Novel approaches to the clinical investigation of glaucoma

Cameron Hudson

Doctor of Philosophy

School of Optometry and Vision Sciences

Cardiff University

2007

ProQuest LLC
789 East Eisenhower Parkway
P.O. Box 1346
Ann Arbor, MI 48106-1346

Form: PGR_Submission_200701

NOTICE OF SUBMISSION OF THESIS FORM: POSTGRADUATE RESEARCH

APPENDIX 1:
Specimen layout for Thesis Summary and Declaration/Statements page to be included in a Thesis

DECLARATION

This work has not previously been accepted in substance for any degree and is not concurrently submitted in candidature for any degree.

Signed ..... (candidate) Date 24.06.08

STATEMENT 1

This thesis is being submitted in partial fulfillment of the requirements for the degree of .....(insert MCh, MD, MPhil, PhD etc, as appropriate)

Signed ..... (candidate) Date 24.06.08

STATEMENT 2

This thesis is the result of my own independent work/investigation, except where otherwise stated. Other sources are acknowledged by explicit references.

Signed ..... (candidate) Date 24.06.08

STATEMENT 3

I hereby give consent for my thesis, if accepted, to be available for photocopying and for inter-library loan, and for the title and summary to be made available to outside organisations.

Signed ..... (candidate) Date 24.06.08

Cardiff University

Novel approaches to the clinical investigation of glaucoma

Cameron Hudson

Doctor of Philosophy

2007

Summary

The aim of the thesis was threefold. Firstly, to undertake a retrospective analysis for the presence of 'dissociating factors' in a longitudinal study designed to investigate the relationship between progressive structural and functional damage in open angle glaucoma (OAG). Secondly, to evaluate, in a prospective cross-sectional study, the diagnostic precision of current promising techniques for the detection of OAG, namely: Optical Coherence Tomography (OCT), Confocal Scanning Laser Ophthalmoscopy (CSLO) and the Multifocal Visual Evoked Potential (mfVEP). Thirdly, to investigate the validity of RNFL thickness measurements obtained using novel software (OCTAnalyse) against those obtained using a commercially available OCT (StratusOCT).

The longitudinal study (follow-up 78.4 ±9.5 months) was concerned with the concordance between progressive damage identified using Heidelberg Retina Tomograph (HRT) Topographic Change Analysis (TCA) and the Humphrey Field Analyzer (HFA) Glaucoma Probability Analysis (GPA) in patients with OAG or 'high risk' ocular-hypertension (OHT). Seventeen out of 23 patients exhibited progressive damage by TCA and/or by GPA; however, only 4 patients exhibited progressive damage by both techniques. In a majority (70%) of the eyes progressing by only one technique, one of three 'dissociating factors' explained the discordance.

The prospective cross-sectional study evaluated the diagnostic precision of retinal nerve fibre layer (RNFL) thickness using StratusOCT, neuroretinal rim area using the HRT and the mfVEP using the Visual Evoked Response Imaging System (VERIS) in a cohort of 20 normal individuals and 23 individuals with OAG. OAG was defined in terms of the subjective assessment of the digital stereoscopic image (DSI) of the ONH by each of 3 masked observers. The sensitivity and specificity of OCT, CSLO, mfVEP for OAG was 91.3% and 65.0%, 43.5% and 95.0%, 69.6% and 60.0%, respectively. In the same cohort, Standard Automated Perimetry (SAP) achieved sensitivity and specificity of 47.8% and 95%, respectively. The best combination of tests for the detection of OAG was OCT and CSLO, which yielded a sensitivity and specificity of 82.6% and 80%, respectively. The topographical correspondence of the ONH abnormality identified by DSI was greatest using CSLO (100%).

The final study utilised custom-derived software, OCTAnalyse, designed for use in instances where StratusOCT yielded erroneous RNFL thickness measurements (such as with a detatched internal limiting membrane and/or in a retina exhibiting poor reflectivity). The validity of the RNFL thickness measurements collected in the cross-sectional study and analysed using OCTAnalyse were compared against those obtained using the standard StratusOCT analysis software. OCTAnalyse RNFL thickness measurements were greater (by approximately 9μm) and exhibited poorer within-session repeatability than those obtained using the StratusOCT.

The overall findings from the three studies provide important information for clinicians implementing the current promising techniques for the routine management of patients with OAG.

Acknowledgements

I would like to thank my supervisor, Professor John Wild, for his help and guidance in producing this thesis.

I am also grateful to Mr James Morgan, Mr Ian Cunliffe, Mr David Garway-Heath and Dr Gavin Powell for their input in the research presented in this thesis.

I am indebted to my colleagues and friends, especially Rishi and Jade, and to my family for their support, tolerance and encouragement throughout the years of my study.

Contents

Chapter 1: Structural and functional relationships in open angle glaucoma (OAG)

1.1 Introduction

The generic term 'glaucoma' refers to a group of ocular disorders characterised by progressive damage to the optic nerve head (ONH) and visual field loss. The pathogenesis of the disease is unclear (Anderson DR 1989, Drance SM 1992, 1997) and the detection of OAG requires the ability to accurately differentiate an ONH that is diseased from one that is healthy. The clinical investigation of glaucoma employs a number of diagnostic techniques to determine abnormality in the structural and/or functional integrity of the eye and/or identify risk factors for the development of the disease.

1.2 Epidemiology

Open-angle glaucoma (OAG) is the most prevalent form of the disease and is the leading cause of blindness in the developed world (Resnikoff S, et al. 2004, Saw S, et al. 2004) affecting between 1.5-8.5% of the population over the age of 40 (Anton A, et al. 2004, Iwase A, et al. 2004, Mitchell P, et al. 2004, Ntim-Amponsah CT, et al. 2004, Tuck MW and Crick RP 1998, Varma R, et al. 2004). Unlike other chronic diseases, OAG is asymptomatic until later stages of the disease; therefore, case finding in groups considered 'at risk' is vital for early detection.

By definition, in OAG, the optic neuropathy manifests in the presence of open anterior chamber angles and is a chronic form of the disease. An acute form of glaucoma, referred to as angle closure glaucoma (ACG), occurs when the anterior chamber angle becomes closed and can occur with (primary) or without (secondary) an anatomical predisposition. Unlike OAG, ACG is associated with a rapid increase in IOP, a painful red eye and a reduction in visual acuity. Angle closure glaucoma is considered a true ophthalmic emergency requiring immediate, appropriate therapy to prevent vision loss. Glaucomatous optic neuropathy can develop in the presence of seemingly normal IOP. This is a condition referred to as normal-tension glaucoma (NTG) and accounts for 25-30% of all open angle glaucoma cases (Klein BE, et al. 1992, Sommer A 1996). Conversely, IOP can be elevated with no evidence of associated ONH damage. This condition is referred to as ocular-hypertension (OHT). Approximately 97% of individuals with IOP between 21mmHg and 25mmHg, and just under 50% of individuals with IOP greater than 35mmHg never develop ONH damage (Kass MA, et al. 1980, Pohjanpelto PE and Palva J 1974).

Risk factors for OAG include: elevated intra-ocular pressure (IOP) (Armaly MF 1969, Kass MA, et al. 1980), older age (Armaly MF, et al. 1980), ethnic origin (Afro-Caribbean's are likely to develop OAG at an earlier age, progress more rapidly, be more resistant to therapy and are more likely to go blind from the disease) (Quigley HA 1996, Tielsch JM, et al. 1991), a family history of the disease (Miller SJ 1978, Tielsch JM, et al. 1994) and moderate to high myopia (>3DS) (Chihara E, et al. 1997, Mitchell P, et al.

1999. Phelps CD 1982). There is much debate as to whether a positive correlation exists between diabetes and OAG. and between systemic hypertension and OAG. Several studies have reported no statistically significant association between diabetes and OAG (Leske MC. et al. 1995. Tielsch JM. et al. 1995). Others. however. report a three-fold increase in the prevalence of OAG (Dielemans I. et al. 1996) and a two-fold increase in the prevalence of OHT (Mitchell P. et al. 1997) in patients with diabetes. Several authors report no association between systemic hypertension and OAG (Jonas JB and Grundler AE 1998. Schulzer M and Drance SM 1987) whilst others report evidence to the contrary (Tielsch JM. et al. 1995).

1.3 Pathophysiology of OAG

The pathological change underlying OAG is atrophy of the retinal ganglion cells (retinal ganglion cells) and neural tissue within the retina. Retinal ganglion cell death manifests as a thinning of the retinal nerve fibre layer (RNFL) and reduction in the width of the neuroretinal rim (NRR) of the ONH with concomitant enlargement of the optic cup. Neuronal death in OAG is not. however. limited to the retina as neurons in the lateral geniculate nucleus (LGN) (Yucel YH. et al. 2000. Yucel YH. et al. 2001. 2003) and visual cortex (Crawford ML. et al. 2001. Yucel YH. et al. 2003) are also lost through retrograde degeneration. The aetiology of glaucomatous optic neuro-degeneration is not fully understood. Elevated IOP is the principal risk factor and is associated with the degeneration of the retinal ganglion cells and optic nerve fibres in a majority of patients with OAG. Elevation of IOP above physiological levels results in an increase in the

pressure gradient across the lamina cribrosa. This, in turn, causes deformation and mechanical stress to the lamina cribrosa and retinal ganglion cell axons (Bellezza AJ, et al. 2003). In addition, mechanical compression of the retinal ganglion cell axons due to elevated IOP, impairs transport of axonal factors supporting a mechanism of cell death that is due to trophic insufficiency (Krishnamoorthy RR, et al. 2001, Pease ME, et al. 2000, Quigley HA, et al. 2000).

Independently, or in addition to elevated IOP, other factors can individually, or collectively, contribute to the death of the retinal ganglion cells and ON fibres in OAG. Localised ischaemia of retinal tissues due to dysfunction of retinal blood flow autoregulation has been implicated as one of these factors (Weinreb RN, et al. 1997). Excessive stimulation of the glutamatergic system, specifically the N-methyl-D-aspartate (NMDA) subtypes, has also been proposed as a contributory factor to the death of retinal ganglion cells in OAG (Dreyer EB, et al. 1996, Lipton SA 2003, Yoles E and Schwartz M 1998). However, it is still unknown whether excess glutamate has a positive or a negative effect on the retinal ganglion cells and whether various sub-classes of retinal ganglion cells respond to glutamate in different ways (Honkanen RA, et al. 2003). Other proposed aetiologies for glaucomatous neuro-degeneration include: poorly functioning cellular pumps and glutamate transporters (Martin KR, et al. 2002), oxidative stress and formation of free radicals (Geiger LK, et al. 2002, Schlieve CR, et al. 2006), autoimmunity (Grus FH, et al. 2004, Schwartz M 2003, Tezel G, et al. 1999, Wax MB 2000) and the effects of inflammatory cytokines such as tumour necrosis factor (TNF) and nitric oxide (NO) (Chiou GC 2001, Dawson VL and Dawson TM 1996, Dreyer EB

1998. Liu B and Neufeld AH 2001. Morgan J. et al. 1999. Yan X. et al. 2000). Evidence also exists suggesting that an initial response to ON insult can lead to a secondary cascade of events causing neuro-degeneration among surviving retinal ganglion cells and their fibres (Liu B and Neufeld AH 2001. Schwartz M 2003). Thus. although primary nerve injury may not directly affect all retinal ganglion cells. it may increase the vulnerability of spared neurones due to subsequent alterations in their environment (Liu B and Neufeld AH 2001. Schwartz M 2003).

1.4 Clinical examination for OAG

The management of OAG principally involves evaluation of the ONH. examination of the visual field and the measurement of IOP.

1.4.1 Evaluation of the Optic Nerve Head (ONH)

Evaluation of the ONH appearance is presently the most sensitive technique for the identification of the earliest pathological changes that occur in OAG (American Academy of Ophthalmology 2000. European Glaucoma Prevention Study (EGPS) Group 2002. Gordon MO and Kass MA - The Ocular Hypertension Treatment Study Group 1999. Leske CM. et al. 1999). Clinically. the ONH is examined stereoscopically and under magnification by slit-lamp binocular indirect ophthalmoscopy (BIO). Slit-lamp BIO provides a quick. simple and non-invasive method to assess the ONH for changes characteristic of OAG. Subjective evaluation of stereoscopic ONH photographs is the recommended standard technique for identifying glaucomatous structural damage

(American Academy of Ophthalmology 2000, European Glaucoma Prevention Study (EGPS) Group 2002, Gordon MO and Kass MA - The Ocular Hypertension Treatment Study Group 1999, Leske CM, et al. 1999).

The neuroretinal rim (NRR) is the intrapapillary projection of the RNFL. The shape of the NRR is governed by the angle at which the optic nerve meets the globe and the size of the ONH relative to the number of retinal ganglion cell axons. As a result, the appearance of the NRR shows great variability between normal individuals (Jonas JB and Grundler AE 1997).

Loss of retinal ganglion cells and neural tissue in OAG reduces the width of the NRR and the size of the optic cup increases, relative to the ONH (Fingeret M, et al. 2005) (Figure 1.0). Attenuation of the NRR and enlargement of the optic cup, referred to as 'cupping', most frequently occurs at the superior and inferior regions of the ONH. Cupping may also manifest as a concentric expansion of the cup due to diffuse loss of retinal ganglion cells (Burgoyne CF, et al. 2005), or as a notch in the regular contour of the NRR due to localised loss of retinal ganglion cells (Javitt JC, et al. 1990, Quigley HA and Addicks EM 1981) (Figure 1.1). A topographical relationship has been shown between regions of the NRR and the visual field (Garway-Heath DF, et al. 2000, Hudson CJ, et al. 2007, Johnson CA, et al. 2003, Strouthidis NG, et al. 2006). Localised retinal ganglion cell death and subsequent focal attenuation of the NRR width is nearly always associated with a corresponding visual field abnormality (Anderson DR 1983).

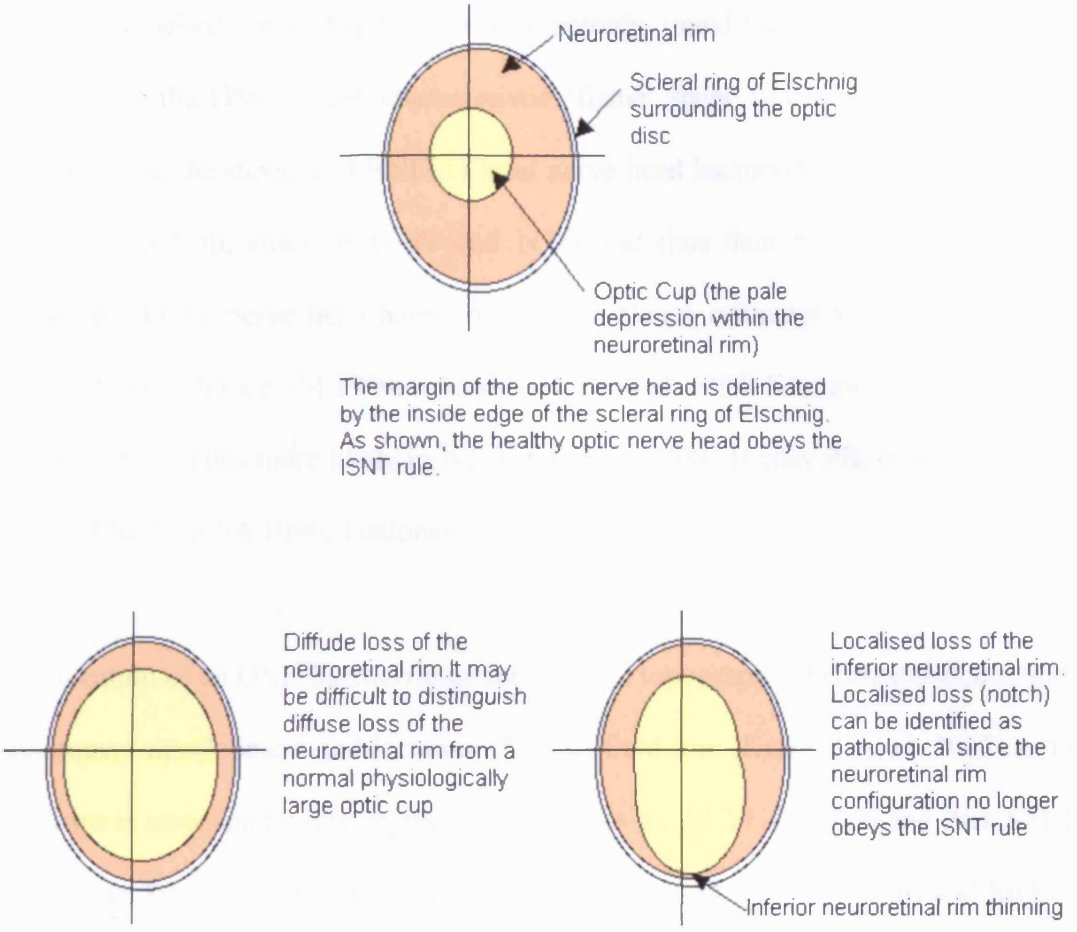

Figure 1.1 – *Schematic representation of the appearance of the ONH in the normal eye (top) and in diffuse (bottom left) and localised (bottom right) neuroretinal rim attenuation from OAG.*

The appearance of an ONH haemorrhage is highly indicative of OAG (Fingeret M, et al. 2005, Soares AS, et al. 2004). The aetiology of ONH haemorrhages is unclear; however, it is postulated that they represent acute ischaemic changes in the retina and/or collapse of small blood vessels at the ONH margin (Sonnsjo B, et al. 1991) and/or disruption of the blood retinal barrier (Grieshaber MC, et al. 2006). Optic nerve head haemorrhages appear

as small, localised flame shaped, or less commonly, round haemorrhages within one disc diameter of the ONH. Their characteristic 'flame' shape is created by virtue of their occurrence in the superficial RNFL. Optic nerve head haemorrhages occur transiently in some, but not all, cases of OAG and NTG and thus their prevalence is difficult to determine. Optic nerve head haemorrhage prevalence estimates vary between 2% and 37% in OAG (Drance SM 1989, Hendrickx KH, et al. 1994, Kitazawa Y, et al. 1986) and are up to four times more likely in NTG (Gloster J 1981, Healey PR, et al. 1998, Siegner SW and Netland PA 1996, Tuulonen A, et al. 1992).

The location of an ONH haemorrhage shows good topographical correspondence with the subsequent development and location of visual field loss (Kono Y, et al. 2003) and their presence is associated with progressive damage to the RNFL (Ahn JK and Park KH 2002, Airaksinen PJ, et al. 1981, Airaksinen PJ and Tuulonen A 1984, Jonas JB and Xu L 1994, Siegner SW and Netland PA 1996, Sugiyama K, et al. 1997, Sugiyama K, et al. 1999) and visual field (Rasker MT, et al. 1997, Siegner SW and Netland PA 1996).

Peripapillary atrophy (PPA) describes a region of cellular degeneration affecting the retinal photoreceptor layer, retinal pigment epithelium (RPE) and chorioretinal tissue adjacent to the ONH. The presence of PPA is non-specific to OAG and is also a physiological effect with ageing; however, the extent of atrophic area is statistically significantly larger in eyes with OAG compared to age-matched normal eyes (Jonas JB 2005, Jonas JB, et al. 1999, Jonas JB, et al. 1992, Jonas JB, et al. 1989, Law SK, et al. 2001). Peripapillary atrophy is divisible ophthalmoscopically and histopathologically into

two distinct regions, namely: the alpha (α) and the beta (β) zones (Figure 1.2). The β-zone occurs at the peripheral edge of the scleral rim of Elshnig and is characterised by complete loss of the RPE and a marked atrophy of the photoreceptor layer and the choriocapillaris. The α- zone borders the peripheral edge of the β-zone and is visible as irregular RPE hypo- and hyperpigmentation and chorioretinal thinning.

Expansion of the PPA regions have been observed in progressive OAG (Heltzer JM 1999, Jonas JB 2005, Uchida H, et al. 1998), patients with OHT converting to OAG and in patients with OAG exhibiting progressive damage to the visual field (Heltzer JM 1999). However, PPA shows large inter-individual variation and the pattern of PPA varies in different types of OAG. Peripapillary atrophy is more common in NTG than OAG, for reasons that are unknown (Wang L, et al. 1998). Similarly, the precise aetiology of PPA is also unknown although vascular ischaemic changes to the choroid have been proposed (Wang L, et al. 1998).

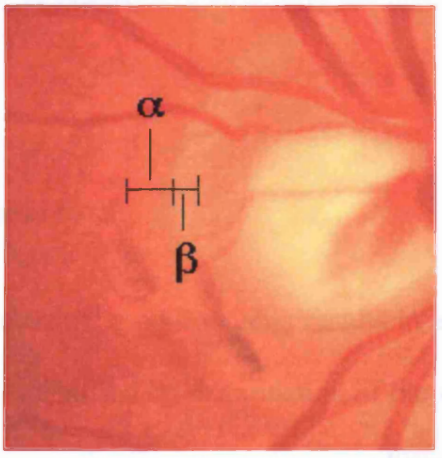

Figure 1.2 – *The alpha (α) and beta (β) zones of peripappilary atrophy (PPA) at the ONH margin.*

Stereoscopic imaging is the current gold standard technique used to assess the ONH in OAG (American Academy of Ophthalmology 2000, European Glaucoma Prevention Study (EGPS) Group 2002). The technique derives objective and archiveable images of the ONH and peripapillary retina useful both in cross-sectional and longitudinal evaluations.

During the last two decades, a number of computer-assisted techniques for evaluating ONH morphometry have evolved for the identification of OAG. These techniques include digital planimetry (Morgan JE, et al. 2005), confocal scanning laser ophthalmoscopy (CSLO) (Bowd C, et al. 2004, Chauhan BC, et al. 2001, Wollstein G, et al. 1998), optical coherence tomography (OCT) (Guedes V, et al. 2003, Wollstein G, et al. 2004), retinal thickness analysis (RTA) (Zeimer R, et al. 1998) and nerve fibre layer polarimetry (GDx) (Medeiros FA, et al. 2004, Reus NJ and Lemij HG 2004). The objective nature of these techniques generally confers high test-retest repeatability of measurements and facilitates their use in the identification of progressive structural damage. Each of these techniques is discussed in section 1.6.

1.4.2 Examination of the visual field

Glaucomatous damage to the retinal ganglion cells results in a functional impairment to vision that is most frequently identified by examination of the visual field. Clinically, the visual field is assessed under standardised recording conditions by a process known as standard automated perimetry (SAP). Standard automated perimetry evaluates the differential light sensitivity at a number of specific and pre-determined locations

throughout the central visual field. The lowest detectable stimulus luminance at each location within the visual field is termed the threshold luminance. The differential light sensitivity, expressed in decibels (dB), is the reciprocal of the threshold luminance. The Humphrey Field Analyzer (HFA, Carl Zeiss Meditec, CA) is the automated perimeter that is most commonly employed in the clinical setting and is therefore the 'gold standard' for visual field examination in OAG.

Evaluation of the visual field by SAP, clinically, is made taking into account any apparent correspondence that exists between the location of the visual field loss and the location of the ONH abnormality. Retinal nerve fibres from the nasal retina project into the ONH in a radial fashion, whereas retinal nerve fibres from temporal retina enter the ONH at the supero-temporal and infero-temporal regions. This asymmetry is due to the relatively large number of retinal nerve fibres originating from the papillomacular region. Retinal nerve fibres from the temporal retina must pass around these nerve fibres and thus enter the ONH closer to the superior and inferior poles. In OAG, damage to the temporal retinal fibres is a common manifestation of the disease and subsequently produces attenuation of the NRR in the supero-temporal and/or infero-temporal regions and a corresponding visual field defect.

Retinal nerve fibres from the temporal retina do not cross the horizontal midline of the retina (Horizontal line of Raphé). This anatomical feature means that in the early stages of OAG, visual field loss can manifest as a marked difference in the differential light sensitivity between the superior and inferior hemifields. The horizontal line of Raphé is

also responsible for the 'nasal step' visual field defect, which occurs due to localised loss of nerve fibres originating from the nasal periphery (Drance SM 1969). The nasal step more commonly manifests in the superior hemifield (Hart WM and Becker B 1982) and is present in up to 40% of OAG patients with visual field loss (Caprioli J and Spaeth GL 1985).

Paracentral visual field defects are also prevalent in OAG and account for approximately 70% of all glaucomatous field loss (Chauhan BC, et al. 1989). Paracentral visual field defects are more commonly found in the superior hemifield between 10^{o} and 20^{o} eccentricity (Hart WM and Becker B 1982, Mickelberg FS and Drance SM 1984).

With progressive damage to the visual field, new regions of field loss appear and/or existing defects become larger, deeper or coalesce. In advanced visual field loss, both hemifields are affected and the extent of the visual field loss can become so profound that the condition drastically impairs mobility and quality of life.

With increasing age, the differential light sensitivity gradually reduces due to the effects of: senile pupil miosis, reduced light transmission of the ocular media, and reduction in the neural integrity of the retina and visual pathway (Johnson CA, et al. 1989). Thus, reduction in the differential light sensitivity that is due to OAG must be separated from that which is due to age.

In the retina, a number of retinal ganglion cell sub-populations exist that comprise

broadly two groups. those that project to the magnocellular layers (M-cells) in the lateral geniculate nucleus (LGN) and those projecting to the parvocellular layers (P-cells) (Perry V. et al. 1984. Silveira L and Perry V 1991). The M. or parasol cells. are widely distributed in the retina and have relatively large cell bodies. axonal diameters and receptive fields (Silveira L and Perry V 1991). The P. or midget cells. tend to be concentrated within the fovea region. and decline rapidly with increase in eccentricity (Dacey D 1993). The P-cells have small cell bodies. axonal diameters and receptive fields and account for about 80-90% of the total retinal ganglion cell population (Curcio CA and Allen KA 1990).

A second group of retinal ganglion cells project to the parvocellular layers of the LGN. namely the K. or small bi-stratified cells. These K-cells have larger cell bodies and larger receptive fields than P-cells and are more sparsely distributed across the retina (Curcio CA and Allen KA 1990). The K-cells receive input from the short-wavelength sensitive (SWS) cone cells. opposed by the combined input from the medium-wavelength sensitive (MWS) cones and long-wavelength sensitive (LWS) cones and convey the SWS cone excitatory signals to the parvocellular layers of the LGN (Dacey D 1993).

Numerous studies have implicated selective damage to retinal ganglion cell sub-populations as the pathological mechanism underlying OAG (Anderson RS and O'Brien C 1997. Glovinsky Y. et al. 1991. Quigley HA. et al. 1988. Quigley HA. et al. 1987). Identifying the mechanism of retinal ganglion cell death is important in terms of our understanding of the disease process and in designing psychophysical tests that exploit

the properties of these cells to identify early disease.

Optic nerve axon counts in monkey and human OAG show a greater loss of the larger than average diameter axons compared to those of the normal optic nerve (Quigley HA, et al. 1988, Quigley HA, et al. 1987). A scarcity of larger diameter axons has also been observed in prepared sections of retinal tissue from glaucomatous eyes (Glovinsky Y, et al. 1991). These observations suggest that large diameter axons may be more susceptible to damage in OAG and supports the use of psychophysical tests that are sensitive to and specific for M-cell properties in the detection of pre-perimetric OAG.

However, some doubts exist as to the interpretation of the histological findings arising from such factors as: cell shrinkage, cell labelling errors, small sample sizes, large between-individual variation in retinal ganglion cell size and differences in tissue preparation (Curcio CA and Allen KA 1990, Morgan JE 1994).

Damage to both magno- and parvocellular pathways is reported in OAG (Weber AJ, et al. 1998). Thus, whether retinal ganglion cell death in OAG is truly selective, or not, has yet to be fully elucidated; however, it is conceivable that there is overlap in the susceptibility of different retinal ganglion cell sub-populations to glaucomatous damage.

Selective and non-selective losses of retinal ganglion cells may be occurring at different locations within the visual field and at different times throughout the course of the disease dependent upon the pathogenesis and stage of glaucomatous damage. Utilizing

this view, some investigators have put forward the hypothesis that sparsely represented retinal ganglion cells, with lower degrees of overlap between adjacent receptive fields, are more likely to exhibit functional deficits not necessarily due to selective damage but because only a small number of cells must be lost before the integrity of the pathway is compromised (the reduced redundancy theory) (Johnson C 1994, Johnson CA 1995).

Evidence for selective loss of retinal ganglion cells and/or the reduced redundancy theory has prompted the development of psychophysical tests that exploit various function-specific retino-cortical pathways. Several of these tests exhibit clinically useful levels of sensitivity and specificity for the identification of early OAG and include: short-wavelength automated perimetry (SWAP) (Bayer AU and Erb C 2002, Bayer AU, et al. 2002, Demirel S and Johnson CA 2001), Frequency Doubling Technology Perimetry (FDT) (Kogure S, et al. 2003, Landers J, et al. 2006, Wadood AC, et al. 2002) and High-pass Resolution Perimetry (HRP) (Birt CM, et al. 1998, Iester M, et al. 1999, Kalaboukhova L and Lindblom B 2003).

1.4.3 Measurement of intra-ocular pressure (IOP)

Elevated intra-ocular pressure (IOP) is the primary treatable risk factor for OAG (Heijl A, et al. 2002, Kass MA, et al. 2002, Lee BL and Wilson MR 2003); however, the precise role of IOP in the pathophysiology of the disease is unknown (Gordon MO, et al. 2002, Leske MC, et al. 2003).

Treatment of OAG is aimed primarily at lowering IOP, either by therapeutic or by surgical or laser intervention, to prevent progressive damage and thus improve the prognosis for the maintenance of 'good' vision (Cioffi GA and Leibmann JM 2002, Leske MC, et al. 2004).

The Goldmann applanation tonometer (GAT) is the internationally accepted standard for IOP measurement. The principal of the technique is based upon the Imbert-Fick Law, which assumes that the cornea is a dry surface that is infinitely thin and behaves as a membrane where by the applanating pressure is equal to the IOP (Gloster J and Perkins ES 1963). In reality, the cornea fulfils none of these criteria; however, the surface tension force created by the tear film and the resistance force created by virtue of corneal thickness are approximately equal and opposite when an applanation area of 7.35mm^2 (diameter 3.06mm) is applied to a cornea of 520μm in thickness (Ehlers N, et al. 1975). Central corneal thickness (CCT) and corneal curvature affect IOP measurements obtained with the GAT (Brandt JD 2004, Brandt JD, et al. 2001, Whitacre MM, et al. 1993). The effect of CCT on GAT measurements has been apparent since the introduction of laser refractive surgery where there is an iatrogenic thinning of the cornea and a reported underestimation of IOP post surgery (Agudelo LM, et al. 2002, Chatterjee A, et al. 1997). Central corneal thickness affects the pressure measurements obtained with the GAT such that IOP may be overestimated or underestimated in thick or thin corneas, respectively (Doughty MJ and Zaman ML 2000, Ehlers N, et al. 1975). The extent of the underestimation and overestimation by GAT has received mixed reviews (Doughty MJ and Zaman ML 2000, Singh RP, et al. 2001, Whitacre MM, et al. 1993). Some authors

report that GAT IOP measurements may span a range of up to 11mmHg in patients normally encountered clinically (Doughty MJ and Zaman ML 2000, Whitacre MM, et al. 1993), whilst others suggest that the effect of CCT on IOP is small and does not need correction in the majority of patients (Singh RP, et al. 2001).

The clinical utility of CCT-corrected IOP measurements lies in the identification of elevated IOP in eyes with thin corneas and of normal eyes falsely classified as OHT. Several correction factors for GAT IOP measurements have been proposed (Doughty MJ and Zaman ML 2000, Gunvant P, et al. 2005, Whitacre MM, et al. 1993) and typically adjust measurements by between 0.19-0.37mmHg for each $\pm$10μm of thickness variation from the normal CCT of 520μm (Doughty MJ and Zaman ML 2000, Gunvant P, et al. 2005, Whitacre MM, et al. 1993). However, none of these correction factors consider the stiffening of the cornea that is thought to occur with age (Friedenwald JS 1937). Age induced stiffening of the cornea results from ultrastructural changes in the collagen fibrils of the corneal stroma (Daxer A, et al. 1998, Malik NS, et al. 1992); thus, a 'one size fits all' correction factor may be unsuitable for patients of different ages.

1.5 Current approaches to OAG detection and management

Throughout the last decade, technological advances have led to the development of new techniques for the investigation of OAG. Many of these techniques appear to exhibit clinically useful levels of diagnostic precision for OAG, and are seemingly useful in the detection of pre-perimetric disease. The techniques which show the greatest level of

promise for the early detection of OAG are reviewed in the following sections and can be classified under the headings: ocular imaging (Section 1.6), ocular electrophysiological techniques (Section 1.7) or psychophysical (Section 1.8) techniques.

1.6 Ocular imaging

It is well established that structural damage to the ONH and RNFL precedes detectable visual field loss by SAP (Harwerth RS, et al. 2004, Quigley HA, et al. 1982). As a result, a number of quantitative ocular imaging techniques have evolved that are capable of identifying structural changes that are believed to represent the earliest pathological changes of the glaucomatous disease process. These techniques include: digital stereoscopic imaging (DSI), optical coherence tomography (OCT), confocal scanning laser ophthalmoscopy (CSLO), retinal thickness analysis (RTA) and scanning laser polarimetery (SLP).

These devices each exhibit clinical utility for the detection of OAG (Bagga H, et al. 2005, Bathija R, et al. 1998, Budenz DL, et al. 2005, Da Pozzo S, et al. 2005, De Leon-Ortega JE, et al. 2006, Garway-Heath DF and Hitchings RA 1998, Hougaard JL, et al. 2004, Huang ML and Chen HY 2005, Iester M, et al. 2000, Jeoung JW, et al. 2005, Kanadani FN, et al. 2006, Kanamori A, et al. 2006, Kanamori A, et al. 2003, Leung CK, et al. 2005, Leung CK, et al. 2005, Mardin CY, et al. 1999, Medeiros FA and Susanna R Jr 2003, Medeiros FA, et al. 2005, Medeiros FA, et al. 2004, Mikelberg FS, et al. 1995, Morgan JE, et al. 2005, Nouri-Mahdavi K, et al. 2004, O'Connor DJ, et al. 1993, Sihota R, et al.

2006. Uchida H. et al. 1996. Wollstein G. et al. 1998. Wollstein G. et al. 2005) and demonstrate topographical correspondence between the location of structural damage and visual field loss in eyes with OAG (Garway-Heath DF. et al. 2000. Sommer A. et al. 1991). However. since in a majority of these studies OAG was defined on the basis of visual field loss. the appreciation of their clinical utility in detecting early/pre-perimetric OAG is limited. The diagnostic ability of the most promising novel imaging techniques in correctly identifying pre-perimetric OAG has yet to be established. In addition. the chronology of structural damage as assessed by each of the different techniques is also unknown.

The application and limitation of the current commercially available imaging techniques for the detection of glaucomatous structural damage is discussed in the following sections.

1.6.1 Stereoscopic ONH-imaging and planimetry

Subjective evaluation of stereoscopic photographic images of the ONH is an effective and recommended standard technique for the evaluation of the glaucomatous optic neuropathy (Abrams LS. et al. 1994. American Academy of Ophthalmology 2000. European Glaucoma Prevention Study (EGPS) Group 2002. Gordon MO and Kass MA - The Ocular Hypertension Treatment Study Group 1999. Leske CM. et al. 1999. Musch DC. et al. 1997). The technique utilises pairs of photographic images. which when viewed together in a specialised stereo-viewer. allows the observer to appreciate depth. A small amount of disparity between two images. created by a lateral displacement in the

axis of image capture between the two acquisitions, is required to create the appreciation of depth when the images are viewed simultaneously.

In order to achieve 'good quality' stereoscopic images, patients should have dilated pupils and have relatively clear media. A skilled ophthalmic photographer is also important.

Stereoscopic imaging provides a permanent and archiveable record of the appearance of the ONH and peripapillary retina at any given time point. Specifically, digital stereoscopic imaging (DSI) is the preferred form of this technique owing to advances in photographic methods and the greater versatility of images in this medium.

Viewing the ONH in three-dimensions improves the discrimination of the NRR, the appreciation of the depth of the optic cup, and provides better visualisation of blood vessel changes. These factors, in combination, enhance the observer's ability to assess characteristics of the ONH with respect to OAG, including; the intra-papillary projection of the retinal nerve fibres; localised and/or generalised attenuation of the NRR; the extent of cupping and/or bowing of the lamina cribrosa; the presence of an acquired pit of the optic nerve (APON); and alterations in the course of retinal blood vessels (Broadway DC, et al. 1999, Piette SD and Sergott RC 2006).

A number of stereo-cameras designed for ophthalmologic application are currently commercially available, including the NIDEK 3-Dx (NIDEK Co., Ltd, Tokyo, Japan) and

Topcon TRC-50EX (Topcon Medical Systems, Inc. [TMS], Paramus, NJ). These two cameras acquire digital stereo–image pairs in different ways. The NIDEK 3-Dx stereo-camera obtains pairs of digital stereo-images simultaneously, whereas the Topcon TRC-50EX stereo-camera obtains the pair of digital stereoscopic images sequentially. Whilst both simultaneous and sequential imaging techniques are capable of obtaining high quality digital stereoscopic images, sequentially acquired digital images are more susceptible to artefacts due to eye movements and to blinking between the first and second successive image. Simultaneously acquired digital stereoscopic images exhibit superior reproducibility to those obtained sequentially and are therefore recommended for use in the detection of progressive structural damage (Varma R, et al. 1992).

Technological advances in digital display equipment have facilitated the evaluation of digital stereoscopic ONH images. In its simplest form, a standard computer monitor with a device capable of dissociating the view (for example, a monitor Z-Screen overlay [StereoGraphics Corp., San Rafael, CA] and passive polarizing eyewear) to each eye is all that is required.

The qualitative assessment of digital ONH images by trained observers exhibits moderate to excellent levels of sensitivity (72-78%) and specificity (60-95%) for the detection of OAG (Abrams LS, et al. 1994, O'Connor DJ, et al. 1993, Wollstein G, et al. 2000).

Digital planimetry is a method for analysing stereoscopic images that permits quantification of the ONH morphometry. At present, there is no established standard

planimetric technique to assess the ONH and studies utilizing digital planimetry have primarily employed custom software (Garway-Heath DF, et al. 1999, Hatch WV, et al. 1999, Kono Y, et al. 1999, Morgan JE, et al. 2005, Shen SY, et al. 2006). Planimetry is capable of measuring parameters of the ONH including the ONH size, ONH area, optic cup area, optic cup to ONH area ratio, α-zone PPA area and β-zone PPA area etc. Such measurements are derived from the area within a boundary that is positioned around the given structure. Therefore, the actual measurement obtained by this technique for any given structure, is subject to between-observer variability (Hatch WV, et al. 1999, Kono Y, et al. 1999).

Digital planimetry can be used to identify an ONH structure that is statistically significantly different from the expected value based upon a distribution of the value found in a population of normal individuals. In this way, planimetry can be applied cross-sectionally provided that differences in refractive error and corneal curvature between patients are corrected. Digital planimetry yields values of specificity and sensitivity of between 67-94.3% and 62-94.4%, respectively for the detection of OAG (Garway-Heath DF, et al. 1998, Morgan JE, et al. 2005, O'Connor DJ, et al. 1993) and typically exceeds that of alternative objective digital imaging devices when compared in a single cohort (Correnti AJ, et al. 2003, Greaney MJ, et al. 2002, Jonas JB, et al. 1998, Wollstein G, et al. 2000).

DSI and digital planimetry exhibit large amounts of within- (Kappa = 0.69-0.96) and between-observer (Kappa = 0.20-0.84) variability (Coleman AL, et al. 1996). Despite the

inherent variability. DSI is clinically appropriate for the evaluation of glaucomatous structural damage since it is offers direct visualisation of the structural status of the neuro-retina (Jonas JB. et al. 1998). In addition. the objective nature by which digital stereo ONH images are obtained results in high repeatability of images between sessions. Thus. DSI is suitable for the identification in progressive structural damage. Although the absence of longitudinal data currently precludes this assumption. statistically significant reductions in manual planimetrically derives rim area measurements were evident over a 10 year follow-up (Airaksinen PJ. et al. 1992).

1.6.2 Confocal Scanning Laser Ophthalmoscopy (CSLO)

The confocal scanning laser ophthalmoscope (CSLO) is an objective imaging device used for *in vivo* topographical mapping of the ONH and peripapillary retina. The procedure is non-invasive and negates the need for pupil dilation in a majority of patients owing to the low intensity. long-wavelength diode laser used to obtain the images. The Heidelberg Retina Tomograph (HRT. Heidelberg Engineering GmbH. Dossenheim. Germany) is a commercially available CSLO. that has demonstrated clinical utility in detecting early and progressive structural damage in OAG (Artes PH and Chauhan BC 2005. Bathija R. et al. 1998. Bowd C. et al. 2004. Chauhan BC. et al. 2000. Chauhan BC. et al. 2001. Ford BA. et al. 2003. Kamal DS. et al. 2000. Kesen MR. et al. 2002. Miglior S. et al. 2003. Uchida H. et al. 1996).

The current version of the HRT. the HRT III. employs a rapid scanning 670nm diode laser to obtain images of the posterior segment. The emitted beam is projected through a

pinhole, a raster scanning system and an objective lens onto the retina. Laser light that is reflected from the retina is then re-directed through a second pinhole and onto a light sensitive detector. The confocal aperture limits the depth from which reflected light reaches the detector to a narrow range centred around the location of a set focal plane on the retinal or ONH surface. Reflected light from structures in front of or behind the focal plane of interest is blocked by the detector pinhole producing an optical section of the posterior pole corresponding to the focal plane. The depth of the focal plane is automatically adjusted by shifting the confocal aperture to acquire multiple image sections through the tissue, creating a layered three-dimensional structure. The HRT III acquires 16 to 64 imaging planes to a depth of up to 4mm, depending on the depth of the optic cup. The sections are then combined to create a three-dimensional topographical map of the ONH surface. The amount of reflected laser light at each point in the image at each point in the z-axis forms the z-profile. The peak of the z-profile is used to determine the retinal surface height at each point in the image, which is presumed to correspond with the internal limiting membrane. The product of this process is a topographic height map containing independent retinal surface height measurements of the ONH and peripapillary retina.

After an initial 'pre-scan', which determines the depth of the optic cup, the HRT III automatically obtains a further three scans for the analysis. Automated quality control measures detect scans that are of inadequate quality due to blinking and/or fixation shifts, and repeat any faulty scans to ensure that three 'adequate' scans are obtained. The scans are then automatically aligned and averaged to create a mean topography image for the

scan session. Heidelberg Retina Tomograph measurements with the current and previous versions of the instrument exhibit high repeatability (Janknecht P and Funk J 1994, Rohschneider K, et al. 1994, Weinreb RN, et al. 1993, Zangwill L, et al. 1997). Once the image is processed and saved, the topography standard deviation (SD) provides a measure of image quality. Standard deviations below 20μm indicate excellent image quality; 20 to 30μm, very good image quality, and 30 to 40μm, acceptable image quality (Schuerle AF and Schmidt E 2004).

The reflectance image is a false-colour image that is similar in appearance to a photograph of the ONH. The image is created by summating the two-dimensional reflectance images and is presented as a 384x384 pixel map illustrating the intensity of the reflections at sites within the ONH and peripapillary retina. Darker areas represent regions of lower reflectance whereas lighter areas indicate higher reflectance.

The topography image provides information regarding the height of the surface contour of the ONH and peripapillary retina. The topography image is derived from the height measurement matrix constructed from the depth of maximal reflection in the z-axis intensity profile. The image is false-colour coded, whereby brighter areas correspond to deeper surfaces and darker areas lie more superficially.

A number of stereometric parameters that describe the morphometry of the ONH are generated by HRT III software following the delineation of the ONH margin. The ONH margin is defined as the inner edge of the scleral ring of Elshnig. The ONH itself usually

appears a slightly pink in colour with a slightly depressed central portion (cup) that is pale pinkish-white in colour. The position of the ONH margin is determined using the same general procedure for all version of the HRT and takes into account both the topography and the reflectance images. Six or more points are placed along the circumference of the ONH margin using a mouse controlled cursor; the HRT automated software then constructs a roughly circular contour line connecting adjacent points. Fine adjustments to the position of the ONH contour line are then made to ensure that it corresponds with the ONH margin throughout the entirety of its circumference. Where evidence of peripapillary atrophy (PPA) and/or a myopic crescent is apparent, extra care is required in order not to confuse the ONH margin with the edge of the atrophic region. Once correctly aligned, the contour line is used during cross-sectional and longitudinal analysis of scans.

The location of the ONH margin dictates the position of a 'reference plane', against which most of the stereometric parameters are derived. The 'standard reference plane' (SRP) lies 50μm below a 6^{o} wide section of the ONH margin corresponding to the site of the papillomacular bundle. This region of the ONH is considered to remain relatively stable throughout the course of OAG such that the position of the SRP is stable throughout the course of the disease. The SRP is positioned below the retinal surface height at this location to account for the inter-individual variability in ONH topography (Burk RO, et al. 2000) (Figure 1.3). However, since demarcation of the ONH margin is a subjective task, the shape, size and location of the ONH contour exhibits considerable between- and within-observer variability (Iester M, et al. 2001).

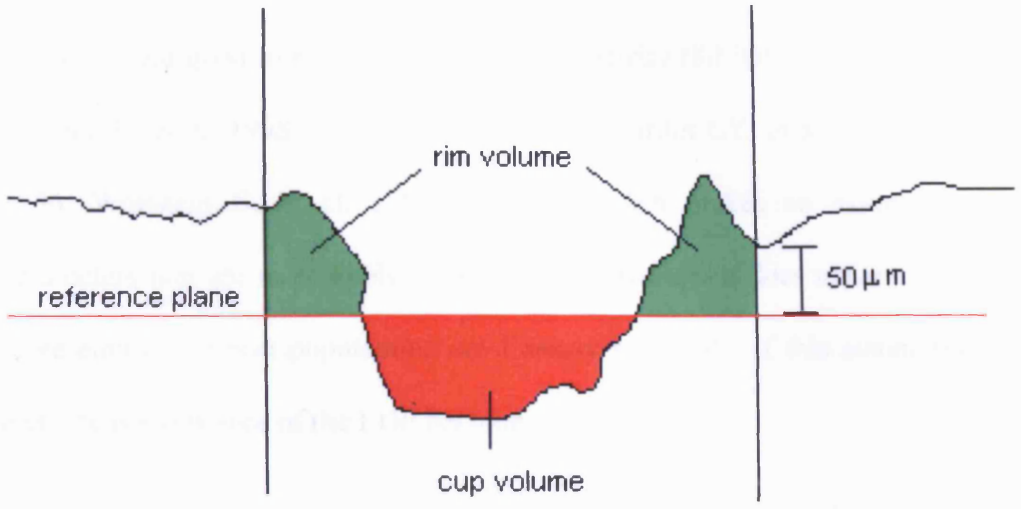

Figure 1.3 - *Position of the standard reference plane (SRP)*

Owing to the considerable between-individual variability in the size, shape and tilt etc, of the ONH, the distinction between a normal and abnormal ONH appearance, the HRT II stereometric parameters can provide limited/misleading information in cases of large (>3.0mm^2), small (<1.9mm^2) and/or tilted ONHs (Schuerle AF and Schmidt E 2004).

Within these constraints, a number of different mathematical approaches have been applied to the problem of deriving a suitable algorithm that can make use of all the HRT data to distinguish between normal and OAG eyes (Bowd C, et al. 2002, Ford BA, et al. 2003, Swindale NV, et al. 2000, Wollstein G, et al. 2000).

Linear discriminant function (LDF) analysis of combinations of optimally weighted stereometric parameters is a method widely used for the detection of glaucomatous ONH abnormalities (Bathija R, et al. 1998, Mardin CY, et al. 1999, Mikelberg FS, et al. 1995).

Analysis of HRT data by LDF analysis exhibits moderate to good levels of sensitivity (62-87%) and good to excellent levels of specificity (80-96%) for the detection of OAG (Bathija R. et al. 1998. Iester M. et al. 2000. Mardin CY. et al. 1999. Uchida H. et al. 1996. Wollstein G. et al. 1998). This approach makes no assumptions about the parameters that are most likely to be useful; however. it does assume that distributions representing different populations are linearly separable. If this assumption is not well met. the performance of the LDF becomes degraded.

The Moorfields Regression Analysis (MRA) is a linear discriminant function that is incorporated into the software of the commercially available HRT II and III. The MRA differs from most other LDFs by incorporating prior knowledge of the physiological dependence of NNR area on ONH size. The MRA algorithm is derived from linear regression of sectoral and global ONH area against the log of the NRR area. Due to increase in the variability of NRR area measurements with increasing NRR area. (Jonas JB. et al. 1988) log scaling of NRR. helps to normalize the observed size of the ONH. With respect to the detection of abnormality. log scaling of NRR area makes the prediction intervals more appropriate for both small and large ONHs.

The first version of the MRA algorithm available with the HRT II employs measurements obtained from 110 normal eyes to determine 95.0%. 99.0% and 99.9% confidence limits for the normal population. The latest software version (3.0) for the HRT III includes a larger and ethnicity-specific normative database. The Heidelberg Retina Tomograph III includes two databases. one of 733 healthy Caucasian eyes and one of 215 healthy

African-American eyes. Based on the enlarged database, the equations of the MRA have been modified. Both for HRT II and HRT III, an ONH is classified as 'within normal limits' if the global and sectoral NRR areas are all within the 95% confidence interval. Where the NRR area lies between the 95% and 99.9% confidence intervals for normality, the ONH is classified to be 'borderline'. If the rim area of any segment falls outside the 99.9% confidence interval then it is deemed to be 'outside normal limits'.

The MRA (Version 1.0) exhibits sensitivity of 74-84% and specificity of 41-96% in detecting glaucoma eyes with glaucomatous field loss by SAP (Miglior S, et al. 2003, Wollstein G, et al. 1998). This, and several other studies have demonstrated that sensitivities and specificities of MRA reduce if the 'borderline' outcomes are considered to be normal (Ford BA, et al. 2003, Miglior S, et al. 2003). The diagnostic performance of the HRT III MRA has not yet been extensively evaluated; although, one study has reported improved diagnostic performance by the HRT III MRA (Area under receiver operating characteristic, AROC 0.934) compared to the HRT II MRA (AROC 0.927) (Burgansky-Eliash Z, et al. 2007).

Several, automated classification systems have employed neural networks to classify eyes as normal or glaucomatous based upon the HRT II stereometric parameters (Bowd C, et al. 2002, Brigatti L, et al. 1996, Uchida H, et al. 1996). Neural networks, or specifically, multilayer perceptrons (MLPs) with back-propagated learning, can be trained to detect a relationship between input data and a pre-defined 'gold standard' diagnosis by comparing its prediction with the labelled diagnosis, and learning from its mistakes (Rumelhart DE,

et al. 1986). In general, neural networks differ from basic statistical techniques, such as LDFs, because they are able to adapt to the distribution of the variable rather than assume a predefined distribution. Neural network classification techniques appear to outperform conventional LDF techniques, including the MRA, in the detection of OAG; however, studies comparing the two methods are scant (Bowd C, et al. 2002, Uchida H, et al. 1996). Neural network classification systems provide good to excellent sensitivity (83%-92%) and excellent specificity (around 90%) for the detection of OAG (Bowd C, et al. 2002, Uchida H, et al. 1996).

Both the HRT III and HRT II are accurate (Dreher AW and Weinreb RN 1991, Janknecht P and Funk J 1994, 1995) and reproducible (Garway-Heath DF, et al. 1999) techniques for the quantification of progressive damage.

To date, there are two general methods that have been used to identify progressive damage to the ONH: one based upon linear regression of stereometric parameters and the other based upon evaluation of longitudinal topographic height change.

Detection of progressive damage by linear regression of stereometric parameters permits quantification of the extent of the progressive damage, but provides little information regarding its location. Conversely, detection of progressive damage by localised reduction in topographic height is a better method for determining the location of progressive damage but is unable to quantify the extent in real terms.

The HRT III and HRT II software uses an automated algorithm to align consecutive images obtained from a series of follow-up examinations. This process ensures that corresponding locations of consecutive images are compared for evidence of progressive damage. The ONH margin contour from the base-line image is then replicated onto the follow-up images and stereometric parameters generated for each image. Due to the heterogeneity of the stereometric parameters, evidence of progressive damage is based upon normalized parameter values. If no detectable damage occurs between consecutive images then normalized parameter values are equal to 0. Where a normal ONH is deemed to progress to advance disease, the normalised values are equal to -1 (Schuerle AF and Schmidt E 2004). The HRT II displays normalised stereometric values for global and three different sector combinations (Schuerle AF and Schmidt E 2004) for evidence of progressive damage.

Topographic change analysis (TCA) is a statistical method, which is incorporated into the standard HRT II software, to compare topographic height values from discrete regions called superpixels (4x4 pixels). Following the alignment of the image series, evidence of statistically significant change in topographic height, from the mean topographical height of two baseline examinations, is determined for each superpixel using standard statistical procedures (Chauhan BC, et al. 2000). The probability that any observed change in topographic height occurring within a superpixel exceeds between-examination variability is evaluated by ANOVA and expressed in the form of a probability map. Regions within the ONH and peripapillary retina that exhibit statistically significant reduction in topographic height from baseline ($p<0.05$) are highlighted by the

superimposition of magenta superpixels in the corresponding region of the HRT II reflectance image. Regions within the ONH and peripapillary retina that exhibit statistically significant elevation in topographic height from baseline ($p<0.05$) are highlighted by the superimposition of green superpixels in the corresponding region of the HRT II reflectance image. The TCA identifies statistically significant progressive damage when a cluster of at least 20 magenta superpixels is present at each of three consecutive follow-up examinations (Chauhan BC, et al. 2001). The clinical utility of TCA has been investigated by a number of studies (Artes PH and Chauhan BC 2005, Chauhan BC, et al. 2001). In addition, topographic correspondence between progressive structural damage by the HRT II TCA and functional progression by SAP is often present when progressive damage is demonstrable by both techniques (Artes PH and Chauhan BC 2005, Chauhan BC, et al. 2001). However, a poor level of agreement generally exists between HRT II TCA and SAP progression analyses (Artes PH and Chauhan BC 2005, Chauhan BC, et al. 2001).

A number of factors that are related to the stage of the glaucomatous disease and/or inherent to the test procedures are believed to be the source of the poor association (Jonas JB, et al. 1988).

1.6.3 Optical Coherence Tomography (OCT)

The first optical coherence tomographer for imaging the retina was demonstrated in 1991 (Huang D, et al. 1991). Optical coherence tomography (OCT) is a non-invasive imaging technique capable of providing sectional imaging in many biomedical situations

especially imaging of the retinal structures. The current generation of the clinical standard OCT used in ophthalmology, StratusOCT (Carl Zeiss Meditec Inc., Dublin, CA) has recently been surpassed by the fourth generation, which exhibits an axial resolution of between 5 and 7μm. Other commercially available instruments include: Niris (Imalux, Clevelend, OH), RT Vue100 (Optovue, Fremont, CA), LightLab (LightLab Imaging, Westford, MA), Bioptigen (Bioptigen Inc., Research Triangle Park, NC), Spectral OCT/SLO (OTI, Ophthalmic Technologies Inc., Toronto, Ontario, Canada) and Spectralis (Heidelberg Engineering GmbH, Dossenheim, Germany).

The principle of OCT is based on low-coherence interferometry (Huang D, et al. 1991). Using broadband light sources generated by using superluminescent diodes or femtosecond lasers, OCT uses the properties of reflected light from the tissue of regard, in the context of this thesis, the retina, to construct a two- or three-dimensional model of the cytoarchitecture. The time-delay of reflected light between points of reflection is used to determine the thickness of the tissues.

The light source in an OCT system is split into two arms: a sample arm (for example, containing the retina) and a reference arm (in most cases, a mirror). The combination of reflected light from the sample arm and from the reference arm gives rise to an interference pattern. Areas of the sample/retina that reflect back a lot of light will create greater interference than areas that don't. This reflectivity profile, called an A-scan contains information about the spatial dimensions and location of structure within the

sample/retina. A cross-sectional tomography (B-scan) is achieved by laterally combining a series of axial depth scans (A-scan).

The lateral resolution of the StratusOCT can be manually varied between 128, 256 and 512 scans per record. The device has a scan rate of 400 scans/second, thus acquisition time can also be controlled between approximately 25ms and 130ms.

The StratusOCT employs a false-colour image to represent the layered retinal architecture. The current StratusOCT software (Version 4.0) incorporates 19 scanning and 18 analysis protocols. Radial scans, along any vector, and circular scans, of varying diameter, can be customised for a range of applications.

Good agreement exists between OCT (StratusOCT and OCT) and histologically derived retinal thickness measurements in post-mortem eyes (Hee MR, et al. 1995, Huang D, et al. 1991, Schuman JS, et al. 2007, Toth CA, et al. 1997); although StratusOCT measurements are typically thinner (Dichtl A, et al. 1999, Varma R, et al. 1996).

The StratusOCT has an axial resolution of around 10μm and yields structural images and measurements that are highly repeatable (SD ±5-8μm) (Blumenthal EZ, et al. 2000, Budenz DL, et al. 2005, Carpineto P, et al. 2003, Paunescu LA, et al. 2004). The StratusOCT has been applied to range of vitreoretinal and retinal disorders; however, given the topic of this thesis the description of its utility will be restricted to retinal applications related to OAG. Due to the very recent arrival of the fourth generation

instrument (Cirus high-definition OCT) this review is limited to versions up to StratusOCT.

The clinical application of OCT/StratusOCT in the detection of OAG has been widely investigated (Bagga H, et al. 2005, Budenz DL, et al. 2005, Burgansky-Eliash Z, et al. 2005, De Leon-Ortega JE, et al. 2006, Huang ML and Chen HY 2005, Jeoung JW, et al. 2005, Kanadani FN, et al. 2006, Kanamori A, et al. 2006, Nouri-Mahdavi K, et al. 2004, Sihota R, et al. 2006). Several of the standard StratusOCT scan protocols exhibit clinically useful levels of sensitivity and specificity for the detection of OAG (Bourne RR, et al. 2005, Bowd C, et al. 2001, Burgansky-Eliash Z, et al. 2005, Kanadani FN, et al. 2006, Leung CK, et al. 2005, Medeiros FA, et al. 2005, Sihota R, et al. 2006, Wollstein G, et al. 2005). However, the RNFL thickness (3.4) protocol yields the highest levels of diagnostic precision for the detection of OAG with (AROC 0.91-0. 93) (Bourne RR, et al. 2005, Bowd C, et al. 2001, Leung CK, et al. 2005, Medeiros FA, et al. 2005, Sihota R, et al. 2006, Wollstein G, et al. 2005) and without visual field loss by SAP (AROC 0.87-0.89) (Bowd C, et al. 2001, Kanamori A, et al. 2006).

Whilst OAG is traditionally associated with structural alterations to the ONH and peripapillary retina, StratusOCT exhibits diagnostic precision for the detection of OAG based upon measurements obtained from the macula region (Burgansky-Eliash Z, et al. 2005, Leung CK, et al. 2005). Anatomically, the macula is defined as the region of the retina where the ganglion cell layer is more than one ganglion cell thick. Since the photoreceptor layer is not considered to decrease in thickness in OAG, it is likely that a

reduction in retinal thickness in the macula region in OAG can be attributed to loss of retinal ganglion cells and the RNFL.

The density of ganglion cells at the macula is greater than at any other region of the retina and accounts for up to 30% of the total retinal thickness (Giovannini A. et al. 2002. Greenfield DS. et al. 2003). This observation lends favour to the hypothesis that the attenuation in retinal thickness at the macula can be used to detect OAG before substantial functional abnormality manifests. Scans obtained from the macula region also have the practical advantage of easier image acquisition and less between-operator and between-session variability (Gurses-Ozden R. et al. 2004).

StratusOCT macula thickness and macula volume protocols exhibit moderate to excellent discriminatory power for the detection of OAG suspect eyes (AROC 0.61) (Leung CK. et al. 2005) and in eyes with advanced OAG (AROC 0.89) (Burgansky-Eliash Z. et al. 2005). respectively. However. the presence of maculopathy. for example. age-related macula degeneration (AMD) and/or diabetic maculopathy. limits the utility of macula scanning across the typical OAG population.

Longitudinal evaluation of eyes with OAG and of eyes of OAG suspects. during a 4.7 year follow-up. shows that twice the number patients exhibited structural progression of the RNFL by StratusOCT (22%) than of the visual field recorded by SAP (9%) (Wollstein G. et al. 2005). However. the lack of an established criterion of what constitutes a statistically significant reduction in RNFL thickness limits the validity of

this finding. The clinical utility of StratusOCT in longitudinal evaluation of OAG by many research groups is ongoing and the results are eagerly awaited. Such studies will determine the true clinical utility of StratusOCT in the detection of progressive structural damage.

1.6.4 Retinal Thickness Analysis (RTA)

The retinal thickness analyser (RTA; Talia Technology Ltd, Neve-Ilan, Israel) is a commercially available objective retinal-imaging device for measurement of retinal thickness and retinal surface topography. Unlike OCT, which analyses retinal thickness as a single section, RTA is able to compile a series of rapidly and consecutively acquired sections, within a small area, to produce a three-dimensional retinal thickness map. This facilitates measurement of both the degree and size of the affected area of atrophy or oedema.

The principal of the technique is similar to slit lamp bio-microscopy (optical triangulation) (Zeimer R, et al. 1998) in that a thin vertical slit of green laser light (540 nm) is projected obliquely onto the retina. The reflected laser light enters an offset, closed circuit digital (CCD), camera and is analysed by software. During a single scan, 500 points along the scan section are obtained. The shape of the back-scatter profile can then be determined and is synonymous with retinal thickness (Zeimer R, et al. 1998). The RTA acquires 16 adjacent sectional scans covering an area of $9mm^2$ (approximately 10^o x 10^o) in approximately 320ms and combines the two-dimensional scan data from each profile to derive the three-dimensional model of retinal topography. Five such scans are

obtained at the macula, three scans at the ONH and an additional 5 scans over the peripapillary region.

The RTA then performs morphometric analysis of the data using automated algorithms. These algorithms divide each optical section into 20 segments with each segment 100 μm in length. The segment information is converted into a light-intensity profile (Zeimer R, et al. 1998) from which the separation between the vitreoretinal interface and the chorioretinal interface can be determined. These provisional thickness estimates are then corrected for erroneous results, arising from fixation instability, media opacity etc using a quality check algorithm. The corrected thickness data from adjacent and surrounding segments are then combined and smoothed using a specialised two-dimensional filter to create an 'un-calibrated' retinal thickness map. The un-calibrated map is sufficient to determine whether there are changes in thickness occurring within an individual over time: however, in order that measurements are comparable cross-sectionally, the effects of the patient's axial length and the refractive error must be accounted for.

The latter two parameters are determined prior to scanning using a built in ultrasound A-scan (axial length), and the spherical focus adjustment necessary to acquire the image (spherical refractive error). A conversion factor is then applied to the un-calibrated data to derive measurements of retinal thickness in micrometers (μm).

The RTA has clinical application in the diagnosis and management of a range of posterior segment abnormalities, particularly those affecting the macula, such as age-related

macula degeneration (Shahidi M. et al. 2002) and diabetic macula oedema (Oshima Y. et al. 1999. Weinberger D. et al. 1998).

The RTA provides a range of comprehensive reports covering the posterior pole. peripapillary and ONH regions. The 'glaucoma complete' protocol analyses the posterior pole. peripapillary retina and ONH regions and is used in the detection and follow-up of OAG. The RTA is able to derive a print-out detailing the rim/cup area map: a colour coded two-dimensional thickness map of the posterior pole and an accompanying deviation probability map: the retinal surface height profile along an operator defined ONH margin contour and indices defining disc area. rim area. cup area. cup volume. rim volume and cup/disc area ratio measurements.

Statistically significant reductions in RTA derived macula thickness ($P<0.05$) in early OAG have been found compared to age-matched normal individuals (Asrani S. et al. 2003. Mori M. et al. 1999. Zeimer R. et al. 1998). The RTA is also able to detect perimacula retinal thinning in corresponding regions of the visual field where the measured sensitivity is beyond the dynamic range of SAP using a size III stimulus (Zeimer R. et al. 1998).

Despite its theoretical advantages. the RTA has failed to receive widespread clinical acceptance. This is principally due to several inherent limitations. Firstly. the accuracy of the RTA measurements is reduced to a greater extent than most other imaging techniques where patients have unclear media and/or a pupil diameter less than 5 mm (Zeimer R. et

al. 1998). Secondly, it is not known how the presence of co-existing maculopathy, such as diabetic maculopathy or age-related macula degeneration, which are also prevalent amongst the glaucomatous population, affects the diagnostic performance of the technique.

Interestingly, no variation in retinal thickness with age is reported with the RTA (Asrani S, et al. 1999, Cvenkel B 2002), which is contrary to observations made using StratusOCT (Alamouti B and Funk J 2003). The most likely explanation for these disparate findings lies in the difference in the axial resolution of the two devices. The axial resolution of the RTA is approximately 5 times that of the StratusOCT, being 50μm and 10μm respectively.

Until the RTA is capable of achieving a level of resolution comparable with other commercially available imaging devices such as the fourth generation of OCT, its application to the early detection of OAG will remain limited.

1.6.5 *Scanning Laser Polarimetry (SLP)*

Scanning laser polarimetery (SLP) is an optical imaging technique for measuring the RNFL thickness (Bagga H and Greenfield DS 2004, Bagga H, et al. 2003, Weinreb RN, et al. 1990). The principal of the technique is similar to CSLO but, instead, uses a longer wavelength laser (780nm) and an integrated polarimeter. The technique utilises the parallel architecture of the axonal tubules of the RNFL and their birefringence properties to measure the amount of retardation of reflected polarised light. Polarised light passing

through the RNFL parallel to the axonal tubules is retarded to a greater extent than polarised light passing through the RNFL perpendicular to the axonal tubules. The net amount of retardation is proportional to the RNFL thickness, whereby approximately 1^{o} of retardation is equivalent to 7.4μm of thickness (Weinreb RN, et al. 1990).

However, the birefringent properties of the eye do not originate solely from the RNFL. The cornea, lens and sclera also produce birefringence and their combined effects must be overcome in order to determine the amount of light retardation that is due to the RNFL (Bowd C, et al. 2003, Greenfield DS, et al. 2000, Greenfield DS, et al. 2003, Weinreb RN, et al. 2002, Weinreb RN, et al. 2003). Early versions of SLP (NFL Analyzer, I and II, GDx and GDx Access [Laser Diagnostic Technology, San Diego, CA]) used a fixed corneal compensation (FCC) factor, derived from median values obtained from a normal population, to correct for anterior segment birefringence. Current versions of SLP, such as the commercially available GDx-VCC (Variable Corneal Compensation) (Carl Zeiss Meditec Inc., Dublin, CA) quantify the amount of anterior segment birefringence compensation (ASBC) prior to determining the RNFL thickness (Weinreb RN, et al. 2002). The ASBC is determined from the axis and magnitude (brightness) of the macula 'bow tie' that appears in the uncompensated SLP image. The 'bow tie' appearance arises from the interaction of the linear birefringence of the anterior segment with the radial birefringence of Henle's RNFL.

The GDx-VCC scan area covers an image field of 40^{o} horizontally and 20^{o} vertically and image are obtained in approximately 0.7 seconds. By virtue of the long wavelength light

(780-798nm) source the procedure is relatively unaffected by mild/moderate media opacity (Hollo G, et al. 1997).

The GDX-VCC printout includes a retardation map of the ONH and peripapillary RNFL and summary statistics of the measured RNFL thickness. The image of the peripapillary retina is superimposed with colour-coded pixels to denote the significance of any reduction in RNFL thickness below an expected level based on the distribution of normal thicknesses contained within the database of the polarimeter. Pixels appear blue if the RNFL thickness falls between a probability for normality of between 2% and 5%; light blue, between 2% and 1%; yellow, between 1.0% and 0.5% and red if the average RNFL thickness is less than the 0.5% prediction limit.

The GDx-VCC also generates six parameters that are based upon segment analysis of the ONH and peripapillary retina nerve fibre layer thickness. The parameter with the highest discriminatory power for OAG is the Nerve Fibre Index (NFI) (AROC 0.89-0.98) (Bowd C, et al. 2001, Medeiros FA, et al. 2004, Reus NJ and Lemij HG 2004, 2004). This parameter represents the output of a support vector machine that has been trained based upon the measurements taken from normal and OAG eyes. The Nerve Fibre Index values range between 0 (normal) and 100 (advanced OAG) and are proportionally related to the stage/severity of OAG. Nerve fibre indicator values between 35 and 44 are considered borderline.

Retinal nerve fibre layer thickness measurements derived by the GDx-VCC exhibit a curvilinear relationship with differential light sensitivity obtained with SAP ($r^2 = 0.640$) (Leung CK, et al. 2005, Reus NJ and Lemij HG 2005). The diagnostic precision of the StratusOCT and GDx-VCC for the detection OAG is approximately equal and generally yield AROCs between 0.85 and 0.94 (Kanamori A, et al. 2006, Leung CK, et al. 2005).

Limitations of GDx-VCC include a reduction in the reliability of RNFL thickness measurements in eyes with large peripapillary atrophic areas and a difficulty in determining ASBC in eyes with moderate to advanced maculopathy and/or a history of corneal refractive surgery (Kook MS, et al. 2002). An alternative algorithm for individual compensation of corneal birefringence, the Enhanced Corneal Compensation (ECC), has been developed for the GDx (Reus NJ, et al. 2006), which appears to exhibit improved diagnostic precision for OAG than the GDx-VCC (Medeiros FA, et al. 2007) although further studies are warranted to confirm this observation.

1.7 Electrophysiology of vision

Electrophysiological assessment of visual function assesses the integrity of specific visual areas and pathways. The clinical appeal of electrophysiology assessment of vision, as with ocular imaging, lies in the objective nature of the procedures. Thus, they are relatively robust to the effects of patient induced variables, such as learning and fatigue. In addition, electrophysiological procedures provide a unique assessment of the electrical and chemical processes underlying vision.

The visual evoked potential (VEP) and electroretinogram (ERG) evaluate the functional integrity of the visual pathway at the level of the visual cortex and retina, respectively. Since the VEP and ERG are typically small (mV), the recording conditions under which these tests are conducted must be carefully standardised and controlled (Marmour MF, et al. 2004, Odom JV, et al. 2004). This ensures that electrophysiological recordings can be more easily replicated and directly compared between institutions.

Several modifications of the standard VEP and ERG techniques have evolved which offer improved spatial resolution of functional abnormality and/or better sensitivity for specific visual pathway damage in OAG, with consequent improved diagnostic precision. These techniques, include the multifocal VEP (mfVEP), pattern electroretinogram (PERG), photopic negative response (PHNR) and the multifocal ERG (mfERG), and are described in further detail in the following sections.

1.7.1 The Visual Evoked Potential (VEP)

The visual evoked potential (VEP) is a small electrical signal that is produced by the primary visual processing area of the Occipital Cortex (V1) in response to a retinal stimulus (Carr RE and Siegel IM 1982). The VEP is typically between 3 and 25μv in magnitude and is embedded within the electroencephalogram (EEG), which is much greater in amplitude (around 100μv). The EEG represents non-specific brain activity that is recorded simultaneously with the VEP. As a result, specialist filtering and amplification procedures are required to separate the VEP from the EEG.

The VEP is recorded using electrodes that are placed in contact with the scalp overlying the visual cortex (Area V1). Specifically, two silver chloride or two gold plated electrodes are positioned above and below each other along the vertical midline of the cranium constitute the active and a reference channels, respectively. This configuration is referred to as a bipolar occipital straddle (BOS). A third channel, or 'ground' electrode, is attached to the centre of the forehead or to an ear lobe.

The VEP can be generated either in response to a Ganzfeld stimulus that is controlled for luminance, presentation rate and/or wavelength, or in response to a patterned stimulus that is controlled for field size, pattern size, contrast, retinal location, presentation rate and wavelength (Odom JV, et al. 2004).

Although the VEP is a mass response from the entire retina it is primarily used as a measure of macula function. This is due to the anatomical arrangement of the visual cortex. The posterior surface of the occipital cortex is responsible for processing information derived from the central retina. Activity within this region is more easily detected by the recording electrodes than activity in the medial aspect of the occipital cortex, deep within the calcarine fissure, that is responsible for processing of information from the peripheral retinal locations. In addition, cortical magnification means that a larger proportion of the visual cortex is responsible for the processing of information derived from the macula than would be expected on the basis of the relative amount of the retina occupied by this region (Duncan RO and Boynton RM 2003). A third reason,

which applies only to patterned stimuli, relates to the fact that only the macula region can resolve high spatial frequency stimuli.

The VEP has traditionally been utilised during the assessment of gross macula function in paediatric and learning-disabled patients by virtue of its non-invasive and objective nature. The VEP has also been applied to a number of diseases including; demyelinating optic neuropathies (Halliday AM, et al. 1972, Nemerow NS and Enns N 1972, Richey ET, et al. 1971) such as optic neuritis, retrobulbar optic neuritis and multiple sclerosis; the investigation of macular disease (Johnson LN, et al. 1986), such as central serous maculopathy, macular holes and macular cysts; and in the investigation of more diffusely occurring optic neuropathies, such as OAG (Kubova Z, et al. 1996-97, Towle VL, et al. 1983). However, the principal limitation of the VEP is the large between-individual variability of the response both in terms of magnitude and waveform. This arises from the physiological variation in cortical anatomy (Steinmetz H, et al. 1989, Stensaas SS, et al. 1972), the magnitude of the EEG, and the thickness and density of bone, skin and fat tissue (Carr RE and Siegel IM 1982).

1.7.2 The Multifocal Visual Evoked Potential (mfVEP)

A major advancement to the VEP technique is the multifocal VEP technique (mfVEP). The mfVEP is a technique that derives multiple and discrete VEPs from localised areas of the retina. The mfVEP occurs in response to a specialised, computer-controlled stimulus that is subdivided into a number of sectors, each of which is responsible for generating a VEP. Each sector contains an array of high contrast black and white checks. The VEP

derived from each sector occurs in response to pattern reversal, as the black and white checks reverse in polarity. The reversal of polarity within each sector is controlled by a computer-driven binary m-sequence, which allows VEPs corresponding to each of the sectors to be recorded simultaneously.

Similar to the VEP, the mfVEP exhibits considerable between-individual variability both in amplitude and in waveform. Consequently, the clinical utility of the procedure has been put under scrutiny (Baseler HA, et al. 1994). However, due to the homogeneity of the mfVEP obtained from the right and left eyes of a normal individual, inter-ocular comparison of mfVEPs is advocated in the uni-ocular and/or asymmetrical conditions including OAG (Hood DC 2000, Hood DC, et al. 2004).

The mfVEP represents a promising objective method for identifying functional deficits in glaucoma (Baseler HA, et al. 1994, Goldberg I, et al. 2002, Graham SL, et al. 2005, Graham SL, et al. 2000, Hasegawa S and Abe H 2001, Hood DC, et al. 2004, Hood DC and Zhang X 2000, Hood DC, et al. 2000, Klistorner AI and Graham SL 2000, Klistorner AI, et al. 1998, Thienprasiddhi P, et al. 2003, Thienprasiddhi P, et al. 2006). Improvements to the technique (see following sections), such as multiple channel recording (Hood DC, et al. 2002, Klistorner AI, et al. 2000), inter-ocular analysis (Graham SL, et al. 2000, Hood DC, et al. 2000) and signal-to-noise amplitude assessment (Klistorner AI and Graham SL 2001, Zhang X, et al. 2002) have helped to increase the clinical utility of the mfVEP.

The mfVEP can accurately discriminate between persons with glaucomatous visual field loss and those with normal vision (Baseler HA, et al. 1994, Goldberg I, et al. 2002, Graham SL, et al. 2005, Graham SL, et al. 2000, Hasegawa S and Abe H 2001, Hood DC, et al. 2004, Hood DC and Zhang X 2000, Hood DC, et al. 2000, Klistorner AI and Graham SL 2000, Klistorner AI, et al. 1998, Thienprasiddhi P, et al. 2003, Thienprasiddhi P, et al. 2006). The mfVEP can identify as abnormal, perimetrically normal areas of the glaucomatous visual field by SAP (Hood DC, et al. 2003, Thienprasiddhi P, et al. 2003), and even in eyes suspected of having OAG with normal visual fields by SAP (Goldberg I, et al. 2002, Graham SL, et al. 2000, Klistorner AI and Graham SL 2000, Thienprasiddhi P, et al. 2006).

The mfVEP stimulus, employed by the clinical 'gold standard' device for measuring the mfVEP, the Visual Evoked Response Imaging System (VERIS, EDI, San Mateo, CA) (Figure 1.4), is a checkerboard style array of checks and is divided into 60 sectors. Each sector contains 16 checks, of which 8 are black and 8 are white (Balachandran C, et al. 2003, Hood DC and Greenstein VC 2003). The luminance of the white checks typically falls between 100-200cd/m^2 and the black checks are typically <1cd/m^2 (Hood DC 2003), depending upon the stimulus delivery system used. The sectors progressively increase in size from the centre to the periphery of the checker-board and are scaled to be approximately equal in their representation in the cortex (Baseler HA, et al. 1994). Modified versions of the stimulus spatial array are available for use with alternative systems, such as the AccuMap (ObjectiVision Pty. Ltd., Sydney, Australia). The typical mfVEP is capable of examining the functional integrity of the central visual field out to

25° eccentricity (Baseler HA, et al. 1994, Goldberg I, et al. 2002, Graham SL, et al. 2005, Graham SL, et al. 2000, Hasegawa S and Abe H 2001, Hood DC, et al. 2004, Hood DC and Zhang X 2000, Hood DC, et al. 2000, Hood DC, et al. 2003, Klistorner AI and Graham SL 2000, Klistorner AI, et al. 1998, Thienprasiddhi P, et al. 2003, Thienprasiddhi P, et al. 2006).

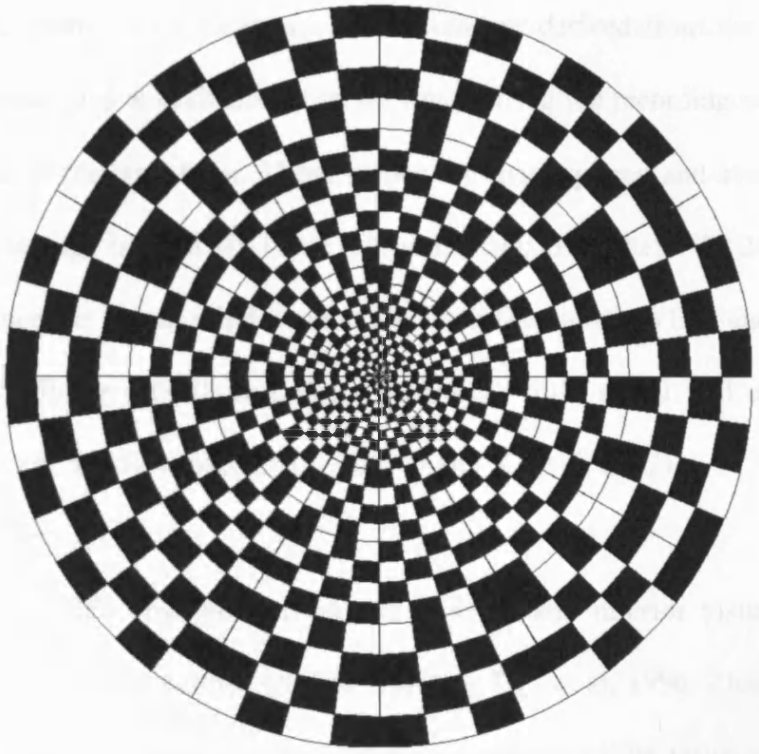

Figure 1.4 - *The typical checkerboard style of the multifocal Visual Evoked Potential (mfVEP) Stimulus.*

A major factor governing the 'quality' of the mfVEP response is the magnitude of the EEG (Klistorner AI and Graham SL 2001). Multifocal VEP recordings must be normalised for the effects of the EEG in order that the mfVEP can be determined. The

established method for this utilises two discrete recording 'windows', of equal duration: one containing the EEG and the mfVEP (signal window) and a second containing only the EEG (noise window) (Hasegawa S and Abe H 2001, Hood DC, et al. 2002, Zhang X, et al. 2002). From these two recordings, the magnitude of the signal window relative to the noise windows is expressed in terms of their root mean squared (RMS) signal-to-noise ratio (SNR). Root mean squared values are a traditional way of representing the magnitude of a waveform. Root mean squared values are derived from the difference between the amplitude (μv) at each time interval (ms) during the recording window and the mean amplitude of the waveform. These values are then squared and averaged. The square root of this average is the RMS value (Hood DC and Greenstein VC 2003, Zhang X, et al. 2002). Since the signal window contains both the signal (VEP) and the noise (EEG), the RMS SNR for mfVEP recordings with very little signal will approach 1, rather than 0 (Hood DC and Greenstein VC 2003, Zhang X, et al. 2002).

In most individuals, VEPs originating from the superior and inferior visual field are opposed in polarity i.e. appear counter-phased (Harding GF, et al. 1996, Zhang X, et al. 2002). This observation is consistent with the known anatomy of the visual cortex (V1) (Clark VP, et al. 1995, Jeffreys DA and Axford JG 1972). Most of area V1 lies within the calcarine fissure, the upper and lower banks of which represent the lower and upper visual field, respectively. The cells in the calcarine fissure generating mfVEP responses are thus oriented in opposite directions and generate dipoles of opposing polarity. The distance of the calcarine fissure varies between 1.5cm below and 3.5cm above the inion (Hood DC and Zhang X 2000). To ensure that the calcarine fissure is below the active

electrode, in a majority of patients the active electrode is mounted between 3 and 4cm above the inion (Hood DC and Zhang X 2000).

The conventional BOS electrode configuration (single vertical midline channel) has a tendency to derive smaller responses in the superior visual field relative to those from the inferior visual field. This is due to the angle between the calcarine sulcus and the reference electrode, which when placed at the inion, favours responses from the upper banks of the calcarine sulcus (lower visual field) (Hood DC and Greenstein VC 2003). One method to overcome this effect is to place the active electrode below the reference electrode (Graham SL, et al. 2000, Klistorner AI and Graham SL 2000, Klistorner AI, et al. 1998); however, mfVEPs recorded in this fashion exhibit only a marginal improvement in superior field response amplitudes in a minority of patients (Hood DC, et al. 2002). In addition, this electrode configuration creates problems associated with attaching the electrodes to the nape of the neck and is contaminated with extra noise from the neck muscles.

The single channel BOS electrode configuration is also limited in its representation of mfVEPs from the lower horizontal region of the visual field (Klistorner AI and Graham SL 2000). At the level of the cortex, this region of the visual field is represented deep within the calcarine fissure at its base. The dipoles in this region of the cortex are generated perpendicular to the vertically oriented BOS electrodes and thus little or no signal is detected (Klistorner AI and Graham SL 2000). The SNR from these regions is improved by utilizing two additional active electrodes, with a common reference, placed

1cm above and 4cm laterally to the Inion on either side (Hood DC, et al. 2002, Klistorner AI and Graham SL 2000). By collating the responses with the greatest SNR from each channel, the visual field is better represented in terms of its true functional capacity (Hood DC, et al. 2002).

The topographical correspondence of area VI with the visual field is symmetrical in the right and left eyes of an individual. Thus, the mfVEP obtained from the right and left eyes in normal individuals are essentially identical (Graham SL, et al. 2000, Hood DC 2000, Hood DC, et al. 2000). This observation, as mentioned earlier, has given rise to inter-ocular mfVEP symmetry analysis as a means of identifying unilateral or asymmetrical visual abnormality (Graham SL, et al. 2000, Hood DC, et al. 2000). One of the drawbacks of this method is the possibility that bilateral damage will not be detected. In other words, defects in the same part of the field in both eyes (e.g., inferotemporal in one eye and inferonasal in the other eye) will not be detected. The mfVEP can be used to detect functional abnormality by comparing the response amplitude, in any given sector, with the statistical confidence interval of the VEP amplitude with the distribution of normal values from the normal population (monocular test) (Goldberg I, et al. 2002, Hood DC 2003, Hood DC, et al. 2003). By combining monocular and interocular methods, the mfVEP exhibits good agreement with SAP in OAG (Goldberg I, et al. 2002, Hood DC and Greenstein VC 2003, Hood DC, et al. 2002, Hood DC, et al. 2004).

The relationship between mfVEP and visual field loss by SAP is difficult to elucidate given that there are clear differences between the techniques. Firstly, mfVEP sectors and

the stimulus locations for Program 30-2 and 24-2, for example, do not correspond spatially. Secondly, the stimulus locations are spaced evenly throughout the visual field, whereas the mfVEP employs a larger proportion of sectors in the regions close to fixation. Finally, there is large variability in the mfVEP RMS SNR even between normal individuals, thus the quantitative relationship with the differential light sensitivity recorded by SAP is difficult to expound especially where RMS SNR is low (Hood DC, et al. 2002).

However, the mfVEP has steadily gained acceptance as an objective method for topographical assessment of visual function in OAG. Multifocal VEP abnormalities have been found in 20% of glaucoma suspects and in 16% of patients with ocular hypertension (Thienprasiddhi P, et al. 2006). In addition, mfVEP abnormalities were found in the non-affected hemifield in 37.5% of eyes (n=16) with glaucomatous SAP abnormality in hemifields, which appeared normal (Thienprasiddhi P, et al. 2003). These observations, combined with the widely accepted consensus that considerable glaucomatous damage occurs prior to visual field loss by SAP supports the use of the mfVEP for the detection of pre-perimetric OAG.

The test-retest variability of the mfVEP has not been widely investigated: One study showed that the between-test variability of mfVEP amplitudes (SD $\pm$1.63-4.3dB) was less than of the between-test variability for SAP (SD $\pm$2.4-8.9dB) in normal individuals (Fortune B, et al. 2006). However, in OAG the mfVEP amplitude exhibits greater variability (SD $\pm$ 13.39dB) than for SAP (SD $\pm$ 9.88dB) (Chen CS, et al. 2003, Fortune B, et al. 2006). Two important factors, which affect the test-retest variability of the

mfVEP are the SNR (Fortune B. et al. 2006) and location of the mfVEP within the visual field. The improvement of SNR over repeated visits is also postulated (Bjerre A. et al. 2004). The precision in repositioning the recording electrodes from one examination to the next will also play a major role in the between-test variability of the mfVEP technique. In addition, it is almost impossible to re-position the recording electrodes on the same person at exactly the same locations on two separate occasions, especially where two different technicians/clinicians conduct the examinations.

Since inter-ocular comparison of mfVEPs is the standard method to detect glaucomatous functional abnormality, it is important to understand how the relationship between the ratio of signal amplitudes from the right and left eyes changes over time. This characteristic of the mfVEP technique has yet to be determined. Standardisation of test procedures will be an important step in optimising the quality/SNR of mfVEP recordings and reducing test-retest variability.

Studies are required to determine the full clinical utility of the mfVEP technique in the identification of progressive functional damage in OAG.

1.7.3 The Electroretinogram (ERG)

The electroretinogram (ERG) is an examination used to assess the functional integrity both of neuronal and non-neuronal components of the retina. The ERG represents the light-evoked changes to the electrical and chemical gradients within the retina that occur following phototransduction.

Published guidelines classify the standard ERG into 5 subtypes (Marmour MF, et al. 2004): the rod ERG, the standard combined ERG, the oscillatory potentials, the single-flash cone ERG and the 30Hz flicker ERG.

The precise waveform for each ERG subtype is governed by a number of parameters (Marmour MF, et al. 2004). For example, the rod ERG, standard combined ERG and the oscillatory potentials are evoked under scotopic conditions from the dark-adapted retina. Conversely, the single-flash cone ERG and the 30Hz flicker ERG are evoked under photopic conditions from the light adapted retina. With the exception of the oscillatory potentials and the 30Hz flicker ERG, the ERG consists of two principal components, namely the a- and b- waves. The retinal origins of these waves have been widely investigated (Friedburg C, et al. 2004, Friedburg C, et al. 2001, Paupoo AA, et al. 2000, Rager G 1979). The a-wave is a small deflection in the ERG waveform and has a latency of around 25ms (Marmour MF, et al. 2004). The a-wave represents photoreceptoral activity and occurs due to the photoreceptor outer segments becoming hyperpolarised as sodium ions enter the cells during phototransduction. In accordance with the published International Society for Clinical Electrophysiology of Vision (ISCEV) guidelines, an ERG a-wave can be obtained that is representative of rod cell activity (rod ERG), cone cell (single flash 'cone ERG') activity, or both (standard combined ERG) (Marmour MF, et al. 2004).

The ERG b-wave is a large positive deflection in the waveform that occurs immediately after the a-wave. The b-wave arises from light-induced changes to the photoreceptors, and the subsequent reduction in neurotransmitter release at their synaptic terminals. This results in an increase in extra-cellular potassium levels in the outer-plexiform layers causing depolarisation of the Muller cells and a transretinal current that is responsible for the b-wave (Newman EA and Odette LL 1984).

The ISCEV standard ERGs are dominated by activity in the outer retinal layers. Since the ERG has limited representation of inner retinal function, their application in OAG is limited; however, several specialised ERGs are described in the literature that are believed to represent inner retinal function, specifically retinal ganglion cells. A number of these specialised ERGs, namely the pattern ERG (PERG) and the photopic negative response (PHNR) have been suggested to be of use for the detection of OAG and are described in the following sections.

1.7.4 The Pattern Electroretinogram (PERG)

The pattern electroretinogram (PERG) evaluates the activity in the retina that is induced when an achromatic chequered stimulus reverses in contrast (Berninger T and Schuurmans RP 1985). The PERG stimulus has equal numbers of light and dark checks, which enables the total luminous flux entering the eye to be kept constant. The PERG is not a response to the pattern element of the stimulus, per se, but rather the local increase or decrease in retinal luminance that occurs when the stimulus polarity reverses. For this

reason, intra-ocular light scatter must be minimised during the procedure (Bach M and Mathieu M 2004).

The PERG is characterised by a prominent positive deflection known as P1, or, P-50, which occurs approximately 50ms after polarity reversal. The P1/P-50 is followed by a negative deflection known as N1, or, N-95 which occurs approximately 95ms after polarity reversal (Berninger T and Schuurmans RP 1985). The PERG is believed to have an inner-retinal source since it is diminished in primate retinas following intravitreal injection of tetrodotoxin (TTX) (a selective blocker of inner retinal spiking activity) (Viswanathan S, et al. 2000); in laser induced OAG (Viswanathan S, et al. 2000); and in primate and cat retinas following optic nerve transection (Maffei L and Fiorentini A 1981). In human retina, the N-95 is diminished in OAG (Harrison JM, et al. 1987, Kirkham TH and Coupland SG 1983, Trick GL and Wintermeyer DH 1982) whilst the P-50 remains relatively unaffected (Porrello G and Falsini B 1999, Toffoli G, et al. 2002, Wanger P and Persson HE 1987). The N-95 also exhibits a contrast dependency and spatial tuning; thus a retinal ganglion cell origin is widely accepted (Bach M 2001, Berninger T and Schuurmans RP 1985, Holder GE 2001, 1987, Schuurmans RP and Berninger T 1985, Thompson DA and Drasdo N 1987, Viswanathan S, et al. 2000). The PERG has demonstrated clinically useful levels of diagnostic precision in correctly identifying OAG (sensitivity and specificity of 92%) (Bayer AU, et al. 2002). PERG abnormalities have also been found in patients with OHT who later develop OAG (Bach M, et al. 1998, Panagachis E and Moschos M 1998, Pfeifer N, et al. 1993, Ruben ST, et al. 2004). Despite these findings, the PERG will not replace current clinical examinations

for the identification of OAG due to the inherently high between-test variability (up to between 30% and 67% of the mean value) (Holopigian K, et al. 1988). The very small magnitude of the PERG also necessitates experienced specialist technicians to derive an adequate SNR for clinical use.

1.7.5 The Photopic Negative Response (PhNR)

The photopic negative response is recorded under specialised conditions and is a slow negative potential following the ERG b-wave. The retinal generators of this component of the ERG are believed to be the retinal ganglion cells (Bui BV and Fortune B 2004, Gotoh Y, et al. 2004, Viswanathan S, et al. 2001). The PhNR is discernable in the conventional achromatic ERG (Colotto A, et al. 2000, Viswanathan S, et al. 2001); however, a much greater amplitude occurs in response to chromatic stimuli (Drasdo N, et al. 2001, Fortune B, et al. 2004). The short wavelength sensitive cone (S-cone) PhNR is derived in response to short duration, blue light (that stimulates S-cone activity) presented on a red background (to suppress long- and medium-wavelength cone activity, respectively) and yields clinically useful levels of diagnostic precision in OAG (AROC 0.86) (Drasdo N, et al. 2001).

The PhNR is believed to arise from the increase in extracellular potassium ions from glial cells in the proximal retina that occurs as a direct result of retinal ganglion cell spiking activity in the inner retina (Viswanathan S, et al. 2000). Thus, either damage to the inner retina or to the glial cells is capable of attenuating the response (Viswanathan S, et al. 2000). In primate models of OAG, damage both to retinal ganglion cells and to glial cells

is hypothesised as the histopathology responsible for reduced PhNR amplitudes (Viswanathan S. et al. 2000).

Both in experimental OAG models and in pharmacological dissection studies using TTX in primates, attenuation of the PhNR occurs in the presence of the relative preservation of a- and b-wave amplitudes (Fortune B. et al. 2004, Viswanathan S. et al. 2000, Viswanathan S. et al. 1999). Thus in primates, at least, the PhNR appears to solely reflect spiking activity of the retinal ganglion cells and their axons. In humans, the time course of the PhNR is reminiscent of the N95 component of the PERG that is reduced in inner retinal dysfunction (Holder GE 1987) and suggests that the two responses share a common retinal origin. Thus, the PhNR is a viable technique for the identification of retinal ganglion cell dysfunction in OAG. In comparison with the PERG, the PhNR has the practical advantages that neither refractive correction nor exact foveal positioning is required to obtain useful responses. Furthermore, the PhNR is affected to a lesser extent by the presence of media opacity and yields an overall larger response than the PERG. However, the PhNR technique is neither new nor has it replaced SAP. This is largely due to the need for trained expert technicians to carry out the procedure in addition to a lack of understanding amongst clinicians of the precise retinal origin of the response in humans.

1.7.6 The Multifocal Electroretinogram (mfERG)

The multifocal ERG (mfERG) permits topographical assessment of retinal function (Bearse MA and Sutter E 1996, Sutter E and Tran D 1992, Sutter EE 2001). The mfERG is an adaptation of the full field ERG and is analogous to the mfVEP in its method of stimulus delivery and response extraction. Several institutions have derived mfERG responses using custom devices; however, several instruments, including the Visual Evoked Response Imaging System (VERIS, EDI, San Mateo, CA) and the Retiscan (Roland Instruments, Germany), are commercially available.

The guidelines for basic mfERG recording recommend the use of a stimulus that consists of an array of alternating black and white hexagonal elements (Marmour MF, et al. 2003) (Figure 1.5). The number of hexagonal elements can be varied (typically either 37, 61 or 103 elements are employed) to control the spatial resolution of the procedure. However, an increase in the spatial resolution of the stimulus reduces the SNR of each mfERG response.

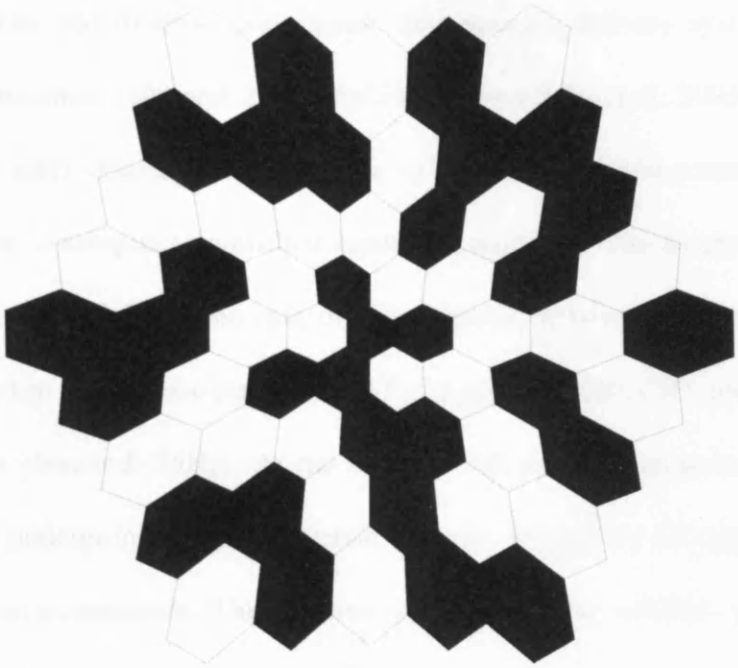

Figure 1.5 - *The typical multifocal Electroretinogram (mfERG) stimulus.*

Achieving accurate recordings at high spatial resolution requires excellent SNR and equally good fixation stability by the patient. Several studies have derived adequate SNR both using 241 (Heinemann-Vernaleken B, et al. 2001, Sutter E and Tran D 1992) and 509 (Poloschek CM and Sutter EE 2002) stimulus elements; however, these protocols required recording times of up to 1 hour, which is unreasonable for clinical use.

The hexagonal elements of the mfERG stimulus increase in size from the centre to the peripheral visual field in order that they elicit approximately equal size mfERG responses in individuals with normal retinal function (Sutter E and Tran D 1992).

As with the conventional ERG, the mfERG is recorded using a corneal electrode and the same amplification and filtering procedures. The stimulus delivery system is typically either a high-luminance (100 and 200 cd/m^2) (Marmour MF, et al. 2003) CRT or LCD monitor, or an LED device. The sequence of stimulus element contrast reversal is predetermined by a computer controlled binary m-sequence. The frequency of contrast reversal is governed by the frame rate of the stimulus delivery and occurs at constant intervals referred to as the base period (bp). For a typical 75Hz CRT monitor, the bp is equal to 13.3ms (1second /75Hz). At the end of each bp, each stimulus element has a 50% chance of undergoing contrast reversal and the probability of contrast reversal is governed by the m-sequence. Under these conditions, the mfERG waveform bears superficial resemblance to the conventional photopic flash ERG waveform; however, residual differences arise from the more rapid rate of contrast reversal for the mfERG and the way in which the responses are extracted (Hood DC 2003, Hood DC, et al. 2002).

In its standard form, the first order mfERG (Figure 1.6) is not considered to provide any information about inner retinal and/or retinal ganglion cell function (Hood DC, et al. 2002). However, under non-standard recording and filtering conditions the mfERG can be used to identify inner retinal abnormality (Bearse MA, et al. 1995, Fortune B, et al. 2002, Hood DC, et al. 2001, Hood DC, et al. 2002, Klistorner AI and Graham SL 2000, Sutter EE and Bearse MA 1999).

The first description of a 'pure' retinal ganglion cell component of the human mfERG was described over a decade ago (Bearse MA, et al. 1995) and originated within the first slice of the second order response kernel (K2.1) (Figure 1.7). The K2.1 response was decomposed into two principal components: the optic nerve head component (ONHC) and the retinal component (RC) (Bearse MA, et al. 1995). The latency of the ONHC exhibits nasal-temporal asymmetry whereby the latency of the waveform increases as a function of the distance between the site of focal stimulation and the ONH. Since the conduction velocity of action potentials along unmyelinated retinal nerve fibres is slower than for myelinated nerve fibres, the response has been attributed to a signal source near to the ONH (Bearse MA, et al. 1995, Sutter EE and Bearse MA 1999). The ONHC is also exhibited by monkey retina (Hood DC, et al. 2001); however, the response is diminished in monkey retinas exposed to TTX (Hood DC, et al. 1999) and to NMDA (Hare WA, et al. 2001). This observation supports the notion that the ONHC has an inner retinal origin in human (Fortune B, et al. 2002).

The magnitude of the ONHC is enhanced by reducing the stimulus contrast to 50% (Hood DC, et al. 1999); by using DTL recording electrodes (Hood DC, et al. 2002); by employing an *in situ* DTL reference electrode in the contralateral eye (Hood DC, et al. 2001, Sutter EE and Bearse MA 1999); and interleaving blank frames between contrast reversals (Fortune B, et al. 2002). When combined, these considerations for optimal ONHC recording will help to define a standard protocol for recording the ONHC. However, further research as to the precise origin of the ONHC and ways to extract the response is needed before the technique can be considered for clinical use.

Non-linearity and m-sequences

The human visual system is described as a 'non-linear' system since chemical and electrical activity within the retina at any time point is governed by preceding events. Thus, the influences of visual events occurring prior to an ERG stimulus, for example, have the power to alter the ERG waveform provided that the event occurs within a finite time period (memory) to the stimulus. In a linear system the memory is equal to the duration of the response. However, in non-linear visual system, visual activity can have a considerable effect on subsequent activity if it falls within the memory of the visual system.

The rate of contrast reversal of the mfERG stimulus is sufficiently slow for the retina to register each contrast reversal as a discrete event; however, the individual responses to successive contrast reversals overlap. The effects of preceding stimuli on the mfERG are expressed in a 'kernel series' for each stimulus element. By analysing mfERGs that occur after preceding stimuli, the properties of non-linear systems, such as adaptive mechanisms, can be assessed. The kernels series derived by the mfERG technique permit topographical mapping of non-linear response properties across the central retina. Higher order kernels represent increasingly more complex interactions between events occurring at each bp interval. An in-depth description of higher order kernel response derivation is beyond the scope of this review; however, a comprehensive review is provided by Sutter (Sutter EE 2000).

The first order kernel of the mfERG represents the average retinal response to a focal flash (the mean difference between a response to a light and dark stimulus event). In a similar way, the second order response reflects the mean difference between responses to a flash, which is preceded by a bright stimulus event, and a flash that is preceded by a dark stimulus event (Figure 1.7). This pattern of data analysis continues for still higher response kernels.

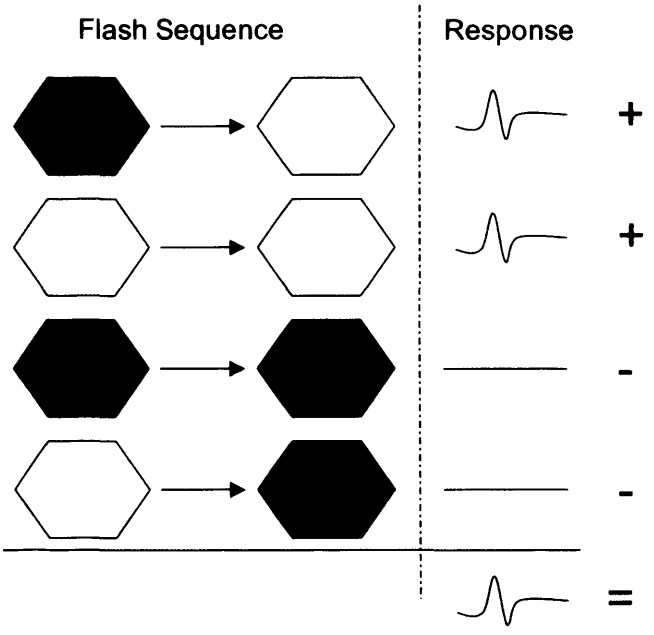

Figure 1.6 – *The derivation of the first order response (K1) based on a CRT stimulus projection system.*

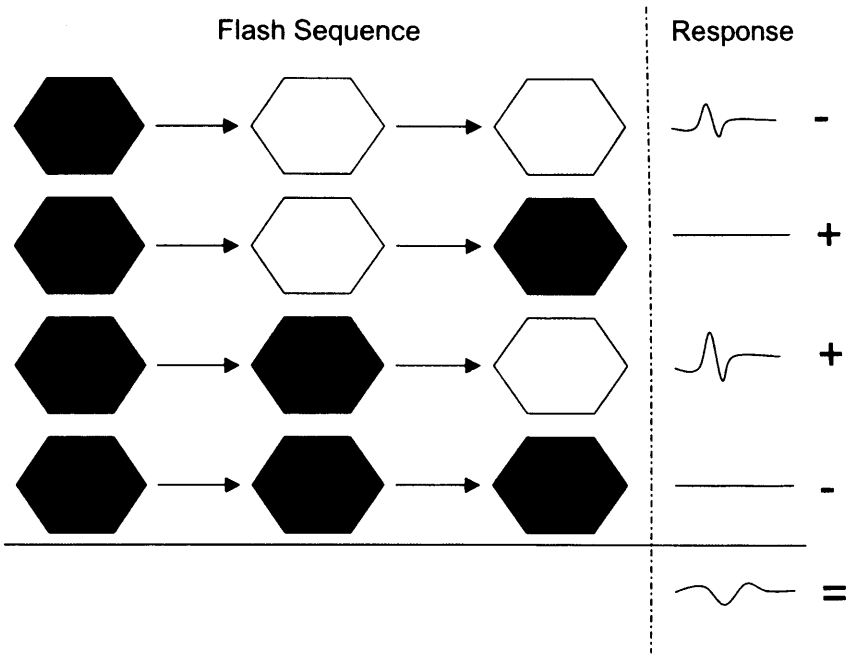

Figure 1.7 – *The derivation of the first slice of the second order response (K2.1) based on a CRT stimulus projection system.*

The rapid rate, at which the mfERG stimulus reverses in contrast, combined with its high luminance, produces a response that is principally mediated by the cones. The first order mfERG response typically exhibits an initial negative trough (N1) proceeded by a positive peak (P1) and a final negative trough (N2). The N1, P1 and N2 components of the first order mfERG bear a superficial resemblance to the a-wave, b-wave and PhNR, respectively, of the photopic flash ERG. However, since the stimulus and analysis conditions under which the two responses are derived are different, in addition to the fact that the mfERG is a mathematical extraction and not a measured electrical potential, the

waveforms are not described using the same nomenclature (Marmour MF, et al. 2003). Slowing down the rate of stimulus presentation such that at least 7bp intervals (106ms) are interleaved between contrast reversals (the average separation being 212ms) further enhances the likeness of the mfERG and flash ERG waveforms (Hood DC, et al. 1999). Thus, the two waveforms are likely to share the same retinal source generators.

1.7.7 The Multifocal Pattern Electroretinogram (mfPERG)

The diagnostic ability of the standard PERG for the detection of glaucomatous abnormality has prompted the development of its multifocal PERG counterpart (mfPERG) (Klistorner AI, et al. 2000, Steifelmeyer S, et al. 2004). In OAG, the mfPERG is attenuated (Klistorner AI, et al. 2000, Steifelmeyer S, et al. 2004) with little/no effect on the latency of the response (Berninger T and Schuurmans RP 1985), unlike the standard PERG: However, the location of the mfPERG abnormality exhibits poor topographical correspondence with the location of the field loss deemed by SAP (Klistorner AI, et al. 2000, Steifelmeyer S, et al. 2004). In OAG, the mfPERG responses corresponding to the central visual field are affected to a greater extent than those from more peripheral areas, irrespective of the location of the field loss (Klistorner AI, et al. 2000, Steifelmeyer S, et al. 2004). This observation raises the possibility that inner retinal damage in OAG may be more widespread and more uniform than SAP suggests and also that examinations directed at the macula may be useful in detecting OAG (Greenfield DS, et al. 2003, Guedes V, et al. 2003).

Despite the lack of topographical agreement between mfPERG abnormality and visual field loss by SAP, the best predictive parameter of the mfPERG, the amplitude difference between P-50 and N-95, exhibits moderate to good sensitivity (88%) and specificity (77%) for the detection of OAG (Klistorner AI, et al. 2000). The AROC for the mfPERG is also marginally better than the standard PERG, being 0.86 (Steifelmeyer S, et al. 2004) and 0.78 (Bayer AU, et al. 2002), respectively.

The clinically useful levels of diagnostic precision exhibited by the mfPERG suggest that the technique is clinically useful in discriminating patients with OAG from normal individuals. However, recording of the mfPERG necessitates lengthy testing times and excellent acuity and accurate fixation (Klistorner AI, et al. 2000, Steifelmeyer S, et al. 2004) and renders the technique unsuitable for the typical OAG population. In addition, the lack of topographical correspondence between mfPERG and SAP abnormalities raises the question whether in fact the two techniques are assessing two different pathological processes. Thus mfPERG technique is not considered to offer improvement over current methods used in clinical management of OAG.

1.8 Psychophysical approaches to OAG detection

1.8.1 The Humphrey Field Analyzer (HFA)

The Humphrey Field Analyzer II (Carl Zeiss Meditec Inc., Dublin, CA) is the current 'gold standard' perimeter for SAP. The HFA employs predefined, computer-controlled examination strategies to rapidly evaluate the differential light sensitivity at a number of pre-defined locations throughout the visual field. By employing standardised recording conditions, the HFA permits better and faster control of the stimulus presentation than with the previous 'gold standard', the Goldmann Perimeter, and reduces the between-test variability that arises between different operators (Flammer J, et al. 1983).

The HFA offers a variety of screening and threshold stimulus programs that meet most clinical needs. Screening tests provide an important clinical function by quickly surveying the visual field for areas that are highly suspect. Areas flagged as abnormal during a screening test warrant re-examination using a threshold strategy. Threshold tests more precisely define the sensitivity of the visual field by calculating the differential light sensitivity at each test location.

As with all psychophysical procedures involving the detection of a 'signal' embedded in 'noise', the HFA exhibits high within- and between-test variability, referred to as short- and long-term variability, respectively (Bebie H, et al. 1976, Flammer J, et al. 1984, Flammer J, et al. 1984, 1983).

The outcome of any given single visual field examination is influenced by many factors including pupil diameter (Blumenthal EZ, et al. 2003, Wood JM, et al. 1988), refractive error (Goldstick BJ and Weinreb RN 1987, Heuer DK, et al. 1987), media opacities (Dengler-Harles M, et al. 1990, Guthauser U and Flammer J 1988, Wood JM, et al. 1988), patient learning (Heijl A, et al. 1989, Wild JM, et al. 1989), patient fatigue (Bjerre A, et al. 2004, Blumenthal EZ, et al. 2003, Gonzalez de la Rosa M and Pajera A 1997, Schmiti RB, et al. 2002, Spry PGD, et al. 2001) and random variations in the physiological status of the patient (Anderson DR 1992). In addition, the long- and short-term variability of a visual field outcome is influenced by factors including the severity of the disease (Bengtsson B 2000, Chauhan BC, et al. 1993), the eccentricity of the test location (Heijl A, et al. 1987), the age of the patient (Heijl A, et al. 1988) and the fixation stability (Henson DB, et al. 1996).

Unless the effects of these factors are minimised, they can mask or mimic either visual field loss in a single examination or, 'true' deterioration between successive examinations. The major factor governing the short-term fluctuation (STF) is fatigue arising from protraction of the examination duration. The HFA is able to minimize the duration of SAP examination, and reduce the effect of the STF, by employing either the Swedish Interactive Thresholding Algorithm (SITA) Standard or the SITA Fast examination protocols. Both SITA Standard and SITA Fast algorithms are effective methods to reduce the duration of SAP without loss of sensitivity or specificity for the detection of glaucomatous visual field loss (Artes PH, et al. 2002, Bengtsson B, et al. 1997, Bjerre A, et al. 2004, Budenz DL, et al. 2002, Wild JM, et al. 1999). The HFA

statistical software, STATPAC, provides statistical analysis of the measured differential light sensitivity in a summary print-out that details the visual field indices: Mean Deviation (MD), Pattern Standard Deviation (PSD) and Corrected Pattern Standard Deviation (CPSD), Total Deviation (TD), Pattern Deviation (PD) as well as deriving indices for the quality of examination (e.g. fixation stability, and false-positive and false–negative catch trial rates) (Wild JM 1988).

The TD index represents the difference between the observed differential light sensitivity and the expected value in an age-matched normal individual. The PD index represents the difference between the observed differential light sensitivity and the expected value adjusted for the general height of the visual field. The general height is determined from the relative depression of the 15^{th} percentile of the TD values. By correcting for diffuse changes to the visual field in this way, PD analyses seek to separate visual field loss that is due to OAG from that which is due to cataract. On the HFA printout, both the TD and PD indices are plotted at points corresponding to the HFA stimulus locations. Total and Pattern Deviation values that fall between the 5% and 2%, the 2% and 1%, the 1.0% and 0.5%, and below the 0.5% prediction limit based upon values expected from a normal population are highlighted using an grey scale, which increases in density as the prediction limit cut-off reduces.

However, the subjective nature of SAP, which confers the greatest source of within- and between-variability (Blumenthal EZ, et al. 2003, Spry PGD, et al. 2001), is the major limitation of the technique. The magnitude of the patient-attributed variability is such that

SAP is rarely, if ever, interpreted in isolation and without careful consideration of the appearance of the fundus.

1.8.2 Non-conventional evaluation of visual function in OAG

The consensus that considerable retinal ganglion cell death occurs prior to the onset of detectable functional deficit by conventional SAP (Harwerth RS, et al. 2004, Kerrigan-Baumrind LA, et al. 2000, Quigley HA, et al. 1982) has prompted the development of alternative psychophysical tests that are designed to exploit the functional deficit specific to OAG. These tests employ specialised stimuli that assess the functional integrity sub-channels within the visual pathway.

1.8.3 Frequency-Doubling Technology (FDT) perimetry

Frequency doubling technology (FDT) perimetry is a specialised visual field examination that is designed to detect functional damage specific to OAG (Johnson CA and Samuels SJ 1997). The technique is based upon the frequency doubling illusion phenomenon (Kelly DH 1981) that is created when a low spatial frequency (<1cyc/deg) sinusoidal grating undergoes counterphase flicker at a high temporal frequency (>15Hz). Under these conditions the grating appears to be twice the actual spatial frequency (Kelly DH 1981). Early studies hypothesised that the frequency doubling phenomenon was mediated by a particular sub-set of cells within the magnocellular pathway, namely the M_y cells (Maddess T and Henry GH 1992). Some authors estimate that M_y cells constitute between 3% and 5% of all retinal ganglion cells (Kaplan E and Shapley RM 1982), whilst

others have questioned whether they exist at all (Anderson AJ and Johnson CA 2002, White AJ, et al. 2002) and have postulated that, at contrast threshold, all magnocellular cells are likely to be responsible for the frequency doubling phenomenon (Anderson AJ and Johnson CA 2002).

The current FDT perimeter, the Humphrey Matrix (Humphrey Systems, Dublin, CA and Welch Allyn, Skaneateles, NY) utilises a number of examination protocols, namely the C-20 (four 10 x 10° stimuli per quadrant plus a 5° diameter central stimulus), N-30 (four 10 x 10° stimuli per quadrant plus a 5° diameter central stimulus, plus two additional stimuli above and below the nasal horizontal midline at 20-30° eccentricity) (Johnson CA and Samuels SJ 1997) and four test patterns analogous to Program 30-2 (69 stimuli), 24-2 (55 stimuli), 10-2 (44 stimuli) and macula (16 stimuli) tests of the HFA which utilize 5° x 5° stimuli to improve the spatial resolution of the technique. By utilizing smaller stimuli, the shape characterisation of visual field defects is improved (Johnson CA, et al. 1999). The Humphrey Matrix software derives summary analyses including the Glaucoma Hemifield Test and serial test overview analyses that facilitate evaluation of the data.

The contrast threshold is measured using a maximum likelihood threshold strategy, ZEST (zippy estimation of sequential thresholds) (King-Smith PE, et al. 1994) and is defined as the minimum contrast at which the frequency-doubling phenomenon is perceived. The ZEST strategy employs a fixed number of presentations at each location and a flat prior probability density function (PDF) to effectively minimize the test duration (Turpin A, et al. 2002, 2002).

Although FDT perimetry is named after the frequency-doubling phenomenon the thresholds measured are in fact contrast detection thresholds, since no direct measure of the presence or absence of frequency-doubling is made. It is thus difficult to ascertain what percept patients respond to when performing the test. The original suggestion was that the percept of frequency-doubling did exist at contrast detection threshold (Kelly DH 1966); however, others propose that at contrast threshold the sinusoidal grating may appear close to its actual spatial frequency (Parker A 1983) or, merely as a zone of amorphous flicker (Kulikowski JJ 1975, Maddess T and Henry GH 1992, McKendrick AM, et al. 2003, Richards W and Felton TB 1973). The importance of correct patient instruction prior to commencing the examination (Maddess T and Henry GH 1992, McKendrick AM, et al. 2003, Parker A 1983) has undermined the validity of the FDT perimetry normative database (Anderson AJ, et al. 2005). The effect of whether the measured thresholds arise either from detection (critical flicker frequency) or resolution (spatial frequency recognition) of the stimulus, on the diagnostic precision of FDT for the detection of OAG is unknown. However, differences between the detection and resolution thresholds of up to 6dB have been reported (Bosworth CF, et al. 1998, Flood T and Flanagan JG 1998, McKendrick AM, et al. 2003).

Frequency doubling technology perimetry is robust to the effects of optical defocus (Anderson AJ and Johnson CA 2003). Humphrey Matrix Pattern Deviation indices, analogous to the PD index of the HFA, is an effective way to separate change caused by glaucoma from that caused by cataract (Kook MS, et al. 2004). A prerequisite for any

perimetric technique is a short, small and predictable learning curve such that 'true' baseline examinations are offset minimally. The FDT perimetry learning effect is well documented (Fujimoto N, et al. 2002, Horani A, et al. 2002, Iester M, et al. 2000, Matsuo H, et al. 2002) and its magnitude is dependent upon patients' prior experience with SAP (Fujimoto N, et al. 2002, Horani A, et al. 2002).

In patients with perimetric or pre-perimetric OAG, FDT perimetry exhibits moderate to good levels of diagnostic precision with AROCs of 0.93 (Brusini P, et al. 2006), 0.79 (Sample PA, et al. 2006) and 0.75 (Brusini P, et al. 2006). In addition, visual field loss recorded by frequency doubling technology perimetry is a positive predictive factor for the subsequent development of corresponding SAP loss (Boden C, et al. 2005, Cello KE, et al. 2000, Kalaboukhova L and Lindblom B 2003, Maddess T, et al. 1999, Medeiros F, et al. 2004).

The Humphrey Matrix Program 24-2 performs similar to HFA Program 24-2 SITA Fast algorithm both in terms of the reliability of the tests (i.e. the number of: fixation losses and abnormal responses to the false-positive and false-negative catch trials) and the duration of the test (median durations are 316 seconds and 309 seconds for FDT and SITA Fast, respectively) (Spry PGD, et al. 2005). However, the STF and LTF of FDT perimetry are less influenced by disease severity and the eccentricity of the stimulus than for SAP (Chauhan BC and Johnson CA 1999, Spry PGD, et al. 2001). Thus, FDT perimetry is suggested to be a better means of identifying progressive functional damage than SAP (Chauhan BC and Johnson CA 1999, Spry PGD, et al. 2001). Indeed, FDT

perimetry can identify progressive functional damage by approximately 12 months before SAP (Bayer AU and Erb C 2002, Haymes SA, et al. 2005), although supplementary longitudinal data is necessary to determine the validity of these findings.

Despite their relative merits, neither the first-generation FDT perimeter nor the current version, the Humphrey Matrix, has successfully replaced SAP in the routine clinical management of OAG. Further studies are warranted to determine the cross-sectional and longitudinal relationship between functional damage differentiated by FDT perimetry in OAG and the corresponding structural damage. However, the principal limitations of FDT perimetry are: the uncertainty of the precise derivation of the measured threshold values and lack of understanding of the retinal mechanisms/pathways exploited by the technique.

1.8.4 *Short-wavelength Automated Perimetry (SWAP)*

Short wavelength automated perimetry (SWAP) is a perimetric technique for evaluating the functional integrity of the short-wavelength sensitive pathway comprising short-wavelength sensitive cone cells (S-cones), S-cone bipolar cells and blue-yellow retinal ganglion cell (Adams AJ, et al. 1982, Dacey D and Lee B 1994). The technique measures detection thresholds for a Goldman size V narrow bandwidth blue stimulus (440nm) presented against a bright ($100cd/m^2$), broad bandwidth yellow background (Sample PA and Weinreb RN 1990). The processing of the blue stimulus in SWAP is believed to be mediated by small bistratified ganglion cells (Dacey D 1993, Dacey D and Lee B 1994). Despite being referred to as 'small' bistratified cells, their dendritic field size is

approximately 50% larger than those retinal ganglion cells serving the medium- and long-wavelength sensitive cone cells (M- and L-cones, respectively). The bright yellow background employed by SWAP is used to suppress the rod cells and the M- and L-cone cells during the examination. Small bistratified ganglion cells have large dendritic field size and sparse neural representation (Glovinsky Y, et al. 1991), which may make the functional consequences of their loss in OAG, more apparent than most other retinal ganglion cells.

Short-wavelength automated perimetry is commercially available for use with HFA 740 and 750 instruments (Carl Zeiss, Meditec, Dublin, CA) and the Octopus 101, 301 and 311 instruments (Interzeag AC, Schlieren, Switzerland). With the exception of the stimulus colour, background colour and duration of the stimulus presentation (200ms) all other aspects of examination are as for SAP. The HFA SWAP yields a dynamic range of approximately 24dB, increasing to approximately 29 dB for SITA versions (Bengtsson B 2003) and has approximately 13dB of isolation before the next most sensitive retinal mechanism is capable of detecting the SWAP stimulus (Sample PA, et al. 1996). The dynamic range and degree of isolation (18dB) is slightly better for the Octopus perimeter (Wild JM 2001).

The hill of vision for SWAP, in normal eyes, is generally steeper than that obtained by SAP. In addition, the hill of vision for SWAP in the superior field is generally steeper than that of the inferior field. The age-related decline in SWAP is approximately 2.2dB/decade, which is up to approximately twice that of the age-related decline by SAP

(approximately 1.2dB/decade) (Gardiner SK, et al. 2006, Johnson C and Marshall D 1995, Wild JM, et al. 1998); however, this difference is reduced to only 0.5dB when the differential light sensitivity thresholds are corrected for the effect of ocular media absorption (Johnson CA, et al. 1995).

The STF for SWAP is larger than for W-W perimetry; estimates for STF using the commercially available SWAP vary between approximately 17% (Wild JM, et al. 1998) and approximately 55% (Kwon YH, et al. 1998). The STF is greater for patients with glaucoma than with ocular hypertension (Wild JM, et al. 1995).

The LF is greater for SWAP compared to W-W perimetry in normal individuals and in patients with glaucoma. In patients with OAG, the LF at each stimulus location was greater by about 0.50 dB than that for W-W perimetry (Gardiner SK, et al. 2006, Wild JM, et al. 1995) especially in peripheral stimulus locations (Gardiner SK, et al. 2006). In clinical terms, the increased STF and the LTF, for SWAP relative to W-W perimetry means that the identification of progressive visual field loss for SWAP between any two given examinations will generally be more difficult to identify than that for W-W perimetry.

Short wavelength automated perimetry is affected to a greater extent by pre-retinal light absorption than SAP (Sample PA, et al. 1988). As a result, differences in lens yellowing, light scatter and macular pigmentation between individuals produces wider confidence limits for normality for SWAP compared to SAP (Wild JM, et al. 1998, Wild JM and

Hudson C 1995). Pattern Deviation Analysis by SWAPPAC effectively reduces the adverse influence of media opacity: however, the between-individual variability remains greater for SWAP than for SAP.

Despite these limitations, SWAP offers several distinct clinical advantages over SAP. Short-wavelength automated perimetry defects are generally larger/deeper than those identified by SAP, and have a greater rate of progressive damage (Johnson CA, et al. 1995) Short-wavelength automated perimetry is more sensitive than SAP for the detection of early glaucomatous visual field loss (Demirel S and Johnson CA 2001, Johnson CA, et al. 1993, Sample PA 2000, Spry PGD, et al. 2005) and generally precede those identified by SAP by as much as 5 years (Demirel S and Johnson CA 2001, Johnson CA, et al. 1993, Sample PA 2000, Spry PGD, et al. 2005). In addition, SWAP exhibits better sensitivity for identifying patients with progressive disc cupping than SAP (72.7% and 59.1%, respectively) (Girkin CA, et al. 2000) and SWAP visual field defects are more prevalent, prominent and persistent than those of SAP abnormalities in OAG (Demirel S and Johnson CA 2001, Reus NJ, et al. 2005). As would be expected, SWAP visual field defects correlate well with glaucomatous NRR abnormalities (Larrosa JM, et al. 2000, Mistelberger A, et al. 2002), RNFL defects (Mistelberger A, et al. 2002, Mok KH, et al. 2003, Mok KH and Lee VWL 2000, Sanchez-Galeana CA, et al. 2004) and ONH damage (Ugurlu S, et al. 2000).

The SITA concept has been applied to SWAP and are available for the HFA 740 and 750 perimeters (Bengtsson B 2003, Bengtsson B and Heijl A 2003) which have been

successful in reducing between-individual variability, shortening the test duration, improving the dynamic range of SWAP and reducing the width of the confidence limits of the normative values compared to the full threshold and FASTPAC algorithms for SWAP (Bengtsson B 2003, Bengtsson B and Heijl A 2003). Despite these advancements, SWAP is not recognised as an improvement over SAP for routine clinical management of OAG. The principal limitation of technique arises from the large within- (STF) (Wild JM, et al. 1995) and between-test (LTF) (Gardiner SK, et al. 2006, Wild JM, et al. 1995) variability and its subsequent effects on the ability of the technique to detect progressive functional damage.

1.8.5 High-pass Resolution Perimetry (HRP)

High-pass resolution perimetry (HRP) is a psychophysical test that provides an estimate of retinal ganglion cell density. High-pass resolution perimetry employs ring shaped, spatially high-pass filtered 'vanishing' targets to determine resolution acuity at a number of pre-determined locations within the central 30^{o} radius of the visual field. The commercially available HRP device is the Ophthimus system (Visumetrics and High Tech Vision, Goteberg, Sweden). High spatial frequency filtered rings are used to determine resolution acuity at 50 predefined locations under photopic conditions. The HRP ring stimuli consist of light core ($25cd/m^2$) and dark ($15cd/m^2$) inner and outer borders. The background luminance is $20cd/m^2$. The width of the ring is 1/5th of the diameter. The stimulus 'value' is defined in terms of its angular size in accordance with conventional resolution acuity tests. If a given target cannot be resolved, it cannot be seen

since the ring's constituents blend imperceptibly into the background i.e. the concept of 'vanishing optotypes' (Frisen L 1986).

The ring values vary between presentations and the patient responds by pushing a button when the stimulus is perceptible. A moving fixation target is used to indicate to the patient approximately when a target can be expected. The test takes approximately 5 to 6 minutes per eye to complete. Fixation stability is monitored by the Heijl-Krakau technique as employed by SAP and SWAP.

The patient views the monitor at a working distance of 16.7cm and wears the appropriate near vision refractive correction. The HRP utilizes 14 different stimuli sizes. The scale factor between consecutive sizes is approximately 1dB. The smallest ring is designated a value of 0. The software automatically scales the rings for constant angular dimensions, irrespective of their actual location on the display screen, i.e. the software corrects for screen curvature and thickness.

Removal of the low spatial frequency information from the HRP stimulus, i.e. high-pass spatial frequency filtering, affects visual perception by narrowing the interval between detection and resolution thresholds. This has important advantages in the perimetric situation: firstly, the perception task is made much easier, and secondly, the result can be interpreted in terms of numbers of functional neural channels. The ease of deciding whether or not a given target is invisible allows a uniquely rapid bracketing of the

threshold level. The measurement probes more complex visual functions than the simple differential light sensitivity measurement employed by SAP.

Several of the summary statistics generated by the HRP are similar to those used in conventional automated perimeters. However, because of the many technical differences, results cannot be compared numerically. A typical HRP printout displays the thresholds at each stimulus location and generates the following indices useful for the detection of OAG, including: global deviation (GD, equivalent to MD with SAP), local deviation (LD, equivalent to PSD with SAP). Combined Deviation (the sum of Global and local deviations, calculated from the standard deviation of the former plus the mean of the latter) and Neural Capacity (NC, based upon the proportional relationship between resolution thresholds, and the spatial separation retinal ganglion cells).

Open angle glaucoma results in an increased separation between remaining, functional retinal ganglion cells. This raises the resolution threshold in the corresponding region of the visual field. Neural Capacity is expressed as a percentage of the average normal whereby the normal average equals 100% (Frisen L and Frisen M 1976). The SD of the NC is approximately $\pm$18%; thus, patients who perform better than average yield results which are greater than 100%.

Other indices produced by HRP provide the observer with information about the validity of a test and of follow-up tests and include: Mean Retest Change, Retest Standard Deviation, Relative Criterion Level (C), Relative Dispersion, Blur Index, elapsed time

(normally 5.5 minutes for a full test), the number of Fixation Losses, and the number of incorrect responses to the false-positive and false-negative catch trials.

High-pass resolution perimetry indices exhibit a statistically significant ($P<0.001$) correlation with those obtained by SAP ($r^2=0.76$) (Chauhan BC, et al. 1993, Iester M, et al. 2003). However, unlike SAP, the variability of the HRP resolution threshold is relatively uniform across the entire visual field and is less affected by the age of the patient (Chauhan BC and House PH 1991, Wall M, et al. 2004, Wall M, et al. 1991). As a result, current evidence suggests that HRP can detect progressive functional damage in OAG by up to 12 months prior to SAP (Chauhan BC, et al. 1993). A high level of concordance is reported between FDT screening and HRP tests (87.7%) in the classification of normal individuals and patients with OAG (Kalaboukhova L and Lindblom B 2003).

Despite being in use for over 14 years, the technique has failed to receive widespread acceptance amongst clinicians and has not replaced SAP as the clinical standard technique for evaluating functional vision in OAG. The principal disadvantage of HRP is attributable to the difficulty in standardising monitor outputs (luminance, homogeneity of output, stability of contrast etc). Consequently, the validity of the normative data is put in question and results obtained from different centres may not be directly comparable.

1.9 Summary

Within the last decade, new and evolving of technology has changed the ways in which OAG is managed clinically. Such advancement has enabled clinicians to currently detect OAG and progressive damage at an earlier stage than previously possible. Future advancements will undoubtedly improve these abilities even further. Currently, stereoscopic ONH-imaging is the recommended 'gold standard' technique to detect OAG. Due to the increased versatility of digital media versus film media, digital stereoscopic ONH-imaging (DSI) will follow-on as the 'gold standard' technique. However, an optimal standard technique for the identification of progressive damage in OAG has yet to be described.

Since the consensus that, in OAG, considerable structural damage occurs prior to visual field loss by SAP, a number of quantitative ocular imaging techniques for detecting OAG have been developed. The two techniques exhibiting the greatest promise for clinical application are based on CSLO and OCT and are the HRT III and CirrusOCT, respectively. In patients with OAG, CSLO and OCT exhibit high repeatability of measurements and suggests that they may be useful for identifying progressive structural damage. CSLO and OCT exhibit high diagnostic precision for the detection of perimetric OAG. However, the clinical utility of CSLO and OCT in detecting OAG, irrespective of any visual field loss is unknown.

Several psychophysical tests, which are designed to exploit specific retinal ganglion cell functional properties, are described in the literature, including; SWAP, FDT and HRP.

Despite yielding generally useful levels of diagnostic precision, these techniques have not replaced SAP as the clinical standard perimetric examination. This is due to poor threshold repeatability and/or uncertainty regarding the physiological basis of the tests. As yet, an optimal psychophysical stimulus for the detection of OAG and progressive functional damage has not been found.

The current-most promising electrophysiology technique for the investigation of OAG is the mfVEP. The appeal of the technique lies in its ability to objectively map visual field loss prior to SAP. Whilst the relative infancy of the technique limits the amount of longitudinal data currently available, the high reproducibility of the mfVEP suggests a role for the technique in detecting progressive functional damage. There is a compelling need for further studies investigating the clinical potential of the mfVEP in OAG management.

Chapter 2: Rationale for the research

2.1 Introduction to OAG management

As described in the previous chapter there is an abundance of examination techniques currently available that facilitate the management of OAG. The 'ideal' examination would rapidly obtain results, which are highly repeatable; exhibit high sensitivity and specificity; and are consistent between diagnosticians and between institutions.

The detection of OAG and of progressive damage at the earliest possible stage is the principal aim of any new or evolving investigative technique for OAG. Currently, the most effective method to detect OAG and/or progressive damage is dependent upon the characteristics and severity of the damage. In the earliest stages of the disease, stereoscopic ONH imaging is currently the most effective method to detect OAG (Gordon MO and Kass MA - The Ocular Hypertension Treatment Study Group 1999, Greaney MJ, et al. 2002, Leske CM, et al. 1999, Musch DC, et al. 1997). However, stereoscopic ONH imaging is confounded by the variation in the ONH size and shape; the number and size of optic nerve fibres; and the related neuroretinal rim (NRR) area, that exists in the normal population. In addition, structural alterations to the ONH that are due to OAG must be accurately differentiated from those that are due to normal ageing (Moya FJ, et al. 1999).

Whilst stereoscopic ONH imaging exhibits the highest sensitivity for early damage, the precise level of diagnostic precision achieved is dependent upon the experience and

expertise of the individual clinician. Objective techniques, which incorporate large databases of age-adjusted normative values, are more favourable for standardising the diagnosis of OAG.

Detection of progressive damage in OAG can generally be identified by retrospective analysis of data over many visits, but is dependent upon the repeatability of measurements obtained both within- and between-visits.

Several objective structural and functional tests stand out on merit as having the greatest clinical utility for use in the management of OAG. These techniques include: the HRT III (Burgansky-Eliash Z, et al. 2007); the StratusOCT (Jeoung JW, et al. 2005, Parikh RS, et al. 2007, Wollstein G, et al. 2005); and the mfVEP (Fortune B, et al. 2007, Graham SL, et al. 2005, Hood DC, et al. 2004, Thienprasiddhi P, et al. 2006). The HRT III and StratusOCT represent the latest generation of established technology; however, the mfVEP is at a much earlier stage of development. Despite the relative infancy of the mfVEP, the literature suggests that the technique represents one of the most promising techniques developed within the last 10 years (Bjerre A, et al. 2004, Fortune B, et al. 2006, Fortune B, et al. 2007, Thienprasiddhi P, et al. 2006). However, none of these techniques have been compared to/validated against the emerging clinical 'gold standard', DSI.

2.2 Previous work

This thesis is a continuation of studies previously undertaken within the School of Optometry and Vision Sciences, Cardiff University, Cardiff and, previously, in the Department of Vision Sciences, Aston University, Birmingham. The studies described in this thesis are the natural development of the previous research concerned with longitudinal and cross-sectional evaluation of OAG. This subject is a constant evolving entity because of technological advancements.

The study described in Chapter 3, investigated the prevalence and concordance of structural and functional progressive damage determined by HRT II and SAP, respectively, in patients with OAG and in patients with 'high risk' OHT. The analysis described in this thesis was with particular respect to 'dissociating factors' between structural and functional progressive damage.

The study described in Chapter 4 investigated the ability of the current most sophisticated and promising novel investigative techniques for identification of abnormality in OAG in patients diagnosed solely using DSI. These techniques include: CSLO (using the HRT II and the HRT III), Optical Coherence Tomography (using StratusOCT), the mfVEP technique and the HFA. This study was an extension of previous work by the Group evaluating the use of retinal imaging techniques to determine early changes in structure of the ONH in patients with OAG and with OHT (Morgan JE, et al. 2005). The study particularly investigated potential combination of techniques for the identification of abnormality; the agreement between techniques; and the topographical relationship of

abnormality between RNFL thickness, neuroretinal rim area, mfVEP RMS amplitude and SAP differential light sensitivity.

The study described in Chapter 5 evolved from the study described in Chapter 4 and was prompted owing to the observed frequency of erroneous RNFL thickness measurements yielded by the standard StratusOCT in patients with OAG. This study validated a novel method for measuring RNFL thickness (OCTAnalyse) against measurements obtained using the commercially available StratusOCT software.

2.3 Rationale

2.3.1 Some dissociating factors in the analysis of structural and functional progressive damage in OAG

Detection of progressive damage in OAG enables clinicians to determine/predict the prognostic outcome for patients receiving a given treatment regimens. Where the rate of progressive damage is deemed to exceed the normal rate of decline expected due to ageing, the treatment strategies are reviewed in an attempt to preserve the remaining vision. Since OAG causes an irreversible loss of vision, the early detection of progressive damage is important in reducing the number of patients who become legally or functionally blind from the disease. Whilst structural changes are believed to precede functional changes in the early stages of OAG the temporal relationship between structure and function is currently unknown.

Specialised computer algorithms for the Heidelberg Retina Tomograph and Humphrey Field Analyzer, namely the Topographic Change Analysis (TCA) and Glaucoma Probability Analysis (GPA), respectively, represent the current-most sophisticated methods to detect progressive structural and functional damage, respectively (Artes PH and Chauhan BC 2005, Bengtsson B, et al. 1997, Chauhan BC, et al. 2000, Chauhan BC, et al. 2001). Both of these algorithms employ complex statistical analyses to determine whether temporal changes to the ONH and visual field, respectively, are statistically significantly different from those expected in normal individuals. Both the HRT and HFA exhibit sensitivity for progressive damage in OAG (Strouthidis NG, et al. 2006); however, poor agreement between the techniques is attributed to one or more unnamed dissociating factors (Artes PH and Chauhan BC 2005, Chauhan BC, et al. 2000, Chauhan BC, et al. 2001). The sensitivity of the latest progression analyses, namely TCA and GPA, for progressive structural and functional damage, respectively, is currently unknown.

This prospective longitudinal study investigated the topographical and temporal relationship between structure and function in progressive OAG. The study identified several dissociating factors, which are largely responsible for the poor level of agreement between the TCA and the GPA in progressive OAG.

2.3.2 Novel approaches to glaucoma detection

Currently, OAG is diagnosed based on subjective evaluation of the ONH appearance. This is most commonly assessed using binocular indirect ophthalmoscopy; however, digital stereoscopic ONH imaging (DSI) is the emerging 'gold standard' technique. The images can be viewed retrospectively, archived and used to derive stereometric data (Morgan JE, et al. 2005, Morgan JE, et al. 2005).

Modern digital stereoscopic ONH imaging instruments can detect glaucomatous abnormalities before conventional psychophysical tests, such as SAP (Morgan JE, et al. 2005).

In recent years, several objective diagnostic techniques have shown promise in glaucomatous structural or functional abnormalities during the early stages of the disease. These techniques include the HRT I, II and III (Burgansky-Eliash Z, et al. 2007, Uchida H, et al. 1996, Wollstein G, et al. 1998), the StratusOCT (Wollstein G, et al. 2004, Wollstein G, et al. 2005) and the mfVEP technique (Goldberg I, et al. 2002, Graham SL, et al. 2005, Hood DC, et al. 2004). In the majority of studies to date, the diagnostic precision of these techniques has been determined in patients with OAG who are diagnosed on the basis of glaucomatous visual field loss.

Currently, the diagnostic precision of these novel techniques has not been referenced to the emerging 'gold standard' technique for assessing ONH abnormality, DSI.

The study was designed to determine the diagnostic performance of the current novel structural and functional investigative techniques in early OAG and/or moderate/advanced OAG diagnosed on the basis of abnormal ONH appearance by DSI, alone. The use of techniques in combination was also investigated since this can improve the sensitivity and specificity of OAG detection (Shah NN, et al. 2006). The agreement in the clinical diagnosis, false-positive rates and topographic correspondence of abnormality between techniques was also determined.

2.3.3 Novel estimation of retinal nerve fibre layer thickness (RNFL) thickness based on subjective evaluation of StratusOCT scan data.

Optical coherence tomography (OCT) is a standard optical imaging technique that exhibits high sensitivity and specificity for the detection of RNFL attenuation in OAG (Budenz DL, et al. 2005, De Leon-Ortega JE, et al. 2006, Jeoung JW, et al. 2005, Leung CK, et al. 2005, Sihota R, et al. 2006). The third generation OCT, namely StratusOCT, has recently been superceded by the fourth generation OCT.

StratusOCT yields highly reproducible, cross-sectional images of the retinal cytoarctitecture to an axial resolution typically between 8 and 10μm. The high reproducibility of scans suggests that the StratusOCT will be suitable for the identification of progressive structural damage.

The commericially available StratusOCT software incorporates several scan and analysis protocols. The standard scan and analysis protocols for the detection of OAG are the RNFL thickness (3.4) and RNFL thickness average protocols, respectively.

StratusOCT is also a standard procedure for the investigation of macula abnormalities, including; macula cysts, macula holes, age-related macula degeneration (AMD), diabetic maculopathy and central serous retinopathy. However, several studies have reported instances where StratusOCT yields erroneous retinal thickness measurements (Ishikawa H, et al. 2002, Ray R, et al. 2005, Sadda SR, et al. 2006). Such measurement error can be found in as many as 92% of scans in eyes with subretinal abnormalities (Ray R, et al. 2005) and most commonly occurs due to misalignment of the individual a-scans (Ray R, et al. 2005, Sadda SR, et al. 2006) and/or misplacement of the retinal inteface markers (Ray R, et al. 2005, Sadda SR, et al. 2006).

Clearly there is compelling need to determine whether measurement errors by StratusOCT occur with the same or similar frequency for RNFL thickness measurement ptotocols. It is important to determine the source of the errors and whether any patient-induced factors increase the likelihood of encountering such errors. Also, alternative methods to obtain RNFL thickness measurements are desireable in instances where the standard StratusOCT analysis procedure yields erroneous RNFL thickness measurements.

The study was designed to evaluate the relationship between RNFL thickness measurements obtained by the RNFL thickness average analysis protocol and by a

custom designed program for measuring RNFL thicknes based on StratusOCT scans, namely OCTAnalyse. The two methods were compared in terms of their within-test repeatability of measurements and their agreement. Several factors which seemingly increase the likelihood of encountering erroneous RNFL thickness measurments by the standard StratusOCT procedure were also determined.

2.4 Logistics

2.4.1 Some dissociating factors in the analysis of structural and functional progressive damage in open-angle glaucoma

The data collection for the study had been undertaken at the Department of Ophthalmology at Birmingham Heartlands Hospital with ethical approval being provided by the Birmingham Heartlands Research and Ethics Committee

Patients with 'high risk' ocular hypertension and patients with OAG who were enrolled in an on-going prospective longitudinal investigation of structural and functional progressive damage who had five years of follow-up, or more, and who conformed to the inclusion criteria of the study were included. Of the original 24 patients with OAG and 27 patients with 'high-risk' OHT, the search, carried out by Cameron Hudson (CH), revealed 14 and 9 patients, respectively, who were eligible. The remaining patients had been either lost to follow-up, had withdrawn from the study or had died.

Some delays were encountered whilst several of the patients were recalled to their final HRT and HFA examinations. The influence of progressive cataract on the study data was retrospectively analysed by re-examination of the clinical notes. Small delays were encountered in retrieving the clinical notes from the hospital archive.

2.4.2 Novel approaches to glaucoma detection

The data collection for the study was undertaken at the Cardiff Eye Unit at the University of Wales Hospital, Cardiff, and the School of Optometry and Vision Sciences, Cardiff. Ethical approval for the study was provided by the Central Office for Research and Ethics Committee.

Patients with OAG attending the Glaucoma Outpatients Clinic at the Cardiff Eye Unit, who conformed to the inclusion criteria, were provided with a general outline of the study. Friends, family and partners of the participants with OAG were encourage to take part in the study as normal individuals and were recruited following a full ophthalmic investigation to confirm their suitability. Further normal individuals were also recruited from the staff at Cardiff University and at the University Hospital of Wales. Informed written consent was obtained from all participants, following a full explanation, verbally and in writing, of the nature of the study.

Patients with OAG were required to attend for a total of 6 visits. The normal individuals attended for one extra pre-study session in order to undergo ophthalmic examination including visual field examination.

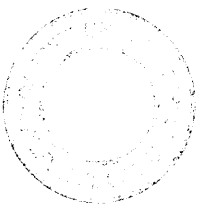

Prior to recruitment of the participants, a period of approximately 12 months was spent becoming proficient in the technical aspects of mfVEP recording as well as compiling a database of normative mfVEP records from normal individuals of different ages. During this time, advice and guidance was sought from experienced technicians at the Department of Clinical Electrophysiology at the Queens Medical Centre, Nottingham. Experts in the mfVEP technique were also consulted during the 2006 ISCEV and 2007 BRISCEV meetings at Glasgow Caledonian University and Stoke Mandeville Hospital, respectively.

Some difficulties in recruiting participants were encountered, as the inclusion criteria were quite restrictive. The presence of moderate/dense cataracts, common in older individuals who are considered to be more likely to develop OAG, can degrade the results from ocular imaging.

Major delays in obtaining mfVEPs occurred due to technical problems with the colour microdisplay stimulus projection system. Replacement hardware was not available until approximately 10 months after the initial problems were reported. Replies from the technical advisers at Electro-Diagnostic Industries (EDI), San Mateo, California, USA, to queries relating to the use of the monitor stimulus projection system were delayed by several months on a number of occasions. In addition, the StratusOCT was only available for use at various times during the working week due to its use in routine Hospital outpatients clinics.

Longer delays, of approximately 6 months, were encountered in obtaining the clinical diagnoses of participants by the expert clinical observers who were located at different centres around the UK.

A total of approximately 600 hours was required to analyse the data; of which approximately half was spent analysing the mfVEP data alone.

2.4.3 Novel estimation of RNFL thickness based on subjective evaluation of StratusOCT scan data

StratusOCT data from 21 patients with OAG and 20 normal individuals, who had taken part in the study described in Chapter 4 were used in the study.

Delays of approximately 6 months were encountered in analysing the data as the OCTAnalyse software was developed and revised. However, the persistence and expertise of professional colleagues ensured that a fully operational version of the software was available for use by the time that most of the OCT data had been collected.

StratusOCT data was obtained over a 20 month period, with approximately 41 hours of data acquisition and approximately 200 hours of data analysis.

Despite the delays encountered during the study, the patience and cooperation shown by participants and professional colleagues ensured that a wealth of valuable information

was collected and could be presented in this study.

A period of 17 months was required to achieve the cohort described in Chapters 4 and 5. In total, 45 volunteers provided 90 SAP visual fields, 90 HRT images, 90 StratusOCT scans, 45 mfVEPs and 45 digital stereoscopic ONH images. In total, over 270 separate visits were attended, each visit lasting on average one hour.

Chapter 3: Some dissociating factors in the analysis of structural and functional progressive damage in OAG

3.1 Introduction

When progressive glaucomatous damage becomes apparent, the given treatment regimens must be re-assessed in order to arrest the deterioration.

In early OAG, changes to the ONH morphology are believed to provide a more sensitive marker of progressive damage than standard automated perimetry (SAP) (Harwerth RS, et al. 2004, Martus P, et al. 2005, Medeiros FA, et al. 2005, Quigley HA, et al. 1980) whilst in advanced cases of OAG, SAP is believed to provide a more sensitive measure of progressive damage than structural assessment of the ONH by biomicroscopic evaluation (Jonas JB and Grundler AE 1997, Jonas JB, et al. 2004). Although this summary of the temporal relationship between progressive structural and functional damage in OAG is useful clinically, the precise relationship is unknown and is currently receiving much attention.

The two digital techniques in longest clinical use for assessment of structural and functional damage and, thus, the current 'gold' standard techniques for the identification of progressive in OAG, are confocal scanning laser ophthalmoscopy (CSLO) and SAP, respectively.

3.1.1 Detecting progressive structural damage with Confocal Scanning Laser Ophthalmoscopy (CSLO)

Confocal scanning laser ophthalmoscopy with the HRT is an accurate and repeatable technique that obtains quantitative topographical information of the ONH and peripapillary retina. The HRT has been widely employed both in research and clinically for the assessment of ONH morphometry in OAG (Balachandran C, et al. 2006, Danesh-Meyer HV, et al. 2006, Iester M, et al. 2006, Janknecht P and Funk J 1994, Jayasundera T, et al. 2005, Pueyo V, et al. 2007, Rohschneider K, et al. 1994, Weinreb RN, et al. 1993). The HRT has shown good test-retest repeatability of measurements in stable OAG both for individual retinal surface height measurements (Chauhan BC, et al. 1994, Strouthidis NG, et al. 2005, Weinreb RN, et al. 1993) and for the automated software derived stereometric parameters (Rohschneider K, et al. 1994). The HRT can thus identify statistically significant changes in the ONH morphology that occur in progressive OAG. The variability of the HRT measurements, and thus its sensitivity to identify 'true' change, has been shown to be greater in regions of the ONH where the topographic gradient is steep and in regions of the ONH/retina underlying the retinal vasculature (Brigatti L, et al. 1995, Chauhan BC, et al. 1994). Thus, variability of the HRT measurements is dependent on the region of the ONH under scrutiny.

An in-depth description of the instrument can be found in Chapter 1, Section 1.4.1.

The Topographic Change Analysis (TCA) of the HRT II and III identifies statistically significant changes in the topographic height of the ONH and of the peripapillary retina

(Chauhan BC, et al. 2000). The TCA identifies changes in the mean retinal height from two baseline examinations that reach statistical significance ($p<0.05$), and is independent of the reference plane and ONH contour. The technique requires a minimum of two baseline and three follow-up examinations in order to fulfil the criterion for 'definite' structural progression. The TCA software corrects the images acquired at baseline and at follow-up for differences in magnification, rotation and tilt. Clusters of 4x4 adjacent pixels are then combined to create super-pixels allowing more sophisticated statistical treatment of the topography data. Height measurements within each superpixel are used to perform an F-statistic, which tests the variances of the local height measurements between baseline and follow-up examinations at each pixel within the image. The resultant value indicates the probability that a measured height change at a given location occurred by chance, alone. If the error probability is less than 5%, a local surface height change is deemed to have occurred. Probability maps display those regions of the ONH that are either elevated or reduced in mean topographic height from baseline, by the superimposition of green or magenta super-pixels, respectively, in the corresponding region of the reflectance image (Chauhan BC, et al. 2001). Since OAG manifests as a loss of neural tissue, this technique assumes that a reduction in topographic height from baseline is descriptive of the disease process. The criterion for topographic height change is a change at the $p<0.05$ within a given superpixel, present over three consecutive sets of follow-up images. This criterion was determined by computer simulation (Chauhan BC, et al. 2000). This criterion has since become the established standard to detect progressive structural damage in OAG (Chauhan BC, et al. 2000, Chauhan BC, et al. 2001).

3.1.2 Detecting progressive functional damage with Standard Automated Perimetry (SAP)

Standard automated perimetry is the current method used to identify progressive functional damage to the visual field in OAG. The subjective nature of SAP yields suboptimal levels of within-test variability of the differential light sensitivity, making 'true' change to the visual field difficult to differentiate from the between-test variability associated with the procedure. Most clinicians employing SAP are reliant upon the visual comparison of printouts over the follow-up period to identify progressive damage to the visual field. However, this method of subjective clinical judgement is inconsistent and even expert observers show considerable within- and between-test variability in their judgement as to whether the results of a given series of visual field examinations exhibit progressive loss, or, are stable (Viswanathan AC, et al. 2003). This stems from the lack of accepted guidelines as to what constitutes a clinically significant progression of the visual field.

Several analytical methods for identifying progressive functional damage have been proposed. However, at present there is no general agreement as to which of these techniques identifies progressive visual field loss with the greatest levels of sensitivity and specificity (Katz J, et al. 1999, Nouri-Mahdavi K, et al. 2004, Spry PGD, et al. 2002, Wild JM, et al. 1993). Several large scale randomized trials, namely the Early Manifest Glaucoma Trial (EMGT) (Bengtsson B, et al. 1997), the Advanced Glaucoma Intervention Study (AGIS) (The AGIS Investigators 1994) and the Collaborative Initial Glaucoma Treatment Study (CIGTS) (Katz J 1999, Musch DC, et al. 1997), for which a

worsening of the visual field has been the primary outcome measure, have developed statistical criteria for the identification of progressive visual field loss. The methods used by these trials for identifying progressive functional damage to the visual field are each based upon different principles. Whilst a standardised criterion for progressive visual field loss is clinically appealing, the justification for using any one technique over another is equivocal.

The prevalence of visual field progression with the EMGT and CIGTS methods is twice that of the AGIS method, being 23%, 22% and 11%, respectively (Katz J, et al. 1999). Due to the lack of a standard for comparison, it cannot be established which of these techniques is the most sensitive for identifying 'true' progressive loss. In addition, a poor level of concordance was observed between those patients deemed as 'progressive' by each method. However, the earlier time to progression and the greater prevalence of improvement with the EMGT criterion compared to the other two approaches suggests that this method may be more sensitive to progressive damage, earlier (Katz J, et al. 1999).

The principal difference between the EMGT criterion and the CIGTS and AGIS criteria is the utilisation of the Pattern Deviation (PD) values to identify visual field progression as opposed to the Total Deviation (TD) values, respectively. As described in Chapter 1, Section 1.8.1, the HFA printout for an individual visual field examination displays both TD and PD probability maps (Heijl A, et al. 1989). The PD probability map indicates the statistical significance of the difference between the measured threshold values and the

age-specific normal threshold values at each location of the visual field after correcting for any generalized depression or elevation of sensitivity.

The rationale for this approach is, that the PD values remove the influence of homogeneous diffuse loss of sensitivity e.g., that caused by cataract (Bengtsson B, et al. 1997).

Studies of the ability of PD compared to TD based criteria to identify progressive visual field damage indicate a lower prevalence of progressive loss for PD based criteria than for TD based criteria (Artes PH, et al. 2005, Katz J 2000). The discrepancy has been attributed to the separation of progressive OAG from progressive cataract (Katz J 2000). However, the prevalence of PD based progressive loss is lower than TD based progressive loss in the presence of stable cataract (Artes PH, et al. 2005).

3.1.3 Temporal relationship between structural and functional progressive damage

Two studies have investigated the temporal relationship between structural and functional progressive damage, assessed using HRT and SAP, respectively (Artes PH and Chauhan BC 2005, Chauhan BC, et al. 2001). Both studies find a lack of concordance between structural and functional progression (Artes PH and Chauhan BC 2005, Chauhan BC, et al. 2001). Whilst this lack of agreement may be a genuine reflection of the temporal relationship between structural and functional abnormality in OAG, it has been proposed that 'dissociating factors' inherent to the test procedures, themselves, may mask the true

relationship (Artes PH and Chauhan BC 2005, Chauhan BC, et al. 2001). Such dissociating factors have yet to be described.

3.2 Study Aims

The purpose of this study was to investigate the prevalence and concordance of structural and functional progressive damage in patients with OAG and in patients with 'high risk' OHT with particular reference to the presence of dissociating factors.

3.3 Materials/ Methods

The material for the study was obtained from an on-going prospective longitudinal investigation of structural and functional progressive damage in OAG undertaken at the Glaucoma Out-patients Clinic at Birmingham Heartlands Hospital, Birmingham.

3.3.1 Cohort

A search of the database for patients who had been followed-up for five years, or more, with the HRT and HFA revealed 14 patients with OAG and 9 patients with 'high-risk' OHT. The mean period of follow-up was 78.4 months (SD ±9.5 months, range 60-101 months). The mean age of the group with OAG was 69.3 years (SD ±9.4, range 51-80) and of the group with OHT was 63.8 years (SD ±12.2, range 46-85).

The combined cohort had undergone a mean of 5.5 (SD ±0.8, range 4-7) examinations with the HRT and a mean of 7.4 (SD ±1.4, range 5-10) examinations with the HFA during the follow-up.

The study had approval from the Research and Ethics Committee of Birmingham Heartlands and Solihull (Teaching) NHS Trust and all patients had given written informed consent. The group mean age, mean duration of follow-up, mean number of examinations with the HRT and HFA, respectively, and mean interval between examinations for each of the two groups are specified in Table 3.1

		OAG (n=14)	OHT (n=9)
Mean Age ± SD (Range)		69.0 ± 9.5 (51-80)	63.8 ± 12.2 (46-85)
Mean duration of follow-up (months) ± SD		77.2 ± 10.0	80.0 ± 9.0
Mean number of exams ± SD	HRT	5.6 ± 0.8	5.3 ± 0.9
	HFA	7.5 ± 1.3	6.9 ± 1.3
Mean interval between exams (months)	HRT	13.8 ± 3.1	15.0 ± 2.7
	HFA	10.3 ± 6.0	11.6 ± 7.0

Table 3.1 - *Demographic characteristics of the study cohort.*

The mean ONH area for those with OAG, derived by the HRT II, was 2.1mm^2 (SD ±0.4; range 1.7-2.9mm^2) and for those with OHT 2.2mm^2 (SD ±0.4; range 1.7-2.8mm^2). Seven of the 14 patients with OAG exhibited a small (<1.99mm^2) (Schuerle AF and Schmidt E 2004) and 7 a normal sized (2.0-3.0mm^2) ONH. Four of the 9 patients with OHT had a

small and 5 a normal sized ONH. The vertical CD ratio in the 4 patients with OHT and a small ONH ranged from 0.5 to 0.7.

3.3.2 Inclusion criteria

Inclusion criteria on entry into the longitudinal study confirmed a best-corrected visual acuity of 6/9 or better; a distance refractive error within the range ±6.00 DS and ±2.50 DC; a crystalline lens appearance, graded according to the Lens Opacity Classification System (LOCS) III (Chylack LT, et al. 1993), was not greater than nuclear colour (NC) 3.0, nuclear opalescence (NO) 3.0, cortical (C) 1.0, or posterior subcapsular (P) 1.0; no systemic medication known to affect the visual field; and no history of diabetes mellitus.

Two patients, one with OAG and one with OHT were pseudophakic at the time of enrolment.

Open angle glaucoma (OAG)

Open angle glaucoma was defined as a characteristic ONH appearance with, or without, a characteristic visual field defect by SAP and with, or without, elevated IOP. A characteristic ONH appearance was considered as one or more of the following: an increase in cup size, an increase in cup to disc (CD) ratio, disc asymmetry, changes in the lamina cribrosa, loss of neuro-retinal rim, pallor, evidence of peripapillary atrophy, vessel changes or ONH haemorrhage. A visual field defect characteristic of OAG was considered as a cluster of three or more locations, on the same side of the horizontal

midline and in a location typical for OAG, exhibiting abnormality on two successive examinations by Pattern Deviation probability analysis at the $p<0.05$ level with at least one location exhibiting abnormality at the $p<0.01$ level (Hodapp E, et al. 1993).

'High risk' ocular hypertension

High-risk OHT was defined as either a presenting IOP >24mmHg; a presenting IOP ≥22mmHg and a vertical cup-to-disc (CD) ratio >0.5; or a presenting IOP ≥22mmHg, a vertical CD ratio ≤ 0.5 and a family history of OAG. The IOP was not corrected for the effects of central corneal thickness (CCT).

All had undertaken at least one examination with SAP prior to inclusion in the study.

One eye from each patient had been examined for the study: the eye with the more advanced glaucomatous disease or, for the participants with OHT, the eye with the greatest risk of developing OAG.

3.3.3 Heidelberg Retina Tomography (HRT)

The HRT images at the initial/baseline visit were acquired with the HRT Version I, and Software Version 1.7. The initial focal plane had been set to the spherical equivalent of the refractive error; the scan depth to 2.5mm; the image frame to 10^{o}x10^{o} and the laser to maximum intensity. The camera objective lens had been positioned approximately 15mm from the cornea and the laser bean had been directed through the pupil (Schuerle AF and

Schmidt E 2004). The patient had been instructed to fixate an internal flashing green light visible nasally to the eye being examined. The ONH image had been centred on the real-time monitor using fine adjustment of the vertical and horizontal position of the camera and focal plane position to achieve optimal illumination of the retina and ONH. The patient had been asked to refrain from blinking and from excessive head and eye movement between each successive scan in order to minimise motion artefacts. A further three scans, of acceptable quality, had been recorded using the same recording settings. The three scans had then been combined to generate a mean topographical image, which improves the repeatability of subsequent topographic measurements (Weinreb RN, et al. 1993).

Once commercially available, the HRT II was used in a similar manner for all subsequent follow-up examinations. The recording procedure for the HRT II differed to that of HRT I, in that the scanning variables fine focus, scan depth and sensitivity were determined by an automated pre-scanning mode. Also, the HRT II images were obtained using automated serial acquisition of scans with built-in quality-control measures and an automated averaging of scans to generate the mean topographical. The images obtained using the HRT I had been transferred to the HRT II using the export E2E option of the HRT software (All versions). Export E2E, facilitates the transfer of HRT data between compatible systems.

A third HRT system without image acquisition capability, was used to analyse data collected from both the HRT I and the HRT II instruments.

3.3.4 Humphrey Field Analyzer (HFA)

At the baseline examination, each participant underwent SAP using Program 24-2 and either the Full Threshold or SITA Standard algorithm with the HFA 750. The distance refractive correction, in the form of a full aperture trial lens, together with any near correction appropriate for the viewing distance of the perimeter bowl, was employed for all SAP examinations.

The follow-up intervals for HRT and SAP examination were determined in accordance with the management criteria of the lead clinician, Mr Ian Cunliffe.

3.3.5 Analysis

HRT progression criterion: Topographic Change Analysis (TCA)

Evidence of progressive structural damage within the ONH and peripapillary retina was assessed using the Topographic Change Analysis (TCA) of the HRT II (Software Version 1.7). Structural progression was defined as a cluster of at least 20 magenta super pixels present in each of 3 consecutive images (Chauhan BC, et al. 2001).

HFA progression criterion: Glaucoma Progression Analysis (GPA)

Evidence of progressive functional damage to the visual field was assessed using the Glaucoma Progression Analysis (GPA) of the HFA. The GPA defines 'likely' visual field progression when at least three stimulus locations exhibit statistically significant

reductions ($p<0.05$) in sensitivity from a baseline comprising the average of two examinations, by Pattern Deviation analysis, on at least each of three consecutive examinations (Heijl A, et al. 2003). This criterion is the same as that employed by the Early Manifest Glaucoma Trial (EMGT) (Heijl A, et al. 2003).

3.5 Results

3.5.1 Structural and functional concordance

Six patients (2 with OAG and 4 with OHT) were stable by both TCA and GPA. Four patients exhibited progression by both techniques (3 with OAG and 1 with OHT) (Figure 3.1). Topographical correspondence between the visual field progression and the ONH progression was present in all four patients (Figure 3.2).

3.5.2 Structural progression, only

Five patients with OAG and two with OHT exhibited progression by TCA only (Figure 3.1). Four of these 7 patients manifested localised field loss, designated as 'out of range' by GPA, which corresponded to the region of structural progression (Figure 3.3). An 'out of range' designation indicates that the variability associated with the measured sensitivity at the given location lies beyond the maximum stimulus luminance of the HFA. Such locations are excluded by the GPA from the analysis of progressive field loss.

Of the remaining 3 patients, one exhibited functional progression over the last two visits of the series, and thus did not meet the GPA criterion for 'likely' progressive damage;

and one showed a protracted perimetric learning effect (Figure 3.4). No explanation could be found for the lack of functional progression in the remaining patient.

3.5.3 Functional progression, only

Four patients with OAG and two with OHT exhibited progression by GPA only (Figure 3.1). All 4 of the patients with OAG exhibited an extensively cupped ONH at baseline (one or more HRT sectors exhibiting a neuro-retinal rim area to disc area ratio of $\leq$0.2). The attenuated neuro-retinal rim width reduced the available area for assessment of reduction in the topographical height within the ONH. Advanced OAG also reduces the available height of the peripapillary retina. Thus, structural progression with the HRT seemingly becomes more difficult to identify as the disease advances (Figure 3.5).

In the two patients with OHT, no explanation could be found for the lack of structural progression.

One patient with OAG and one with OHT underwent 4 HRT examinations; both exhibited functional progression in the presence of stable structural damage at each of the two follow-up examinations.

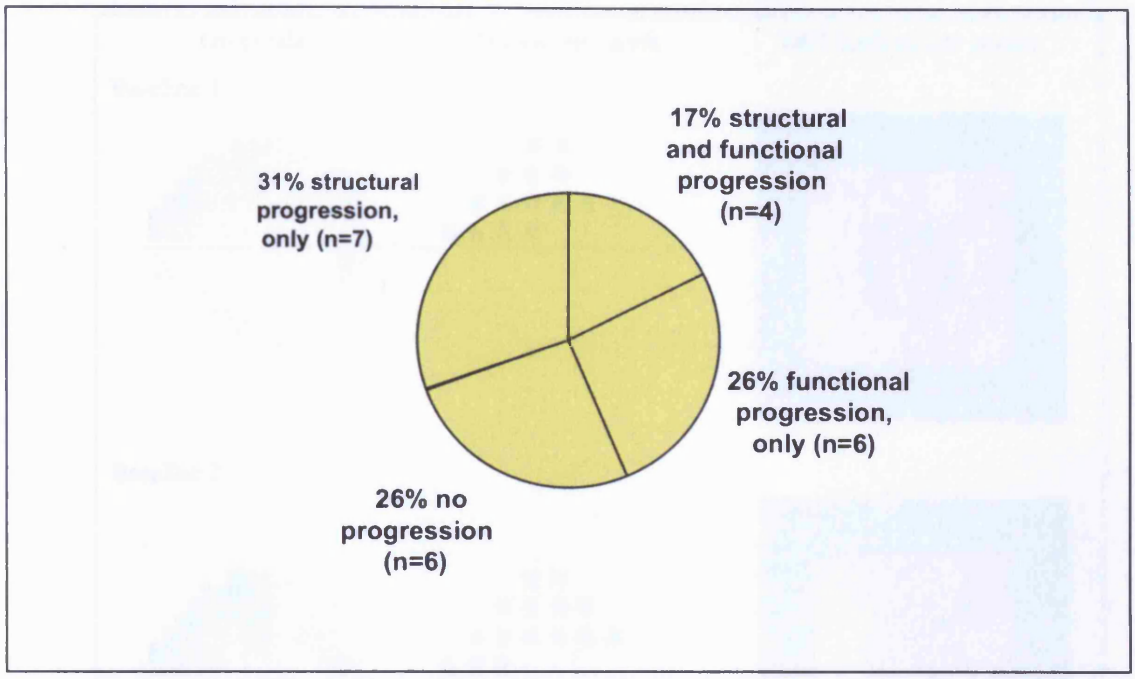

Figure 3.1 – *The proportions of patients exhibiting structural and/or functional progressive damage.*

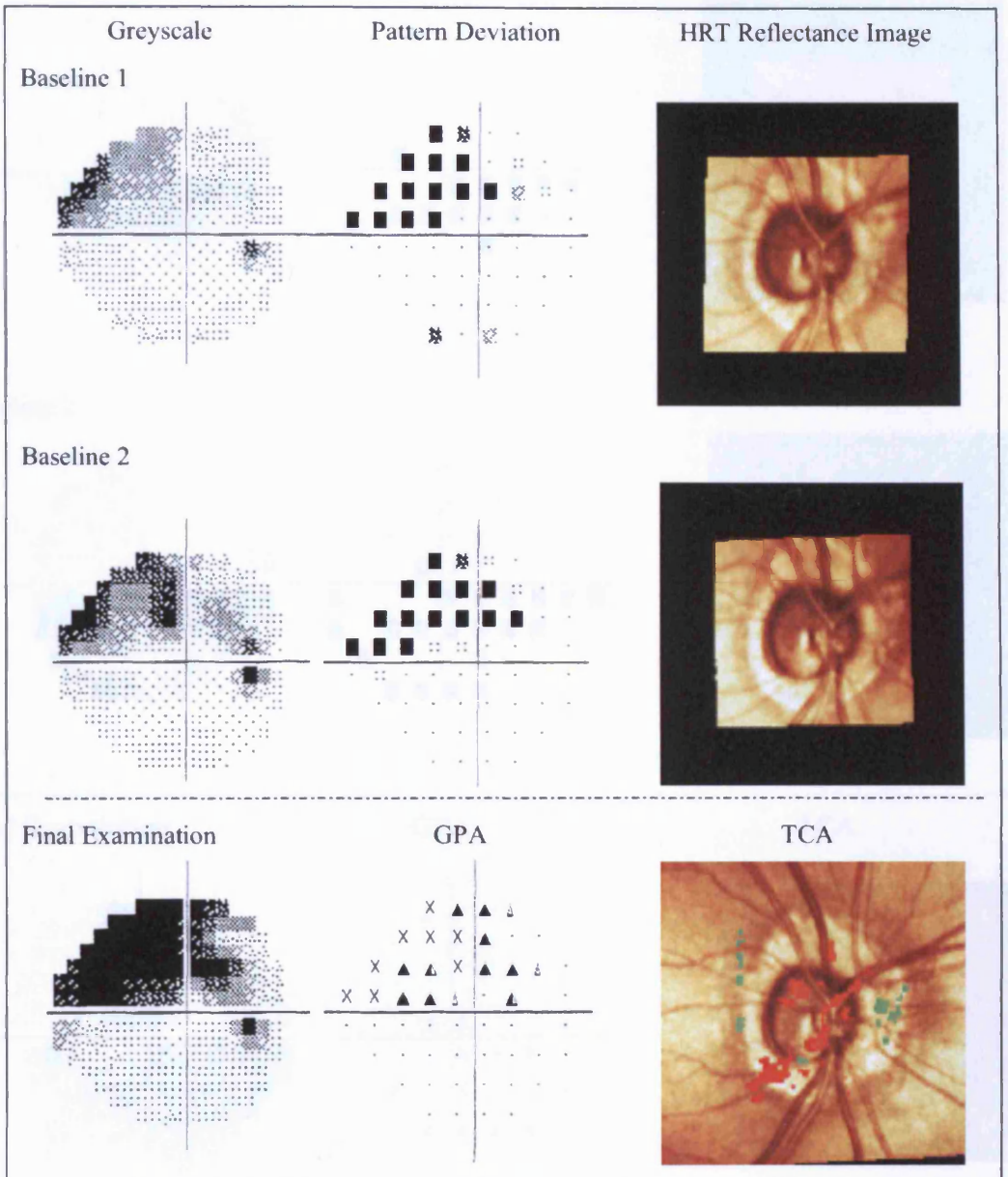

Figure 3.2 Topographic correspondence of structural and functional progressive damage

(*Male, aged 71 at baseline, Dx OAG*).
The baseline TCA images of the ONH and peripapillary region and GPA print-out of the baseline visual fields are shown above the dotted line. The most recent visit of a 72 month follow-up is shown below the dotted line. Progressive structural damage to the inferior temporal region of the ONH is apparent by the TCA (indicated in red) and corresponds to the progressive functional damage in the superior temporal visual field apparent by the GPA.

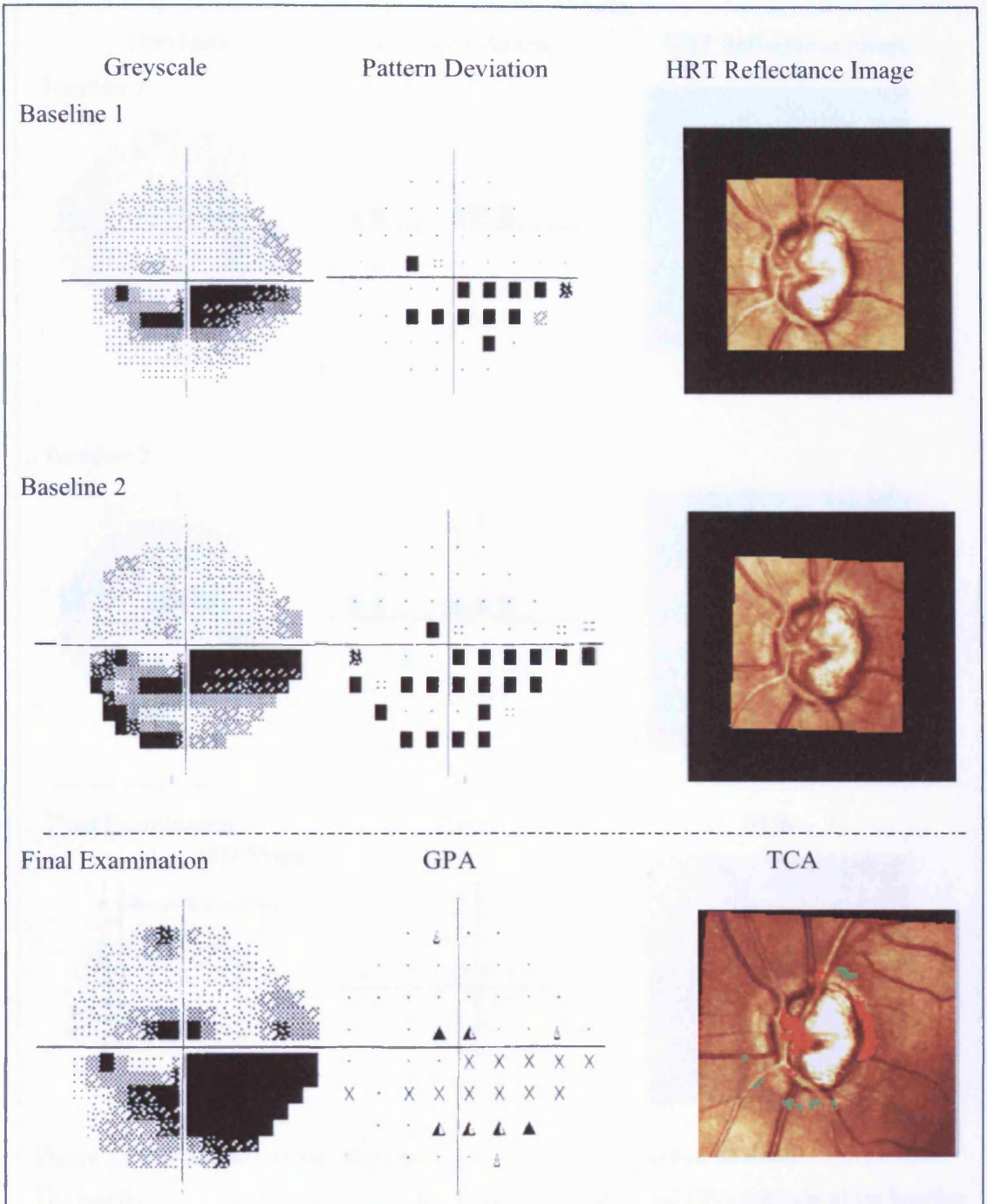

Figure 3.3 Advanced field loss at baseline (*Female, aged 68 at baseline, Dx OAG*).
The baseline TCA images of the ONH and peripapillary region and GPA print-out of the baseline visual fields are shown above the dotted line. The most recent visit of a 76 month follow-up is shown below the dotted line. Progressive structural damage to the superior temporal region of the ONH is apparent by the TCA (indicated in red); however, the corresponding region of the visual field cannot be evaluated by the GPA due to the depth of the defect (indicated with a cross).

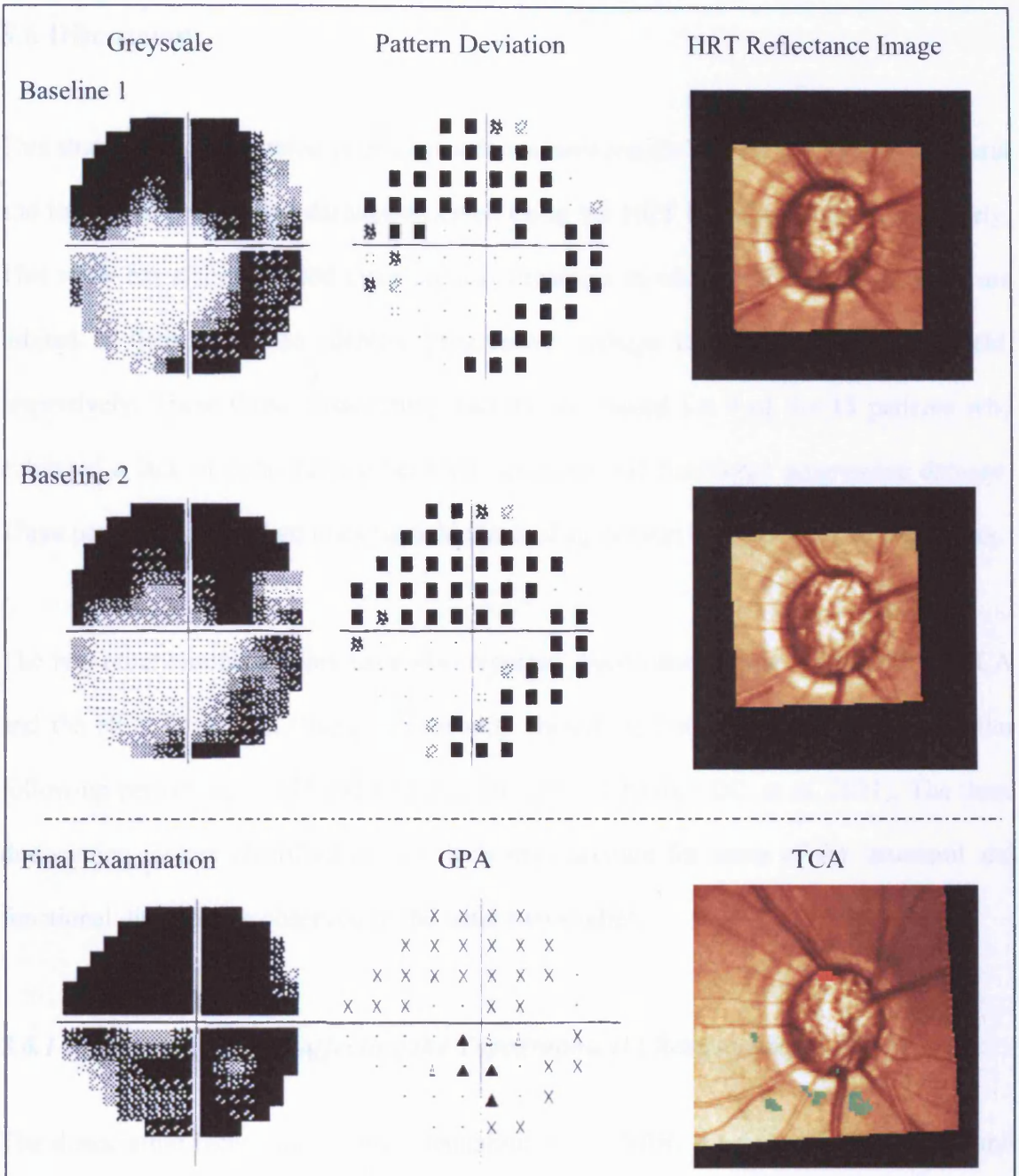

Figure 3.5 Attenuated neuroretinal rim (*Male, aged 74 at baseline, Dx OAG*)

The baseline TCA images of the ONH and peripapillary region and GPA print-out of the baseline visual fields are shown above the dotted line. The most recent visit of a 76 month follow-up is shown below the dotted line. Progressive visual field loss was identified by GPA (indicated by the solid triangles); however, topographic height reduction, although present at the superior disc margin (indicated in red), did not fulfill the criteria for structural progression due to the presence of an attenuated neuroretinal rim.

3.6 Discussion

This study has demonstrated poor concordance between the current criteria for structural and functional progressive damage assessed using the HRT II and the HFA, respectively. This study has also identified three clinical situations in which, either, TCA or GPA are limited in their ability to identify progressive damage to the ONH or visual field, respectively. These three 'dissociating factors' accounted for 9 of the 13 patients who exhibited a lack of concordance between structural and functional progressive damage. Three patients exhibited an unexplainable lack of agreement between the two techniques.

The two other similar studies have also reported discordance between the HRT II TCA and the HFA Glaucoma Change Probability (based on Total Deviation) over a similar follow-up period (Artes PH and Chauhan BC 2005, Chauhan BC, et al. 2001). The three dissociating factors identified in this study may account for some of the structural and functional discordance observed in the latter two studies.

3.6.1 Dissociating factors affecting the Topographical Change analysis (TCA)

The dissociating factor, the severe attenuation of the NRR, for the analysis of structural progression with the HRT II (Figure 3.5) is in addition to the limitation arising from sub-optimal image quality due to such factors as media opacity, fixation instability, and pupil miosis which also impair the identification of progressive damage (Zangwill L, et al. 1997). It is recommended by the manufacturer, that the standard deviation of the height measurements for the HRT should not exceed 30μm to ensure 'high quality' images,

(Schuerle AF and Schmidt E 2004). All images in the study were less than the recommended value and thus considered to be of 'high quality'. However, it would be expected that the sensitivity of the TCA to identify progressive loss would decline with reduction in image quality even within the acceptable range of image quality.

The diagnostic performance of the HRT II is influenced by the ONH size (Medeiros FA, et al. 2006). The HRT II, Moorfields regression analysis is associated with an increase in diagnostic sensitivity in large ONHs compared with that of smaller ONHs (Medeiros FA, et al. 2006). The effect of ONH size on the sensitivity of the TCA to identify progressive structural damage is not known and cannot be determined from the present study due to the small range of ONH sizes and to the small cohort size. Optic nerve head size is not a predictive factor for the progression of functional damage (Jonas JB, et al. 2004); however, the precise relationship between ONH size and sensitivity of the TCA to detect progressive structural damage requires further investigation.

3.6.2 Dissociating factors affecting the Glaucoma Progression Analysis (GPA)

The detection of functional progression with the HFA is clearly limited by the two dissociating factors, namely the dynamic range and the learning effect, are illustrated in Figure 3.3 and Figure 3.4. The present version of the GPA is limited by its inability to identify progressive loss in regions of the visual field where the variability of the differential light sensitivity is beyond the dynamic range of the HFA at the baseline examinations. The stimulus locations corresponding to these regions of the visual field are designated as 'out of range' and excluded from the GPA in subsequent examinations.

This limitation could conceivably be overcome by the use of a size V stimulus. However, such an approach would require the development of a new GPA based upon the larger stimulus size.

The second source of dissociation between the progression analyses arises when evidence of a perimetric learning effect is apparent. Clinicians should exercise caution when accepting baseline HFA data for use with GPA, particularly in patients inexperienced in SAP. The GPA software alerts the clinician to a significant learning effect between the first and second examinations and, in such cases, recommends that the second and third examinations be used as the baseline. However, the appropriate baseline visual field examination for GPA should only be designated when it is apparent that the learning effect is no longer operative. The learning effect is complex in its format (Heijl A, et al. 1989) and can last beyond the third examination and, as illustrated in Figure 3.4, can also be associated with large variations in MD.

The time to detection of progressive functional loss should also, theoretically, be retarded by one or more examinations in the series deemed to be unreliable on the basis of an unacceptable number of incorrect responses to one or more of the three types of catch trials. However, with the exception of those examinations exhibiting $\geq$15% incorrect responses to the false-positive catch trials, recorded by either of the SITA algorithms, which are excluded from the baseline, the GPA software incorporates those examinations deemed to be unreliable into the analysis of progressive field loss. The criterion for low reliability for any given type of catch trial is empirically derived and the utility, or

otherwise, of incorporating an unreliable field into the analysis of progressive loss has yet to be determined. In the current study, all patients exhibited reliable responses in terms of the incorrect responses to the false-negative (≤30%) and false-positive (≤15%) catch trials across all the examinations. Six patients each exhibited one examination at which the incorrect responses to the fixation loss catch trials was beyond 30%. One patient with OAG exhibited an unacceptable number of incorrect responses to the fixation loss trials in 7 of 10 examinations. This was attributed to the difficulty in locating the blind spot, which was due, in turn, to the difficulty in fixating as a consequence of a small focal defect close to the macula; however, fixation mediated by the gaze tracker was considered to be stable. This patient was not identified as progressing by GPA, due to the depth of the central focal defect lying 'out of range', but showed evidence of structural progression by TCA.

3.6.3 Topographical correspondence of structural and functional progressive damage

Topographical correspondence of the ONH and visual field was present in all four patients exhibiting both structural and functional progression, an example of which is given in Figure 3.2. The topographical relationship between structural damage to the ONH and functional damage to the visual field has been investigated previously (Anton A, et al. 1998, Bowd C, et al. 2006, Danesh-Meyer HV, et al. 2006, Gardiner SK, et al. 2005, Garway-Heath DF, et al. 2000, Yamagishi N, et al. 1997). The retinotopic organization of the retinal nerve fibres at the ONH is equivocal (Minckler DS 1980, Ogden TE 1983, 1974, Radius RL and Anderson DR 1979) and exhibits variability between individuals (Garway-Heath DF, et al. 2000, Wirtschafter JD, et al. 1982). There

is an apparent organisation of the retinal nerve fibres with respect to the circumferential origin of the axons. The course of axons above and below the macula show clear, mirrored symmetry: however, the position of the ONH relative to the horizontal meridian governs their precise point of entry and accounts for the between-individual differences in topographical correspondence (Garway-Heath DF, et al. 2000). The organisation of the retinal nerve fibres with respect to the eccentricity of their origin is less well understood. Some studies report that the longer axons, from more peripheral regions tend to lie deeper within nerve fibre bundles (Minckler DS 1980, Radius RL and Anderson DR 1979). Other studies conclude that the longer axons are intermixed with the shorter ones (Ogden TE 1973), or, that the longer axons lie more superficially (Ogden TE 1974). A more recent study found no apparent organisation of nerve fibres within the nerve fibre bundle with respect to the eccentricity of its origin (Garway-Heath DF, et al. 2000). Whilst the findings of the present study do not further the understanding of the topographical correspondence in progressive OAG, they do serve to corroborate the likelihood of 'true' progression having occurred in these four patients.

3.6.4 Identification of progressive damage and disease severity

Another likely contributor to the discordance between the HRT II TCA and the HFA GPA is the failure of the respective progression analyses to consider the severity of the disease. The reduction in differential light sensitivity, in dBs, for each ganglion cell lost in OAG, increases exponentially as the total number of remaining retinal ganglion cells declines (Harwerth RS, et al. 2004). Thus, the amount of structural damage required to produce an equivalent amount of functional damage will vary dependent upon the

severity of the condition. Thus, the amount of neuronal damage required to produce a given functional deficit is likely to be smaller in advanced stages of OAG than in the early stages. The current TCA software (HRT Version 3.0) is unlikely to overcome this issue, since, like earlier software versions; it employs a fixed progression criterion that is independent of disease severity.

Since loss of the retinal ganglion cells is the primary neuronal damage occurring in OAG, the ideal study of structure and function should occur at the level of the retinal ganglion cell and its axon. Currently, this cannot be achieved *in vivo* and clinicians must rely upon surrogate measures of structural deficit, such as morphometric assessment of the ONH, and functional deficit, such as measurement of differential light sensitivity. Precisely how well these surrogate measures are a true reflection of retinal ganglion cell damage in OAG is not yet fully understood. Experimental studies on primate have shown that despite complete optic nerve transection, the ONH fails to undergo cupping, which is the hallmark of OAG (Agapova OA, et al. 2003, Morrison JC, et al. 1990). Similarly, assessment of the visual field can be affected by many pre- and post-retinal factors that are independent of retinal ganglion cell dysfunction. Thus, the clinical appropriateness of CSLO and SAP as surrogate measures of retinal ganglion cell integrity is questionable.

In OAG, ONH cupping occurs as a result of retinal ganglion cell axonal loss and the physical backward compression of the connective tissue of the lamina cribrosa. Individuals with OAG, exhibit different amounts of physical tissue alteration and retinal ganglion cell loss that, together, constitute the final disc topography. However, only the

retinal ganglion cell axon loss is correlated directly with functional loss. Since the HRT II is unable to differentiate these different types of structural alteration, this may further add to the disparity between the HRT II and HFA progression analyses. It has yet to be determined whether imaging technologies that assess progressive damage due to axonal integrity by means other than ONH morphometry yield better concordance with progressive functional damage. It has been proposed that RNFL thickness may be a more suitable surrogate for determining retinal ganglion cell integrity (Schlottmann PG, et al. 2004); however, within- and between-individual variability of the RNFL thickness measurement may ultimately limit the clinical utility of this modality. Equally so, a psychophysical test that is less dependent on pre-retinal factors may yield a truer reflection of retinal ganglion integrity.

3.7 Conclusion

A poor concordance was present between structural and functional progressive damage in OAG assessed using the TCA of the HRT II and the GPA of the HFA, respectively. It can be speculated that this is due to the three dissociating factors identified in this study. It may also arise from the failure of the TCA and the GPA criteria for progressive damage to account for disease severity and by the inappropriateness of ONH morphometry and measurement of differential light sensitivity as surrogate measures of retinal ganglion cell integrity. Such factors highlight the potential limitations of current techniques, and in particular CSLO and SAP, for the identification of progressive structural and functional damage in OAG.

Chapter 4: Novel approaches to glaucoma detection

4.1 Introduction

Since the widespread consensus that retinal ganglion cell damage precedes detectable functional damage, by conventional SAP in the earliest stages of OAG (Harwerth RS, et al. 2004, Kerrigan-Baumrind LA, et al. 2000, Quigley HA, et al. 1989), evaluation of the optic nerve head (ONH) and retinal nerve fiber layer (RNFL) has become the core of OAG management (American Academy of Ophthalmology 2000, European Glaucoma Prevention Study (EGPS) Group 2002, Gordon MO and Kass MA - The Ocular Hypertension Treatment Study Group 1999, Leske CM, et al. 1999, Musch DC, et al. 1997).

Subjective evaluation of the ONH is hampered by high within- and between-observer variability (Harper R, et al. 2000, Shuttleworth GN, et al. 2000, Tielsch J, et al. 1988, Varma R, et al. 1992, Zeyen T, et al. 2003). Similarly, the most widely used functional test in the management of OAG, namely SAP, is fraught with high within- and between-test variability and, as mentioned above, is relatively insensitive to early glaucomatous damage. Several alternative perimetric techniques, including; Frequency Doubling Technology (FDT) perimetry, Short Wavelength Automated Perimetry (SWAP) and High-Pass Resolution Perimetry (HRP), have shown promise in identifying OAG-specific functional abnormality (Bayer AU and Erb C 2002, Johnson CA, et al. 1993, Kalaboukhova L and Lindblom B 2003, Martin L, et al. 2003, Sample PA 2000, Spry PGD, et al. 2005). However, none of these tests have gained wide spread clinical acceptance.

4.1.1 Current clinical standards

With the advent of newer optical imaging technology, such as confocal scanning laser ophthalmoscopy (CSLO) and optical coherence tomography (OCT), assessment of the ONH and peripapillary morphometry has become more objective and quantitative. The current clinical standard for confocal scanning laser ophthalmoscopy, the HRT, is capable of producing highly reproducible, three-dimensional topographic images of the ONH (Chauhan BC, et al. 1994, Rohschneider K, et al. 1994, Zangwill L, et al. 1995). The HRT is clinically useful for the detection of OAG (Burgansky-Eliash Z, et al. 2007, Uchida H, et al. 1996, Wollstein G, et al. 1998) and progressive structural damage (Chauhan BC, et al. 2000, Chauhan BC, et al. 2001).

The current clinical standard for optical coherence tomography, the StratusOCT, yields cross-sectional, high-resolution images of the retinal cytoarchitecture that are highly reproducible (Budenz DL, et al. 2005, Paunescu LA, et al. 2004). The RNFL Thickness (3.4) Scan exhibits the highest level of diagnostic precision for glaucomatous damage of all of the StratusOCT scan protocols and is the current clinical standard protocol (Wollstein G, et al. 2004, Wollstein G, et al. 2005).

The multifocal visual evoked potential (mfVEP) has steadily gained acceptance as an objective method for topographical assessment of functional vision (Hasegawa S and Abe H 2001, Hood DC 2000, Klistorner AI and Graham SL 2000, Klistorner AI, et al. 1998). With refinements to the standard technique, such as inter-ocular comparisons (Graham SL, et al. 2000, Hood DC, et al. 2000) and signal-to-noise analyses (Klistorner AI and Graham SL 2001, Zhang X, et al. 2002), the mfVEP can accurately discriminate glaucomatous visual field loss (Goldberg I, et al. 2002, Graham SL, et al.

2005, Hood DC, et al. 2004). The mfVEP technique can also detect abnormalities in seemingly unaffected regions of the glaucomatous visual field (Hood DC, et al. 2004, Thienprasiddhi P, et al. 2003) and in persons with suspected OAG who manifest normal visual fields by SAP (Goldberg I, et al. 2002, Hood DC, et al. 2004, Klistorner AI and Graham SL 2000).

4.1.2 Limitations of previous studies

Traditionally, the diagnostic performance of new and emerging OAG diagnostic tests is compared with the most widely used method of functional assessment, namely SAP. This methodology poses a critical problem since any new test that is capable of detecting OAG prior to SAP will appear to yield a high false-positive rate and thus exhibit poor specificity for OAG. In addition, all but a few studies are confounded by the use of SAP as the diagnostic 'gold standard' used to define OAG (Bowd C, et al. 2001). Embracing current perspectives, it is justifiable to define OAG based solely on the appearance of the ONH, using the emerging 'gold standard' technique, digital stereoscopic imaging (DSI) (Morgan JE, et al. 2005).

No single study, to date, has investigated the diagnostic performance of the most promising structural and functional techniques, namely HRT III, StratusOCT and the mfVEP, in detecting early OAG in a single cohort, and referenced the outcome to DSI.

4.2 Study Aims

The aims of this study were fourfold. Firstly, to evaluate the diagnostic utility, in terms of sensitivity and specificity, of the current promising techniques to detect early OAG based solely on the appearance of the ONH using the current diagnostic gold standard, DSI. Secondly, to determine whether by combining structural and/or functional techniques the diagnostic precision for OAG of the promising techniques would be improved. Thirdly, to determine the agreement in the diagnostic outcome between the structural and/or functional techniques. Fourthly, to investigate the topographical relationship between structural and/or functional damage as assessed by these techniques.

4.3 Materials/Methods

This prospective cross-sectional study took place at the Cardiff Eye Unit in the Ophthalmology department at the University Hospital of Wales (UHW), Cardiff and at the School of Optometry and Vision Sciences at Cardiff University, Cardiff.

4.3.1 Cohort

In total, 23 patients with OAG (12 female, 11 male) and 20 normal individuals (14 female, 6 male) were recruited to the study. The mean age (±SD) of the OAG group was 67.3 (±11.2) years (range 46-85). The mean age of the normal individuals was 66.9 (±9.3) years (range 51-82).

The study had approval from the Central Office for Research Ethics Committees (COREC), London and the Cardiff and Vale NHS Trust, Research and Development committee. All participants had given written informed consent.

4.3.2 Inclusion criteria

The suitability of participants was determined prior to entry into the study in accordance with the following inclusion criteria: all participants exhibited a best-corrected visual acuity of 6/9 or better in the designated eye; a distance refractive error within the range of ±5.00 DS and ±2.50 DC; a crystalline lens appearance, graded according to the Lens Opacity Classification System (LOCS) III (Chylack LT, et al. 1993), not greater than nuclear colour (NC) 2.0, nuclear opalescence (NO) 2.0, cortical (C) 2.0 or posterior subcapsular (P) 1.0; no systemic medication known to affect the visual field; no history of diabetes mellitus and no history of ocular surgery in the designated eye. Patients with pigment dispersion symdrome and/or pseudoexfoliation syndrome were deemed unsuitable for the study.

Each participant underwent a detailed ophthalmologic examination including measurement of best-corrected visual acuity, Goldmann applanation tonometry (GAT), and measurement of central corneal thickness (CCT) and corneal radius with the Oculus Pentacam (Oculus, Inc., Lynwood, WA). All intra-ocular pressure (IOP) measurements were corrected for the effects of CCT (Ehlers N, et al. 1975). Gonioscopy was not performed.

Both eyes from each participant were examined. Suitable participants were classified either as normal or glaucomatous (early OAG or moderate/advanced OAG) on the

basis of their ONH appearance by DSI, alone. This procedure is described in further detail in the following section (Section 4.3.3).

In total, 20 normal, Caucasian individuals and 23 patients with OAG (22 Caucasian patients and 1 patient of African origin) were recruited into the study. Fifteen of the 23 OAG eyes were from patients with unilateral OAG. The remaining 8 eyes were from patients with bilateral OAG. All normal eyes used during the present study were obtained from individuals who exhibited a normal ONH appearance in both eyes. None of the patients had undergone laser refractive surgery.

The mean age, mean CCT, Goldmann IOP and cornea corrected IOP (cc-IOP) of the Normal, Early OAG and Moderate/Advanced OAG participants is given in Table 5.1.

Each participant underwent the schedule of appointments given in Table 4.2. The mean interval (±SD) between visits was 2.4 (±1.8) weeks (range 1-12 weeks). The mean duration (±SD) between visit 1 and visit 6 was 12.1 weeks (±4.9) weeks, (range 6-25 weeks).

	Normal (n=20)	Early OAG (n=15)	Moderate/Advanced OAG (n=8)
Gender (M:F)	6:14	9:6	2:6
Mean age ±SD (range) (years)	66.9 ±9.3 (31-82)	67.4 ±11.3 (46-85)	69.2 ±10.6 (58-83)
Mean CCT ±SD (range) (μm)	556.5 ±30.6 (497-615)	522.9 ±27.2 (477-576)	532.8 ±40.3 (473-605)
Mean IOP±SD (range) (mmHg)	15.5 ±3.6 (10-19)	21.8 ±5.2 (11-29)	18.0 ±4.1 (12-25)
Mean cc-IOP±SD (range) (mmHg)	14.6 ±3.1 (9-19)	22.1±5.5 (12-30)	19.8 ±4.4 (14-24)
Mean SAP MD±SD (range) (dB)	-0.3 ± 2.2 (-8.3 - 2.2)	-1.0± 1.5 (-3.6 - 0.8)	-3.0 ± 6.6 (-18.9 - 1.0)
Mean SAP PSD ±SD (range) (dB)	1.7 ± 0.8 (1.1 - 4.7)	2.3 ± 0.9 (1.3 - 3.9)	3.5 ± 3.7 (1.7 - 12.7)

Table 4.1 – *Gender, mean age, mean central corneal thickness (CCT), mean intra-ocular pressure (IOP) and mean cornea corrected IOP (cc-IOP) for the normal individuals and for the individuals with early and moderate/advanced OAG, repectively. Where appropriate, the IOPs and cc-IOPs indicate treated values.*

	Visit 1	Visit 2	Visit 3	Visit 4	Visit 5	Visit 6
Procedures	DSI	SAP HRT CCT Keratometry	mfVEP	OCT	SAP HRT	OCT
Mean duration post previous visit ±SD (range) (weeks)	-	2.7 ±1.5 (1-6)	2.5 ±1.8 (1-10)	2.3 ±2.5 (1-12)	2.7 ±1.8 (1-8)	1.9 ±1.4 (1-6)

Table 4.2 – *Visit schedule completed by all study participants*

4.3.3 Digital Stereoscopic ONH-imaging (DSI)

Sequential ONH stereo-photographs were obtained for both eyes of each particpant, after dilation of the pupil (Tropicamide, 0.5%), using a digital fundus camera (Topcon TRC 50EX, Topcon Medical Systems, Inc. [TMS], Paramus, NJ). During the procedure, the patient was seated in front of the camera with their chin and forehead in contact with the chin rest and forehead strap, respectively. The camera objective lens was brought to within approximately 15mm of the cornea and the patient was instructed to look at a fixation target attached to the camera. The image of the ONH, visible through the eyepiece of the camera, was centred and brought into sharp focus using the camera joystick. The image brightness was optimised using a rheostat and the patient was instructed to refrain from blinking and to keep their eye still for approximately 5 seconds. Two images of the ONH were captured in rapid succession with a small 10^0 separation in the viewing angle between the first and second images.

The two images were automatically transferred to a computer and displayed on a monitor using IMAGEnet^{TM} 2000 software (Version 2.1) (Topcon Medical Systems, Inc. [TMS], Paramus, NJ). A subjective assessment of the image quality was performed. Images that appeared out of focus, or, were under or over exposed were re-taken. Acceptable image pairs were saved to the hard-drive of the computer and copies of the images were transferred to a custom DSI software program (StereoDxResearch) on a stand-alone PC. Using a specialist graphics card (VX1 graphics card (3Dlabs, Milpitas, CA), a Z-Screen monitor overlay (StereoGraphics Corp., San Rafael, CA) and passive polarizing eyewear, StereoDxResearch enables an observer to view ONH image pairs simultaneously, thereby creating the perception of a single, three dimensional ONH stereo-image. The Digital stereo ONH images were reviewed by three expert observers (Mr James E Morgan [JEM], Mr Ian A Cunliffe [IAG] and Mr David Garway-Heath [DGH]), each trained to fellowship level in OAG. Observers were masked to the individual's identities and diagnoses. All images were independently graded by each observer on three separate occasions. An interval of at least one week was interleaved between each grading session. The three observers graded the digital stereoscopic ONH images as either normal, early OAG or moderate/advanced OAG at each of the three grading sessions in accordance with the following definitions:

A normal ONH appearance was defined as: an ONH exhibiting no evidence of structural abnormality to the neuroretinal rim, peripapillary RNFL and peripapillary retina and with no other characteristic associated with OAG.

Early OAG was defined as: an abnormal ONH appearance which, in the opinion of

the observer, would not yield corresponding glaucomatous visual field loss by SAP.

Moderate/advanced OAG was defined as: an abnormal ONH appearance which, in the opinion of the observer, would yield corresponding glaucomatous visual field loss by SAP. Each observer was also required to indicate the severity (based on an arbitrary scale between 1 [early] and 10 [advanced]), and location, of any apparent abnormality for each stereo ONH image designated as glaucomatous. Agreement in the topographic location of abnormality in, at least, two out of three observers was used to construct the final diagnosis (See Figure 4.1).

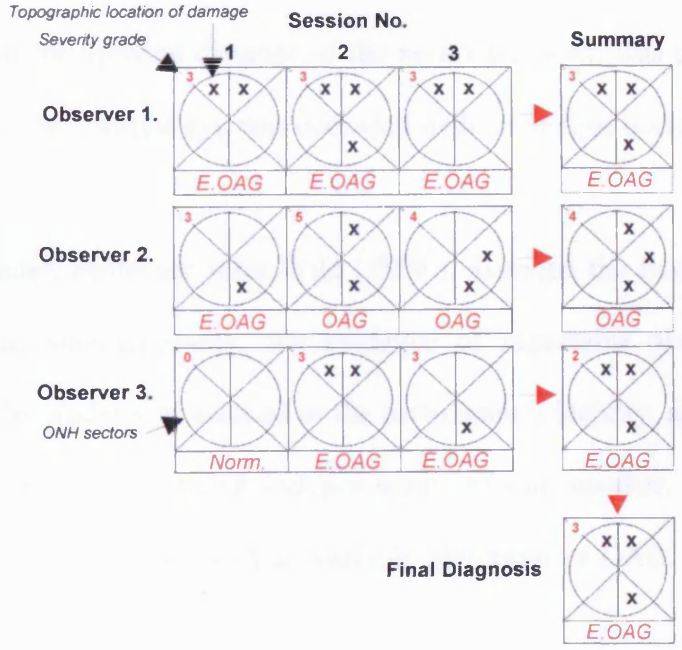

Figure 4.1 – *Flow diagram depicting the mechanism for establishing the diagnosis of each ONH (Norm. indicates normal, E.OAG indicates early OAG and OAG indicates moderate/advanced OAG).*

4.3.4 Standard Automated Perimetry (SAP)

Each individual underwent SAP using Program 24-2 and the SITA Standard algorithm of the Humphrey Field Analyzer (HFA) 750 (Carl Zeiss Meditec, Dublin, CA, USA) on two occasions. The mean interval (±SD) between SAP examinations was 7.5 (±3.4) weeks (range 3-15 weeks). Both eyes of each participant were examined on each occasion. All participants had undertaken at least one visual field examination by SAP prior to inclusion in the study. The HFA examination protocol was the same as described in Chapter 3, Section 3.3.4. The distance refractive correction, in the form of a full aperture trial lens, together with any near correction appropriate for the viewing distance of the perimeter bowl, was used during all SAP examinations. The non-test eye was occluded with an opaque occluder.

An expert grader, Professor John Wild (JMW), assessed the first and second visual field printouts, simultaneously, for evidence of repeatable abnormality for each participant. The grader was masked to the participant's identity, age and diagnosis by DSI. Fellow eyes were graded independently of one another. Visual fields were graded as: normal, variable normal, variable abnormal or OAG, in accordance with the following criteria:

The criterion for a normal visual field was defined as:

A pair of fields, each containing fewer than 3 non-adjacent locations, excluding locations adjacent to the blind spot and the upper locations corresponding to the upper lid region in Sectors 4 and 5 of the Glaucoma Hemifield Test (Asman P and Heijl A

1992) (Figure 4.2), which exhibited abnormality at the p<5% level and/or two or fewer non-adjacent locations in either hemifield exhibiting repeatable abnormality at the p<5% level.

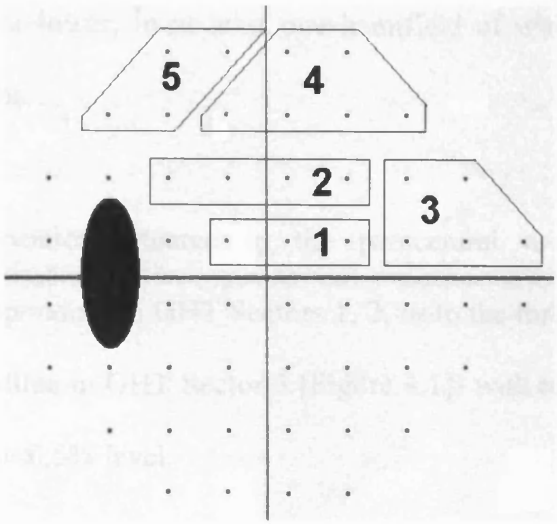

Figure 4.2 – *Distribution of sectors in the superior hemifield for the Glaucoma Hemifield Test (GHT). The distribution of GHT sectors is mirrored in the inferior hemifield.*

The criterion for a variable normal visual field was defined as:

A pair of fields, with at least one field containing more than 3 locations (excluding locations as above) exhibiting abnormal sensitivity at the p<5% level, or lower; and/or with two or fewer non-adjacent locations per hemifield, exhibiting repeatable abnormality at the p<5% level, or lower.

The criteria for a glaucomatous visual field were defined as fields exhibiting:

1). Three, or more, locations with repeatable abnormality at the $p<0.05$ level, or lower, in at least one hemifield of which two locations are adjacent.

2). One location situated in the paracentral or nasal step regions (corresponding to GHT Sectors 1, 2, or to the three locations closest to the midline in GHT Sector 3 [Figure 4.1]) with repeatable abnormality at the $p<0.5\%$ level.

3). Two or more locations situated in a cluster both with repeatable abnormality at the $p<1.0\%$ level, or lower; or, one location in the cluster with repeatable abnormality at the $p<0.05\%$ level and the remaining location at $p<2\%$ level, or lower.

4). Two or more locations situated in a cluster exhibiting repeatable abnormality, one of which is at the $p<1.0\%$ level, or lower, by Pattern Deviation probability analysis in the arcuate regions corresponding to the two locations in GHT Sector 3 farthest from the midline, and to the locations closest to the midline in GHT Sectors 4 and 5.

5). Three or more locations situated in a cluster exhibiting repeatable abnormality one of which is at the $p<2.0\%$ level, or lower, in the

arcuate regions corresponding to the two locations in GHT Sector 3 farthest from the midline, and to the locations closest to the midline in GHT Sectors 4 and 5.

Locations exhibiting apparent abnormality arising from the presence of obvious artefacts such as lens rim, upper lid contamination or seed point (i.e. those at 9°, 9° eccentricity) errors; and those locations immediately adjacent to the blind spot were not considered in the evaluation of the field.

In all categories, the adjacent locations could vertically straddle the division within GHT sector 3 and/or straddle either horizontally or vertically the adjacent sectors, but not straddle the horizontal midline.

4.3.5 Corneal curvature and corneal thickness assessment

Each participant underwent Oculus Pentacam assessment to determine the radius of corneal curvature (keratometry values) and central corneal thickness. The Oculus Pentacam uses a rotating Scheimpflug camera to obtain 3-D images of the anterior segment of the eye.

The patient was seated in front of the Oculus Pentacam with their chin on the chin rest and forehead in contact with the forehead restraint. The instrument was aligned in front of the eye using the joystick. The patient was instructed to fixate the centre of a blue light, visible within the instrument and to refrain from blinking for a period of approximately 3 seconds. The live Scheimpflug image, visible on the LCD screen of

the instrument assisted in aligning the instrument at the correct working distance from the anterior apical surface of the cornea. Once correctly aligned, the images were taken automatically. Image quality was assessed subjectively prior to saving to the hard drive. Poor quality images or those containing artifacts were retaken. Central corneal thickness measurement was used to calibrate the IOP measurements (Table 4.1). The corneal curvature measurement was used prior to acquisition of the HRT images (Section 4.3.6).

4.3.6 Confocal Scanning Laser Ophthalmoscopy (CSLO)

Each individual underwent confocal Scanning Laser Ophthalmoscopy (CSLO) using the HRT II (Version 1.4.1) on two occasions. The mean interval (±SD) between examinations was 7.2 (±4.3) weeks (range 3-20 weeks). Both eyes of each participant were scanned on each occasion.

Heidelberg Retina Tomograph images were obtained using the methodology described in Chapter 3, Section 3.3.3. In addition, a cylindrical lens correction was attached to the condensing lens system for patients with astigmatism ≥1.00 DC (Schuerle AF and Schmidt E 2004). Corneal curvature values obtained by Oculus Pentacam were input into the HRT II during the scan preparation (Section 4.3.5). In all but one of the scans, image quality was considered excellent according to the manufacturers guidelines (Mean SD = 17.9μm, SD ±5.8μm, Range 8-30μm). The slight reduction in image quality (SD 32μm) in the one case occurred due to the patient having a mild tremor.

The ONH margin contour line, defined as the inner edge of the scleral ring, was demarcated by a trained observer (CH) for all images used during the study. The topographical information from within the ONH margin contour was used to calculate the likelihood of glaucomatous optic neuropathy based upon the Moorfields Regression analysis (MRA) (Full description given in Chapter 1, Section 1.6.2). The HRT II images were exported to the HRT III analysis software (Version 3.0), when it became commercially available, using the export E2E option for analysis. Export E2E, facilitates the transfer of HRT data between compatible systems. The HRT III incorporates a larger and ethnicity-specific normative database than the HRT II, and comprises a database of 733 healthy Caucasian eyes and 215 healthy African American eyes. The MRA by HRT III is based upon this enlarged database.

Moorfields regression analyses on the first and second HRT scans, both for HRT II and III, were evaluated for evidence of repeatable abnormality at, or beyond, the 5% prediction limit based upon the distribution of expected values from the respective normative databases. Glaucomatous abnormality both by HRT II and HRT II MRAs were defined as repeatable abnormality within one or more disc sector/s at or below the 5% prediction limit.

4.3.7 Optical Coherence Tomography (OCT)

Each participant underwent RNFL thickness measurement and ONH topographic imaging using StratusOCT. Both eyes of each participant were examined on two occasions. The mean interval (±SD) between the first and second examinations was 7.2 (±3.1) weeks (range 3-17 weeks).

Each participant received Tropicamide (0.5%) to dilate the pupil prior to examination. Retinal nerve fibre layer thickness measurements were obtained using a commercially available StratusOCT, with the Standard RNFL (3.4) Scan protocol. During the scan acquisition, participants were seated with their chin on the chin rest and their forehead in contact with the forehead restraint. The scanning module was correctly aligned and the StratusOCT objective lens was adjusted for the participant's refractive error. The participant was instructed to fixate a target, which brought the ONH within view of the examiner on the real-time video window. The Z-offset and polarization were optimized to bring the OCT scan into view and to maximize the reflectivity of the signal, respectively. The aiming circle was adjusted so that the ONH was in the centre of the scan circumference. All StratusOCT scans were obtained by a single operator (CH). All scans used in the analysis were free from blink and eye movement artefacts, had a signal to noise ratio (SNR) of at least 33dB and had 100% of A-scans accepted.

Global and quadrant average RNFL thicknesses were automatically calculated for the first and second scan using the commercially available StratusOCT analysis software (Version 3.0).

The RNFL thickness data was analyzed using the RNFL thickness average analysis protocol of the standard StratusOCT software (Version 3.0). For each participant, RNFL thickness measurements were compared with the expected values based upon the StratusOCT normative database. Printouts were considered abnormal if they showed evidence of a repeatable abnormality beyond the 5% and/or 1% prediction limit based upon the distribution of expected RNFL thickness from a normal population.

4.3.8 Multifocal Visual Evoked Potential (mfVEP)

The Multifocal VEP was obtained using the Visual Evoked Response Imaging System (VERIS) Science, Version 5.1 (EDI, San Mateo, CA). Both eyes were examined, monocularly and a standard 60-sector dartboard stimulus was used to generate the evoked response. The stimulus was displayed on a 22-inch colour monitor (Mitsubishi Diamond Pro 2070SB, Mitsubishi Electric & Electronics, Cypress, CA), which had a refresh rate of 75Hz. The mfVEP stimulus consisted of 60 individual sectors each sector containing 16 checks, 8 white (102.0 cd/m2) and 8 black (2.1 cd/m2). The luminance of the stimulus was measured using a Minolta LS-110 luminance meter (Konica Minolta, Ramsey, NJ).

A single, vertical midline channel (Bipolar Occipital Straddle, BOS) was recorded for each participant. The active and reference electrodes were positioned 3cm above and 1cm below the inion, respectively. The ground electrode was attached to the forehead. The skin area for the electrode was prepared with Nuprep (D.O. Weaver & Co, Aurora, CO). Disposable, silver chloride coated plastic disc electrodes (Oxford Instruments, Surrey, UK) were then fixed in place using Ten20 conductive paste (D.O. Weaver & Co, Aurora, CO). Electrode impedance was measured prior to recording using a custom-made impedance meter and was maintained below 5kσ.

During the recording, the participant was seated in an armchair and encouraged to relax their neck and shoulders. The stimulus projection monitor was brought towards the patient to a working distance of 52cm. At this distance the stimulus subtended a

viewing angle of 25 degrees from fixation to the outermost edge of the stimulus. The distance refractive correction, in the form of a full aperture trial lens, together with any near correction appropriate for the viewing distance, was used during all mfVEP examinations. The non-test eye was occluded with an opaque patch. The stimulus was viewed through natural pupils. The contrast polarity of the stimulus was modulated temporally and controlled by a computer-driven binary m-sequence. The mfVEP recording was divided 16 segments each segment lasting 27.31 seconds. At the end of each segment, participants were allowed a brief rest period before the recording of the next segment began. On average, the mfVEP recording lasted between 8-10 minutes per eye. Signals were amplified (Grass model 15LT), band pass filtered from 3 to 30Hz, sampled at 1200Hz and notch filtered.

Multifocal VEPs within 16 discrete regions were averaged to improve the amplitude of the signals using the standard VERIS analysis software. The spatial distribution of these regions is shown in Figure 4.3. The raw data for the 16 responses was exported from VERIS. No spatial smoothing was applied to the data prior to the export. Additional data analyses were performed using commercially available software (Microsoft Excel; Microsoft Corporation, Redmond, WA). The root-mean-square (RMS) amplitude of a 'signal' and 'noise' window, between 45 to 150ms and 325 to 430ms, respectively, was calculated for each mfVEP waveform. The RMS signal-to-noise ratio (SNR) was determined by dividing the RMS of the signal by the RMS of the noise.

A standard analysis of inter-ocular mfVEP signal amplitude was undertaken by dividing the log RMS signal in the right eye with the log RMS signal in the left eye.

The observed values, in each of the 16 mfVEP sectors, were compared with the 95% confidence limits for the inter-ocular ratio of signal amplitudes, derived from a database of mfVEPs obtained both eyes of 30 normal age-matched individuals (13 males and 17 females) (mean age [±SD] 65.2 [±9.1] years, range 49-82 years). Probability plots, similar to HFA Total Deviation plots, were produced, whereby the colour of the mfVEP sector indicated which eye, left (blue) or right (red) was affected (see Figure 4.4). The saturation of the color indicated the level of significance of the difference between the observed value and value expected from the distribution normal values. Lighter colours were used to indicate abnormality, within any given sector, between the 5% and 1% prediction limit. Deeper colours were used to indicate abnormality, within any given sector, beyond the 1% prediction limit.

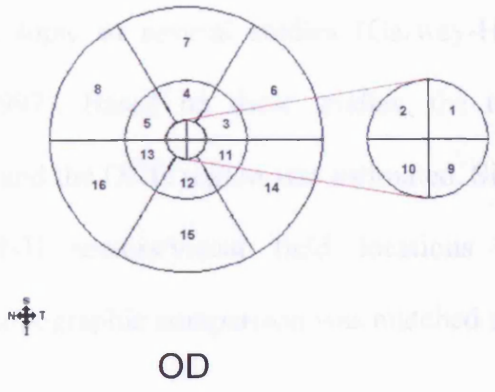

Figure 4.3 – The *spatial distribution of mfVEP responses*

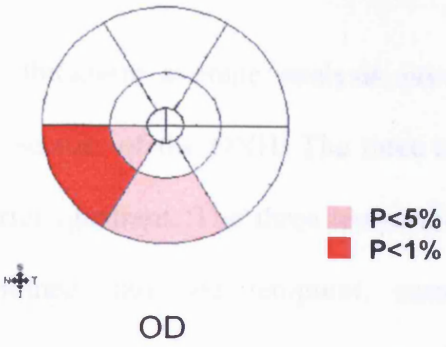

Figure 4.4 – *Multifocal VEP printout showing a nasal step defect in the right eye. The deeper colour indicates abnormality beyond the 1% prediction limit and the lighter colour indicates abnormality between the 5% and 1% prediction limits.*

4.3.9 Topographic correspondence

The topographic relationship between the region of the visual field and the region of the ONH has been the topic of several studies (Garway-Heath DF, et al. 2002, Yamagishi N, et al. 1997). Based on these studies, the topographic correlation between the visual field and the ONH region was estimated. Since the size and spatial distribution of the ONH sectors/visual field locations varied between each examination technique, topographic comparison was matched as closely as possible.

On DSI, the final diagnosis plot (Figure 4.1) reports summary findings of the ONH appearance as assessed by three expert observers. The superior-temporal and superior–nasal sectors and the inferior-temporal and inferior–nasal sectors were combined into superior and inferior quadrants, respectively. These quadrants were considered to be abnormal if either of the sectors was classified as abnormal by at least two out of the three observers. The temporal, superior, nasal and inferior quadrants were numbered 1 to 4, respectively, as shown in Figure 4.5a.

The StratusOCT RNFL thickness average analysis protocol displays the RNFL thickness for each of 12 sectors of the ONH. The three superior-most sectors were combined into one superior quadrant. The three temporal-, nasal- and inferior-most sectors were also combined into one temporal, nasal and inferior quadrant, respectively. Quadrants were considered to be abnormal if any of the three sectors was classified as abnormal at the 5% or 1% confidence limit. The temporal, superior, nasal and inferior quadrants were numbered 1 to 4, respectively, as shown in Figure 4.5b.

The Heidelberg Retina Tomograph II and III display MRA for each of 6 sectors of the ONH. The superior-temporal and superior-nasal sectors and the inferior-temporal and inferior-nasal sectors were combined into superior and inferior quadrants respectively. These quadrants were considered to be abnormal if either of the sectors was classified as abnormal or borderline. The temporal, superior, nasal and inferior quadrants were numbered 1 to 4, respectively, as shown in Figure 4.5c.

For the mfVEP print-out, the temporal sector of the ONH was considered to correspond to Sectors1, 2, 3, 9, 10 and 11 in right eye format and sectors 1, 2, 5, 9, 10 and 13 in left eye format i.e. the central-most 5^{o} of the visual field and the region corresponding to the papillomacular bundle. The nasal quadrant of the ONH was considered to correspond to Sectors 6 and 14 in right eye format and 8 and 16 in left eye format. The superior and inferior quadrants of the ONH were considered to correspond to the remaining sectors in the inferior and superior quadrants,

respectively. The mfVEP regions corresponding to the temporal, superior, nasal, and inferior ONH were numbered 1 to 4, respectively, and are shown in Figure 4.5d.

For Program 24-2 of the HFA, the temporal quadrant on the ONH was considered to correspond to the stimulus locations, above and below the midline, in GHT Sector 1. The nasal quadrant was considered to correspond to the four stimulus locations temporal to the blind spot. The superior and inferior quadrants of the ONH were considered to correspond to the remaining GHT Sectors in the inferior and superior hemifield, respectively. For consistency the upper most locations of GHT Sectors 4 and 5 in the superior hemifield, only, were excluded from the analysis (see Section 4.3.4). The regions of the visual field corresponding to the temporal, superior, nasal and inferior ONH were numbered 1 to 4, respectively, as shown in Figure 4.5e.

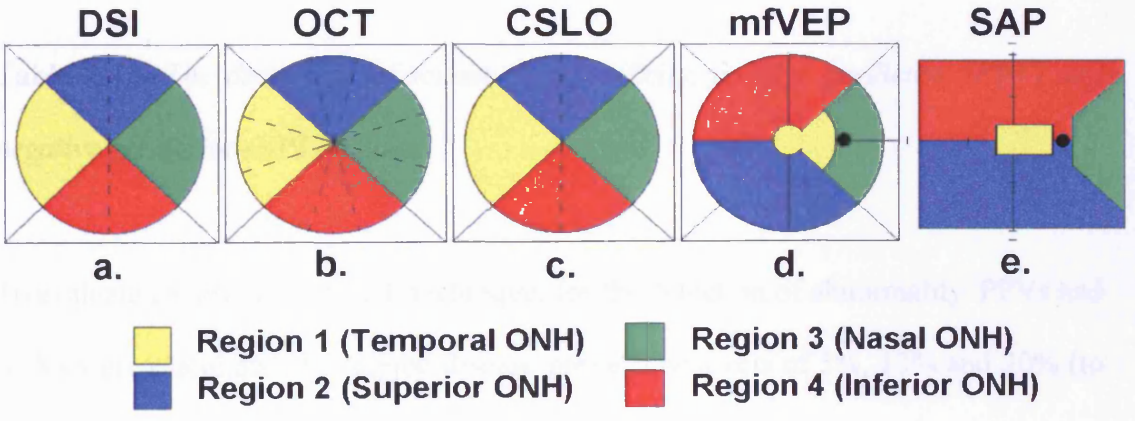

Figure 4.5*a-e* - *The topographic delineation of the results for each of the investigative techniques. DSI denotes digital stereoscopic ONH-imaging, OCT denotes Optical coherence Tomography, CSLO denotes Confocal Scanning Laser Ophthalmoscopy, mfVEP denotes multifocal Visual Evoked Potential and SAP denotes Standard Automated Perimetry.*

4.3.10 Analysis

The Sensitivity, specificity, positive predictive value (PPV) and negative predictive value (NPV) were calculated using conventional 2x2 contingency tables (Table 4.3).

		DSI		
		OAG*	Normal	
Examination	OAG	True Positive (TP)	False Positive (FP)	$PPV = \frac{TP}{(TP + FP)}$
	Normal	False Negative (FN)	True Negative (TN)	$NPV = \frac{TN}{(TN + FN))}$
		$Sens. = \frac{TP}{(TP + FN)}$	$Spec. = \frac{TN}{(FP + TN)}$	

OAG* includes participants with early OAG and patients with moderate/advanced OAG

Table 4.3 – *The derivation of sensitivity, specificity, positive predictive (PPV) and negative predictive (NPV) values.*

To evaluate the efficacy of each technique, for the detection of abnormality, PPVs and NPVs were calculated at assumed disease prevalence levels of 5%, 10% and 30% (to simulate populations at various levels of risk).

Positive (LR) and negative (LR) likelihood ratios were also calculated for each technique (Deeks JJ and Altman DG 2004). Specifically, the likelihood ratio is the probability of the specific test result in individuals who do have the disease compared to the probability of the specific test result in people who do not, expressed as a ratio. A likelihood ratio greater than 1 indicates that the test result is associated with the

presence of the disease, whereas a likelihood ratio less than 1 indicates that the test result is associated with the absence of disease.

4.4 Results

4.4.1 Agreement in clinical diagnosis by DSI

The cohort comprised 19 right eyes and 24 left eyes. Twenty eyes were designated as normal, 15 as early OAG and 8 as moderate/advanced OAG. The demographic characteristics of the groups are described in Table 4.1.

The agreement between observers in the clinical diagnosis is given in Table 4.4. A moderate level of agreement was present between JEM and DGH (Kappa = 0.61). A fair level of agreement was present between IAC and DGH (Kappa = 0.31) and between IAC and JEM (Kappa = 0.40).

		IAC vs. DGH	*IAC vs. JEM*	*JEM vs. DGH*
Kappa Statistic		0.31	0.40	0.61
Agreement (%)		69.8	73.2	81.4
SE		0.11	0.10	0.09
95% CI	Upper	0.53	0.60	0.78
	Lower	0.10	0.20	0.44

Table 4.4 - *Agreement rates in clinical diagnosis between the three observers: Mr David Garway-Heath (DGH), Mr Ian Cunliffe (IAC) and Mr James Morgan (JEM).*

The distribution of severity scores of the ONH provided by each observer is given in Figure 4.6 The mean severity score diagnosed by DGH, IAC and JEM, and was 4.1, 4.5 and 4.2, respectively. The median severity score for abnormal ONHs diagnosed by TGH, IAC and JEM was 4, 5 and 4, respectively. A Kolmogorov-Smirnov test of the data demonstrated that severity scores did not follow a normal distribution for any of the observers, and that no statistically significant difference in the distribution of the severity scores existed between any two observers (Table 4.5).

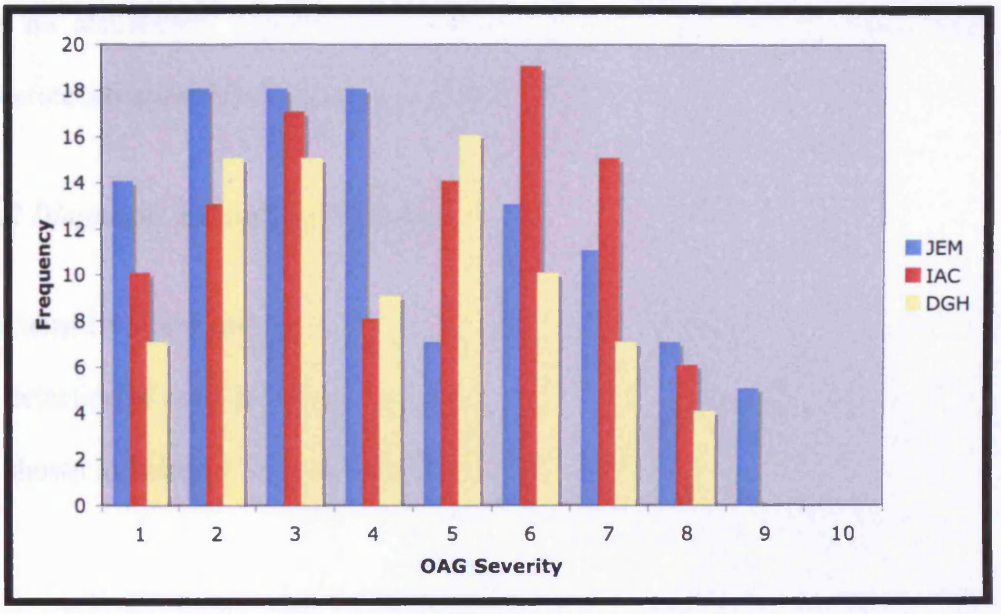

Figure 4.6 – *The distribution of severity scores for the three observers: Mr David Garway-Heath (DGH), Mr Ian Cuniliffe (IAC) and Mr James Morgan (JEM).*

	IAC vs. DGH	*IAC vs. JEM*	*JEM vs. DGH*
Maximum difference between cumulative distributions, D	*0.16 (p =0.16)*	*0.14 (p =0.22)*	*0.10 (p =0.68)*

Table 4.5 – *The results of the Kolmogorov-Smirnov test to identify differences in the distribution of severity scores between observers*

The SAP visual field Mean Deviation (MD) and Pattern Standard Deviation (PSD) values for the normal, early OAG and moderate/advanced OAG groups are given in Table 4.1. A students T-Test revealed that there was no statistically significant difference in the MD between the normal group and the group with early OAG (p=0.23), for the normal and moderate/advanced OAG groups (p=0.11) and for the early OAG and moderate/advanced OAG (p=0.28) groups. The difference in mean PSD statistically significant between the normal and early OAG groups (p=0.046) and between the normal and moderate/advanced OAG groups (p=0.045). However, there was no statistically significant difference in PSD between the early OAG and moderate/advanced OAG groups (p=0.23).

4.4.2 Diagnostic precision of techniques

The sensitivity and specificity of OCT, CSLO (HRT II and III), mfVEP and SAP for the detection of early OAG, moderate/advanced OAG and for both groups, combined, are shown in Tables 4.6a, 4.6b and 4.6c, respectively.

Early OAG (n=15)	OCT	CSLO II	CSLO III	mfVEP	SAP
Sensitivity (%)	**40.0**	**73.3**	**86.7**	**66.7**	**40.0**
Specificity (%)	**95.0**	**80.0**	**65.0**	**60.0**	**95.0**
PPV	0.86	0.73	0.65	0.56	0.86
PPV (5%)	0.26	0.16	0.12	0.08	0.30
PPV (10%)	0.47	0.29	0.22	0.16	0.47
PPV (30%)	0.77	0.61	0.51	0.42	0.77
NPV	0.68	0.80	0.87	0.71	0.68
NPV (5%)	0.08	0.13	0.20	0.09	0.08
NPV (10%)	0.15	0.25	0.35	0.17	0.15
NPV (30%)	0.40	0.56	0.68	0.44	0.40
PLR	8.00	3.67	2.47	1.67	8.00
NLR	0.63	0.33	0.21	0.56	0.63

Table 4.6a – *Sensitivity, specificity, positive predictive value (PPV) (at 5, 10 and 30% prevalence), negative predictive value (NPV) (at 5, 10 and 30% prevalence), positive likelihood ratio (PLR) and negative likelihood ratio (NLR) for Optical Coherence Tomography (OCT), Confocal Scanning Laser Ophthalmoscopy (CSLO II using the Heidelberg Retina Tomograph II and CSLO III using the Heidelberg Retina Tomograph III), multifocal Visual Evoked Potential (mfVEP) and Standard Automated Perimetry (SAP) for the early OAG group (n=15).*

Moderate/Advanced OAG (n=8)	OCT	CSLO II	CSLO III	mfVEP	SAP
Sensitivity (%)	**50.0**	**87.5**	**100.0**	**75.0**	**62.5**
Specificity (%)	**95.0**	**80.0**	**65.0**	**60.0**	**95.0**
PPV	0.80	0.64	0.53	0.43	0.83
PPV (5%)	0.34	0.19	0.13	0.09	0.40
PPV (10%)	0.53	0.33	0.24	0.17	0.58
PPV (30%)	0.81	0.65	0.55	0.45	0.84
NPV	0.83	0.94	1.00	0.85	0.86
NPV (5%)	0.09	0.25	1.00	0.11	0.12
NPV (10%)	0.17	0.42	1.00	0.21	0.22
NPV (30%)	0.45	0.73	1.00	0.51	0.52
PLR	10.00	4.38	2.86	1.88	12.5
NLR	0.52	0.16	0	0.41	0.39

Table 4.6b – *Sensitivity, specificity, positive predictive value (PPV) (at 5, 10 and 30% prevalence), negative predictive value (NPV) (at 5, 10 and 30% prevalence), positive likelihood ratio (PLR) and negative likelihood ratio (NLR) for Optical Coherence Tomography (OCT), Confocal Scanning Laser Ophthalmoscopy (CSLO II using the Heidelberg Retina Tomograph II and CSLO III using the Heidelberg Retina Tomograph III), multifocal Visual Evoked Potential (mfVEP) and Standard Automated Perimetry (SAP) for the moderate/advanced OAG group (n=8).*

Combined OAG Groups (n=23)	OCT	CSLO II	CSLO III	mfVEP	SAP
Sensitivity (%)	**43.5**	**78.2**	**91.3**	**69.6**	**47.8**
Specificity (%)	**95.0**	**80.0**	**65.0**	**60.0**	**95.0**
PPV	0.91	0.82	0.75	0.67	0.92
PPV (5%)	0.31	0.17	0.12	0.08	0.29
PPV (10%)	0.49	0.30	0.22	0.16	0.47
PPV (30%)	0.79	0.63	0.53	0.43	0.77
NPV	0.59	0.76	0.86	0.63	0.61
NPV (5%)	0.08	0.16	0.28	0.37	0.07
NPV (10%)	0.16	0.29	0.45	0.18	0.15
NPV (30%)	0.42	0.61	0.76	0.46	0.40
PLR	8.70	3.91	2.61	1.74	7.83
NLR	0.59	0.27	0.13	0.51	0.55

Table 4.6c – *Sensitivity, specificity, positive predictive value (PPV) (at 5, 10 and 30% prevalence), negative predictive value (NPV) (at 5, 10 and 30% prevalence), positive likelihood ratio (PLR) and negative likelihood ratio (NLR) for Optical Coherence Tomography (OCT), Confocal Scanning Laser Ophthalmoscopy (CSLO II using the Heidelberg Retina Tomograph II and CSLO III using the Heidelberg Retina Tomograph III), multifocal Visual Evoked Potential (mfVEP) and Standard Automated Perimetry (SAP) for the early and moderate/advanced OAG groups combined (n=23).*

Optical Coherence Tomography with the StratusOCT detected abnormality in early OAG eyes with a sensitivity and specificity of 40.0% and 95.0%, respectively (Table 4.6a). It detected abnormality in moderate/advanced OAG eyes with a sensitivity and specificity of 50.0% and 95.0%, respectively (Table 4.6b). When the early OAG and moderate/advance OAG groups were combined, the sensitivity and specificity was 43.5% and 95.0%, respectively (Table 4.6c).

Confocal Scanning Laser Ophthalmoscopy with the HRT II detected abnormality in early OAG eyes with a sensitivity and specificity of 73.0% and 80.0%, respectively (Table 4.6a). It detected abnormality in moderate/advanced OAG eyes with a sensitivity and specificity of 87.5% and 80.0%, respectively (Table 4.6b). When the early OAG and moderate/advanced OAG groups were combined, the sensitivity and specificity was 78.2% and 80.0%, respectively (Table 4.6c).

Confocal Scanning Laser Ophthalmoscopy with the HRT III detected abnormality in early OAG eyes with a sensitivity and specificity of 86.6% and 65.0%, respectively (Table 4.6a). It detected abnormality in moderate/advanced OAG eyes with a sensitivity and specificity of 100.0% and 65.0%, respectively (Table 4.6b). When the early OAG and moderate/advanced OAG groups were combined, the sensitivity and specificity was 91.3% and 65.0%, respectively (Table 4.6c).

The mfVEP with the VERIS detected abnormality in early OAG eyes with a sensitivity and specificity of 66.7% and 60.0%, respectively (Table 4.6a). It detected abnormality in moderate/advanced OAG eyes with a sensitivity and specificity of 75.0% and 60.0%, respectively (Table 4.6b). When the early OAG and

moderate/advanced OAG groups were combined, the sensitivity and specificity was 69.6% and 60.0%, respectively (Table 4.6c).

Standard Automated Perimetry with the HFA detected abnormality in early OAG eyes with a sensitivity and specificity of 40% and 95%, respectively (Table 4.6a). It detected abnormality in moderate/advanced OAG eyes with a sensitivity and specificity of 62.5% and 95.0%, respectively (Table 4.6b). When the early OAG and moderate/advanced OAG groups were combined, the sensitivity and specificity was 47.8% and 95%, respectively (Table 4.6c).

The highest PPV was achieved by SAP (0.92) for the early OAG and moderate/advanced OAG groups (Table 4.6c). The lowest PPV was achieved by mfVEP (0.43) in individuals with moderate/advanced OAG (Table 4.6b). The highest NPV was achieved with the CSLO (1.00) in individuals with moderate/advanced OAG (Table 4.6b). The lowest PPV was achieved by OCT (0.43) for the group with early OAG or moderate/advanced OAG (Table 4.6c).

The highest PLR was achieved by SAP for the moderate/advanced OAG group whereby a positive SAP result (i.e. visual field loss) increase the odds of having OAG by 12.5 times (Table 4.6b). The lowest PLR was achieved by mfVEP for the early OAG group whereby an abnormal mfVEP response increases the odds of having OAG by 1.67 times. The lowest (best) NLR was achieved by CSLO using HRT III for the moderate/advanced OAG group whereby a negative result seemingly excludes the disease. The highest (worst) NLR was achieved by SAP and OCT equally, for the

early OAG group, such that a negative test result reduced the odds of having OAG by only 0.63 times.

4.4.3 Combining techniques

The diagnostic precision of two tests combined, when a positive result by both tests was required to detect abnormality, is given in Table 4.7a. Under these conditions, the specificity for the detection of OAG is generally higher; however, the observed levels of sensitivity are lower. The best overall combination of tests was observed using the HRT II MRA and the HRT III MRA. In cases where either of these tests yielded an abnormal result the sensitivity and specificity for OAG was 78.3% (in early and moderate/advanced groups combined) and 85%, respectively.

The diagnostic precision of two tests combined, when a positive result by either test was required to detect abnormality, is given in Table 4.7b. Under these conditions the sensitivity for the detection of OAG is generally higher; however, the observed levels of specificity are lower. The best overall combination of tests was OCT and CSLO with the StratusOCT and the HRT II MRA, respectively. In cases where either of these tests yielded an abnormal result the sensitivity and specificity for OAG was 82.6% (in early and moderate/advanced groups combined) and 80.0%, respectively.

Abnormal by test 1 AND test 2	Specificity (%)	Sensitivity (%)		
		Early OAG (n=15)	Moderate/ Advanced OAG (n=8)	Combined OAG groups (n=23)
OCT and CSLO II	95.0	40.0	37.5	39.1
OCT and CSLO III	100.0	40.0	50.0	43.5
OCT and mfVEP	100.0	20.0	37.5	26.1
OCT and SAP	100.0	26.7	25.0	26.1
CSLO II and CSLO III	85.0	73.3	87.5	78.3
CSLO II and mfVEP	95.0	46.7	62.5	52.2
CSLO II and SAP	100.0	33.3	37.5	34.8
CSLO III and mfVEP	90.0	60.0	75.0	65.2
CSLO III and SAP	95.0	33.3	37.5	34.8
mfVEP and SAP	100.0	26.7	25.0	26.1

Table 4.7a – *The sensitivity and specificity of combinations of two techniques in OAG based upon an abnormal result with both tests.*

Abnormal by test 1 OR test 2	Specificity (%)	Sensitivity (%)		
		Early OAG (n=15)	Moderate/ Advanced OAG (N=8)	Combined OAG groups (N=23)
OCT and CSLO II	80.0	73.3	100.0	82.6
OCT and CSLO III	60.0	86.7	100.0	91.3
OCT and mfVEP	55.0	86.7	87.5	87.0
OCT and SAP	90.0	53.3	75.0	60.9
CSLO II and CSLO III	60.0	86.7	100.0	91.3
CSLO II and mfVEP	45.0	93.3	100.0	95.7
CSLO II and SAP	75.0	80.0	87.5	82.6
CSLO III and mfVEP	35.0	93.3	100.0	95.7
CSLO III and SAP	65.0	93.3	100.0	95.7
MfVEP and SAP	55.0	80.0	87.5	82.6

Table 4.7b – *The sensitivity and specificity of combinations of two techniques in OAG based upon an abnormal result by one of the two tests.*

4.4.4 Rates of agreement between tests

The agreement between tests in detecting abnormality in normal individuals (false-positives), in early OAG and in moderate/advanced OAG are shown in Figure 4.7, Figure 4.8 and Figure 4.9, respectively. The percentage agreement, Kappa statistic and standard error between test outcomes in normal individuals and in early OAG, in moderate/advanced OAG and in the two groups OAG, combined, are given in Tables 4.8a, 4.8b, 4.8c and 4.8d, respectively.

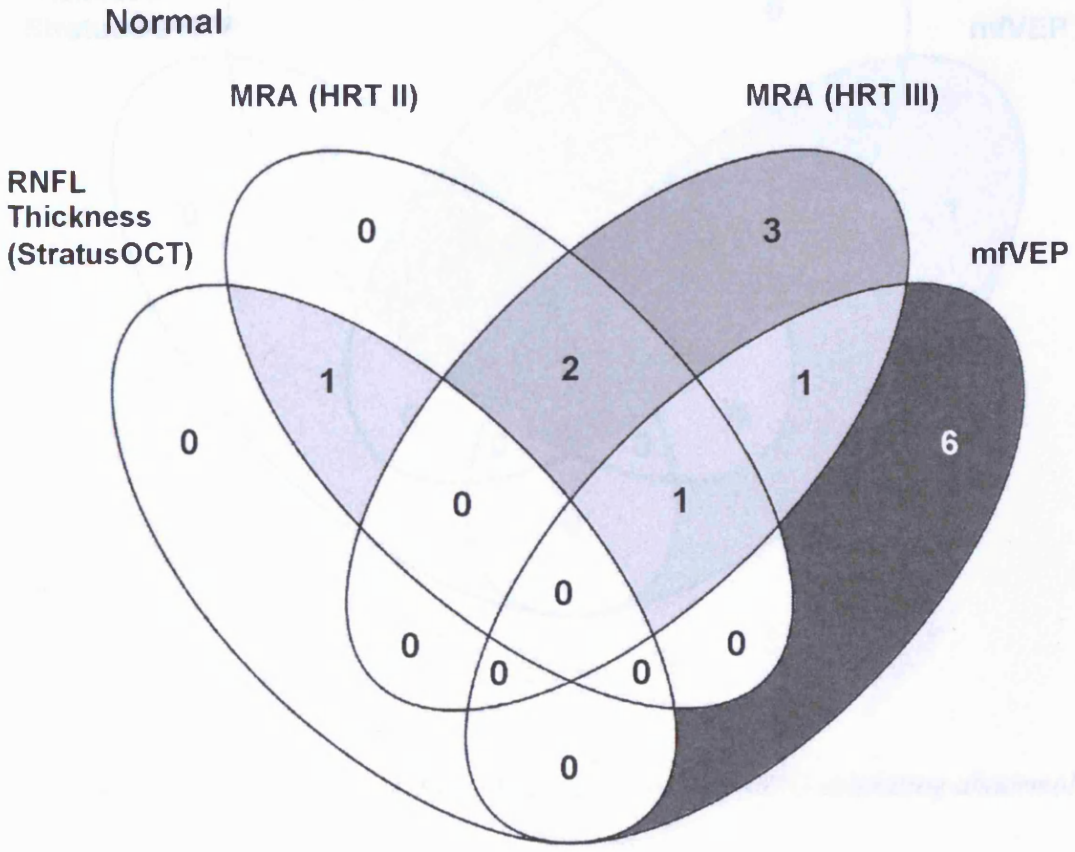

Figure 4.7 *– The number of the 20 normal individuals exhibiting abnormality with the given investigative technique.*

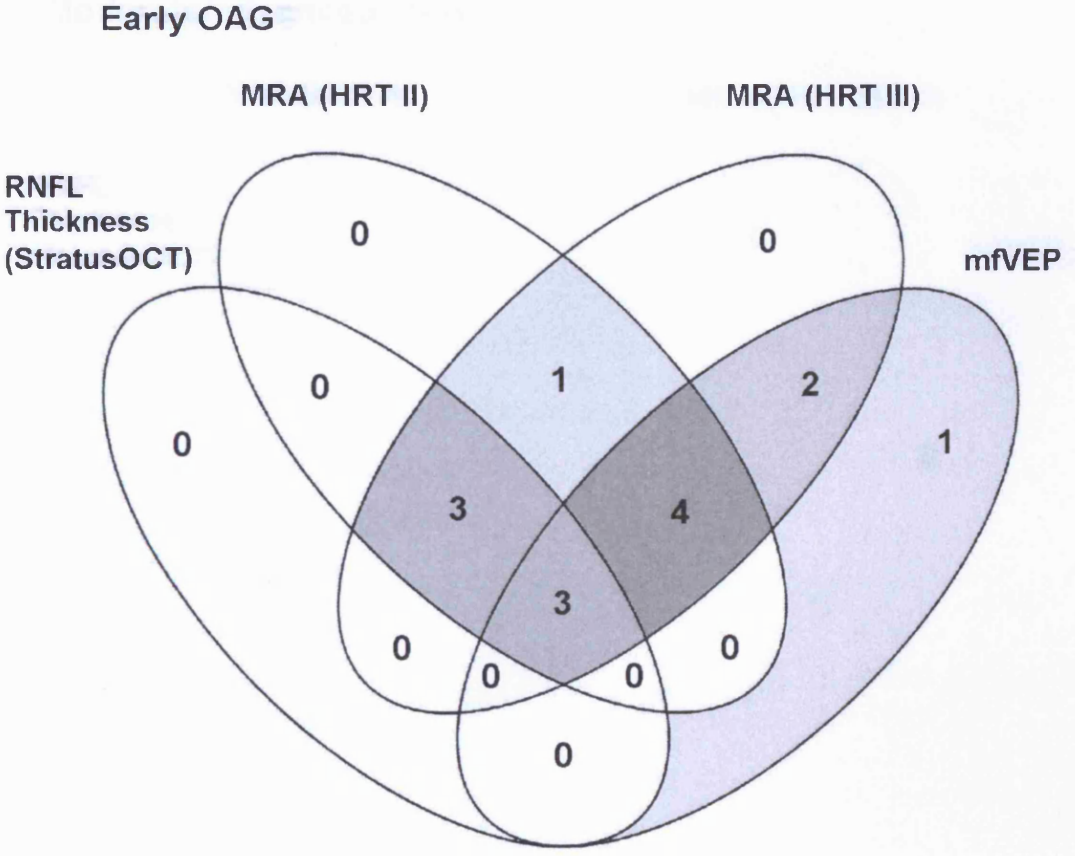

Figure 4.8 *– The number of the 15 individuals with early OAG exhibiting abnormality with the given investigative technique.*

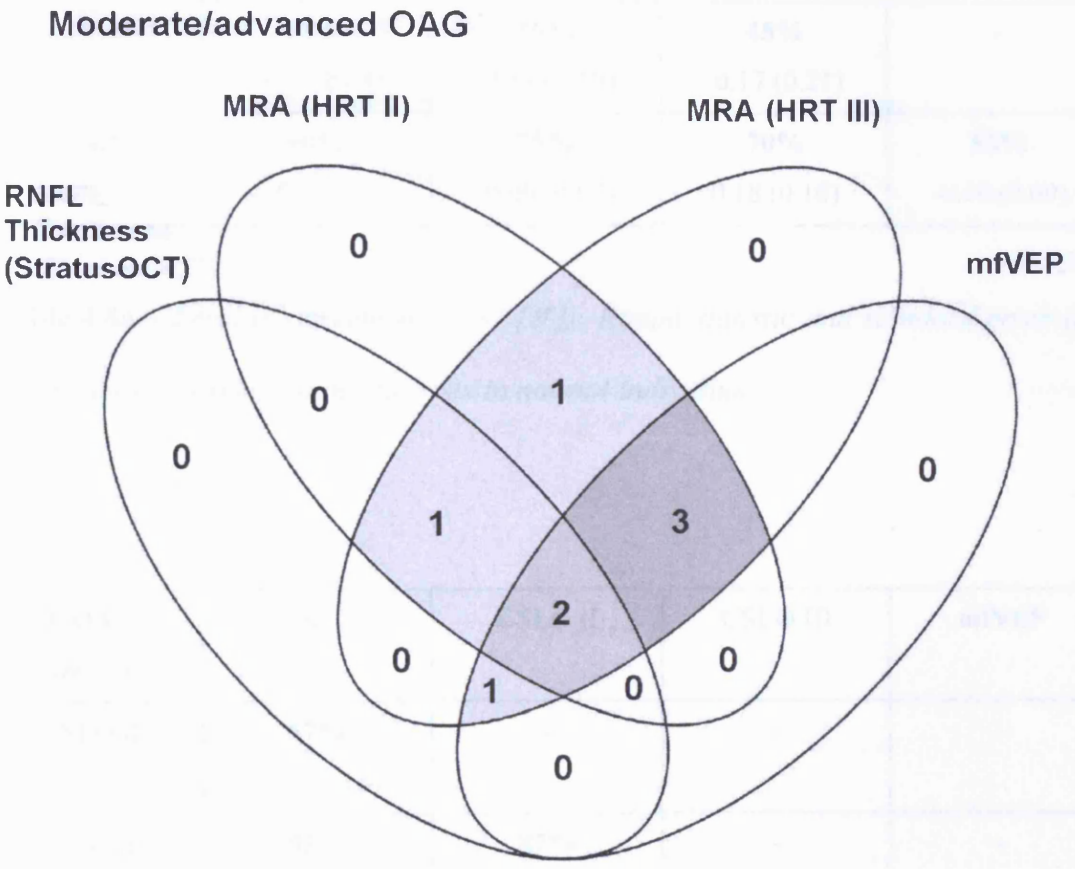

Figure 4.9 *– The number of the 8 individuals with moderate/advanced OAG exhibiting abnormality with the given investigative technique.*

Normal (n=20)	OCT	CSLO II	CSLO III	mfVEP
CSLO II	**85%** 0.35 (0.26)	-	-	-
CSLO III	**60%** -0.10 (0.09)	**75%** 0.39 (0.21)	-	-
mfVEP	**55%** -0.10 (0.09)	**50%** -0.14 (0.19)	**45%** -0.17 (0.21)	-
SAP	**90%** -0.05 (0.04)	**75%** -0.09 (0.07)	**70%** 0.18 (0.16)	**55%** -0.10 (0.09)

Table 4.8a – *Level of agreement (bold [%]), Kappa statistic and standard error (in parentheses) between diagnostic tests in normal individuals.*

E.OAG (n=15)	OCT	CSLO II	CSLO III	mfVEP
CSLO II	**67%** 0.39 (0.18)	-	-	-
CSLO III	**53%** 0.19 (0.13)	**87%** 0.60 (0.24)	-	-
mfVEP	**33%** -0.25 (0.23)	**53%** -0.10 (0.24)	**67%** 0.12 (0.24)	-
SAP	**73%** 0.44 (0.24)	**53%** 0.15 (0.20)	**40%** -0.05 (0.16)	**47%** 0 (0.22)

Table 4.8b – *The level of agreement (bold [%]), Kappa statistic and Standard Error (in parentheses) between diagnostic tests in the individuals with early OAG.*

M/A. OAG (n=8)	OCT	CSLO II	CSLO III	mfVEP
CSLO II	**38%** -0.25 (0.23)	-	-	-
CSLO III	**50%** 0.00 (0.00)	**88%** 0.00 (0.00)	-	-
mfVEP	**50%** 0.00 (0.31)	**75%** 0.33 (0.38)	**75%** 0.00 (0.00)	-
SAP	**63%** 0.25 (0.33)	**50%** 0.16 (0.16)	**38%** 0.00 (0.00)	**33%** -0.13 (0.24)

Table 4.8c – *The level of agreement (bold [%]), Kappa statistic and Standard Error (in parentheses) between diagnostic tests in the individuals with moderate/advanced (M/A.) OAG.*

OAG Combined (n=23)	OCT	CSLO II	CSLO III	mfVEP
CSLO II	**57%** 0.19 (0.15)	-	-	-
CSLO III	**52%** 0.14 (0.10)	**87%** 0.51 (0.23)	-	-
mfVEP	**39%** -0.16 (0.18)	**61%** 0.04 (0.21)	**70%** 0.10 (0.18)	-
SAP	**70%** 0.37 (0.20)	**52%** 0.15 (0.14)	**39%** -0.03 (0.10)	**42%** -0.06 (0.17)

Table 4.8d – *The level of agreement (bold [%]), Kappa statistic and Standard Error (in parentheses) between diagnostic tests in all individuals with OAG.*

4.4.5 Topographic correspondence of abnormality

The topographic correspondence of abnormality was determined between each of the diagnostic techniques for individuals classified as early OAG and for individuals classified as moderate/advanced OAG and for both groups of patients combined. The rates of agreement between techniques are given in Table 4.9

In eyes with early OAG, the best topographic correspondence with the diagnostic standard DSI was achieved by CSLO using the HRT III (80%). The worst topographic correspondence was for SAP using the HFA (13.3%) and the mfVEP using VERIS (13.3%), equally.

In eyes with moderate/advanced OAG, the best topographic correspondence with the diagnostic standard DSI was achieved by CSLO using the HRT III (100%). The worst topographic correspondence was for SAP using the HFA (25%).

In eyes with early OAG or moderate/advanced OAG, combined, the best topographic correspondence of abnormality with the diagnostic standard DSI was achieved by CSLO using the HRT III (87%). The worst topographic correspondence was for SAP using the HFA (17.4%).

Agreement between:	**E.OAG (%)** (n=15)	**M/A. OAG (%)** (n=8)	**Combined (%)** (n=23)
DSI and OCT	33.3	37.5	34.8
DSI and CSLO II	66.7	87.5	73.9
DSI and CSLO III	80.0	100.0	87.0
DSI and mfVEP	13.3	37.5	21.7
DSI and SAP	13.3	25.0	17.4
OCT and CSLO II	40.0	37.5	39.1
OCT and CSLO III	40.0	37.5	39.1
OCT and mfVEP	13.3	0	8.7
OCT and SAP	20.0	12.5	17.4
CSLO II and CSLO III	73.3	87.5	78.3
CSLO II and mfVEP	26.7	12.5	21.7
CSLO II and SAP	26.7	37.5	30.4
CSLO III and mfVEP	26.7	12.5	21.7
CSLO III and SAP	26.7	37.5	30.4
mfVEP and SAP	13.3	12.5	13.0

Table 4.9 – *The agreement in the topographical location of abnormality between the 4 techniques in individuals with early OAG, in individuals with moderate/advanced OAG and for the two groups combined.*

4.5 Discussion

Subjective evaluation of stereoscopic ONH images is the 'gold standard' technique for detecting structural damage (American Academy of Ophthalmology 2000, European Glaucoma Prevention Study (EGPS) Group 2002, Gordon MO and Kass MA - The Ocular Hypertension Treatment Study Group 1999). The natural development of stereoscopic ONH imaging and thus the emerging 'gold standard' is digital stereoscopic ONH imaging (DSI) (Morgan JE, et al. 2005). Since the consensus, that in OAG structural damage precedes functional damage by SAP (Harwerth RS, et al. 2004, Kerrigan-Baumrind LA, et al. 2000, Quigley HA, et al. 1989), several techniques that are sensitive to structural changes to the ONH and peripapillary retina have shown promise in the detection of the disease. Two of the most promising of these techniques, namely CSLO and OCT, that measure structural aspects of ONH morphometry and RNFL thickness, respectively, have been shown to detect structural abnormalities in glaucomatous patients with visual field loss by SAP (Burgansky-Eliash Z, et al. 2007, Danesh-Meyer HV, et al. 2006, Naithani P, et al. 2007, Pueyo V, et al. 2007, Sihota R, et al. 2006). However, the detection of OAG in patients without visual field loss presents a much greater diagnostic challenge and the use of these imaging techniques in this type of OAG is less well documented. The mfVEP technique has also demonstrated clinical utility in detecting functional deficits in patients with OAG manifesting visual field loss by SAP (Graham SL, et al. 2005, Hood DC, et al. 2000, Hood DC, et al. 2004) and in patients with OAG without visual field loss (Hood DC, et al. 2003, Thienprasiddhi P, et al. 2003).

This study is the first to determine the diagnostic performance of the current state-of-the-art techniques for detecting OAG in a single study cohort who were classified

solely according to the emerging 'gold standard' technique, DSI. The results of this study demonstrate the various diagnostic performances of OCT, CSLO, mfVEP and SAP in their respective ability to detect OAG.

This study has also demonstrated the various diagnostic capabilities of techniques used in combination, as well as the levels of agreement between tests and the level topographical correspondence of abnormality.

4.5.1 Diagnostic Precision

Sensitivity

In early OAG, in moderate/advanced OAG and for both groups combined, CSLO using the HRT III MRA exhibited the highest levels of sensitivity for OAG. In early OAG, moderate/advanced OAG and combined groups HRT III MRA yielded sensitivities of 86.7%, 100% and 91.3%, respectively, with a specificity of 95% in all groups. The lowest sensitivity was OCT of the RNFL using the StratusOCT (40%) and for SAP using the HFA (40%) in the early OAG group. In the combined group, the HRT II MRA (78.2%), the HRT III MRA (91.3%) and the mfVEP (69.6%) technique each exhibited sensitivity for glaucomatous abnormality exceeding that of the HFA (47.8%). This finding may indicate that these techniques are capable of detecting glaucomatous damage before it can be detected as visual field loss by SAP.

The sensitivity of StratusOCT RNFL thickness measurements to detect OAG is lower than reported in other studies (Balachandran C, et al. 2006, Hougaard JL, et al. 2007, Medeiros FA, et al. 2006, Naithani P, et al. 2007). However, this discrepancy can be

explained in one of two ways. Firstly, since the analysis of StratusOCT RNFL thickness measurements in this study was based solely on the normative database of RNFL thickness values employed by the commercially available StratusOCT, rather than using a LDF of the best diagnostic parameters, it may be the case that, due to the wide inherent variation in RNFL thickness, the confidence intervals yielded by the StratusOCT normative data are, in fact, too wide to detect OAG accurately. In addition, the fact that the StratusOCT RNFL thickness average protocol takes no account of the between individual differences in ONH size, which has been shown to result in relative under- and overestimation of RNFL thickness in small and large ONHs, respectively (Medeiros FA, et al. 2006) may be a confounding limitation of the StratusOCT RNFL thickness average analysis protocol. A second explanation relates to the fact that all diagnostic tests tend to be more sensitive in advanced stages of the disease and that measures of diagnostic precision obtained from studies that include patients with moderate or severe OAG may not be applicable to patients in the early stages of the OAG or OAG suspects (Medeiros FA, et al. 2006, Ransohoff DF and Feinstein AR 1978). In the present study, a relatively large proportion of patients (15 of 23) presented with what are believed to be the 'earliest' detectable signs of OAG according to the emerging 'gold standard', DSI. Thus, the relatively low sensitivity of StratusOCT to detect OAG may represent differences in the distribution of OAG severity between the present study and other recent studies (Hougaard JL, et al. 2007, Medeiros FA, et al. 2006, Parikh RS, et al. 2007, Pueyo V, et al. 2007). A recent study investigating the diagnostic capability of StratusOCT based on RNFL thickness in patients with OAG without visual field loss (Kim TW, et al. 2007), showed sensitivity and specificity of $\leq$40.8% and $\leq$100%, which is more consistent with the values observed in this study.

Despite yielding only moderately levels of sensitivity (69.6%, in early and moderate/advanced groups combined), the mfVEP technique appeared to be more sensitive for OAG than SAP (47.8%, in early and moderate/advanced groups combined). Previous studies investigating the mfVEP have reported sensitivities of 29% (Fortune B, et al. 2007) and 80.9% (Graham SL, et al. 2005) in patients with OAG without visual field loss. Thus, the observed sensitivity of the mfVEP is in agreement with these earlier reports. The low sensitivity of SAP (47.8%, in early and moderate/advanced groups combined) is not surprising considering the stage of OAG exhibited by a majority of the individuals.

It has been speculated that the mfVEP and SAP may be detecting slightly different functional deficits in OAG (Fortune B, et al. 2007). This may, in part, be responsible for the poor level of agreement (33-55%) shown between the mfVEP and SAP in the present study. The fact that the mfVEP outperformed SAP, in terms of sensitivity, and that the two techniques agreed in only 33% to 55% of cases, suggests that the mfVEP detects abnormality that SAP is missing and vice versa. This may arise due to differences in the spatial sampling of the visual field used by each technique or due to the variability in SNR that exists between patients and within the visual field.

Specificity

In all analyses (early OAG, moderate/advance OAG and the two groups combined), RNFL thickness by OCT and differential light sensitivity by SAP exhibited joint highest specificity (95%) for OAG of all of the techniques used. The lowest specificity was exhibited by the mfVEP using VERIS (60%) and the CSLO using the HRT III MRA (65%) (Figure 4.6). An explanation for the apparent lack of specificity

of mfVEP is presented later; however, the lack of specificity exhibited by HRT III MRA is also noteworthy since the MRA represents one of the most sophisticated analysis techniques for the detection of OAG.

The HRT III MRA outperformed the HRT II MRA with respect to sensitivity for OAG, although the HRT II MRA exhibited better specificity for the disease. A good level of agreement was between the HRT II MRA and the HRT III MRA outcomes. Recent studies comparing the HRT II MRA and HRT III MRA report similar findings (Burgansky-Eliash Z, et al. 2007, Ferreras A, et al. 2007). In both studies, a higher degree of abnormality is shown by the HRT III MRA than by the HRT II MRA, which has the effect of increasing sensitivity and reducing specificity for the newer analysis (Burgansky-Eliash Z, et al. 2007, Ferreras A, et al. 2007). It can be speculated that this might be due to the narrower confidence interval in the enlarged normative database and consequently the tendency to yield a greater proportion of abnormal classifications.

Another point, worthy of note, is that all individuals in the normal group were recruited as normal i.e. none of the individuals had been falsely classified in terms of the ONH appearance using DSI. Considering the deliberate exclusion of normal individuals who had risk factors for OAG, the normal individuals classified as abnormal by the techniques in this study would appear to be 'true' false-positive classifications.

Seeking to explain the low specificity yielded by the CSLO, a retrospective analysis of the HRT images in the false-positive cases revealed no evidence of a tilted, small

(<1.9mm^2) or large (>3mm^2) ONHs, which are known to affect the accuracy of MRA classifications (Medeiros FA, et al. 2006, Schuerle AF and Schmidt E 2004). However, a longitudinal follow-up of these patients will be required to identify if any of these individuals subsequently go on to develop OAG.

4.5.2 Combining techniques

The use of diagnostic tests in combination can improve the sensitivity and specificity for the detection of OAG than if the same techniques were used, alone (Shah NN, et al. 2006). In addition, the severity of OAG may have an influence on the diagnostic capability of each test but to different extents (Hougaard JL, et al. 2007). Hence, combining techniques that exploit different diagnostic parameters to quantify glaucomatous damage may improve the diagnostic precision over a broader range of severity.

This study has demonstrated that by using tests in combination the clinical utility of the tests and diagnostic precision for OAG is improved. This is achieved by stipulating either that both or one of the tests must be abnormal in order to yield a glaucomatous classification.

The combination of RNFL thickness by StratusOCT and the HRT II MRA, using an abnormal result by one or other of the tests to designate OAG, exhibited the most clinically useful diagnostic precision of all the possible combinations of techniques, yielding a sensitivity and specificity of 82.6% (in early and moderate/advanced groups combined) and 80%, respectively.

The combination of the HRT II MRA and the HRT III MRA performed similarly well using an abnormal result by both tests to confirm OAG, yielding a sensitivity and a specificity of 78.3% (in early and moderate/advanced groups combined) and 85%, respectively. However, since both versions of the HRT MRA employ the same diagnostic parameter to detect OAG i.e. normalised rim area measurements, it is speculated that this combination of tests may be less effective in detecting OAG over a broader spectrum of disease severity than for other combinations of investigative techniques that offer different diagnostic parameters.

This is the first study that has examined the combined diagnostic precision for the detection of OAG, in terms of any two of the following diagnostic parameters: RNFL thickness (OCT); neuroretinal rim area (CSLO); the mfVEP; and differential light sensitivity (SAP).

The combined use of tests to detect OAG has been investigated previously in terms of visual function-specific perimetry with optical imaging (Shah NN, et al. 2006), early-generation photographic ONH image analysis and SAP (Caprioli J 1992) and early-generation HRT, OCT and stereoscopic image analysis (Greaney MJ, et al. 2002). Each of these studies demonstrated superior level of diagnostic precision for OAG by combining one or more tests than if tests were used in isolation (Caprioli J 1992, Greaney MJ, et al. 2002, Shah NN, et al. 2006).

4.5.4 Agreement between techniques

It is important to determine the agreement between the glaucomatous ONH appearance (DSI) and tests for RNFL thickness (OCT) and neuroretinal rim area

(CSLO) and visual sensitivity (mfVEP and SAP) since it provides an indication of the relationship between structural and functional parameters in OAG.

The best levels agreement between structural tests and functional tests were observed between the OCT RNFL thickness analysis and SAP differential light sensitivity (63-90%) and between the HRT II MRA and the mfVEP (45-75%). Better agreement between SAP and OCT than between SAP and CSLO has been previously reported (Bowd C, et al. 2006).

In this study, the diagnostic agreement between techniques varied considerably in normal individuals, and in individuals with either early OAG or with moderate/advanced OAG. Much of the agreement that occurred between the tests seemingly occurred by chance alone i.e. tests agreed only because the diagnostic precision was similar between tests. As might be expected, the best level of agreement was seen between the two versions of the MRA of the HRT II and the HRT II; however, even still only a poor to moderate likelihood existed that the observed agreement occurred by chance alone (Kappa, 0.0 to 0.6). The generally poor Kappa values observed in this study may be, in part, due to the relatively small cohort size.

This, and several other studies, provide evidence that the temporal onset of structural and functional defects, using the current state-of-the art technology, is different based on different diagnostic parameters (Kass MA, et al. 2002, Miglior S, et al. 2005). In some eyes, glaucomatous structural deficits precede functional deficits and in some

cases the opposite is true (Kass MA, et al. 2002, Miglior S, et al. 2005). Thus, the characterisation of structural and functional damage in terms of the agreement between tests will depend upon the type of OAG and the temporal lag/severity of the disease.

Whilst the levels of agreement between techniques demonstrated by the present study reflect patterns in predominantly early OAG, the precise level of agreement between any two of the techniques will vary depending upon to diagnostic performance of the technique at a given level of OAG severity (Medeiros FA, et al. 2006, Zangwill LM, et al. 2007).

4.5.5 Topographical correspondence

Topographic correspondence between two different tests serves to corroborate the likelihood that 'true' damage has occurred. This is especially the case when topographical agreement occurs between two types of test that utilize different diagnostic parameters (Greaney MJ, et al. 2002, Hoh ST, et al. 2000, Iester M, et al. 2006, Sihota R, et al. 2006).

The topographical correspondence between structure and function has been investigated previously (Ajtony C, et al. 2007, Bowd C, et al. 2006, Gardiner SK, et al. 2005, Garway-Heath DF, et al. 2000, Strouthidis NG, et al. 2006). In this study, the greatest level of topographical correspondence was observed between two structural tests, namely the HRT III MRA and DSI in patients with

moderate/advanced OAG (100%). The HRT II MRA corresponded only slightly less well with DSI in this group of patients (87.5%). The correspondence with DSI for the remaining 3 methods was 34.8%, 21.8% and 17.4% for the StratusOCT, the mfVEP and the HFA, respectively.

The level of topographical agreement between structural and functional tests was generally poor (less than approximately 30%). This finding may be because the cohort consisted predominantly of patients with early OAG who perhaps had not undergone sufficient functional deficits. However, it is also interesting to note that a higher rate of topographical agreement was observed between the SAP and the CSLO than between the SAP and DSI.

Another possible explanation for the weak structure-function associations observed in this study is that the structure-function topography map upon which the analysis was based (Garway-Heath DF, et al. 2000) is not optimal and/or, due to the inherent variation in the RNFL between individuals, devising a 'true' structure-function map is not possible.

A recent study demonstrated that although predicted topographical agreements occur, unpredicted topographical agreements also occur (Gardiner SK, et al. 2005). This latter study investigators showed that although topographical agreement was present between the outcomes of the CSLO and SAP, some degree of topographical inconsistency was also present (Gardiner SK, et al. 2005).

4.5.6 Limitations of the study

A key limitation of this study, and of any method comparison study, is that the different diagnostic techniques are at different stages of development. In general, more established techniques, like the CSLO and OCT, benefit from more robust normative databases and more sophisticated statistical analyses than newer techniques such as the mfVEP.

In this study, the mfVEP analysis did not need to be corrected for the effects of ageing since an interocular comparison was undertaken. This analysis was possible due to the inclusion in the study of patients without cataracts. However, the technique may be limited in patients with a marked difference in the severity of the cataract between the right and left eyes.

The criterion for glaucomatous abnormality by mfVEP was less stringent (operative at a $p<0.05$ level) compared with the criteria used for the other techniques. However, this did not correspond with a relatively higher level of sensitivity by the mfVEP, as may be expected. Recent refinements to the mfVEP technique, which may yield improved diagnostic ability for OAG include: multi-channel recording and use of 'the best array' i.e. the best responses from the six channels available for each eye (Fortune B, et al. 2007, Hood DC and Greenstein VC 2003, Hood DC, et al. 2002); probability based cluster analysis (Fortune B, et al. 2007, Fortune B, et al. 2004); and combining monocular and interocular mfVEP responses (Hood DC, et al. 2004).

Several reports have suggested that the latency of the mfVEP may be useful in detecting OAG (Bach M 2006, Hood DC, et al. 2006, Rodarte C, et al. 2006). However, these delays in the mfVEP are small (<2ms) (Rodarte C, et al. 2006), even based on the most sophisticated recording methods, and are not specific to OAG (Hood DC, et al. 2006).

Due to the rate of technological advancements concerning structural and functional associations in OAG, this area of research is constantly evolving. Cross-sectional and longitudinal studies, which employ state-of-the-art techniques at the study outset, are often out of date by the time the study is complete and/or published.

In the present study, and inherent in all studies evaluating the diagnostic performance of various techniques, there exists no perfect gold standard for diagnosis. Although DSI is derived from the current 'gold standard' technique, it is possible that newly developed instruments are better at detecting OAG. Thus, estimates of diagnostic precision are reliant on the quality of the gold standard applied. The greatest limitation of DSI as a gold standard technique is the lack of an established diagnostic standard of what constitutes a glaucomatous ONH appearance. Diagnoses by DSI are subjective and based upon the gestalt appearance of the disc by the observer. Expert observers using DSI achieved fair to moderate levels of agreement in their clinical diagnoses (Kappa 0.31-0.61). This outcome is also consistent with that for non-digital stereoscopic ONH-imaging (Harper R, et al. 2000, Shuttleworth GN, et al. 2000, Tielsch J, et al. 1988, Varma R, et al. 1992, Zeyen T, et al. 2003). Thus the diagnostic precision of the technique, clinically, will vary with each individual clinician. This

finding highlights the importance that, in research, diagnoses by DSI should be made by consensus agreement and not by one diagnostician, alone.

Longitudinal studies are justified to evaluate whether one, or a combination of the techniques, used in this study, are useful in predicting those patients in a clinical situation likely to convert to OAG over time and also which patients with OAG are most likely to undergo progressive damage.

4.6 Conclusion

This is the first cross-sectional study to compare the diagnostic performance of the 3 most promising techniques (OCT, CSLO and mfVEP) for detection of OAG in a single cohort of individuals classified solely using the emerging 'gold-standard' technique, DSI. The main outcomes of this study are that the CSLO using the HRT III MRA exhibited the highest level of sensitivity for OAG of all the techniques investigated in this study. Thus, the HRT III MRA seemingly identifies OAG at an earlier stage than any other of the techniques. However, along with the mfVEP using VERIS, CSLO using the HRT III MRA exhibited one of the lowest levels of specificity. The greatest levels of specificity were exhibited by for OCT using the StratusOCT and SAP using the HFA.

Based on the results of this study, the precise utility of each of these technologies remains an issue of clinical judgement. The clinical diagnoses made by different observers based on DSI, will govern the precise level of diagnostic precision achieved by each technique.

Combining diagnostic techniques can improve the detection of OAG (Shah NN, et al. 2006). The combination of techniques yielding the greatest diagnostic performance was the OCT (StratusOCT) with the CSLO (HRT II MRA). Based upon a diagnostic criteria of abnormality by either one of the techniques sensitivity and specificity for the detection of OAG of 82.6% and 80%, respectively, was achieved.

The best levels of agreement between structure and function were present between StratusOCT and the HFA and between the HRT and the mfVEP. However, due to the similarities in the diagnostic precision between these pairs of tests, combined with a relatively small cohort size it was difficult to determine whether the observed agreement was due more than just to chance alone.

Chapter 5: Novel estimation of RNFL thickness based on subjective evaluation of StratusOCT scan data

5.1 Introduction

Measurement of RNFL thickness by optical coherence tomography (OCT) is becoming an established standard procedure in the detection and management of patients with OAG (Budenz DL, et al. 2005, De Leon-Ortega JE, et al. 2006, Jeoung JW, et al. 2005, Leung CK, et al. 2005, Sihota R, et al. 2006).

The current clinical standard for OCT, the StratusOCT, defines the anterior and posterior borders of the RNFL as the two points along the A-scan reflectivity profile where the amount of reflectivity just exceeds and just falls below, respectively, a specified threshold. The axial distance between these two points is taken as the measure of the RNFL thickness. A similar approach is adopted for the measurement of macular and retinal thicknesses.

5.1.1 Erroneous RNFL thickness measurement by StratusOCT

In a number of instances, the StratusOCT analysis yields erroneous measurements of RNFL and retinal thickness (Ishikawa H, et al. 2002, Ray R, et al. 2005, Sadda SR, et al. 2006). In these instances an alternative means to obtain RNFL thickness measurements, based on standard StratusOCT data, would add clinical value to the technique.

In eyes with sub-macula and/or sub-retinal disease, erroneous retinal thickness measurements are commonplace in StratusOCT scans (Ishikawa H, et al. 2002, Ray R, et al. 2005, Sadda SR, et al. 2006). Some errors are operator dependent, such as eye movement and blink artefacts (Ray R, et al. 2005), whilst others are operator independent, such as misidentification of the outer/inner retina (Leung CK, et al. 2007, Sadda SR, et al. 2006) and misalignment of adjacent A-scans (Leung CK, et al. 2007, Ray R, et al. 2005, Sadda SR, et al. 2006).

The likelihood of encountering erroneous retinal/RNFL thickness measurements is greater for scans exhibiting low to poor SNR (Ishikawa H, et al. 2002), for an attenuated RNFL (Ishikawa H, et al. 2002), for a poorly reflective RNFL (Ishikawa H, et al. 2002), for a detached internal limiting membrane (ILM) (Ray R, et al. 2005) and/or where abnormalities of the subretinal tissues are apparent, for example, the presence of subretinal fluid (Sadda SR, et al. 2006). Operator independent measurement errors most commonly occur either due to misplacement of the RNFL interface boundary, or due to misalignment of adjacent a-scans by the StratusOCT automated analysis software (Leung CK, et al. 2007, Sadda SR, et al. 2006). Such operator independent errors occur during automated analysis of scan data by StratusOCT and have been identified in individuals undergoing macula thickness scans. The influence of such errors in individuals undergoing RNFL thickness measurement is unknown.

As was described in Chapter 4, the StratusOCT RNFL thickness (3.4) scan, averages the 512 independent measurements from around the ONH to yield one global, 4 quadrant and 12 clock hour averaged RNFL thickness values. Under optimal

recording conditions. StratusOCT RNFL thickness measurements exhibit high within-test repeatability (ICC 0.92-0.97) (Budenz DL, et al. 2005, De Leon-Ortega JE, et al. 2007, Paunescu LA, et al. 2004).

In some cases, erroneous measurements can be rectified, simply by re-scanning the patient. However, where this is not immediately possible and/or where patients consistently yield erroneous RNFL thickness measurements, the application of StratusOCT to detect OAG, or progressive structural damage due to OAG, is limited.

5.1.2 Justification for alternative RNFL thickness measurement methods

During the study described in Chapter 4, it became apparent that a relatively high proportion of the first acquisition StratusOCT RNFL thickness measurements contained errors, which, if persistent, could have led to the exclusion of participants due to unusable RNFL thickness measurements by StratusOCT. As a consequence, novel software was developed to permit the measurement of RNFL thickness in such instances. The basic program, OCTAnalyse, was written by a computer programmer, Gavin Powell (GP), who, in collaboration with two of the study investigators (JEM and CJH), refined the basic software to yield a user-friendly subjective technique for obtaining peripapillary RNFL thickness measurements based on the standard StratusOCT procedure.

The validity of OCTAnalyse needed to be established in terms of the level of agreement between OCTAnalyse and the StratusOCT. The repeatability of OCTAnalyse RNFL thickness measurements governs the clinical utility in cross-sectional and longitudinal evaluation of OAG.

5.2 Study Aims

The purpose of the study was: to determine the level of agreement of RNFL thickness measurements obtained by OCTAnalyse with those obtained by StratusOCT; to determine the test-retest repeatability of RNFL thickness measurements obtained by OCTAnalyse and by StratusOCT; and to investigate the presence and likely cause of measurement errors in RNFL thickness obtained by StratusOCT.

5.3 Materials/ Methods

A retrospective study was undertaken using 21 of the patients described in Chapter 4 and all 20 normal individuals. The inclusion criteria were as described in Chapter 4, Section 4.3.2.

5.3.1 Digital stereoscopic ONH-imaging (DSI)

The classification of eyes as normal or glaucomatous (OAG) was based solely on the appearance of the ONH by subjective grading using DSI in accordance with the procedure described in Chapter 4, Section 4.3.3.

Although both eyes of each participant were assessed with the novel techniques, the results of one randomly chosen eye for each individual are reported in Chapter 4. The eye chosen for the present study was also selected at random but on a separate occasion.

Twelve eyes were classified by DSI as OAG and 29 of the eyes were normal. Nine of the 29 normal eyes had a fellow eye which had OAG. These 9 eyes, defined as

suspect eyes, were analysed alongside, but independently of, the remaining 20 eyes in the normal group. The 12 eyes with OAG were derived from 8 patients with bilateral OAG and 4 patients with unilateral OAG.

One suspect eye was receiving topical anti-glaucoma drugs; all other suspect eyes were not receiving medical therapy of any kind. All of the eyes with OAG were receiving topical anti-glaucoma drugs with the exception of one patient who had undergone a trabeculectomy 30 months prior to entry into the study.

All of the normal and suspect eyes exhibited a normal visual field by SAP. Nine of the 12 OAG eyes exhibited a repeatable visual field defect, characteristic of OAG, by SAP. The remaining 3 OAG eyes exhibited a normal visual field by SAP. In all cases, visual field printouts were interpreted by an expert (JMW). The definitions of a normal and abnormal visual field used in the present study were as described in Chapter 4, Section 4.3.4.

The gender, mean age, mean central corneal thickness (CCT), mean Goldmann intra-ocular pressure (IOP) and mean corneal corrected IOP (cc-IOP) of the Normal, Suspect and OAG participants is given in Table 1.

Group	Gender (M:F)	Mean age ±SD, years (range)	Mean CCT ±SD, μm (range)	IOP ±SD, mmHg (range)	cc-IOP ±SD, mmHg (range)
Normal (n=20)	6:14	65.3 ± 11.2 (31-82)	559.6 ± 28.4 (508-615)	16.4 ± 3.1 (9-20)	14.4 ± 3.5 (9-18)
Suspect (n=9)	4:5	72.4 ± 7.2 (59-83)	531.4 ± 16.8 (502-554)	15.9 ± 3.2 (10-18)	16.4 ± 3.3 (10-19)
OAG (n=12)	7:5	65.6 ± 12.2 (46-85)	521.5 ± 35.5 (480-552)	19.5 ± 5.6 (8-26)	21.2 ± 5.4 (9-26)

Table 5.1 - *Gender, mean age, mean central corneal thickness (CCT), mean intra-ocular pressure (IOP) and mean cornea corrected IOP (cc-IOP) for normal and suspect individuals and individuals with OAG. Where appropriate, the IOPs and cc-IOPs are treated values.*

5.3.2 *StratusOCT*

StratusOCT scans were obtained in accordance with the same methodology described in Chapter 4, Section 4.3.7. After the first scan, the patient was instructed to sit back from the instrument for a moment to rest. The patient was then asked to resume their position in preparation for a second scan. The z-offset and polarization were re-optimized for second scan. The position of the scan circle, relative to the ONH was adjusted, if necessary, to account for any difference in head/eye position between the first and second scans. Both the first and second scan were analysed in the same way using the RNFL thickness average analysis protocol.

5.3.3 OCTAnalyse

The OCTAnalyse software was created in Delphi utilizing the OpenGL application-programming interface (API) (Figure 4.1). The OCTAnalyse software allowed an observer to view StratusOCT scan data, and to subjectively measure RNFL thickness, via a stand-alone PC. The software was designed to allow the data to be viewed in a consistent manner whatever the resolution of the scan (512 or 256 A-scans). StratusOCT data files were imported via a memory stick to OCTAnalyse for each participant. The OCTAnalyse software included a thresholding algorithm that enabled the observer to view the detail within the image analogous to the typical scan pattern seen on the StratusOCT. An independent viewing window, which allowed the observer to visualise any single A-scan reflectivity profile was also incorporated into the program.

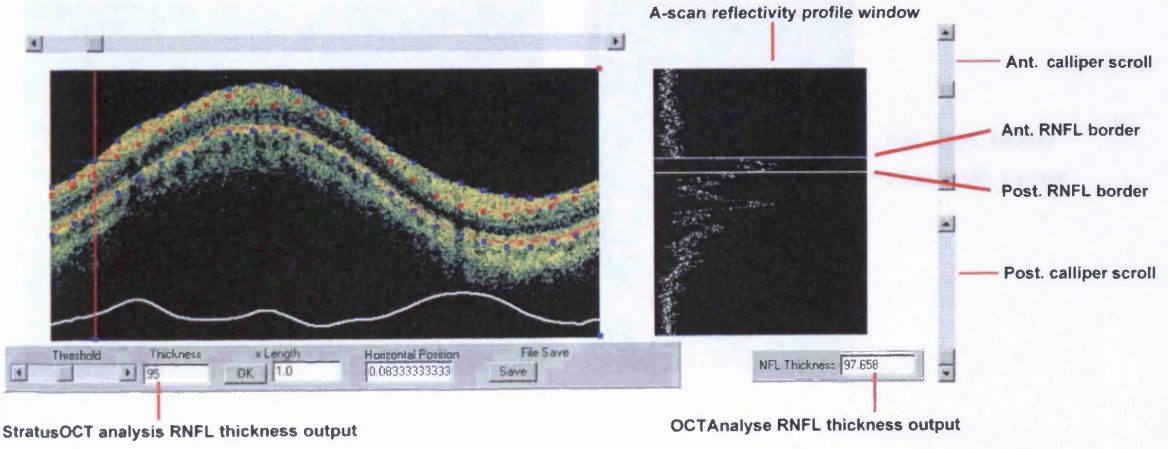

Figure 5.1 – *The display generated by the OCTAnalyse software*

The software permitted manual delineation, with a caliper, of the anterior and posterior RNFL borders based upon specific landmarks in the A-scan reflectivity profile. The axial location of the anterior RNFL border was defined as the base of the first major peak in reflectivity along the A-scan reflectivity profile (Figure 5.2). In several cases, the first reflectivity peak corresponded to a detached inner limiting membrane (ILM). In these instances, the anterior RNFL border was defined at the base of the second major deflection in reflectance intensity on the A-scan reflectivity profile (Figure 5.3). The axial location of the posterior RNFL border was defined as the mid-point along the descending limb of the first reflectance spike. In the presence of a detached ILM, the posterior RNFL border was defined as the mid-point along the descending limb of the second reflectance spike. The distance between the two cursors provided a direct measurement of RNFL thickness.

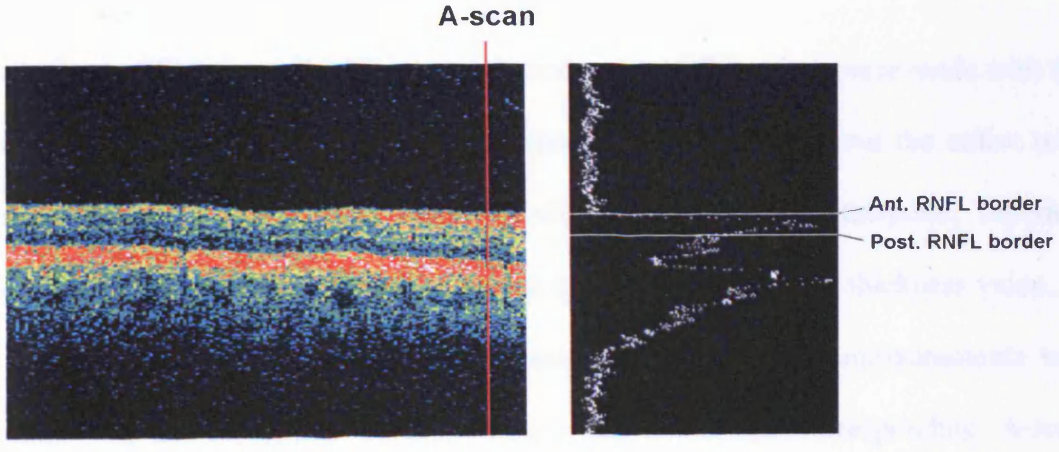

Figure 5.2 – *The axial definition of the anterior and posterior retinal nerve fibre layer (RNFL) borders on the A-scan reflectivity profile (right) corresponding to the highlighted A-scan (left).*

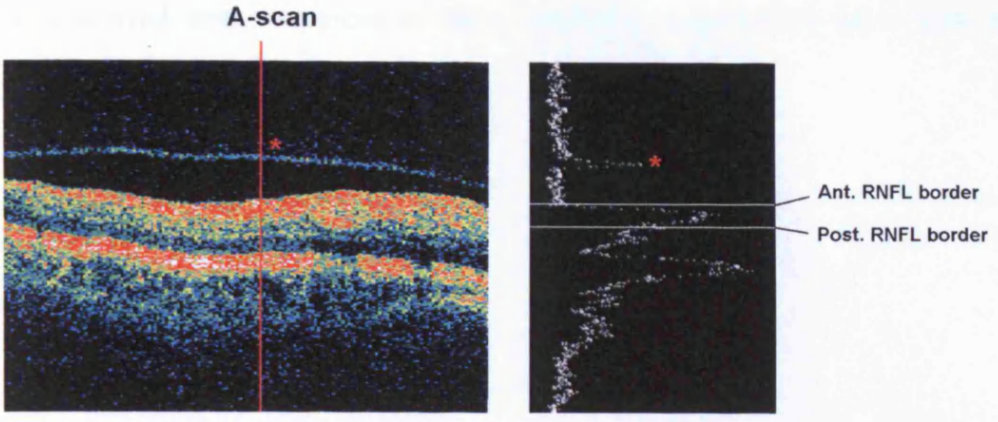

Figure 5.3 –*The axial definition of the anterior and posterior retinal nerve fibre layer (RNFL) borders on the A-scan reflectivity profile in the presence of a detatched internal limiting membrane (ILM) (*) (right) corresponding to the highlighted A-scan (left).*

5.3.4 RNFL thickness measurement

Retinal nerve fibre layer thickness measurements by OCTAnalyse were made with the caliper at 24 predetermined and equally spaced A-scans throughout the entire scan length. The six measurements obtained within each quadrant (temporal, superior, nasal and inferior) were averaged to give a quadrant mean RNFL thickness value. In order that the sampling density of the manual and automated measurements was equal, 24 thickness measurements were obtained at the corresponding A-scan locations to those from the automated StratusOCT analysis. This number of measurements represented an optimum trade-off between sampling density and the length of time taken to obtain measurements from the entire length of the scan. The quadrant mean RNFL thickness corresponding to the StratusOCT analysis was

similarly derived from the mean of the 6 manual measurements taken from each quadrant.

5.3.5 Analysis

Within-session repeatability

The repeatability of the RNFL thickness measurements was assessed using an established method (Bland JM and Altman DG 1999). The difference between the first and second measurements was plotted against the mean of the two values for both the manual (OCTAnalyse) and the automated (StratusOCT) measurements. The 95% confidence intervals for the difference the first and second measurement for both the manual and the automated RNFL thickness measurements were separately determined (Bland JM and Altman DG 1999, 1986). Differences in measurements within particular quadrants and between patient groups were also determined in the same way both for the manual (OCTAnalyse) and for the automated (StratusOCT) measurement methods.

The test-retest repeatability within a session of the RNFL thickness measurements for both the StratusOCT and OCTAnalyse measurements was also assessed using a second method, namely the intraclass correlation coefficient (ICC). Intraclass correlation coefficients were calculated for global average, quadrant average and group average measurements.

Agreement (repeated measures)

The level of agreement between the manual and automated measurements was analyzed in a pair-wise manner. Similar to the first analysis, plots were produced which related the difference between the mean manual and mean automated measurements with the mean of the two values. The SD of the differences from these pairs of means was corrected for the effect of repeated measurement error. The agreement between the methods was quantified by calculating the 95% limits of agreement (LOA) between the methods. The standard error (SE) and 95% confidence interval (CI) for the LOA were also determined.

5.4 Results

5.4.1 Within-test repeatability of measurements by OCTAnalyse and StratusOCT

The difference between the first and second measurements against the mean of the two measurements for OCTAnalyse and for StratusOCT is given in Figures 5.4a-h for each quadrant for all 41 individuals. The corresponding differences for the groups, normal, suspect and OAG are given in Figures 5.5a-d.

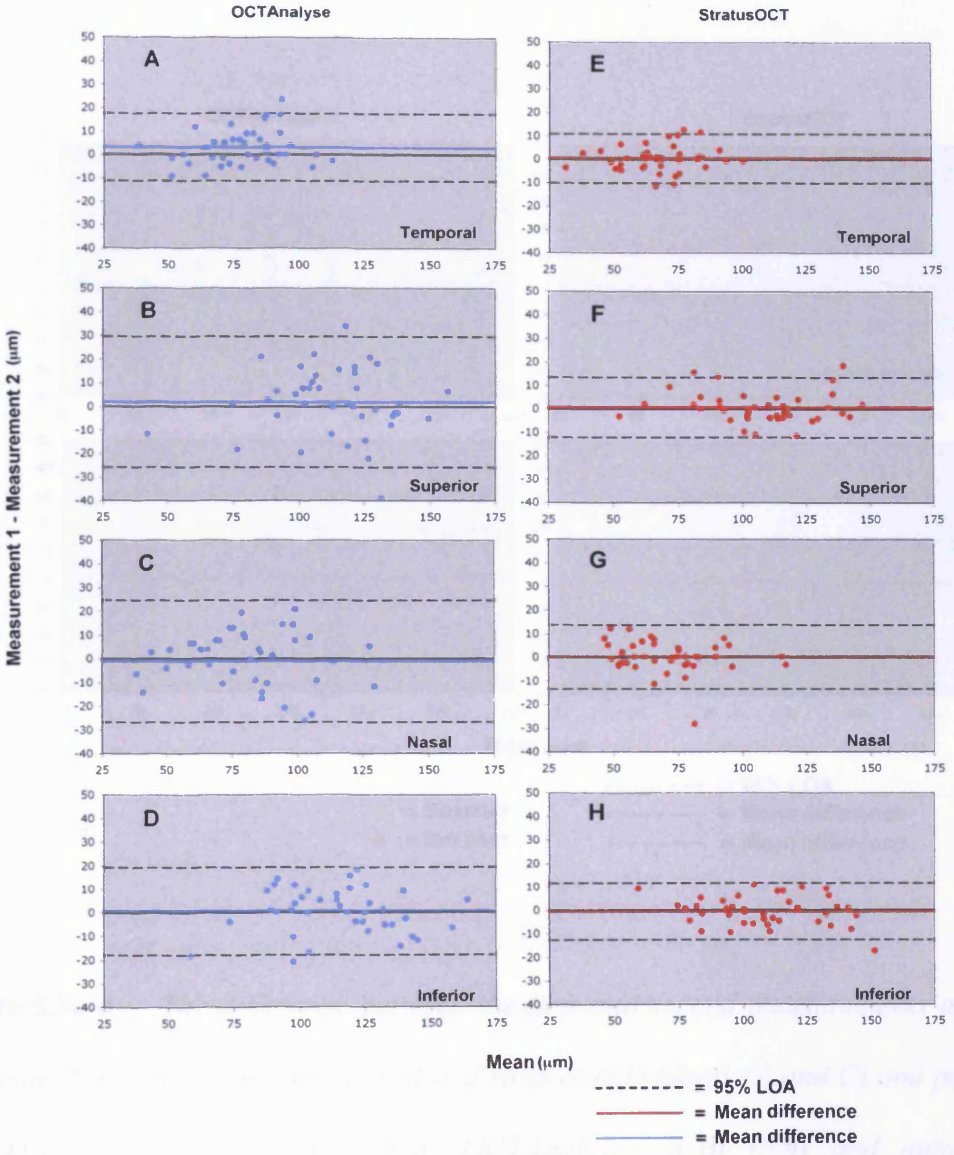

Figure 5.4e-h. – *The difference between the first and second measurements against the mean of the two values in the Temporal (A and E), Superior (B and F), Nasal (C and G) and Inferior (D and H) quadrants for manual (OCTAnalyse) (A-D) (left) and automated (StratusOCT) (E-H) (right) measurement methods for all 41 individuals.*

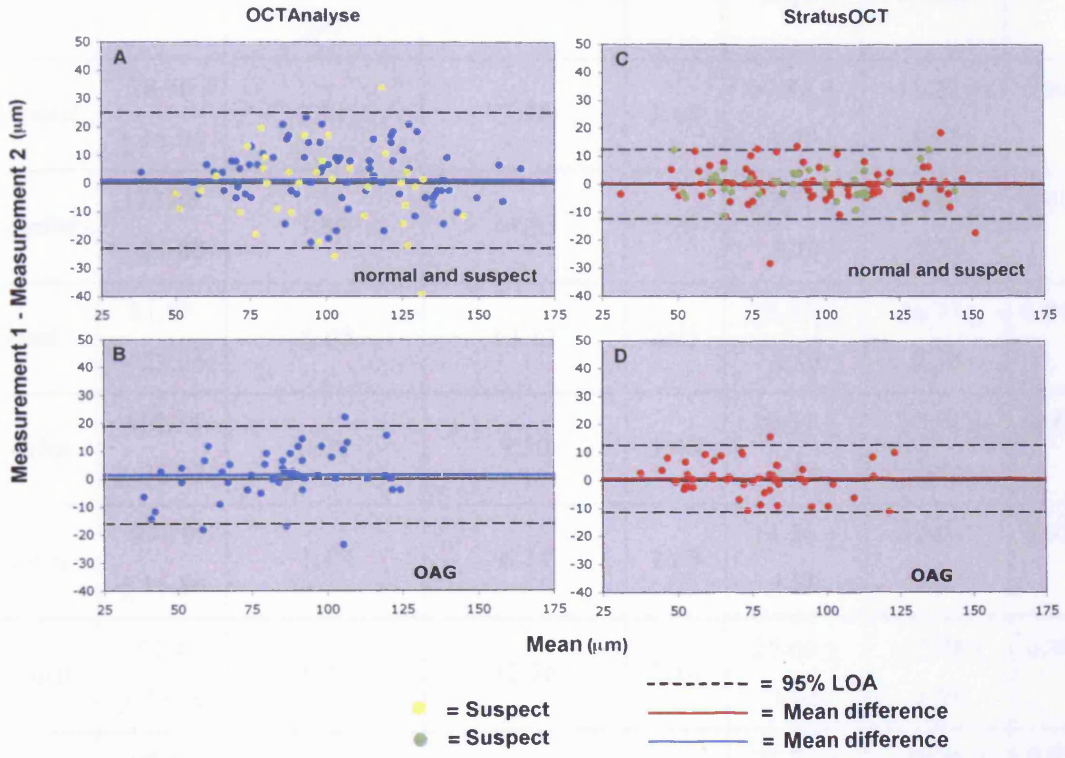

Figure 5.5a-d. – *The difference between the first and second measurements against the mean of the two values for normal and suspect individuals (A and C) and patients with OAG (B and D) for manual (OCTAnalyse) (A-B) (left) and automated (StratusOCT) (C-D) (right) measurement methods.*

Variable	Mean, μm	Mean Difference Manual 1- 2, μm	SD (Difference), μm	SE, μm	95% CI (± 1.71 SE), μm		ICC
					Upper	Lower	
Temporal	78.70 ± 16.04	3.11	7.31	1.14	17.44 ± 1.95	-11.22 ± 1.95	0.90
Superior	113.66 ± 21.88	1.84	14.15	2.21	29.57 ± 3.78	-25.89 ± 3.78	0.81
Nasal	81.67 ± 22.06	-1.05	13.12	2.05	24.67 ± 3.50	-26.77 ± 3.50	0.84
Inferior	114.74 ± 22.23	0.70	9.50	1.49	19.32 ± 2.54	-17.92 ± 2.54	0.91
Global	97.19 ± 16.86	1.15	6.74	1.05	14.36 ± 1.80	-12.06 ± 1.80	0.92
Normal	102.48 ± 26.59	1.04	12.26	1.14	25.06 ± 1.95	-22.98 ± 1.95	0.90
Suspect	98.67 ± 27.32	-1.81	14.07	2.34	25.76 ± 4.01	-29.38 ± 4.01	0.85
OAG	84.42 ± 22.56	1.41	8.92	1.29	18.89 ± 2.20	-16.07 ± 2.20	0.93

Table 5.2 - *The mean, mean difference, standard deviation (SD) of the difference, standard error (SE) of the difference, the upper and lower 95% confidence interval (CI) and intraclass correlation coefficient (ICC) for repeated RNFL thickness measurments obtained by OCTAnalyse for the 43 individuals (above the double line) and for each diagnostic category (below the double line).*

Variable	Mean, μm	Mean Difference Automated 1-2, μm	SD (Difference), μm	SE, μm	95% CI (± 1.71SE), μm		ICC
					Upper	Lower	
Temporal	67.63 ± 14.62	0.42	5.37	0.84	10.94 ± 1.43	-10.11 ± 1.43	0.94
Superior	107.73 ± 21.97	0.72	6.47	1.01	13.40 ± 1.73	-11.96 ± 1.73	0.96
Nasal	71.11 ± 17.18	0.17	6.92	1.08	13.73 ± 1.85	-13.39 ± 1.85	0.92
Inferior	108.76 ± 21.90	-0.49	6.20	0.97	11.66 ± 1.66	-12.64 ± 1.66	0.96
Global	88.81 ± 15.01	0.21	2.74	0.73	5.58 ± 0.73	-5.16 ± 0.73	0.98
Normal	94.05 ± 13.14	0.06	6.30	0.43	12.40 ± 1.00	-12.29 ± 1.00	0.97
Suspect	89.62 ± 14.62	0.33	5.15	0.86	10.44 ± 1.47	-9.78 ± 1.47	0.98
OAG	76.13 ± 20.77	0.57	6.09	0.88	12.5 ± 1.50	-11.37 ± 1.50	0.96

Table 5.3 - *The mean, mean difference, standard deviation (SD) of the difference, standard error (SE) of the difference, the upper and lower 95% confidence interval (CI) and intraclass correlation coefficient (ICC) for repeated RNFL thickness measurments obtained by StratusOCT for the 43 individuals (above the double line) and for each diagnostic category (below the double line).*

Table 5.2 and Table 5.3 show summary statistics for RNFL thickness measurements obtained by OCTAnalyse and StratusOCT, respectively. Intraclass correlation coefficients (ICCs) were excellent (>0.80) and were higher for measurements obtained by StratusOCT in all cases. The highest ICC was obtained for the global average RNFL thickness measurements by automated StratusOCT analysis (0.98). The lowest ICC obtained was for superior quadrant mean RNFL thickness measurements by OCTAnalyse (0.81).

The within-test repeatability (95% CI) of RNFL thickness measurements obtained by OCTAnalyse ranged between ±13.6 μm (global average) and ±28.5 μm (Superior quadrant). The within-test repeatability (95% CI) of RNFL thickness measurements obtained by StratusOCT ranged between ±5.5 μm (global average) and ±13.9 μm (Nasal quadrant). Retinal nerve fibre layer thickness measurements obtained by OCTAnalyse exhibited greatest within-test repeatability in the temporal quadrant (95% CI, ±14.3 μm) followed by the inferior (95% CI, ±18.6 μm), nasal (95% CI, ±23.6 μm) and superior (95% CI, ±27.7 μm) quadrants, respectively. The repeatability of measurements obtained by StratusOCT was greatest in the temporal quadrant (95% CI, ±10.5 μm) followed by the inferior (95% CI, ±12.2 μm), superior (95% CI, ±12.7 μm) and nasal (95% CI, ±13.6 μm) quadrants, respectively. In all quadrants, within-test repeatability of RNFL thickness measurements was greater for automated StratusOCT analysis than for manual OCTAnalyse measurements.

5.4.2 Agreement between OCTAnlayse and StratusOCT

The difference between the mean manual (OCTAnalyse) and mean automated (StratusOCT) measurements against the mean of the two measurements, are given in Figure 5.6a-d for quadrant average data and Figure 5.7a and 5.7b for all quadrants for the normal, suspect and OAG groups. Table 5.3 provides summary statistics for the agreement between OCTAnalyse and StratusOCT RNFL thickness measurements.

Variable	Mean, μm	Difference, (Manual – Automated) μm	$SD_{Corrected}$ Difference, μm	SE, μm	95% CI, μm	
					Upper	Lower
Temporal	73.17	11.07	8.29	1.30	27.32 ± 2.22	-5.18 ± 2.22
Superior	110.70	5.93	13.74	2.16	32.87 ± 3.67	-21.01 ± 3.67
Nasal	76.39	10.56	17.58	2.74	45.01 ± 4.69	-23.90 ± 4.69
Inferior	111.75	5.98	9.64	1.50	24.87 ± 2.57	-12.91 ± 2.57
Global	93.00	8.38	8.01	1.25	24.09 ± 2.14	-7.32 ± 2.14
Normal	98.27	8.42	13.10	2.04	34.10 ± 3.49	-17.26 ± 3.49
Suspect	94.15	9.01	10.00	1.67	28.67 ± 2.75	-10.75 ± 2.75
OAG	80.27	8.29	12.81	2.00	33.40 ± 3.42	-16.82 ± 3.42

Table 5.4 - *The mean, mean difference, corrected standard deviation ($SD_{Corrected}$), standard error (SE) and upper and lower 95% confidence interval (CI) for the agreement between manual and automated RNFL thickness measurement techniques.*

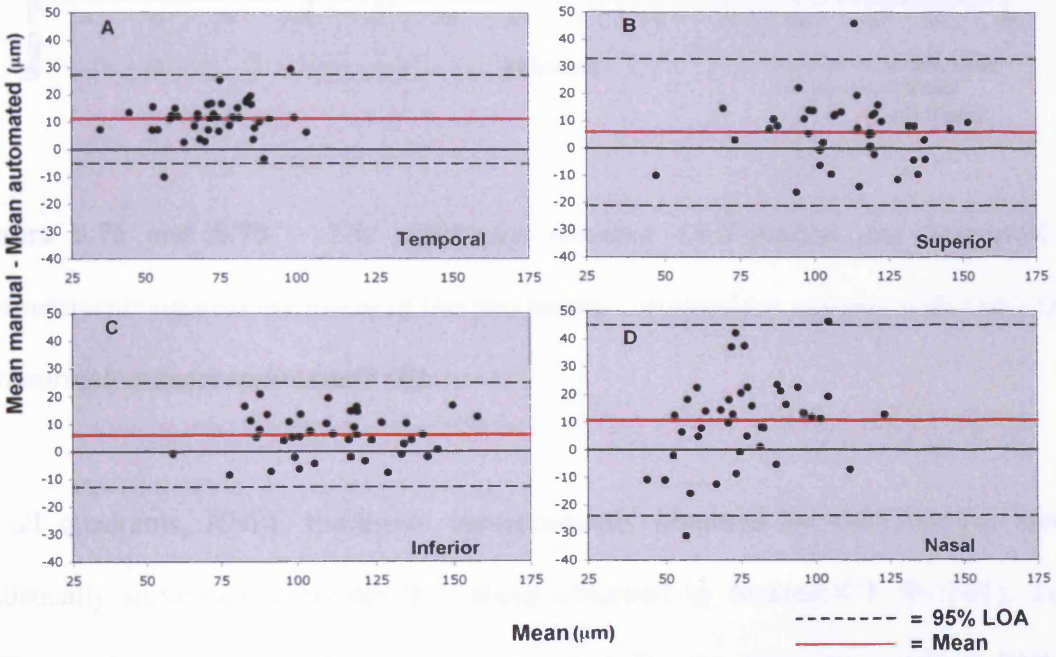

Figure 5.6a-d. – *The difference between OCTAnalyse and StratusOCT measurements against the mean of the two values obtained for the Temporal (A), Superior (B), Inferior (C) and Nasal (D) quadrants.*

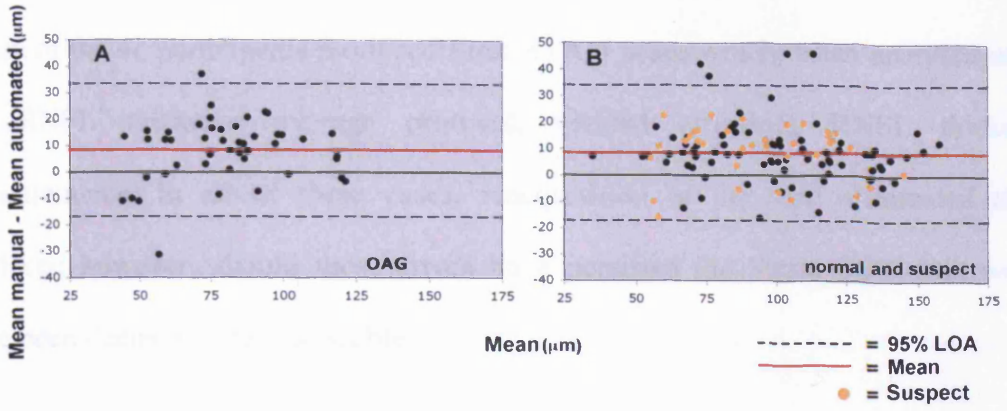

Figure 5.7a and **5.7b** – *The difference between OCTAnalyse and StratusOCT measurements against the mean of the two values obtained for patients with OAG (A) and normal/ suspect individuals (B).*

In all quadrants, RNFL thickness measurements obtained by OCTAnalyse were statistically significantly greater than those obtained by StratusOCT ($P<0.01$). The difference between the techniques was greatest for the temporal quadrant RNFL thickness (11.07 µm) followed by the nasal (10.56 µm), inferior (5.98 µm) and superior (5.93 µm) quadrant measurements.

Retinal nerve fibre layer thickness measurements obtained by OCTAnalyse were greater than those obtained by StratusOCT in normal (8.42 µm), suspect (9.05 µm) and OAG (8.29 µm) groups, which in all cases was statistically significant ($p<0.01$).

5.4.3 Erroneous RNFL thickness measurements by StratusOCT

Seven of the 41 participants produced Stratus OCT scans which, when analysed using the RNFL thickness average protocol, yielded erroneous RNFL thickness measurements. In all of these cases, reacquisition of the scan eliminated these artefacts; however, should these errors have persisted the StratusOCT data would have been deemed to be un-useable.

Several examples of erroneous RNFL thickness measurements are given below. Seemingly, the origin of these errors is consistent with the literature (Ray R, et al. 2005, Sadda SR, et al. 2006) and in all cases arose either due to detachment of the internal limiting membrane (ILM) (Figure 5.8a and Figure 5.8b) or due to a localised area of reduced a-scan reflectivity (Figure 5.9a and Figure 5.9b).

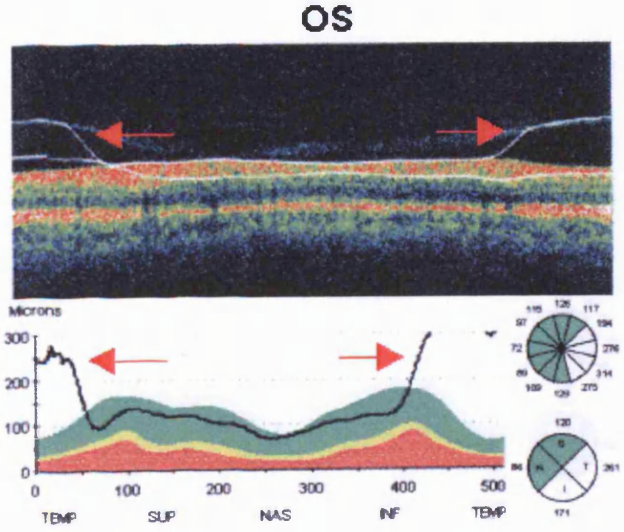

Figure 5.8a *–Erroneous retinal nerve fibre layer (RNFL) thickness measurment due to a detached ILM in a 59 year old male patient with OAG. The red arrow indicates the affected region.*

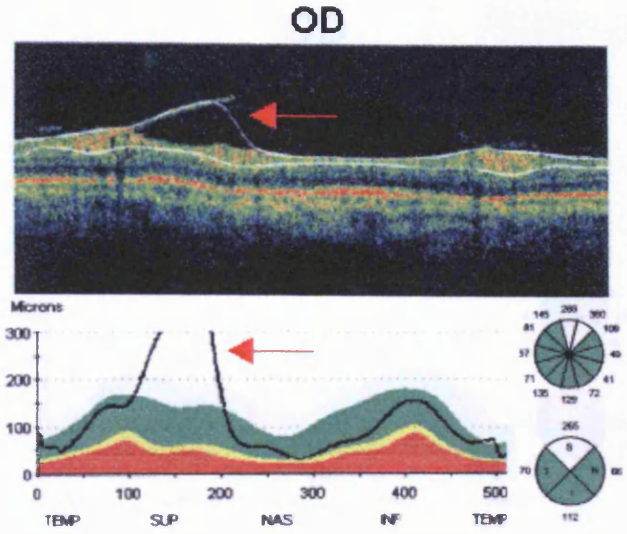

Figure 5.8b - *Erroneous retinal nerve fibre layer (RNFL) thickness measurment due to a detached ILM in a 64 year old female patient with OAG. The red arrow indicates the affected region.*

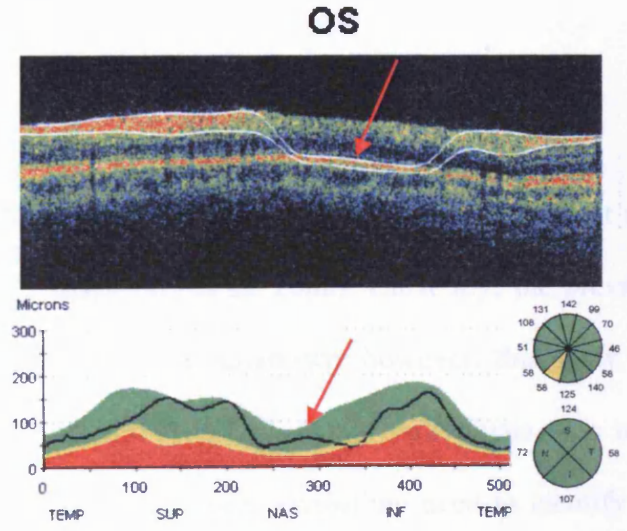

Figure 5.9a - *Erroneous retinal nerve fibre layer (RNFL) thickness measurment due to low RNFL reflectivity in a 52 year old male patient with OAG. The red arrow indicates the affected region.*

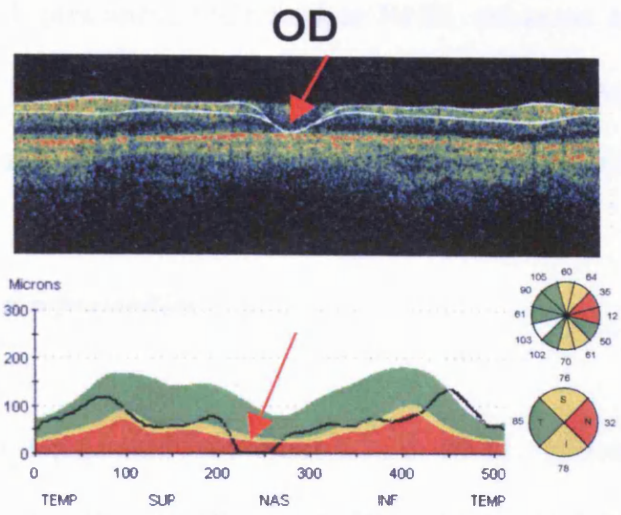

Figure 5.9b - *Erroneous retinal nerve fibre layer (RNFL) thickness measurement due to low RNFL reflectivity in a 55 year old female patient with OAG. The red arrow indicates the affected region.*

5.5 Discussion

Errors in macula thickness by StratusOCT are reported to affect up to 92% of scans (Ray R, et al. 2005, Sadda SR, et al. 2006). Currently, the prevalence of erroneous RNFL thickness measurements is unknown; however, this study observed in RNFL thickness measurements in 17% (7 of 41) of individuals who underwent scanning with the StratusOCT. Thus there is a compelling need to identify the causes of such measurement error and develop ways to overcome such errors in order that the clinical utility of StratusOCT can be improved.

In this study, new and novel software (OCTAnalyse) was developed that permits subjective measurement of RNFL thickness based on data obtained during the

standard StratusOCT procedure. OCTAnalyse RNFL thickness measurements were validated in terms of their agreement with those obtained using StratusOCT. The within-session repeatability of measurements was also determined for each technique.

5.5.1 Within-session repeatability

The within-session repeatability of StratusOCT RNFL measurements has been investigated previously (Budenz DL, et al. 2005, Paunescu LA, et al. 2004). The levels of within-session repeatability of StratusOCT RNFL thickness measurements are consistent with previous values (Budenz DL, et al. 2005, Paunescu LA, et al. 2004). In this study, both the StratusOCT and OCTAnalyse yielded the best within-session repeatability in the temporal quadrant, with 95% LOA of $\pm$10.5 μm and $\pm$14.3 μm, respectively. StratusOCT yielded lowest within-session repeatability for mean RNFL thickness in the nasal quadrant followed by the superior, inferior and temporal quadrants, which is consistent with an earlier study (Budenz DL, et al. 2005). OCTAnalyse, however, yielded lowest within-session repeatability for mean RNFL thickness in the superior quadrant followed by the nasal, inferior and temporal quadrants.

In previous studies, the repeatability of StratusOCT RNFL thickness measurements is greater in normal individuals than in patients with OAG (Budenz DL, et al. 2005, De Leon-Ortega JE, et al. 2007). However, there was no statistically significant difference in the repeatability of RNFL thickness measurements between normal, suspect and OAG eyes, either by OCTAnalyse or StratusOCT.

5.5.2 Agreement between StratusOCT and OCTAnalyse

The level of agreement between two measurement techniques provides an indication of how well the given techniques can be used interchangeably.

The validity of OCT RNFL measurements in providing a clinically reliable estimate of RNFL thickness has been reported in a number of previous studies (Jones AL, et al. 2001, Schuman JS, et al. 1996, Skaf M, et al. 2006, Toth CA, et al. 1997). This relationship is important since it serves to validate imaging-derived data, as well as help improve our understanding of RNFL loss in OAG. Optical coherence tomography RNFL thickness measurements have been evaluated against histological measurements obtained using ex vivo retinal sections (Blumenthal EZ, et al. 2007, Skaf M, et al. 2006, Toth CA, et al. 1997) as well as against RNFL thickness measurements obtained by other imaging techniques (Blumenthal EZ, et al. 2007, Greaney MJ, et al. 2002, Leung CK, et al. 2005). In general, StratusOCT RNFL thickness measurements appear qualitatively similar when compared to the histologically derived data (Blumenthal EZ, et al. 2007, Greaney MJ, et al. 2002, Leung CK, et al. 2005). Quantitative differences have been attributed either to scaling differences or histological artifacts related to cell shrinkage and dehydration of tissues post mortem (Blumenthal EZ, et al. 2007, Skaf M, et al. 2006).

This study observed a consistent tendency for OCTAnalyse to yield statistically significantly greater RNFL thickness ($p<0.01$) measurements than those obtained by StratusOCT. Based on quadrant averaged RNFL thickness measurements across the three groups, this discrepancy was greatest in the temporal and nasal quadrants than in the superior and inferior quadrants.

Similarly, RNFL thickness measurements obtained using OCTAnalyse were statistically significantly greater ($p<0.01$) than those obtained by StratusOCT in normal and suspect individuals and in patients with OAG.

Since the measurement scaling factors used by OCTAnalyse and StratusOCT were equal, the consistent tendency for OCTAnalyse to yield thicker values is most likely to be due to the criteria used to define the axial location of the anterior and posterior RNFL borders on the a-scan reflectivity profile with OCTAnalyse (see Section 5.3.4). Whilst alternative criteria could theoretically be applied to improve the agreement between the techniques, the current criteria utilise points on the a-scan reflectivity profile that are easy to distinguish in order to reduce the influence of between-observer effects on measurement variability.

The magnitude of the difference in the measured RNFL thickness between the two techniques constitutes a caveat when implementing the OCTAnalyse clinically.

5.5.3 Erroneous RNFL thickness measurements

OCTAnalyse was designed to overcome the clinical situation where the standard StratusOCT procedure yields erroneous RNFL thickness measurements. Where errors persist upon re-scanning and/or where re-scanning of the patient is not immediately possible, as in many clinical situations, OCTAnalyse offers an alternative method to obtain RNFL thickness measurements. OCTAnalyse reduces the amount of lost clinical time and resources due to erroneous RNFL thickness measurements by StratusOCT. Erroneous RNFL thickness measurements, by StratusOCT, were present

in 17% of individuals who underwent imaging; however, some reports suggest that a much greater proportion scans may be affected (Ray R, et al. 2005, Sadda SR, et al. 2006).

The erroneous RNFL thickness measurements seen in this study arose either due to mislocation of the retinal interface borders arising from a detachment of the ILM (Figure 5.8a and b) or due to a localised reduction in a-scan reflectivity within the scan profile (Figure 5.9a and b).

Thus, there is a clear clinical need for alternative methods to measure RNFL thickness based on StratusOCT data. In view of its wider potential, OCTAnalyse is also capable of measuring retinal thickness from macula scans where a higher proportion of erroneous measurements are reported to arise (Ray R, et al. 2005, Sadda SR, et al. 2006). Thus OCTAnalyse is a clinically useful tool, which can be applied to a wide range retinal and macula abnormalities.

However, despite yielding high ICCs (>0.80) for repeated measurements, the 95% LOA for OCTAnalyse were large, and ranged between $\pm$13.2 μm and $\pm$27.7 μm. It can be speculated that these limits of agreement may in fact be too wide to accurately detect longitudinal changes in RNFL thickness, although further investigation is warranted.

5.6 Conclusion

This study has demonstrated the clinical utility of novel computer software (OCTAnalyse) that permits subjective quantification of RNFL thickness, based on data obtained from the standard StratusOCT procedure. OCTAnalyse was designed for clinical use in instances where standard StratusOCT yields erroneous RNFL thickness measurements, although the software can be used with StratusOCT scans which yield erroneous macula/retinal thickness measurements.

Retinal nerve fibre layer thickness measurements obtained by OCTAnalyse are statistically significantly thicker ($p<0.01$) than those obtained by standard StratusOCT. The within-session repeatability of OCTAnalyse was, in all analyses, greater for StratusOCT.

In its current form, OCTAnalyse seems unlikely to offer clincians the ability to accurately detect progressive damage due to OAG due to the wide 95% LOA of the technique although further studies are warranted. With refinements to the current OCTAnalyse software, such as the development of an intuitive (semi-automated) algorithm for retinal interface recognition, the longitudinal clinical utility of the technique could potentially be improved. The fourth generation OCT, CirrusOCT, which images the retina with greater resolution, may further improve the repeatability, and thus clinical utility, of OCTAnalyse.

Chapter 6: Conclusions and proposals for future work

6.1 Conclusions

6.1.1 Some dissociating factors in the analysis of structural and functional progressive damage in OAG

The longitudinal study demonstrated poor concordance between two of the current-most sophisticated techniques for the identification of structural and functional progressive damage in OAG namely, the HRT II TCA and the HFA GPA, respectively. Seventeen out of 23 patients with OAG or with 'high risk' ONH exhibited progressive damage by TCA and/or by GPA; however, only 4 patients exhibited progressive damage by both techniques. In a majority (70%) of the eyes progressing by only one of the techniques, one of three dissociating factors were, at least in part, to be responsible for the poor concordance. These dissociating factors were: the perimetric learning effect; the inability of GPA to detect progressive functional damage in regions of the visual field where the variability of the differential light sensitivity is beyond the dynamic range of the HFA at the baseline examinations; and the inability of TCA to detect progressive structural damage where the neuroretinal rim is markedly attenuated, as in advanced OAG.

6.1.2 Novel approaches to glaucoma detection

The cross-sectional study investigated the diagnostic precision of the current-most promising techniques for the detection of OAG, namely; Optical Coherence Tomography (OCT), Confocal Scanning Laser Ophthalmoscopy (CSLO), and the Multifocal Visual Evoked Potential (mfVEP), in participants classified solely

according to the emerging 'gold standard' technique, DSI. Confocal Scanning Laser Ophthalmoscopy, using the Heidelberg Retina Tomograph (HRT) III Moorfields Regression Analysis (MRA), yielded the highest sensitivity for OAG (86.7% to 100%). Optical Coherence Tomography, using the StratusOCT, and SAP using the Humphrey Field Analyzer (HFA) yielded the highest specificity for OAG (95%). The combined use of the StratusOCT and the HRT II MRA yielded the best overall diagnostic precision for OAG (sensitivity, 82.6% and specificity, 80%) of all possible combinations of tests and was higher than if any of the techniques were used alone. The relationship between techniques was determined in terms of their agreement in diagnostic outcome and their topographic correspondence of abnormality. The best agreement between structural and functional techniques was observed between the StratusOCT and the HFA and between the HRT II/III and the mfVEP, although because of the co-variance the observed values are likely to be inflated.

The best topographical concordance was observed between DSI and HRT III (up to 100%) and serves to strengthen the qualitative relationship between the two techniques. The techniques that is the 'best' for detecting OAG is a matter of clinical judgement, which based upon the most promising techniques, inevitably, involves a trade-off between sensitivity and specificity.

6.1.3 Novel estimation of RNFL thickness based on subjective evaluation of StratusOCT scan data

The study investigated the validity of a novel clinical tool (OCTAnalyse) that permits subjective measurement of RNFL thickness based on information obtained from the commercially available StratusOCT. The development of the software was prompted

by observations of erroneous RNFL thickness measurements by the standard StratusOCT analysis procedure during the study described in Chapter 4. OCTAnalyse was designed to overcome this limitation where errors persist on re-scanning and/or where re-scanning is not immediately possible.

The results of the study indicate that both automated (StratusOCT) and manual (OCTAnalyse) exhibit excellent within-test repeatability of measurements, (ICC 0.81-0.98), although measurements obtained by StratusOCT were more repeatable than those obtained using OCTAnalyse. In addition, measurements obtained by OCTAnalyse were statistically significantly greater than those obtained by StratusOCT.

Erroneous measurement of RNFL thickness were present from 7 of 41 patients examined with the StratusOCT. In all of these cases, the measurement errors were due to mislocation of the retinal interface borders and occurred either due to a detached internal limiting membrane or localised diminution in retinal reflectivity.

The study demonstrated the utility and caveats for the use of OCTAnalyse in a clinical setting. In its current form, OCTAnalyse can improve the ability of StratusOCT to detect OAG. With refinements to the current OCTAnalyse, as suggested in Section 6.2.3, the software is likely to be a useful add-on to the commercially available StratusOCT for both cross-sectional and longitudinal use in patients exhibiting persistant errors in RNFL thickness measurement by the standard technique.

6.2 Proposals for future work

6.2.1 Some dissociating factors in the analysis of structural and functional progressive damage in OAG

The failure of the TCA and the GPA to account for disease severity is an important clinical issue, which limits the ability of the both techniques to identify structural and functional progressive damage, respectively. The development of progression criteria for use with the HRT and HFA instruments, which account for both the severity and characteristics of the disease, would enhance the ability to detect progressive damage throughout the entire course of the disease process than is presently possible. This may involve: scaling the number of magenta super-pixels that are necessary in follow-up scans to confirm progressive structural damage with the available neuroretinal rim area for a given ONH, or employing a Size V stimulus to measure differential light sensitivity at visual field locations exhibiting variability beyond the dynamic range of the HFA.

More longitudinal studies, involving large numbers of participants, are required to determine the appropriateness of retinal surface height (TCA) and differential light sensitivity (GPA) as surrogate measures of progressive RGC damage. The ability of other promising techniques, such as OCT and the mfVEP, has yet to be determined as part of a longitudinal investigation.

The first step in corroborating the validity of new and evolving methods, as clinically reliable techniques for detecting progressive damage, will be improving the level of concordance between structural and functional tests for OAG.

6.2.2 Novel approaches to glaucoma detection

Based on the outcomes of the study, future work involving further development of the statistical analyses employed by each of the techniques. For example, this may involve determining how the diagnostic precision of the StratusOCT RNFL thickness measurements is affected when measurements are corrected for between-individual differences in ONH size; determining how the diagnostic precision of the HRT III MRA is affected when additional stereometric parameters, such as RNFL thickness, are incorporated into the algorithm; determining the clinical utility of interocular differences in the RNFL thickness and ONH topography using the StratusOCT and the HRT III, respectively, as means to detect glaucomatous structural damage; enlargement of the mfVEP normative database appropriate for the local recording environment and the development of more sophisticated analysis methods for mfVEP, analogous to Statpac for the HFA.

A longitudinal follow-up of the normal participants classified as abnormal by one, or more, of the techniques should be undertaken to determine whether any of these individuals developed OAG at a later date.

The 'ideal' diagnostic technique for OAG would provide objective, reproducible and rapid measurements that are a direct representation of ganglion cell injury/death and thus exhibit high diagnostic precision for the disease at the earliest stage. The current promising techniques for the detection of OAG, including the emerging 'gold standard', DSI, provide a surrogate assessment of the structural or functional integrity in OAG. It is speculated that a more appropriate evaluation for glaucomatous damage

would involve direct assessment of RGC function. One emerging technology, namely functional ultra-high resolution OCT (Optophysiology), represents perhaps the most promising techniques for directly assessing RGC function (Bizheva K, et al. 2006). Further studies are necessary to determine whether this and/or other new techniques are capable of advancing the ability to detect OAG to an earlier stage than is currently possible.

6.2.3 Novel estimation of RNFL thickness based on subjective evaluation of StratusOCT scan data

Based on the findings in this study, it will be important to determine the 'true' prevalence of erroneous RNFL thickness measurements in the population since this is currently unknown and has the potential to affect the longitudinal utility of OCT RNFL thickness measurements. It is possible that other artefacts, in addition to those described in this study, may be responsible for measurement errors. Thus a cross-sectional study involving a larger cohort of individuals will be necessary to determine the prevalence of erroneous measurements and whether, or nor, other types of artefacts exist.

Whether, or not, the fourth generation OCT will overcome the limitation of erroneous measurements is also grounds for future work. However, unless the interface recognition software for the new device is more intuitive to the artefacts described in this study, it can be speculated that measurement errors will persist even with the fourth generation instrument.

With respect to the current version of OCTAnalyse software, it is of interest to determine the between-observer and between-test effects on repeatability of RNFL thickness measurements. However, with a view to improving the overall repeatability of the technique, future developments of the OCTAnalyse software should involve removing the subjective component of the measurement procedure, for example, by incorporating a fully/semi-automated and intuitive interface recognition algorithm. This would provide a more standardised criteria for retinal interface recognition and also permit more rapid measurement and use of information from all of the 512 A-scans, rather than 24 A-scans as at present.

There is a clear role for software such as revised versions of OCTAnalyse in routine clinical management of patients with OAG. With the suggested refinements to the current OCTAnalyse software, it is feasible that the RNFL thickness measurements obtained by this technique could be superior to those obtained using the automated OCT analysis, in terms of fewer erroneous measurements and greater within- and between-test repeatability, and could become the analysis method of choice for all individuals with OAG.

6.3 Overall conclusions

The overall findings from the three studies provide important information for clinicians implementing the promising techniques for the routine management of patients with OAG. Interestingly, each of the techniques has shown major limitations for their use clinically.

In the case of OCT, which in the cross-sectional study (Chapter 4) exhibited high specificity for OAG (95.0%), the technique exhibited poor sensitivity for OAG (43.5%, for OAG using the StratusOCT). A proportion of the participants (7 of 41) yielded StratusOCT scans which occurred due to mis-location of the anterior or posterior RNFL interface. An investigation into the validity of an alternative method to measure RNFL thickness was prompted by this finding (Chapter 5). However, the new method, namely OCTAnalyse, whilst permitting measurement of RNFL thickness in scans containing measurement errors, yielded measurements which were statistically significantly thicker than those obtained by the standard technique and exhibited poorer within-session repeatability of measurements.

In the case of the mfVEP, the cross-sectional study (Chapter 4) showed that this technique exhibited sub-optimal diagnostic precision, both in terms of sensitivity (69.6%, for OAG using VERIS) and specificity (60.0%), for clinical use in detecting OAG. It should, however, be noted that the mfVEP technique is at a much earlier stage in its development than other more established promising techniques such as CSLO using the HRT and OCT using the StratusOCT.

In the case of CSLO, which in the cross-sectional study (Chapter 4), exhibited high sensitivity for OAG (91.3%, for OAG using the HRT III MRA), the technique exhibited poor specificity for OAG (65.0%, using HRT III MRA and 80.0%, using the HRT II MRA). In the longitudinal study (Chapter 3), whilst demonstrating the ability to detect progressive structural damage (HRT II Topographical Change Analysis [TCA]), CSLO was limited in its ability to detect progressive damage in individuals

with marked attenuation of the neuroretinal rim and exhibited poor concordance with progressive functional damage by SAP.

Whilst not considered as a promising technique for the detection of OAG, SAP also showed several inherent limitations. In the cross-sectional study (Chapter 5), whilst exhibiting high specificity for OAG (95.0%), the sensitivity of SAP was below a level now deemed acceptable for clinical use (47.8%, for OAG using the HFA). In the longitudinal study (Chapter 3), SAP was able to detect progressive functional damage; however, the technique failed to detect progressive damage in the presence of the perimetric learning effect and/or where regions of the visual field loss exhibit variability of the threshold response beyond the dynamic range of the HFA during the baseline examinations.

In the cross-sectional study (Chapter 4), the standard technique used to determine the diagnostic performance of all other techniques was DSI. Digital stereoscopic ONH-imaging was able to correctly classified 100% of individuals originally recruited either as normal or glaucomatous on the basis of consensus agreement; however, there was some overlap in agreement between observers in several participants. The Gestalt principles used by a clinician to define OAG using digital and/or standard stereoscopic ONH-imaging are the same as those employed when using conventional ophthalmoscopy, which was devised over 100 years ago. Thus, despite providing clinicians with the state-of-the-art means to quantify the structural and functional status in OAG, there is little evidence to support the use of any of the promising techniques as the 'complete' technique in OAG management.

References

Abrams LS, Scott IU, Spaeth GL, Quigley HA and Varma R. Agreement among optometrists, ophthalmologists, and residents in evaluating the optic disc for glaucoma. Ophthalmology 1994;101:1662-7.

Adams AJ, Rodic R, Husted R and Stamper R. Spectral sensitivity and colour vision discrimination changes in glaucoma and glaucoma-suspect patients. Investigative Ophthalmology and Visual Science 1982;23:516-24.

Agapova OA, Kaufman PL, Lucarelli MJ, Gabelt BT and Hernandez MR. Differential expression of matrix metalloproteinases in monkey eyes with experimental glaucoma or optic nerve transection. Brain Research 2003;967:132-43.

Agudelo LM, Molina CA and Alvarez DL. Changes in the intraocular pressure after laser in situ keratomileusis for myopia, hyperopia, and astigmatism. Journal of Refractive Surgery 2002;18:472-4.

Ahn JK and Park KH. Morphometric change analysis of the optic nerve head in unilateral disk hemorrhage cases. American Journal of Ophthalmology 2002;134:920-2.

Airaksinen PJ, Mustonen E and Alanko HI. Optic disc haemorrhages precede retinal nerve fibre layer defects in ocular hypertension. Acta Ophthalmologica (Copenh.) 1981;59:627-41.

Airaksinen PJ and Tuulonen A. Early glaucoma changes in patients with and without an optic disc haemorrhage. Acta Ophthalmologica (Copenh.) 1984;62:197-202.

Airaksinen PJ, Tuulonen A and Alanko HI. Rate and pattern of neuroretinal rim area decrease in ocular hypertension and glaucoma. Archives of Ophthalmology 1992;110:206-10.

Ajtony C, Balla Z, Somoskeoy S and Kovacs B. Relationship between visual field sensitivity and retinal nerve fiber layer thickness as measured by optical coherence tomography. Investigative Ophthalmology and Visual Science 2007;48:258-63.

Alamouti B and Funk J. Retinal thickness decreases with age: an OCT study. British Journal of Ophthalmology 2003;87:899-901.

American Academy of Ophthalmology. Primary open angle glaucoma. Preffered practice pattern. American Academy of Ophthalmology 2000:1-36.

Anderson AJ and Johnson CA. Frequency-Doubling Technology perimetry and optical defocus. Investigative Ophthalmology and Visual Science 2003;44:4147-52.

Anderson AJ and Johnson CA. Mechanisms isolated by Frequency-Doubling Technology perimetry. Investigative Ophthalmology and Visual Science 2002;43:398-401.

Anderson AJ, Johnson CA, Fingeret M, Keltner JL, Spry PG, Wall M and Werner JS. Characteristics of the normative database for the Humphrey Matrix perimeter. Investigative Ophthalmology and Visual Science 2005;46:1540-8.

Anderson DR. Basis of quantitative perimetry. In: Kist K, editor. Automated Static Perimetry. St. Louis: Mosby-Year Book; 1992. p. 10-29.

Anderson DR. Glaucoma: the damage caused by pressure. XLVI Edward Jackson memorial lecture. American Journal of Ophthalmology 1989;108:485-95.

Anderson DR. What happens to the optic disc and retina in glaucoma? Ophthalmology 1983;90:766-70.

Anderson RS and O'Brien C. Psychophysical evidence for selective loss of M ganglion cells in glaucoma. Vision Research 1997;37:1079-83.

Anton A, Andrada MT, Mujica V, Calle MA, Portela J and Mayo A. Prevalence of primary open-angle glaucoma in a Spanish population: the Segovia study. Journal of Glaucoma 2004;13:371-6.

Anton A, Yamagishi N, Zangwill L, Sample PA and Weinreb RN. Mapping structural to functional damage in glaucoma with standard automated perimetry and confocal scanning laser ophthalmoscopy. American Journal of Ophthalmology 1998;125:436-46.

Armaly MF. Ocular pressure and visual fields: A ten-year follow-up study. Archives of Ophthalmology 1969;81:25-40.

Armaly MF, Krueger DE, Maunder L, Becker B, Hetherington J Jr, Kolker AE, Levene RZ, Maumenee AE, Pollack IP and Shaffer RN. Biostatistical analysis of the collaborative glaucoma study. I. Summary report of the risk factors for glaucomatous visual-field defects. Archives of Ophthalmology 1980;98:163-71.

Artes PH and Chauhan BC. Longitudinal changes in the visual field and optic disc in glaucoma. Progress in Retinal Eye Research 2005;24:333-54.

Artes PH, Iwase A, Ohno Y, Kitazawa Y and Chauhan BC. Properties of perimetric threshold estimates from Full Threshold, SITA Standard, and SITA Fast strategies. Investigative Ophthalmology and Visual Science 2002;43:2654-9.

Artes PH, Nicolela MT, LeBlanc RP and Chauhan BC. Visual field progression in glaucoma: Total versus Pattern Deviation analyses. Investigative Ophthalmology and Visual Science 2005;46:4600-6.

Asman P and Heijl A. Glaucoma Hemifield Test. Automated visual field evaluation. Archives of Ophthalmology 1992;110:812-9.

Asrani S, Challa P, Herndon L, Lee P, Stinnett S and Allingham RR. Correlation among retinal thickness, optic disc and visual field in glaucoma patients and suspects: a pilot student. Journal of Glaucoma 2003;12:119-28.

Asrani S, Zou S, D' Anna S, Vitale S and Zeimer R. Noninvasive mapping of the normal retinal thickness at the posterior pole. Ophthalmology 1999;106:269-73.

Bach M. Electrophysiologic approaches for early detection of glaucoma. European Journal of Ophthalmology 2001;2:S41-9.

Bach M. Latency of the mfVEP to diagnose glaucoma? British Journal of Ophthalmology 2006;90:1076-7.

Bach M and Mathieu M. Different effect of dioptric focus vs. light scatter on the pattern electroretinogram (PERG). Documenta Ophthalmologica 2004;108:99-106.

Bach M, Sullima F and Gerling J. Little correlation of the pattern electroretinogram (PERG) and visual field measures in early glaucoma. Documenta Ophthalmologica 1998;94:253-63.

Bagga H and Greenfield DS. Quantitative assessment of structural damage in eyes with localized visual field abnormalities. American Journal of Ophthalmology 2004;137:797-805.

Bagga H, Greenfield DS, Feuer W and Knighton RW. Scanning laser polarimetry with variable corneal compensation and optical coherence tomography in normal and glaucomatous eyes. American Journal of Ophthalmology 2003;135:521-9.

Bagga H, Greenfield DS and Knighton RW. Macular symmetry testing for glaucoma detection. Journal of Glaucoma 2005;5:358-63.

Balachandran C, Graham SL, Klistorner A and Goldberg I. Comparison of objective diagnostic tests in glaucoma: Heidelberg Retinal Tomography and multifocal visual evoked potentials. Journal of Glaucoma 2006;15:110-6.

Balachandran C, Klistorner AI and Graham SL. Effect of stimulus check size on multifocal visual evoked potentials. Documenta Ophthalmologica 2003;106:183-8.

Baseler HA, Sutter EE, Klein SA and Carney T. The topography of the visual evoked response properties across the visual field. Electroencephalography and Clinical Neurophysiology 1994;90:65-81.

Bathija R, Zangwill L, Berry CC, Sample PA and Weinreb RN. Detection of early glaucomatous structural damage with confocal scanning laser tomography. Journal of Glaucoma 1998;7:121-7.

Bayer AU and Erb C. Short wavelength automated perimetry, Frequency Doubling Technology perimetry and pattern electroretinography for prediction of progressive glaucomatous standard visual field defects. Ophthalmology 2002;109:1009-17.

Bayer AU, Maag KP and Erb C. Detection of optic neuropathy in glaucomatous eyes with normal standard visual fields using a test battery of short-wavelength automated perimetry and pattern electroretinography. Ophthalmology 2002;109:1350-61.

Bearse MA and Sutter E. Imaging localized retinal dysfunction with the multifocal electroretinogram. Journal of the Optical Society of America 1996;13:634-40.

Bearse MA, Sutter EE, Smith DN and Stamper R. Ganglion cell components of the human multi-focal ERG are abnormal in optic nerve atrophy and glaucoma. Investigative Ophthalmology and Visual Science 1995;36:445.

Bebie H, Fankhauser F and Spahr J. Static perimetry: accuracy and fluctuations. Acta Ophthalmologica (Copenh.) 1976;53:339-48.

Bellezza AJ, Rintalan CJ, Thompson HW, Downs JC, Hart RT and Burgoyne CF. Deformation of the lamina cribrosa and anterior scleral canal wall in experimental glaucoma. Investigative Ophthalmology and Visual Science 2003;44:623-37.

Bengtsson B. A new rapid algorithm for short-wavelength automated perimetry. Investigative Ophthalmology and Visual Science 2003;44:1388-94.

Bengtsson B. Reliability of computerized perimetric threshold tests as assessed by reliability and threshold reproducibility in patients with suspect and manifest glaucoma. Acta Ophthalmologica Scandinavica 2000;78:519-22.

Bengtsson B and Heijl A. Normal intersubject threshold variability and normal limits of SITA SWAP and Full Threshold SWAP perimetric programs. Investigative Ophthalmology and Visual Science 2003;44:5029-34.

Bengtsson B, Lindgren A, Heijl A, Lindgren G, Asman P and Patella M. Perimetric probability maps to separate change caused by glaucoma from that caused by cataract. Acta Ophthalmologica Scandinavica 1997;75:184-8.

Bengtsson B, Olsson J, Heijl A and Rootzen H. A new generation of algorithms for computerized threshold perimetry, SITA. Acta Ophthalmologica Scandinavica 1997;75:368-75.

Berninger T and Schuurmans RP. Spatial tuning of the pattern ERG across temporal frequency. Documenta Ophthalmologica 1985;61:17-25.

Birt CM, Shin DH, McCarty B, Kim C, Lee DT and Chung HS. Comparison between High-pass Resolution perimetry and differential light sensitivity perimetry in patients with glaucoma. Journal of Glaucoma 1998;7:111-6.

Bizheva K, Pflug R, Hermann B, Povazay B, Sattmann H, Qiu P, Anger E, Reitsamer H, Popov S, Taylor JR, Unterhuber A, Ahnelt P and Drexler W. Optophysiology: depth-resolved probing of retinal physiology with functional ultrahigh-resolution optical coherence tomography. Proceedings of the National Academy of Sciences of the United States of America 2006;28:5066-71.

Bjerre A, Grigg JR, Parry NRA and Henson DB. Test-retest variability of multifocal visual evoked potential and SITA Standard perimetry in glaucoma. Investigative Ophthalmology and Visual Science 2004;45:4035-40.

Bland JM and Altman DG. Measuring agreement in method comparison studies. Statistical Methods in Medical Research 1999;8:135-60.

Bland JM and Altman DG. Statistical methods for assessing agreement between two methods of clinical measurement. Lancet 1986;i:307-10.

Blumenthal EZ, Parikh RS, Pe'er J, Naik M, Kaliner E, Cohen MJ, Prabakaran S, Kogan M and Thomas R. Retinal nerve fibre layer imaging compared with histological measurements in a human eye. Eye 2007;24:Epub ahead of print.

Blumenthal EZ, Sample PA, Berry CC, Lee AC, Girkin CA, Zangwill LM, Caprioli J and Weinreb RN. Evaluating several sources of variability for standard and SWAP visual fields in glaucoma patients, suspects, and normals. Ophthalmology 2003;110:1895-902.

Blumenthal EZ, Williams JM, Weinreb RN, Girkin CA, Berry CC and Zangwill LM. Reproducibility of nerve fiber layer thickness measurements by use of optical coherence tomography. Ophthalmology 2000;107:2278-82.

Boden C, Pascaul J, Medeiros FA, Athara M, Weinreb RN and Sample PA. Relationship of SITA and Full-threshold Standard perimetry to Frequency-Doubling Technology perimetry. Investigative Ophthalmology and Visual Science 2005;46:2433-9.

Bosworth CF, Sample PA, Gupta N, Bathija R and Weinreb RN. Motion automated perimetry identifies early glaucomatous field defects. Archives of Ophthalmology 1998;116:1153-8.

Bourne RR, Medeiros FA, Bowd C, Jahanbakhsh K, Zangwill LM and Weinreb RN. Comparability of retinal nerve fiber layer thickness measurements of optical coherence tomography instruments. Investigative Ophthalmology and Visual Science 2005;46:1280-5.

Bowd C, Chan K, Zangwill LM, Goldbaum MH, Lee T, Sejnowski TJ and Weinreb RN. Comparing neural networks and linear discriminant functions for glaucoma

detection using confocal scanning laser ophthalmoscopy of the optic disc. Investigative Ophthalmology and Visual Science 2002;43:3444-54.

Bowd C, Zangwill LM, Berry CC, Blumenthal EZ, Vasile C, Sanchez-Galeana C, Bosworth CF, Sample PA and Weinreb RN. Detecting early glaucoma by assessment of retinal nerve fibre layer thickness and visual function. Investigative Ophthalmology and Visual Science 2001;42:1993-2003.

Bowd C, Zangwill LM, Medeiros FA, Hao J, Chan K, Lee T, Sejnowski TJ, Goldbaum MH, Sample PA, Crowston JG and Weinreb RN. Confocal scanning laser ophthalmoscopy classifiers and stereophotograph evaluation for prediction of visual field abnormalities in glaucoma-suspect eyes. Investigative Ophthalmology and Visual Science 2004;45:2255-62.

Bowd C, Zangwill LM, Medeiros FA, Tavares IM, Hoffmann EM, Bourne RR, Sample PA and Weinreb RN. Structure-function relationships using confocal scanning laser ophthalmoscopy, optical coherence tomography, and scanning laser polarimetry. Investigative Ophthalmology and Visual Science 2006;47:2889-95.

Bowd C, Zangwill LM and Weinreb RN. Association between scanning laser polarimetry measurements using variable corneal polarization compensation and visual field sensitivity in glaucomatous eyes. Archives of Ophthalmology 2003;121:961-6.

Brandt JD. Corneal thickness in glaucoma screening, diagnosis, and management. Current Opinion in Ophthalmology 2004;15:85-9.

Brandt JD, Beiser JA, Kass MA and Gordon MO. Central corneal thickness and the Ocular Hypertension Treatment Study (OHTS). Ophthalmology 2001;108:1779-88.

Brigatti L, Hoffman D and Caprioli J. Neural networks to identify glaucoma with structural and functional measurements. American Journal of Ophthalmology 1996;121:511-21.

Brigatti L, Weitzman M and Caprioli J. Regional test-retest variability of confocal scanning laser tomography. American Journal of Ophthalmology 1995;120:433-40.

Broadway DC, Nicolela MT and Drance SM. Optic disk appearances in primary open-angle glaucoma. Survey of Ophthalmology 1999;Suppl 1:S223-43.

Brusini P, Salvetat ML, Zeppieri M and Parisi L. Frequency doubling technology perimetry with the Humphrey Matrix 30-2 test. Journal of Glaucoma 2006;15:77-83.

Budenz DL, Chang RT, Huang X, Knighton RW and Tielsch JM. Reproducibility of retinal nerve fiber thickness measurements using the StratusOCT in normal and glaucomatous eyes. Investigative Ophthalmology and Visual Science 2005;46:2440-3.

Budenz DL, Michael A, Chang RT, McSoley J and Katz J. Sensitivity and specificity of the StratusOCT for perimetric glaucoma. Ophthalmology 2005;112:3-9.

Budenz DL, Rhee P, Feuer WJ, McSoley J, Johnson CA and Anderson DR. Sensitivity and specificity of the Swedish interactive threshold algorithm for glaucomatous visual field defects. Ophthalmology 2002;109:1052-8.

Bui BV and Fortune B. Ganglion cell contributions to the rat full-field electroretinogram. Journal of Physiology 2004;555:153-73.

Burgansky-Eliash Z, Wollstein G, Bilonick RA, Ishikawa H, Kagemann L and Schuman JS. Glaucoma detection with the Heidelberg retina tomograph 3. Ophthalmology 2007;114:466-71.

Cello KE, Nelson-Quigg JM and Johnson CA. Frequency Doubling Technology perimetry for detection of glaucomatous visual field loss. American Journal of Ophthalmology 2000;129:314-22.

Chatterjee A, Shah S, Bessant DA, Naroo SA and Doyle SJ. Reduction in intraocular pressure after excimer laser photorefractive keratectomy. Correlation with pretreatment myopia. Ophthalmology 1997;104:355-9.

Chauhan BC, Blanchard JW, Hamilton DC and LeBlanc RP. Technique for detecting serial topographic changes in the optic disc and peripapillary retina using scanning laser tomography. Investigative Ophthalmology and Visual Science 2000;41:775-82.

Chauhan BC, Drance SM, Douglas GR and Johnson CA. Visual field damage in normal-tension and high-tension glaucoma. American Journal of Ophthalmology 1989;108:636-42.

Chauhan BC and House PH. Intratest variability in conventional and High-pass Resolution perimetry. Ophthalmology 1991;98:79-83.

Chauhan BC and Johnson CA. Test-retest variability of Frequency-Doubling perimetry and conventional perimetry in glaucoma patients and normal subjects. Investigative Ophthalmology and Visual Science 1999;40:648-56.

Chauhan BC, Le Blanc RP, McCormick TA and Rogers JB. Test-retest variability of topographic measurements with confocal scanning laser tomography in patients with glaucoma and control subjects. American Journal of Ophthalmology 1994;118:9-15.

Chauhan BC, McCormick TA, Nicolela MT and LeBlanc RP. Optic disc and visual field changes in a prospective longitudinal study of patients with glaucoma:

comparison of scanning laser tomography with conventional perimetry and optic disc photography. Archives of Ophthalmology 2001;119:1492-9.

Chauhan BC, Tompkins J, Le Blanc RP and McCormick TA. Characteristics of frequency of seeing curves in normal subjects, patients with suspected glaucoma, and patients with glaucoma. Investigative Ophthalmology and Visual Science 1993;34:3534-40.

Chen CS, Hood DC, Zhang X, Karam EZ, Liebmann JM, Ritch R, Thienprasiddhi P and Greenstein VC. Repeat reliability of the multifocal visual evoked potential in normal and glaucomatous eyes. Journal of Glaucoma 2003;12:399-408.

Chihara E, Liu X, Dong J, Takashima Y, Akimoto M, Hangai M, Kuriyama S, Tanihara H, Hosoda M and Tsukahara S. Severe myopia as a risk factor for progressive visual field loss in primary open-angle glaucoma. Ophthalmologica 1997;211:66-71.

Chiou GC. Review: Effects of nitric oxide on eye diseases and their treatment. Journal of Ocular Pharmacology and Therapeutics 2001;17:189-98.

Chylack LT, Wolfe JK, Singer DM, Leske CM, Bullimore MA, Bailey IL, Friend J, McCarthy D and Wu SK. The Lens Opacities Classification System III. Archives of Ophthalmology 1993;111:831-6.

Cioffi GA and Leibmann JM. Translating the OHTS results into clinical practice. Journal of Glaucoma 2002;11:375-7.

Clark VP, Fan S and Hillyard SA. Identification of early visually evoked potential generators by retinotopic and topographic analysis. Human Brain Mapping 1995;2:170-87.

Coleman AL, Sommer A and Enger C. Interobserver and intraobserver variability in the detection of glaucomatous progression of the optic disc. Journal of Glaucoma 1996;5:384-9.

Colotto A, Falsini B, Salgarello T, Iarossi G, Galan ME and Scullica L. Photopic negative response of the human ERG: losses associated with glaucomatous damage. Investigative Ophthalmology and Visual Science 2000;41:2205-11.

Correnti AJ, wollstein G, Price LL and Schuman JS. Comparison of optic nerve head assessment with a digital stereoscopic camera (Discam), scanning laser ophthalmoscopy, and stereophotography. Ophthalmology 2003;110:1499-505.

Crawford ML, Harwerth RS, Smith III EL, Mills S and Ewing B. Experimental glaucoma in primates: changes in cytochrome oxidase blobs in V1 cortex. Investigative Ophthalmology and Visual Science 2001;42:358-64.

Curcio CA and Allen KA. Topography of ganglion cells in the human retina. Journal of Comparative Neurology 1990;300:5-25.

Cvenkel B. Retinal thickness at the posterior pole in glaucoma and ocular hypertension. Graefe's Archives for Clinical and Experimental Ophthalmology 2002;242:920-5.

Da Pozzo S, Fuser M, Vattovani O, Di Stefano G and Ravalico G. GDx-VCC performance in discriminating normal from glaucomatous eyes with early visual field

loss. Graefe's Archives for Clinical and Experimental Ophthalmology 2005;244:689-95.

Dacey D. The mosaic of midget ganglion cells in the human retina. Journal of Neuroscience 1993;13:5334-55.

Dacey D and Lee B. The 'blue-on' opponent pathway in primate retina originates from a distinct bistratified ganglion cell type. Nature 1994;367:731-5.

Danesh-Meyer HV, Gaskin BJ, Jayusundera T, Donaldson M and Gamble GD. Comparison of Disc Damage Likelihood Scale, cup to disc ratio, and Heidelberg Retina Tomograph in the diagnosis of glaucoma. British Journal of Ophthalmology 2006;90:437-41.

Danesh-Meyer HV, Ku JY, Papchenko TL, Jayasundera T, Hsiang JC and Gamble GD. Regional correlation of structure and function in glaucoma, using the Disc Damage Likelihood Scale, Heidelberg Retina Tomograph, and visual fields. Ophthalmology 2006;113:603-11.

Dawson VL and Dawson TM. Nitric oxide actions in neurochemistry. Neurochemistry International 1996;29:97-110.

Daxer A, Misof K, Grabner B, Ettl A and Fratzl P. Collagen fibrils in the human corneal stroma: structure and aging. Investigative Ophthalmology and Visual Science 1998;39:644-8.

De Leon-Ortega JE, Arthur SN, McGwin G Jr, Xie A, Monheit BE and Girkin CA. Discrimination between glaucomatous and nonglaucomatous eyes using quantitative

imaging devices and subjective optic nerve head assessment. Investigative Ophthalmology and Visual Science 2006;47:3374-80.

De Leon-Ortega JE, Sakata LM, Kakati B, McGwin G Jr, Monheit BE, Arthur SN and Girkin CA. Effect of glaucomatous damage on repeatability of confocal scanning laser ophthalmoscope, scanning laser polarimetry, and optical coherence tomography. Investigative Ophthalmology and Visual Science 2007;48(3):1156-63.

Deeks JJ and Altman DG. Diagnostic tests 4: likelihood ratios. British Medical Journal 2004;329:168-169.

Demirel S and Johnson CA. Incidence and prevalence of short wavelength automated perimetry deficits in ocular hypertensive patients. American Journal of Ophthalmology 2001;131:709-15.

Dengler-Harles M, Wild JM, Cole MD, O'Neill EC and Crews SJ. The influence of forward light scatter on the visual indices in glaucoma. Graefe's Archives for Clinical and Experimental Ophthalmology 1990;228:326-31.

Dichtl A, Jonas JB and Naumann GO. Retinal nerve fiber layer thickness in human eyes. Graefe's Archives for Clinical and Experimental Ophthalmology 1999;237:474-9.

Dielemans I, de Jong PT, Stolk R, Vingerling JR, Grobbee DE and Hofman A. Primary open-angle glaucoma, intraocular pressure, and diabetes mellitus in the general elderly population. The Rotterdam Study. Ophthalmology 1996;103:1271-5.

Doughty MJ and Zaman ML. Human corneal thickness and its impact on intraocular pressure measures: A review and meta-analysis approach. Survey of Ophthalmology 2000;44:367-408.

Drance SM. Bowman Lecture. Glaucoma--changing concepts. Eye 1992;6:337-45.

Drance SM. Disc haemorrhages in glaucomas. Survey of Ophthalmology 1989;33:331-7.

Drance SM. The early field defects in glaucoma. Investigative Ophthalmology and Visual Science 1969;8:84-91.

Drance SM. Glaucoma: a look beyond intraocular pressure. American Journal of Ophthalmology 1997;123:817-9.

Drasdo N, Aldebasi YH, Chiti Z, Mortlock KE, Morgan JE and North RV. The S-cone PHNR and pattern ERG in primary open angle glaucoma. Investigative Ophthalmology and Visual Science 2001;42:1266-72.

Dreher AW and Weinreb RN. Accuracy of topographic measurements in a model eye with the laser tomographic scanner. Investigative Ophthalmology and Visual Science 1991;32:2992-6.

Dreyer EB. A proposed role for excitotoxicty in glaucoma. Journal of Glaucoma 1998;7:62-7.

Dreyer EB, Zurakowski D, Schumer RA, Podos SM and Lipton SA. Elevated glutamate levels in the vitreous body of humans and monkeys with glaucoma. Archives of Ophthalmology 1996;114:299-305.

Duncan RO and Boynton RM. Cortical magnification within human primary visual cortex correlates with acuity thresholds. Neuron 2003;22:659-71.

Ehlers N, Bramsen T and Sperling S. Applanation tonometry and central corneal thickness. Acta Ophthalmologica (Copenh.) 1975;53:34-43.

European Glaucoma Prevention Study (EGPS) Group. The European Glaucoma Prevention Study design and baseline description of the participants. Ophthalmology 2002;110:340-4.

Ferreras A, Pablo LE, Larrosa JM, Polo V, Pajarin AB and Honrubia FM. Discriminating between normal and glaucoma-damaged eyes with the Heidelberg Retina Tomograph 3. Ophthalmology 2007;Epub ahead of print.

Fingeret M, Medeiros F, Susanna R Jr and Weinreb RN. Five rules to evaluate the optic disc and retinal nerve fibre layer for glaucoma. Optometry 2005;76:661-8.

Flammer J, Drance SM, Fankhauser F and Augustiny L. Differential light threshold in automated static perimetry. Factors influencing short-term fluctuation. Archives of Ophthalmology 1984;102:876-9.

Flammer J, Drance SM and Schulzer M. Covariates of the long-term fluctuation of the differential light threshold. Archives of Ophthalmology 1984;102:880-2.

Flammer J, Drance SM and Schulzer M. The estimation and testing of the components of Long-term Fluctuation of the differential light threshold. Documenta ophthalmologica. Proceedings series 1983;35:383-9.

Flood T and Flanagan JG. The influence of detection versus resolution threshold criteria in Frequency Doubling perimetry (Abstract). Optometry and Vision Science 1998;75:31.

Ford BA, Artes PH, McCormick TA, Nicolela MT, Le Blanc RP and Chauhan BC. Comparison of data analysis tools for the detection of glaucoma with the Heidelberg Retina Tomograph. Ophthalmology 2003;110:1145-50.

Fortune B, Bearse MA, Cioffi GA and Johnson CA. Selective loss of an oscillatory component from the temporal retinal multifocal ERG responses in glaucoma. Investigative Ophthalmology and Visual Science 2002;43:2638-47.

Fortune B, Bui BV, Morrison JC, Johnson EC, Dong J, Cepurna WO, Jia L, Barber S and Cioffi GA. Selective ganglion cell functional loss in rats with experimental glaucoma. Investigative Ophthalmology and Visual Science 2004;45:1854-62.

Fortune B, Demirel S, Zhang X, Hood DC and Johnson CA. Repeatability of normal multifocal VEP: implications for detecting progression. Journal of Glaucoma 2006;15:131-41.

Fortune B, Demirel S, Zhang X, Hood DC, Patterson E, Jamil A, Mansberger SL, Cioffi GA and Johnson CA. Comparing multifocal VEP and standard automated perimetry in high-risk ocular hypertension and early glaucoma. Investigative Ophthalmology and Visual Science 2007;48:1173-80.

Fortune B, Zhang X, Hood DC, Demirel S and Johnson CA. Normative ranges and specificity of the multifocal VEP. Documenta Ophthalmologica 2004;109:87-100.

Friedburg C, Allen CP, Mason PJ and Lamb TD. Contribution of cone photoreceptors and post-receptoral mechanisms to the human photopic electroretinogram. Journal of Physiology 2004;556:819-34.

Friedburg C, Thomas MM and Lamb TD. Time course of the flash response of dark- and light-adapted human rod photoreceptors derived from the electroretinogram. Journal of Physiology 2001;534:217-42.

Friedenwald JS. Contribution to the theory and practice of tonometry. American Journal of Ophthalmology 1937;20:985.

Frisen L. Vanishing Optotypes. New type of acuity test letters. Archives of Ophthalmology 1986;104:1194-8.

Frisen L and Frisen M. A simple relationship between the probability distribution of visual acuity and the density of retinal output channels. Acta Ophthalmologica 1976;54:437-44.

Fujimoto N, Minowa K and Miyauchi O. Learning effect for Frequency Doubling perimetry in patients with glaucoma. American Journal of Ophthalmology 2002;133:269-70.

Gardiner SK, Johnson CA and Cioffi GA. Evaluation of the structure-function relationship in glaucoma. Investigative Ophthalmology and Visual Science 2005;46:3712-7.

Gardiner SK, Johnson CA and Spry PG. Normal age-related sensitivity loss for a variety of visual functions throughout the visual field. Optometry and Vision Science 2006;83:438-43.

Garway-Heath DF and Hitchings RA. Quantitative evaluation of the optic nerve head in early glaucoma. British Journal of Ophthalmology 1998;82:352-61.

Garway-Heath DF, Holder GE, Fitzke FW and Hitchings RA. Relationship between electrophysiological, psychophysical, and anatomical measurements in glaucoma. Investigative Ophthalmology and Visual Science 2002;43:2213-20.

Garway-Heath DF, Poinoosawmy D, Fitzke FW and Hitchings RA. Mapping the visual field to the optic disc in normal tension glaucoma. Ophthalmology 2000;107:1809-15.

Garway-Heath DF, Poinoosawmy D, Wollstein G, Viswanathan A, Kamal D, Fontana L and Hitchings RA. Inter- and intraobserver variation in the analysis of optic disc images: comparison of the Heidelberg Retina Tomograph and computer assisted planimetry. British Journal of Ophthalmology 1999;83:664-9.

Garway-Heath DF, Rudnicka AR, Lowe T, Foster PJ, Fitzke FW and Hitchings RA. Measurement of optic disc size: equivalence of methods to correct for ocular magnification. British Journal of Ophthalmology 1998;82:643-9.

Geiger LK, Korteum KR, Alexejum C and Levin LA. Reduced redox state allows prolonged survival of axotomized neonatal retinal ganglion cells. Neuroscience 2002;109:641-6.

Giovannini A, Amato G and Mariotti C. The macular thickness and volume in glaucoma: an analysis in normal and glaucomatous eyes using OCT. Acta Ophthalmologica Scandinavica 2002;Suppl. 236(80):34-6.

Girkin CA, Emdadi A, Sample PA, Blumenthal EZ, Lee AC, Zangwill LM and Weinreb RN. Short-wavelength automated perimetry and standard perimetry in the detection of progressive optic disc cupping. Archives of Ophthalmology 2000;118:1231-6.

Gloster J. Incidence of optic disc haemorrhages in chronic simple glaucoma and ocular hypertension. British Journal of Ophthalmology 1981;65:452-6.

Gloster J and Perkins ES. The validity of the Imbert-Fick law as applied to applanation tonometry. Experimental Eye Research 1963;44:274-83.

Glovinsky Y, Quigley HA and Dunkelberger GR. Retinal ganglion cell loss is size dependent in experimental glaucoma. Investigative Ophthalmology and Visual Science 1991;32:484-91.

Goldberg I, Graham SL and Klistorner AI. Multifocal objective perimetry in the detection of glaucomatous field loss. American Journal of Ophthalmology 2002;133(1):29-39.

Goldstick BJ and Weinreb RN. The effect of refractive error on automated global analysis Program G-1. American Journal of Ophthalmology 1987;104:229-32.

Gonzalez de la Rosa M and Pajera A. Influence of the "fatigue effect" on the Mean Deviation measuement in perimetry. European Journal of Ophthalmology 1997;7:29-34.

Gordon MO, Beiser JA, Brandt JD, Heuer DK, Higginbotham EJ, Johnson CA, Keltner JL, Miller JP, Parrish II RK, Wilson R and Kass MA. The Ocular

Hypertension Treatment Study: Baseline factors that predict the onset of primary open-angle glaucoma. Archives of Ophthalmology 2002;120:714-20.

Gordon MO and Kass MA - The Ocular Hypertension Treatment Study Group. The Ocular Hypertension Treatment Study: Design and Baseline Description of the Participants. Archives of Ophthalmology 1999;117:573-83.

Gotoh Y, Machida S and Tazawa Y. Selective loss of the photopic negative response in patients with optic nerve atrophy. Archives of Ophthalmology 2004;122:341-6.

Graham SL, Klistorner AI and Goldberg I. Clinical application of objective perimetry using multifocal visual evoked potentials in glaucoma practice. Archives of Ophthalmology 2005;123:729-39.

Graham SL, Klistorner AI, Grigg JR and Bilson FA. Objective VEP perimetry in glaucoma: asymmetry analysis to identify early deficits. Journal of Glaucoma 2000;9:10-9.

Greaney MJ, Hoffman DC, Garway-Heath DF, Nakla M, Coleman AL and Caprioli J. Comparison of optic nerve imaging methods to distinguish normal eyes from those with glaucoma. Investigative Ophthalmology and Visual Science 2002;43:140-5.

Greenfield DS, Bagga H and Knighton RW. Macular thickness changes in glaucomatous optic neuropathy detected using optical coherence tomography. Archives of Ophthalmology 2003;121:41-6.

Greenfield DS, Knighton RW and Huang XR. Effect of corneal polarization axis on assessment of retinal nerve fiber thickness by scanning laser polarimetry. American Journal of Ophthalmology 2000;129:715-22.

Greenfield DS, Knighton RW, schiffman J and Feuer W. Normative retardation data corrected for corneal polarization axis using scanning laser polarimetry. Ophthalmic Surgical Lasers 2003;34:165-71.

Grieshaber MC, Terhorst T and Flammer J. The pathogenesis of optic disc splinter haemorrhages: a new hypothesis. Acta Ophthalmologica Scandinavica 2006;84:62-8.

Grus FH, Joachim SC, Hoffman EM and Pfeiffer N. Complex autoantibody repertoires in patients with glaucoma. Molecular Vision 2004;25:132-7.

Guedes V, Schuman JS, Hertzmark E, Wollstein G, Correnti A, Mancini R, Lederer D, Voskanian S, Velazquez L, Pakter HM, Pedut-Kloizman T, Fujimoto JG and Mattox C. Optical coherence tomography measurement of macular and nerve fibre layer thickness in normal and glaucomatous human eyes. Ophthalmology 2003;110:177-89.

Gunvant P, O'Leary DJ, Baskaran M, Broadway DC, Watkins RJ and Vijaya L. Evaluation of tonometric correction factors. Journal of Glaucoma 2005;14:337-43.

Gurses-Ozden R, Teng C, Vessani R, Zafar S, Liebmann JM and Ritch R. Macular and retinal nerve fiber layer thickness measurement reproducibility using optical coherence tomography (OCT-3). Journal of Glaucoma 2004;13:238-44.

Guthauser U and Flammer J. Quantifying visual field damage caused by cataract. American Journal of Ophthalmology 1988;106:480-4.

Halliday AM, McDonald WI and Mushin J. Delayed visual evoked response in optic neuritis. Lancet 1972;1:982-985.

Harding GF, Odom JV, Spiliers W and Sperkreijse H. Standard for visual evoked potentials 1995. The International Society for the Clinical Electrophysiology of Vision. Vision Research 1996;36:3567-72.

Hare WA, Ton H, Ruiz G, Feldman B, Wijono M and Woldemussie E. Characterization of retinal injury using ERG measures obtained with both conventional and multifocal methods in ocular chronic hypertensive primates. Investigative Ophthalmology and Visual Science 2001;42:127-36.

Harper R, Reeves B and Smith B. Observer variability in optic disc assessment: implications for glaucoma shared care. Ophthalmic and Physiological Optics 2000;20:265-73.

Harrison JM, O'Connor PS, Young RS, Kincaid M and Bentley R. The pattern ERG in man following surgical resection of the optic nerve. Investigative Ophthalmology and Visual Science 1987;28:492-9.

Hart WM and Becker B. The onset and evolution of glaucomatous visual field defects. Ophthalmology 1982;89:268-79.

Harwerth RS, Carter-Dawson L, Smith III EL, Barnes G, Holt WF and Crawford ML. Neural losses correlated with visual losses in clinical perimetry. Investigative Ophthalmology and Visual Science 2004;45:3152-60.

Hasegawa S and Abe H. Mapping glaucomatous visual field defects by multifocal VEP's. Investigative Ophthalmology and Visual Science 2001;42:3341-8.

Hatch WV, Trope GE, Buys YM, Macken P, Etchells EE and Flanagan JG. Agreement in assessing glaucomatous discs in a clinical teaching setting with

stereoscopic disc photographs, planimetry, and laser scanning tomography. Journal of Glaucoma 1999;8:99-104.

Haymes SA, Hutchison DM, McCormick TA, Varma DK, Nicolela MT, LeBlanc RP and Chauhan BC. Glaucomatous visual field progression with Frequency-Doubling Technology and standard automated perimetry in a longitudinal prospective study. Investigative Ophthalmology and Visual Science 2005;46:547-54.

Healey PR, Mitchell P, Smith W and Wang JJ. Optic disc haemorrhages in a population with and without signs of glaucoma. Ophthalmology 1998;105:216-23.

Hee MR, Izatt JA, Swanson EA, Huang D, Schuman JS, Lin CP, Puliafito CA and Fujimoto JG. Optical coherence tomography of the human retina. Archives of Ophthalmology 1995;113:325-32.

Heijl A, Leske CM, Bengtsson B, Bengtsson B and Hussein M - The Early Manifest Glaucoma Group. Measuring visual field progression in the Early Manifest Glaucoma Trial. Acta Ophthalmologica Scandinavica 2003;81:286-93.

Heijl A, Leske MC, Bengtsson B, Hyman L, Bengtsson B and Hussein M - The Early Manifest Glaucoma Group. Reduction of intraocular pressure and glaucoma progression: Results from the Early Manifest Glaucoma Trial. Archives of Ophthalmology 2002;120:1268-79.

Heijl A, Lindgren G and Olsson J. The effect of perimetric experience in normal subjects. Archives of Ophthalmology 1989;107:81-6.

Heijl A, Lindgren G and Olsson J. Normal variability of static perimetric threshold values across the central visual field. Archives of Ophthalmology 1987;105:1544-9.

Heijl A, Lindgren G and Olsson J. Perimetric threshold variability and age. Archives of Ophthalmology 1988;106:450-2.

Heijl A, Lindgren G, Olsson J and Asman P. Visual field interpretation with empirical probability maps. Archives of Ophthalmology 1989;107:204-8.

Heinemann-Vernaleken B, Palmowski AM, Allgayer R and Ruprecht KW. Comparison of different high resolution multifocal electroretinogram recordings in patients with age-related maculopathy. Graefe's Archives for Clinical and Experimental Ophthalmology 2001;239:556-61.

Heltzer JM. Progression of peripapillary atrophy. Ophthalmology 1999;106:857.

Hendrickx KH, van den Enden A, Rasker MT and Hoyong PFJ. Cumulative incidence of patients with disc haemorrhages in glaucoma and the effect of therapy. Ophthalmology 1994;101:1165-72.

Henson DB, Evans J, Chauhan BC and Lane C. Influence of fixation accuracy on threshold variability in patients with open angle glaucoma. Investigative Ophthalmology and Visual Science 1996;37:444-50.

Heuer DK, Anderson DR, Feuer WJ and Gressel MG. The influence of refractive accuracy on automated perimetric threshold measurements. Ophthalmology 1987;94:1550-3.

Hodapp E, Parrish II RK and Anderson DR. Clinical decisions in glaucoma. St Louis: Mosby; 1993.

Hoh ST, Greenfield DS, Mistelberger A, Leibmann JM, Ishikawa H and Ritch R. Optical coherence tomography and scanning laser polarimetry in normal and glaucomatous eyes. American Journal of Ophthalmology 2000;129:129-35.

Holder GE. Pattern electroretinography (PERG) and an integrated approach to visual pathway diagnosis. Progress in Retinal Eye Research 2001;20:531-61.

Holder GE. Significance of abnormal pattern electroretinography in anterior visual pathway dysfunction. British Journal of Ophthalmology 1987;71:166-71.

Hollo G, Suveges I, Nagymihaly A and Vargha P. Scanning laser polarimetry of the retinal nerve fibre layer in primary open angle and capsular glaucoma. British Journal of Ophthalmology 1997;81:857-61.

Holopigian K, Snow J, Seiple W and Seigel I. Variability of the pattern electroretinogram. Documenta Ophthalmologica 1988;70:103-15.

Honkanen RA, Baruah S, Zimmerman MB, Khanna CL, Weaver YK, Narkiewicz J, Waziri R, Gehrs KM, Weingeist TA, Boldt HC, Folk JC, Russell SR and Kwon YH. Vitreous amino acid concentrations in patients with glaucoma undergoing vitrectomy. Archives of Ophthalmology 2003;121:183-8.

Hood DC. Assessing retinal function with the multifocal technique. Progress in Retinal Eye Research 2000;19:607-46.

Hood DC. Objective measurement of visual function. Current Opinion in Ophthalmology 2003;14:78-82.

Hood DC, Bearse MA, Sutter EE, Viswanathan S and Frishman LJ. The optic nerve head component of the monkey's (Macaca Mulatta) multifocal electroretinogram (mERG). Vision Research 2001;41:2029-41.

Hood DC, Chen JY, Yang EB, Rodarte C, Wenick AS, Grippo TM, Odel JG and Ritch R. The role of the multifocal visual evoked potential (mfVEP) latency in understanding optic nerve and retinal diseases. Transactions of the American Ophthalmological Society 2006;104:71-7.

Hood DC, Frishman LJ, Saszik S and Viswanathan S. Retinal origins of the primate multifocal ERG: Implications for the human response. Investigative Ophthalmology and Visual Science 2002;43:1673-85.

Hood DC, Frishman LJ, Viswanathan S, Robson JG and Ahmed J. Evidence for a ganglion cell contribution to the primate electroretinogram (ERG): effects of TTX on the multifocal ERG in Macaque. Visual Neuroscience 1999;16:411-6.

Hood DC and Greenstein VC. Multifocal VEP and ganglion cell damage: applications and limitations for the study of glaucoma. Progress in Retinal Eye Research 2003;22:201-251.

Hood DC, Greenstein VC, Frishman LJ, Holopigian K, Viswanathan S, Seiple W, Ahmed J and Robson JG. Identifying inner retinal contributions to the human multifocal ERG. Vision Research 1999;39:2285-91.

Hood DC, Greenstein VC, Odel JG, Zhang X, Ritch R, Leibmann JM, Hong JE, Chen CS and Thienprasiddhi P. Visual field defects and multifocal visual evoked potentials. Evidence of a linear relationship. Archives of Ophthalmology 2002;120:1672-81.

Hood DC, Thienprasiddhi P, Greenstein VC, Winn BJ, Ohri N, Liebmann JM and Ritch R. Detecting early to mild glaucomatous damage: a comparison of the multifocal VEP and automated perimetry. Investigative Ophthalmology and Visual Science 2004;45:492-8.

Hood DC and Zhang X. Multifocal ERG and VEP responses and visual fields: comparing disease related change. Documenta Ophthalmologica 2000;100:115-37.

Hood DC, Zhang X, Greenstein VC, Kangovi S, Odel JG, Leibmann JM and Ritch R. An interocular comparison of the multifocal VEP: a possible technique for detecting local damage to the optic nerve. Investigative Ophthalmology and Visual Science 2000;41:1580-7.

Hood DC, Zhang X, Hong JE and Chen CS. Quantifying the benefits of additional channels of multifocal VEP recording. Documenta Ophthalmologica 2002;104:303-20.

Hood DC, Zhang X, Rodarte C, Yang EB, Ohri N, Fortune B and Johnson CA. Determining abnormal interocular latencies of multifocal visual evoked potentials. Documenta Ophthalmologica 2004;109:177-87.

Hood DC, Zhang X and Winn BJ. Detecting glaucomatous damage with the multifocal visual evoked potentials: how can a monocular test work? Journal of Glaucoma 2003;12:3-15.

Horani A, Frenkel S, Yahalom C, Farber MD, Ticho U and Blumenthal EZ. The learning effect in visual field testing of healthy subjects using Frequency Doubling Technology. Journal of Glaucoma 2002;11:511-6.

Hougaard JL, Heijl A and Bengtsson B. Glaucoma detection by StratusOCT. Journal of Glaucoma 2007;16:302-6.

Hougaard JL, Heijl A and Krogh E. The nerve fibre layer symmetry test: computerized evaluation of human retinal nerve fibre layer thickness as measured by optical coherence tomography. Acta Ophthalmologica Scandinavica 2004;82:410-8.

Huang D, Swanson EA, Lin CP, Schuman JS, Stinson WG, Chang W, Hee MR, Flotte T, Gregory K and Puliafito CA. Optical Coherence Tomography. Science 1991;254:1178-81.

Huang ML and Chen HY. Development and comparison of automated classifiers for glaucoma diagnosis using Stratus optical coherence tomography. Investigative Ophthalmology and Visual Science 2005;46:4121-9.

Hudson CJ, Kim LS, Hancock SA, Cunliffe IA and Wild JM. Some dissociating factors in the analysis of structural and functional progressive damage in open-angle glaucoma. British Journal of Ophthalmology 2007;91:624-8.

Iester M, Altieri M, Vittone P, Calabria G, Zingirian M and Traverso CE. Detection of glaucomatous visual field defect by nonconventional perimetry. American Journal of Ophthalmology 2003;135:35-9.

Iester M, Capris P, Altieri M, KZingirian M and Traverso CE. Correlation between High-pass Resolution perimetry and standard threshold perimetry in subjects with glaucoma and ocular hypertension. Documenta Ophthalmologica 1999;23:99-103.

Iester M, Capris P and Pandolfo A. Learning effect, Short-term Fluctuation, and Long-term Fluctuation in frequency doubling technique. American Journal of Ophthalmology 2000;130:160-4.

Iester M, Jonas JB, Mardin CY and budde WM. Discriminant analysis models for early detection of glaucomatous optic disc changes. British Journal of Ophthalmology 2000;84:464-8.

Iester M, Mikelberg FS, Courtright P, Burk ROW, Caprioli J, Jonas JB, Weinreb RN and Zangwill LM. Interobserver variability of optic disk variables measured by confocal scanning laser tomography. American Journal of Ophthalmology 2001;132:57-62.

Iester M, Zanini M, Vittone P and Calabria G. Detection of glaucomatous optic nerve head by using Heidelberg topographic maps. Eye 2006;21:609-13.

Ishikawa H, Piette S, Liebmann JM and Ritch R. Detecting the inner and outer borders of the retinal nerve fiber layer using optical coherence tomography. Graefe's Archive for Clinical and Experimental Ophthalmology 2002;240(5):362-71.

Iwase A, Suzuki Y, Araie M, Yamamoto T, Abe H, Shirato S, Kuwayama Y, Mishima HK, Shimizu H, Tomita G, Inoue Y, Kitazawa Y and The Tajimi Study Group; Japan Glaucoma Society. The prevalence of primary open-angle glaucoma in Japanese: the Tajimi Study. Ophthalmology 2004;111:1641-8.

Janknecht P and Funk J. Optic Nerve Head Analyser and Heidelberg Retina Tomograph: accuracy and reproducibility of topographic measurements in a model eye and in volunteers. British Journal of Ophthalmology 1994;78:760-8.

Janknecht P and Funk J. Optic Nerve Head Analyzer and Heidelberg Retina Tomograph: relative error and reproducibility of topographic measurements in a model eye with simulated cataract. Graefe's Archives for Clinical and Experimental Ophthalmology 1995;233:523-9.

Javitt JC, Spaeth GL, Katz LJ, Poryees E and Addiego R. Acquired pits of the optic nerve. Increased prevalence in patients with low-tension glaucoma. Ophthalmology 1990;97:1038-43.

Jayasundera T, Danesh-Meyer HV, Donaldson M and Gamble G. Agreement between stereoscopic photographs, clinical assessment, Heidelberg Retina Tomograph and digital stereoscopic optic disc camera in estimating vertical cup:disc ratio. Clinical and Experimental Ophthalmology 2005;33:259-63.

Jeffreys DA and Axford JG. Source locations of pattern-specific component of human visual evoked potentials. I. Component of striate cortical origin. Experimental Brain Research 1972;16:1-21.

Jeoung JW, Park KH, Kim TW, Khwang SI and Kim DM. Diagnostic ability of optical coherence tomography with a normative database to detect localized retinal nerve fibre layer defects. Ophthalmology 2005;112:2157-63.

Johnson C. Selective versus non-selective losses in glaucoma. Journal of Glaucoma 1994;3:32-44.

Johnson C and Marshall D. Aging effects for opponent mechanisms in the central visual field. Optometry and Vision Science 1995;72:75-82.

Johnson CA. The Glen A. Fry award lecture. Early losses of visual function in glaucoma. Optometry and Vision Science 1995;72:359-70.

Johnson CA, Adams AJ, Casson EJ and Brandt JD. Blue-on-yellow perimetry can predict the development of glaucomatous visual field loss. Archives of Ophthalmology 1993;111:645-50.

Johnson CA, Adams AJ and Lewis RA. Evidence for a neural basis of age-related visual field loss in normal observers. Investigative Ophthalmology and Visual Science 1989;30:2056-64.

Johnson CA, Brandt JD, Khong AM and Admas AJ. Short-wavelength automated perimetry in low-, medium-, and high-risk ocular hypertensive eyes: initial baseline results. Archives of Ophthalmology 1995;113:70-6.

Johnson CA, Cioffi GA and Van Buskirk EM. Frequency Doubling Technology perimetry using a 24-2 stimulus presentation pattern. Optometry and Vision Science 1999;76:571-81.

Johnson CA, Sample PA, Zangwill LM, Vasile CG, Cioffi GA, Leibmann JR and Weinreb RN. Structure and function evaluation (SAFE): II. Comparison of optic disc and visual field characteristics. American Journal of Ophthalmology 2003;135:148-54.

Johnson CA and Samuels SJ. Screening for glaucomatous visual field loss with Frequency-Doubling perimetry. Investigative Ophthalmology and Visual Science 1997;38:413-25.

Johnson LN, Yee RD, Hepler RS and Martin DA. Alteration of the visual evoked potential by macular holes: comparison with optic neuritis. Graefe's Archives for Clinical and Experimental Ophthalmology 1986;225:123-8.

Jonas JB. Clinical implications of peripapillary atrophy in glaucoma. Current Opinion in Ophthalmology 2005;16:84-8.

Jonas JB, Budde WM and Panda-Jonas S. Ophthalmoscopic evaluation of the optic nerve head. Survey of Ophthalmology 1999;43:293-320.

Jonas JB, Fernandez MC and Naumann GO. Glaucomatous parapapillary atrophy. Occurrence and correlations. Archives of Ophthalmology 1992;110:214-22.

Jonas JB and Grundler AE. Correlation between mean visual field loss and morphometric optic disc variables in the open-angle glaucomas. American Journal of Ophthalmology 1997;124:488-397.

Jonas JB and Grundler AE. Prevalence of diabetes mellitus and arterial hypertension in primary and secondary open-angle glaucomas. Graefe's Archives for Clinical and Experimental Ophthalmology 1998;236:202-6.

Jonas JB, Gusek GC and Naumann GO. Optic disc, cup and neuroretinal rim size, configuration and correlations in normal eyes. Investigative Ophthalmology and Visual Science 1988;29:1151-8.

Jonas JB, Mardin CY and Grundler AE. Comparison of measurements of neuroretinal rim area between confocal laser scanning tomography and planimetry of photographs. British Journal of Ophthalmology 1998;82:362-6.

Jonas JB, Martus P, Horn FK, Junemann A, Korth M and Budde WM. Predictive factors of the optic nerve head for development or progression of glaucomatous visual field loss. Investigative Ophthalmology and Visual Science 2004;45:2613-8.

Jonas JB, Nguyen NX, Gusek GC and Naumann GOH. Parapapillary chorioretinal atrophy in normal and glaucoma eyes. I. Morphometric data. Investigative Ophthalmology and Visual Science 1989;30:908-18.

Jonas JB and Xu L. Optic disc hemorrhages in glaucoma. American Journal of Ophthalmology 1994;118:1-8.

Jones AL, Sheen NJ, North RV and Morgan JE. The Humphrey optical coherence scanner: quantitative analysis and reproducibility study of the normal human retinal nerve fibre layer. British Journal of Ophthalmology 2001;85:673-677.

Kalaboukhova L and Lindblom B. Frequency Doubling Technology and High-pass Resolution perimetry in glaucoma and ocular hypertension. Acta Ophthalmologica Scandinavica 2003;81:247-52.

Kamal DS, Garway-Heath DF, Hitchings RA and Fitzke FW. Use of sequential Heidelberg Retina Tomograph images to identify changes at the optic disc in ocular hypertensive patients at risk of developing glaucoma. British Journal of Ophthalmology 2000;84:993-8.

Kanadani FN, Hood DC, Grippo TM, Wangsupadilok B, Harizman N, Greenstein VC, Liebmann JM and Ritch R. Structural and functional assessment of the macular region in patients with glaucoma. British Journal of Ophthalmology 2006;90:1393-7.

Kanamori A, Nagai-Kusuhara A, Escano MFT, Maeda H, Nakamura M and Negi A. Comparison of confocal scanning laser ophthalmoscopy, scanning laser polarimetry and optical coherence tommography to discriminate ocular hypertension and glaucoma at an early stage. Graefe's Archives for Clinical and Experimental Ophthalmology 2006;244:58-68.

Kanamori A, Nakamura M, Escano MFT, Seya R, Maeda H and Negi A. Evaluation of the glaucomatous damage on retinal nerve fiber layer thickness measured by optical coherence tomography. American Journal of Ophthalmology 2003;135:513-20.

Kaplan E and Shapley RM. X and Y cells in the lateral geniculate nucleus of macaque monkeys. Journal of Physiology 1982;330:125-43.

Kass MA, Hart WM Jr, Gordon M and Miller JP. Risk factors favoring the development of glaucomatous visual field loss in ocular hypertension. Survey of Ophthalmology 1980;25:155-62.

Kass MA, Heuer DK, Higginbotham EJ, Johnson CA, Keltner JL, Miller JP, Parrish II RK, Wilson MR and Gordon MO. The Ocular Hypertension Treatment Study: a randomized trial determines that topical ocular hypotensive medication delays or prevents the onset of primary open-angle glaucoma. Archives of Ophthalmology 2002;120:701-13.

Katz J. A comparison of the Pattern- and Total Deviation-based glaucoma change probability programs. Investigative Ophthalmology and Visual Science 2000;41:1012-6.

Katz J. Scoring systems for measuring progression of visual field loss in clinical trials of glaucoma treatment. Ophthalmology 1999;106:391-5.

Katz J, Congdon N and Friedman DS. Methodological variations in estimating apparent progressive visual field loss in clinical trials of glaucoma treatment. Archives of Ophthalmology 1999;117:1137-42.

Kelly DH. Frequency doubling in visual responses. Journal of the Optical Society of America 1966;56:1628-33.

Kelly DH. Nonlinear visual responses to flickering sinusoidal gratings. Journal of the Optical Society of America 1981;71:1051-5.

Kerrigan-Baumrind LA, Quigley HA, Pease ME, Kerrigan DF and Mitchell RS. Number of ganglion cells in glaucoma eyes compared with threshold visual field tests in the same persons. Investigative Ophthalmology and Visual Science 2000;41:741-8.

Kesen MR, Spaeth GL, Henderer JD, Pereira MLM, Smith AF and Steinmann WC. The Heidelberg Retina Tomograph vs clinical impression in the diagnosis of glaucoma. American Journal of Ophthalmology 2002;133:613-6.

Kim TW, Park UC, Park KH and Kim DM. Ability of Stratus OCT to identify localized retinal nerve fiber layer defects in patients with normal standard automated perimetry results. Investigative Ophthalmology and Visual Science 2007;48:1635-41.

King-Smith PE, Grigsby SS, Vingrys AJ, Benes SC and Supowit A. Efficient and unbiased modifications of the QUEST threshold method: theory, simulations, experimental evaluation and practical implementation. Vision Research 1994;34:885-912.

Kirkham TH and Coupland SG. The pattern electroretinogram in optic nerve demyelination. The Canadian Journal of Neurological Sciences 1983;10:256-60.

Kitazawa Y, Shirato S and Yamamoto T. Optic disc haemorrhage in low-tension glaucoma. Ophthalmology 1986;93:853-7.

Klein BE, Klein R, Sponsel WE, Franke T, Cantor LB, Martone J and Menage MJ. Prevalence of glaucoma. The Beaver Dam Eye Study. Ophthalmology 1992;99:1499-504.

Klistorner AI and Graham SL. Electroencephalogram-based scaling of multifocal visual evoked potentials: effect on intersubject amplitude variability. Investigative Ophthalmology and Visual Science 2001;42:2145-52.

Klistorner AI and Graham SL. Objective perimetry in glaucoma. Ophthalmology 2000;107:2283-99.

Klistorner AI, Graham SL, Grigg JR and Bilson FA. Multifocal topographic visual evoked potential: improving objective detection of local visual fields defects. Investigative Ophthalmology and Visual Science 1998;39:937-50.

Klistorner AI, Graham SL and Martins A. Multifocal pattern electroretinogram does not demonstrate localised field defects in glaucoma. Documenta Ophthalmologica 2000;100:155-65.

Kogure S, Toda Y, Crabb D, Kashiwagi K, Fitzke FW and Tsukahara S. Agreement between Frequency Doubling perimetry and static perimetry in eyes with high tension glaucoma and normal tension glaucoma. British Journal of Ophthalmology 2003;87:604-8.

Kono Y, Jonas JB, Zangwill L, Berry CC and Weinreb RN. Agreement of measurement of parapapillary atrophy with confocal scanning laser ophthalmoscopy and planimetry of photographs. Journal of Glaucoma 1999;8:105-10.

Kono Y, Sugiyama K, Ishida K, Yamamoto T and Kitazawa Y. Characteristics of visual field progression in patients with normal-tension glaucoma with optic disc haemorrhages. American Journal of Ophthalmology 2003;135:499-503.

Kook MS, Lee S, Tchah HW, Sung K, Park R and Kim K. Effect of laser in situ keratomileusis on retinal nerve fiber layer thickness measurments by scanning laser polarimetry. Journal of Cataract and Refractive Surgery 2002;28:670-5.

Kook MS, Yang SJ, Kim S, Chung J, Kim ST and Tchah H. Effect of cataract extraction on Frequency Doubling Technology perimetry. American Journal of Ophthalmology 2004;138:85-90.

Krishnamoorthy RR, Agarwal P, Prasanna G, Vopat K, Lambert W, Sheedlo HJ, Pang IH, Shade D, Wordinger RJ, Yorio T, Clark AF and Agarwal N. Characterization of a transformed rat retinal ganglion cell line. Brain Research. Molecular Brain Research 2001;86:1-12.

Kubova Z, Kuba M, Hrochova J and Sverak J. Motion-onset visual evoked potentials improve the diagnosis of glaucoma. Documenta Ophthalmologica 1996-97;92:211-21.

Kulikowski JJ. Apparent fineness of briefly presented gratings: balance between movement and pattern channels. Vision Research 1975;15:673-80.

Kwon YH, Park HJ, Jap A, Ugurlu S and Caprioli J. Test-retest variability of blue-on-yellow perimetry is greater than white-on-white perimetry in normal subjects. American Journal of Ophthalmology 1998;126:29-36.

Landers J, Sharma A, Goldberg I and Graham SL. Topography of the Frequency Doubling perimetry visual field compared with that of short wavelength and achromatic automated perimetry visual fields. British Journal of Ophthalmology 2006;90:70-4.

Larrosa JM, Polo V and Pablo L. Short-wavelength automated perimetry and neuroretinal rim area. European Journal of Ophthalmology 2000;10:116-20.

Law SK, Choe R and Caprioli J. Optic disk characteristics before the occurrence of disk hemorrhage in glaucoma patients. American Journal of Ophthalmology 2001;132:411-3.

Lee BL and Wilson MR. Ocular Hypertension Treatment Study (OHTS) commentary. Current Opinion in Ophthalmology 2003;14:74-7.

Leske CM, Heijl A, Hyman L and Bengtsson B. Early Manifest Glaucoma Trial design and baseline data. Ophthalmology 1999;106:2144-53.

Leske MC, Connell AM, Wu SY, Hyman LG and Schachat AP. Risk factors for open-angle glaucoma. The Barbados Eye Study. Archives of Ophthalmology 1995;113:918-24.

Leske MC, Heijl A, Hussein M, Bengtsson B, Hyman L, Kamaroff E and The Early Manifest Glaucoma Trial Group. Factors for glaucoma progression and the effect of

treatment: the Early Manifest Glaucoma Trial. Archives of Ophthalmology 2003;121:48-56.

Leske MC, Heijl A, Hyman L, Bengtsson B and Komaroff E. Factors for progression and glaucoma treatment: the Early Manifest Glaucoma Trial. Current Opinion in Ophthalmology 2004;15:102-6.

Leung CK, Chan W, Chong KK, Yung W, Tang K, Woo J, Chan W and Tse K. Comparative study of retinal nerve fibre layer measurement by Stratus OCT and GDx VCC, I: correlation analysis in glaucoma. Investigative Ophthalmology and Visual Science 2005;46:3214-20.

Leung CK, Chan W, Yung W, Ng ACK, Woo J, Tsang M and Tse RKK. Comparison of macular and peripapillary measurements for the detection of glaucoma. Ophthalmology 2005;112:391-400.

Leung CK, Chan WM, Chong KK, Chan KC, Yung WH, Tsang MK, Tse RK and Lam DS. Alignment artifacts in optical coherence tomography analyzed images. Ophthalmology 2007;114:263-70.

Leung CK, Chong KK, Chau W, Yiu CK, Tso M, Woo J, Tsang M, Tse K and Yung W. Comparative study of retinal nerve fibre layer measurement by StratusOCT and GDx VCC, II: Structure/function regression analysis in glaucoma. Investigative Ophthalmology and Visual Science 2005;46:3702-11.

Lipton SA. Possible role for memantine in protecting retinal ganglion cells from glaucomatous damage. Survey of Ophthalmology 2003;48 (Suppl 1):S38-46.

Liu B and Neufeld AH. Nitric oxide synthase-2 in human optic nerve head astrocytes induced by elevated pressure in vitro. Archives of Ophthalmology 2001;119:240-5.

Maddess T, Goldberg I, Dobinson J, Wine S, Welsh AH and James AC. Testing for glaucoma with the spatial frequency doubling illusion. Vision Research 1999;39:4258-73.

Maddess T and Henry GH. Performance of nonlinear visual units in ocular hypertension and glaucoma. Clinical Visual Science 1992;7:371-83.

Maffei L and Fiorentini A. Electroretinographic responses to alternating gratings before and after section of the optic nerve. Science 1981;211:953-5.

Malik NS, Moss SJ, Ahmed N, Furth AJ, Wall RS and Meek KM. Ageing of the human corneal stroma: structural and biochemical changes. Biochimica et Biophysica Acta 1992;1138:222-8.

Mardin CY, Horn FK, Jonas JB and Budde WM. Preperimetric glaucoma diagnosis by confocal scanning laser tomography of the optic disc. British Journal of Ophthalmology 1999;83:299-304.

Marmour MF, Holder GE, Seeliger MW and Yamamoto S. Standard for clinical electroretinography (2004 update). Documenta Ophthalmologica 2004;108:107-14.

Marmour MF, Hood DC, Keating D, Kondo M, Seeliger MW and Miyake Y. Guidelines for basic multifocal electroretinography (mfERG). Documenta Ophthalmologica 2003;106:105-15.

Martin KR, Levkovitch-Verbin H, Valenta D, Baumrind L, Pease ME and Quigley HA. Retinal glutamate transporter changes in experimental glaucoma and after optic

nerve transection in the rat. Investigative Ophthalmology and Visual Science 2002;43:2236-43.

Martin L, Wanger P, Vancea L and Gothlin B. Concordance of High-pass Resolution perimetry and Frequency Doubling Technology perimetry results in glaucoma: no support for selective ganglion cell damage. Journal of Glaucoma 2003;12:40-4.

Martus P, Stroux A, Budde WM, Mardin CY, Korth M and Jonas JB. Predictive factors for progressive optic nerve damage in various types of chronic open-angle glaucoma. American Journal of Ophthalmology 2005;139:999-1009.

Matsuo H, Tomita G, Suzuki Y and Araie M. Learning effect and measurement variability in Frequency Doubling Technology perimetry in chronic open-angle glaucoma. Journal of Glaucoma 2002;11:467-73.

McKendrick AM, Anderson AJ, Johnson CA and Fortune B. Appearance of the frequency doubling stimulus in normal subjects and patients with glaucoma. Investigative Ophthalmology and Visual Science 2003;44:1111-6.

Medeiros F, Sample PA and Weinreb RN. Frequency Doubling Technology perimetry abnormalities as predictors of glaucomatous visual field loss. American Journal of Ophthalmology 2004;137:863-71.

Medeiros FA, Bowd C, Zangwill LM, Patel C and Weinreb RN. Detection of glaucoma using scanning laser polarimetry with enhanced corneal compensation. Investigative Ophthalmology and Visual Science 2007;48:3146-53.

Medeiros FA and Susanna R Jr. Comparison of algorithms for detection of localised nerve fiber layer defects using scanning laser polarimetry. British Journal of Ophthalmology 2003;87:413-9.

Medeiros FA, Zangwill LM, Bowd C, Sample PA and Weinreb RN. Influence of disease severity and optic disc size on the diagnostic performance of imaging instruments in glaucoma. Investigative Ophthalmology and Visual Science 2006;47:1008-15.

Medeiros FA, Zangwill LM, Bowd C, Sample PA and Weinreb RN. Use of progressive glaucomatous optic disk change as the reference standard for evaluation of diagnostic tests in glaucoma. American Journal of Ophthalmology 2005;139:1010-1018.

Medeiros FA, Zangwill LM, Bowd C, Vessani RM, Susanna R Jr and Weinreb RN. Evaluation of retinal nerve fiber layer, optic nerve head, and macular thickness measurements for glaucoma detection using optical coherence tomography. American Journal of Ophthalmology 2005;139:44-55.

Medeiros FA, Zangwill LM, Bowd C and Weinreb RN. Comparison of the GDx VCC scanning laser polarimeter, HRT II confocal scanning laser ophthalmoscope, and StratusOCT optical coherence tomograph for the detection of glaucoma. Archives of Ophthalmology 2004;122:827-37.

Mickelberg FS and Drance SM. The mode of progression of visual field defects in glaucoma. American Journal of Ophthalmology 1984;98:443-5.

Miglior S, Guareschi M, Albe E, Gomarasca S, Vavassori M and Orzalesi N. Detection of glaucomatous visual field changes using Moorfields Regression Analysis

of the Heidelberg Retina Tomograph. American Journal of Ophthalmology 2003;136:26-33.

Miglior S, Zeyen T, Pfeiffer N, cunha-Vaz J, Torri V and Adamsons I. Results of the European Glaucoma Prevention Study. Ophthalmology 2005;112:366-75.

Mikelberg FS, Parfitt CM, Swindale NV, Graham SL, Drance SM and Gosine R. Ability of the Heidelberg Retina Tomograph to detect early glaucomatous visual field loss. Journal of Glaucoma 1995;4:242-7.

Miller SJ. Genetics of glaucoma and family studies. Transactions of the Ophthalmological Societies of the United Kingdom 1978;98:290-2.

Minckler DS. The organization of nerve fiber bundles in the primate optic nerve head. Archives of Ophthalmology 1980;98:1630-6.

Mistelberger A, Liebmann JM, Greenfield DS, Hoh S, Ishikawa H, Marmor MF and Ritch R. Assessment of optic disc anatomy and nerve fiber layer thickness in ocular hypertensive subjects with normal short-wavelength automated perimetry. Ophthalmology 2002;109:1362-6.

Mitchell P, Hourihan F, Sandbach J and Wang JJ. The relationship between glaucoma and myopia: the Blue Mountains Eye Study. Ophthalmology 1999;106:2010-5.

Mitchell P, Lee AJ, Rochtchina E and Wang JJ. Open-angle glaucoma and systemic hypertension: the Blue Mountains Eye Study. Journal of Glaucoma 2004;13:319-26.

Mitchell P, Smith W, Chey T and Healey PR. Open-angle glaucoma and diabetes: the Blue Mountains Eye Study, Australia. Ophthalmology 1997;104:712-8.

Mok KH, Lee VW and So KF. Retinal nerve fibre layer measurement by optical coherence tomography in glaucoma suspects with short-wavelength perimetry abnormalities. Journal of Glaucoma 2003;12:45-9.

Mok KH and Lee VWL. Nerve fiber analyzer and short-wavelength automated perimetry in glaucoma suspects: a pilot study. Ophthalmology 2000;107:2101-4.

Morgan J, Caprioli J and Koseki Y. Nitric oxide mediates excitotoxic and anoxic damage in rat retinal ganglion cells cocultured with astroglia. Archives of Ophthalmology 1999;117:1524-9.

Morgan JE. Selective cell death in glaucoma: does it really occur? British Journal of Ophthalmology 1994;78:875-9.

Morgan JE, Sheen NJL, North RV, Choong Y and Ansari E. Digital imaging of the optic nerve head: monoscopic and stereoscopic analysis. British Journal of Ophthalmology 2005;89:879-84.

Morgan JE, Sheen NJL, North RV, Goyal R, Morgan S, Ansari E and Wild JM. Discrimination of glaucomatous optic neuropathy by digital stereoscopic analysis. Ophthalmology 2005;112:855-62.

Mori M, Shahidi E, Gracia-Valenzuela DP and Wilensky EJ. Mapping of the peripappillary retinal thickness in normal and glaucomatous eyes. Investigative Ophthalmology and Visual Science 1999;40:S839.

Morrison JC, Dorman-Pease ME, Dunkelberger GR and Quigley HA. Optic nerve head extracellular matrix in primary optic atrophy and experimental glaucoma. Archives of Ophthalmology 1990;108:1020-4.

Moya FJ, Brigatti L and Caprioli J. Effect of aging on optic nerve appearance: a longitudinal study. British Journal of Ophthalmology 1999;83:567-72.

Musch DC, Lichter PR, Guire KE and Standardi CL. The Collaborative Initial Glaucoma Treatment Study: a study design, methods, and baseline characteristics of enrolled patients. Ophthalmology 1997;106:653-62.

Naithani P, Sihota R, Sony P, Dada T, Gupta V, Kondal D and Pandey RM. Evaluation of optical coherence tomography and Heidelberg Retinal Tomography parameters in detecting early and moderate glaucoma. Investigative Ophthalmology and Visual Science 2007;48(7):3138-45.

Nemerow NS and Enns N. Visual evoked responses in people with multiple sclerosis. Journal of Neurology, Neurosurgery and Psychiatry 1972;34:275-80.

Newman EA and Odette LL. Model of electroretinogram b-wave generation: a test of the K+ hypothesis. Journal of Neurophysiology 1984;51:164-82.

Nouri-Mahdavi K, Hoffman D, Gaasterland D and Caprioli J. Prediction of visual field progression in glaucoma. Investigative Ophthalmology and Visual Science 2004;45:4346-51.

Nouri-Mahdavi K, Hoffman D, Tannenbaum DP, Law SK and Caprioli J. Identifying early glaucoma with optical coherence tomography. American Journal of Ophthalmology 2004;137:228-35.

Ntim-Amponsah CT, Amoaku WM, Ofosu-Amaah S, Ewusi RK, Idirisuriya-Khair R, Nyatepe-Coo E and Adu-Darko M. Prevalence of glaucoma in an African population. Eye 2004;18:491-7.

O'Connor DJ, Zeyen T and Caprioli J. Comparison of methods to detect glaucomatous optic nerve damage. Ophthalmology 1993;100:1498-503.

Odom JV, Bach M, Barber C, Brigell M, Marmor MF, Tormene AP, Holder GE and Vaegan. Visual evoked potentials standard (2004). Documenta Ophthalmologica 2004;108:1-10.

Ogden TE. Nerve fibre layer of the macaque retina: retinotopic organization. Investigative Ophthalmology and Visual Science 1983;24:85-98.

Ogden TE. The nerve-fibre layer of the primate retina: an autoradiographic study. Investigative Ophthalmology 1974;1974:95-100.

Ogden TE. The oscillatory waves of the primate electroretinogram. Vision Research 1973;13:1059-74.

Oshima Y, Emi K, Yamanishi S and Motokura M. Quantitative assessment of macular thickness in normal subjects and patients with diabetic retinopathy by scanning retinal thickness analyser. British Journal of Ophthalmology 1999;83:54-61.

Panagachis E and Moschos M. Pattern ERG changes in suspected glaucoma. Ophthalmologica 1998;212:112-4.

Parikh RS, Parikh S, Chandra Sekhar G, Kumar RS, Prabakaran S, Ganesh Babu J and Thomas R. Diagnostic capability of optical coherence tomography (Stratus OCT 3) in early glaucoma. 2007;Epub ahead of print.

Parker A. The effects of temporal modulation on the perceived spatial structure of sine-wave gratings. Perception 1983;12:663-82.

Paunescu LA, Schuman JS, Price LL, Stark PC, Beaton S, Ishikawa H, Wollstein G and Fujimoto JG. Reproducibility of nerve fiber layer thickness, macular thickness, and optic nerve head measurements using StratusOCT. Investigative Ophthalmology and Visual Science 2004;45:1716-24.

Paupoo AA, Mahroo OA, Friedburg C and Lamb TD. Human cone photoreceptor responses measured by the electroretinogram [correction of electoretinogram] a-wave during and after exposure to intense illumination. Journal of Physiology 2000;529:469-82.

Pease ME, McKinnon SJ, Quigley HA, Kerrigan-Baumrind LA and Zack DJ. Obstructed axonal transport of BDNF and its receptor TrkB in experimental glaucoma. Investigative Ophthalmology and Visual Science 2000;41:764-74.

Perry V, Oehler R and Cowey A. Retinal ganglion cells that project to the dorsal lateral geniculate nucleus. Neuroscience 1984;12:1101-23.

Pfeifer N, Tilmon B and Bach M. Predictive value of the pattern electroretinogram in high risk ocular hypertension. Investigative Ophthalmology and Visual Science 1993;34:1710-5.

Phelps CD. Effect of myopia on prognosis in treated primary open-angle glaucoma. American Journal of Ophthalmology 1982;93:622-8.

Piette SD and Sergott RC. Pathological optic-disc cupping. Current Opinion in Ophthalmology 2006;17:1-6.

Pohjanpelto PE and Palva J. Ocular hypertension and glaucomatous optic nerve damage. Acta Ophthalmologica (Copenh.) 1974;52:194-200.

Poloschek CM and Sutter EE. The fine structure of multifocal ERG topographies. Journal of Vision 2002;2:577-7.

Porrello G and Falsini B. Retinal ganglion cell dysfunction in humans following post-geniculate lesions: specific spatio-temporal losses revealed by pattern ERG. Vision Research 1999;39:1739-48.

Pueyo V, Polo V, Larrosa JM, Ferreras A, Pablo LE and Honrubia FM. Diagnostic ability of the Heidelberg Retina Tomograph, optical coherence tomograph, and scanning laser polarimeter in open-angle glaucoma. Journal of Glaucoma 2007;16:173-7.

Quigley HA. The number of people with glaucoma worldwide. British Journal of Ophthalmology 1996;80:389-93.

Quigley HA and Addicks EM. Regional differences in the structure of the lamina cribrosa and their relation to glaucomatous optic nerve damage. Archives of Ophthalmology 1981;99:137-43.

Quigley HA, Addicks EM and Green WR. Optic nerve damage in human glaucoma III. Quantitative correlation of nerve fibre loss and visual field defect in glaucoma, ischaemic neuropathy, papilloedema and toxic neuropathy. Archives of Ophthalmology 1982;100:135-46.

Quigley HA, Dunkelberger GR and Green WR. Chronic human glaucoma causing selectively greater loss of large optic nerve fibres. Ophthalmology 1988;95:357-63.

Quigley HA, Dunkelberger GR and Green WR. Ganglion cell atrophy correlated with automated perimetry in human eyes with glaucoma. American Journal of Ophthalmology 1989;107:453-64.

Quigley HA, McKinnon SJ, Zack DJ, Pease ME, Kerrigan-Baumrind LA, Kerrigan DF and Mitchell RS. Retrograde axonal transport of BDNF in retinal ganglion cells is blocked by acute IOP elevation in rats. Investigative Ophthalmology and Visual Science 2000;41:3460-6.

Quigley HA, Miller NR and George T. Clinical evaluation of nerve fibre layer atrophy as an indicator of glaucomatous optic nerve damage. Archives of Ophthalmology 1980;98:1564-71.

Quigley HA, Sanchez RM, Dunkelberger GR, L'Hernault NL and Baginski TA. Chronic glaucoma selectively damages larger optic nerve fibers. Investigative Ophthalmology and Visual Science 1987;28:913-20.

Radius RL and Anderson DR. The course of axons through the retina and optic nerve head. Archives of Ophthalmology 1979;97:1154-8.

Rager G. The cellular origin of the b-wave in the electroretinogram -- a developmental approach. Journal of Comparative Neurology 1979;15:225-44.

Ransohoff DF and Feinstein AR. Problems of spectrum bias in evaluating the efficacy of diagnostic tests. New England Journal of Medicine 1978;299:926-30.

Rasker MT, van den Enden A, Bakker D and Hoyng PF. Deterioration of visual fields in patients with glaucoma with and without optic disc hemorrhages. Archives of Ophthalmology 1997;115:1257-62.

Ray R, Stinnett SS and Jaffe GJ. Evaluation of image artifact produced by optical coherence tomography of retinal pathology. American Journal of Ophthalmology 2005;139:18-29.

Resnikoff S, Pascolini D, Etya'ale D, Kocur I, Pararajasegaram R, Pokharel GP and Mariotti SP. Global data on visual impairment in the year 2002. Bulletin of the World Health Organization 2004;82:844-51.

Reus NJ, Colen TP and Lemij HG. The prevalence of glaucomatous defects with short-wavelength automated perimetry in patients with elevated intraocular pressures. Journal of Glaucoma 2005;14:26-9.

Reus NJ and Lemij HG. Diagnostic accuracy of the GDx-VCC for glaucoma. Ophthalmology 2004;111:1860-5.

Reus NJ and Lemij HG. Relationships between standard automated perimetry, HRT confocal scanning laser ophthalmoscopy, and GDx VCC scanning laser polarimetry. Investigative Ophthalmology and Visual Science 2005;46:4182-8.

Reus NJ and Lemij HG. Scanning laser polarimetry of the retinal nerve fibre layer in perimetrically unaffected eyes of glaucoma patients. Ophthalmology 2004;111:2199-2203.

Reus NJ, Zhou Q and Lemij HG. Enhanced imaging algorithm for scanning laser polarimetry on eyes with atypical polarisation pattern. Investigative Ophthalmology and Visual Science 2006;47:3870-7.

Richards W and Felton TB. Spatial frequency doubling: retinal or central? Vision Research 1973;13:2129-37.

Richey ET, Kooi KA and Tourtellotte WW. Visual evoked responses in multiple sclerosis. Journal of Neurology, Neurosurgery and Psychiatry 1971;34:275-80.

Rodarte C, Hood DC, Yang EB, Grippo T, Greenstein VC, Liebmann JM and Ritch R. The effects of glaucoma on the latency of the multifocal visual evoked potential. British Journal of Ophthalmology 2006;17:1132-6.

Rohschneider K, Burk ROW, Kruse FE and Volcker HE. Reproducibility of the optic nerve head topography with a new laser tomographic scanning device. Ophthalmology 1994;101:1044-9.

Ruben ST, Hitchings RA, Fitzke F and Arden GB. Electrophysiology and psychophysics in ocular hypertension and glaucoma: Evidence of mechanisms in early glaucoma. Eye 2004;8:516-20.

Rumelhart DE, Hinton G and Williams R. Learning representations of back-propagation errors. Nature 1986;323:533-6.

Sadda SR, Wu Z, Walsh AC, Richine L, Dougall J, Cortez R and LaBree LD. Errors in retinal thickness measurements obtained by optical coherence tomography. Ophthalmology 2006;113(2):285-93.

Sample PA. Short-wavelength automated perimetry: its role in the clinic and for understanding ganglion cell function. Progress in Retinal Eye Research 2000;19:369-83.

Sample PA, Esterson FD, Weinreb RN and Boynton RM. The ageing lens: in vivo assessment of light absorption in 84 human eyes. Investigative Ophthalmology and Visual Science 1988;31:1869-75.

Sample PA, Johnson CA, Haegerstrom-Portnoy G and Adams AJ. Optimum parameters for short-wavelength automated perimetry. Journal of Glaucoma 1996;5:375-83.

Sample PA, Medeiros FA, Racette L, Pascual JP, Boden C, Zangwill LM, Bowd C and Weinreb RN. Identifying glaucomatous vision loss with visual-function-specific perimetry in the diagnostic innovations in glaucoma study. Investigative Ophthalmology and Visual Science 2006;47:3381-9.

Sample PA and Weinreb RN. Color perimetry for assessment of primary open-angle glaucoma. Investigative Ophthalmology and Visual Science 1990;31:1869-75.

Sanchez-Galeana CA, Bowd C, Zangwill LM, Sample PA and Weinreb RN. Short-wavelength automated perimetry results are correlated with optical coherence tomography retinal nerve fiber thickness measurements in glaucomatous eyes. Ophthalmology 2004;111:1866-1872.

Saw S, Foster P, Gazzard G and Seah S. Causes of blindness, low vision, and questionnaire-assessed poor visual function in Singaporean Chinese adults: The Tanjong Pagar Survey. Ophthalmology 2004;111:1161-8.

Schlieve CR, Lieven CJ and Levin LA. Biochemical activity of reactive oxygen species scavengers do not predict retinal ganglion cell survival. Investigative Ophthalmology and Visual Science 2006;47:3878-86.

Schlottmann PG, De Cilla S, Greenfield DS, Caprioli J and Garway-Heath DF. Relationship between visual field sensitivity and retinal nerve fibre layer thickness as measured by scanning laser polarimetry. Investigative Ophthalmology and Visual Science 2004;45:1823-9.

Schmiti RB, Avelino RR, Kara-Jose N and Costa VP. Full-threshold versus Swedish Interactive Threshold Algorithm (SITA) in normal individuals undergoing automated perimetry for the first time. Ophthalmology 2002;109:2084-92.

Schuerle AF and Schmidt E. Atlas of laser scanning ophthalmoscopy. Germany: Springer-Verlag; 2004.

Schulzer M and Drance SM. Intraocular pressure, systemic blood pressure, and age: a correlational study. British Journal of Ophthalmology 1987;71:245-9.

Schuman JS, Pedut-Kloizman T, Hertzmark E, Hee MR, Wilkins JR, Coker JG, Puliafito CA, Fujimoto JG and Swanson EA. Reproducibility of nerve fiber layer thickness measurements using optical coherence tomography. 1996;103:1889-98.

Schuman JS, Pedut-Kloizman T, Pakter H, Wang N, Guedes V, Huang L, Pieroth L, Scott W, Hee MR, Fujimoto JG, Ishikawa H, Bilonick RA, Kagemann L and Wollstein G. Optical coherence tomography and histologic measurements of nerve fiber layer thickness in normal and glaucomatous monkey eyes. Investigative Ophthalmology and Visual Science 2007;48:3645-54.

Schuurmans RP and Berninger T. Luminance and contrast responses recorded in man and cat. Documenta Ophthalmologica 1985;59:187-97.

Schwartz M. Neurodegenration and neuroprotection in glaucoma: development of a therapeutic neuroprotective vaccine - the Friedenwald lecture. Investigative Ophthalmology and Visual Science 2003;44:1407-11.

Shah NN, Bowd C, Medeiros FA, Weinreb RN, Sample PA, Hoffmann EM and Zangwill LM. Combining structural and functional testing for detection of glaucoma. Ophthalmology 2006;113:1593-602.

Shahidi M, Blair NP, Mori M, Gieser J and Pulido JS. Retinal topography and thickness mapping in atrophic age related macular degeneration. British Journal of Ophthalmology 2002;86:623-6.

Shen SY, Baskaran M, Fong AC, Chan YH, Lim LS, Husain R, Gazzard G, Seah SK and Aung T. Changes in the optic disc after acute primary angle closure. Ophthalmology 2006;113:924-9.

Shuttleworth GN, Khong CH and Diamond JP. A new digital optic disc stereo camera: intraobserver and interobserver repeatability of optic disc measurements. British Journal of Ophthalmology 2000;84:403-7.

Siegner SW and Netland PA. Optic disc hemorrhages and progression of glaucoma. Ophthalmology 1996;103:1014-24.

Sihota R, Sony P, Gupta V, Dada T and Singh R. Diagnostic capability of optical coherence tomography in evaluatuing the degree of glaucomatous retinal nerve fiber damage. Investigative Ophthalmology and Visual Science 2006;47:2006-10.

Silveira L and Perry V. The topography of the magnocellular projecting ganglion cells (M-ganglion cell) in the primate retina. Neuroscience 1991;40:217-37.

Singh RP, Goldberg I, Graham SL, Sharma A and Mohsin M. Central corneal thickness, tonometry and ocular dimensions in glaucoma and ocular hypertension. Journal of Glaucoma 2001;10:206-10.

Skaf M, Bernardes AB, Cardillo JA, Costa RA, Melo LA Jr, Castro JC and Varma R. Retinal nerve fibre layer thickness profile in normal eyes using third-generation optical coherence tomography. Eye 2006;20:431-9.

Soares AS, Artes PH, Andreou P, Leblanc RP, Chauhan BC and Nicolela MT. Factors associated with optic disc hemorrhages in glaucoma. Ophthalmology 2004;111:1653-7.

Sommer A. Glaucoma: facts and fancies. Eye 1996;10:295-301.

Sommer A, Katz J, Quigley HA, Miller NR, Robin AL, Richter RC and Witt KA. Clinically detectable nerve fibre atrophy precedes the onset of glaucomatous visual field loss. Archives of Ophthalmology 1991;109:77-83.

Sonnsjo B, Holmin C and Krakau CE. Occurrence of disc haemorrhages in open-angle glaucoma treated with pilocarpine or timolol. Acta Ophthalmologica (Copenh.) 1991;69:217-24.

Spry PGD, Hussin HM and Sparrow JM. Clinical evaluation of Frequency Doubling Technology perimetry using the Humphrey Matrix 24-2 Threshold strategy. British Journal of Ophthalmology 2005;89:1031-5.

Spry PGD, Johnson CA, Bates AB, Turpin A and Chauhan BC. Spatial and temporal processing of threshold data for detection of progressive glaucomatous visual field loss. Archives of Ophthalmology 2002;120:173-180.

Spry PGD, Johnson CA, Mansberger SL and Cioffi GA. Psychophysical investigation of ganglion cell loss in early glaucoma. Journal of Glaucoma 2005;14:11-9.

Spry PGD, Johnson CA, McKendrick AM and Turpin A. Variability components of standard automated perimetry and Frequency Doubling Technology perimetry. Investigative Ophthalmology and Visual Science 2001;42:1404-10.

Steifelmeyer S, Neubauer AS, Berninger T, Arden GB and Rudolph G. The multifocal pattern electroretinogram in glaucoma. Vision Research 2004;44:103-12.

Steinmetz H, Gunter F and Bernd-Ulrich M. Craniocerebral topography within the international 10-20 system. Electroencephalography and Clinical Neurophysiology 1989;72:499-506.

Stensaas SS, Eddington DK and Dobelle WH. The tompography and variability of the primary visual cortex in man. Journal of Neurosurgery 1972;40:747-55.

Strouthidis NG, Scott A, Peter NM and Garway-Heath DF. Optic disc and visual field progression in ocular hypertensive subjects: detection rates, specificity, and agreement. Investigative Ophthalmology and Visual Science 2006;47:2904-10.

Strouthidis NG, Vinciotti V, Tucker AJ, Gardiner SK, Crabb DP and Garway-Heath DF. Structure and function in glaucoma: The relationship between a functional visual field map and an anatomic retinal map. Investigative Ophthalmology and Visual Science 2006;47:5356-62.

Strouthidis NG, White ET, Owen VMF, Ho TA, Hammond CJ and Garway-Heath DF. Factors affecting the test-retest variability of Heidelberg Retina Tomograph and Heidelberg Retina Tomograph II measurements. British Journal of Ophthalmology 2005;89:1427-32.

Sugiyama K, Tomita G, Kitazawa Y, Onda E, Shinohara H and Park KH. The associations of optic disc hemorrhage with retinal nerve fiber layer defect and peripapillary atrophy in normal-tension glaucoma. Ophthalmology 1997;104:1926-33.

Sugiyama K, Uchida H, Tomita G, Sato Y, Iwase A and Kitazawa Y. Localized wedge-shaped defects of retinal nerve fiber layer and disc hemorrhage in glaucoma. Ophthalmology 1999;106:1762-7.

Sutter E and Tran D. The field topography of ERG components in man-I. The photopic luminance response. Vision Research 1992;32:433-46.

Sutter EE. Imaging visual function with the multifocal m-sequence technique. Vision Research 2001;41:1241-55.

Sutter EE. The interpretation of multifocal binary kernels. Documenta Ophthalmologica 2000;100:49-75.

Sutter EE and Bearse MA. The optic nerve head component of the human ERG. Vision Research 1999;39:419-36.

Swindale NV, Stjepanovic G, Chin A and Mikelberg FS. Automated analysis of normal and glaucomatous optic nerve head topography images. Investigative Ophthalmology and Visual Science 2000;41:1730-42.

Tezel G, Edward DP and Wax MB. Serum autoantibodies to optic nerve head glycosaminoglycans in patients with glaucoma. Archives of Ophthalmology 1999;117:917-24.

The AGIS Investigators. The Advanced Glaucoma Intervention Study. 2. Visual field test scoring and reliability. Ophthalmology 1994;101:1445-55.

Thienprasiddhi P, Greenstein VC, Chen CS, Liebmann JM, Ritch R and Hood DC. Multifocal visual evoked potential responses in glaucoma patients with unilateral hemifield defects. American Journal of Ophthalmology 2003;136:399-408.

Thienprasiddhi P, Greenstein VC, Chu DH, Xu L, Liebmann JM, Ritch R and Hood DC. Detecting early functional damage in glaucoma suspect and ocular hypertensive patients with the multifocal VEP technique. Journal of Glaucoma 2006;15:321-7.

Thompson DA and Drasdo N. Computation of the luminance and pattern components of the bar pattern electroretinogram. Documenta Ophthalmologica 1987;66:233-44.

Tielsch J, Katz J, Quigley HA, Miller NR and sommer A. Intraobserver and interobserver agreement in measurement of optic disc characteristics. Ophthalmology 1988;95:350-6.

Tielsch JM, Katz J, Quigley HA, Javitt JC and Sommer A. Diabetes, intraocular pressure, and primary open-angle glaucoma in the Baltimore Eye Survey. Ophthalmology 1995;102:48-53.

Tielsch JM, Katz J, Sommer A, Quigley HA and Javitt JC. Family history and risk of primary open angle glaucoma. The Baltimore Eye Survey. Archives of Ophthalmology 1994;112:69-73.

Tielsch JM, Sommer A, Katz J, Royall RM, Quigley HA and Javitt J. Racial variations in the prevalence of primary open-angle glaucoma. The Baltimore Eye Survey. Journal of the American Medical Association 1991;17:369-74.

Toffoli G, Vattovani O, Cecchini P, Pastotri G, Rinaldi G and Ravalicao G. Correlation between the retinal nerve fibre layer thickness and the pattern electroretinogram amplitude. Ophthalmologica 2002;216:159-63.

Toth CA, Narayan DG, Boppart SA, Hee MR, Fujimoto JG, Birngruber R, Cain CP, DiCarlo CD and Roach WP. A comparison of retinal morphology viewed by optical coherence tomography and by light microscopy. Archives of Ophthalmology 1997;115:1425-8.

Towle VL, Moskowotiz A, Sokol S and Schwartz B. The visual evoked potential in glaucoma and ocular hypertension: effects of check size, field size and stimulation rate. Investigative Ophthalmology and Visual Science 1983;24:175-83.

Trick GL and Wintermeyer DH. Spatial and temporal frequency tuning of pattern-reversal retinal potentials. Investigative Ophthalmology and Visual Science 1982;23:774-9.

Tuck MW and Crick RP. The age distribution of primary open angle glaucoma. Ophthalmic Epidemiology 1998;5:173-83.

Turpin A, McKendrick AM, Johnson CA and Vingrys AJ. Development of efficient threshold strategies for Frequency Doubling Technology perimetry using computer simulation. Investigative Ophthalmology and Visual Science 2002;43:322-31.

Turpin A, McKendrick AM, Johnson CA and Vingrys AJ. Performance of efficient test procedures for Frequency Doubling Technology perimetry in normal and glaucomatous eyes. Investigative Ophthalmology and Visual Science 2002;43:709-15.

Tuulonen A, Airaksinene PF and Alanko HI. Optic disc size in eyes with and without an optic disc hemorrhage. Investigative Ophthalmology and Visual Science 1992;33(Suppl):883.

Uchida H, Brigatti L and Caprioli J. Detection of structural damage from glaucoma with confocal laser image analysis. Investigative Ophthalmology and Visual Science 1996;37:2393-401.

Uchida H, Ugurlu S and Caprioli J. Increasing peripapillary atrophy is associated with progressive glaucoma. Ophthalmology 1998;105:1541-5.

Ugurlu S, Hoffman D and Garway-Heath DF. Relationship between structural abnormalities and short-wavelength automated perimetric defects in eyes at risk of glaucoma. American Journal of Ophthalmology 2000;129:592-8.

Varma R, Skaf M and Barron E. Retinal nerve fiber layer thickness in normal human eyes. Ophthalmology 1996;103:2144-9.

Varma R, Steinmann WC and Scott IU. Expert agreement in evaluating the optic disc for glaucoma. Ophthalmology 1992;99:215-21.

Varma R, Ying-Lai M, Francis BA, Nguyen BB, Deneen J, Wilson MR and Azen SP - The Los Angeles Latino Eye Study Group. Prevalence of open-angle glaucoma and ocular hypertension in Latinos: the Los Angeles Latino Eye Study. Ophthalmology 2004;111:1439-48.

Viswanathan AC, Crabb DP, McNaught AI, Westcott MC, Kamal D, Garway-Heath DF, Fitzke FW and Hitchings RA. Interobserver agreement on visual field

progression in glaucoma: a comparison of methods. British Journal of Ophthalmology 2003;87:726-30.

Viswanathan S, Frishman LJ and Robson JG. The uniform field and pattern ERG in macaques with experimental glaucoma: removal of spiking activity. Investigative Ophthalmology and Visual Science 2000;41:2797-810.

Viswanathan S, Frishman LJ, Robson JG, Harwerth RS and Smith III EL. The photopic negative response of the macaque electroretinogram: reduction by experimental glaucoma. Investigative Ophthalmology and Visual Science 1999;40:1124-36.

Viswanathan S, Frishman LJ, Robson JG and Walters JW. The photopic negative response of the flash electroretinogram in primary open angle glaucoma. Investigative Ophthalmology and Visual Science 2001;42:514-22.

Wadood AC, Azuara-Blanco A, Aspinall P, Taguri A and King AJW. Sensitivity and specificity of Frequency-Doubling Technology, Tendency-Oriented Perimetry, and Humphrey Swedish Interactive Threshold Algorithm-Fast perimetry in a glaucoma practice. American Journal of Ophthalmology 2002;133:327-32.

Wall M, Chauhan BC, Frisen L, House PH and Brito C. Visual field of High-pass Resolution perimetry in normal subjects. Journal of Glaucoma 2004;13:15-21.

Wall M, Lefante J and Conway M. Variability of High-pass Resolution perimetry in normals and patients with idiopathic intracranial hypertension. Investigative Ophthalmology and Visual Science 1991;32:3091-5.

Wang L, Cioffi GA and Van Buskirk EM. The vascular pattern of the optic nerve and its potential relevance in glaucoma. Current Opinion in Ophthalmology 1998;9:24-9.

Wanger P and Persson HE. Pattern-reversal electroretinograms from normotensive, hypertensive and glaucomatous eyes. Ophthalmologica 1987;195:205-8.

Wax MB. Is there a role for the immune system in glaucomatous optic neuropathy? Current Opinion in Ophthalmology 2000;11:145-50.

Weber AJ, Kaufman PL and Hubbard WC. Morphology of single ganglion cells in the glaucomatous primate retina. Investigative Ophthalmology and Visual Science 1998;39:2304-20.

Weinberger D, Axer-Siegel R, Landau D and Yassur Y. Retinal thickness variation in the diabetic patient measured by the Retinal Thickness Analyser. British Journal of Ophthalmology 1998;82:1003-6.

Weinreb RN, Bowd C, Greenfield DS and Zangwill LM. Measurement of the magnitude and axis of corneal polarization with scanning laser polarimetry. Archives of Ophthalmology 2002;120:901-6.

Weinreb RN, Bowd C and Zangwill LM. Glaucoma detection using scanning laser polarimetry with variable corneal polarization compensation. Archives of Ophthalmology 2003;120:218-24.

Weinreb RN, Cioffi GA and Harris A. Optic nerve blood flow. In: Sheilds B, editor. 100 Years of progress in glaucoma. Philadelphia: Lipincott Raven Healthcare; 1997. p. 59-79.

Weinreb RN, Dreher AW, Coleman AL, Quigley HA, Shaw B and Reiter K. Histopathological validation of fourier-ellipsometry measurements of retinal nerve fibre layer thickness. Archives of Ophthalmology 1990;108:557-60.

Weinreb RN, Lusky M, Bartsch DU and Morsman D. Effect of repetitive imaging on topographic measurements of the optic nerve head. Archives of Ophthalmology 1993;111:636-8.

Whitacre MM, Stein RA and Hassanien K. The effect of corneal thickness on applanation tonometry. American Journal of Ophthalmology 1993;115:592-6.

White AJ, Sun H, Swanson WH and Lee BB. An examination of physiological mechanisms underlying the frequency doubling illusion. Investigative Ophthalmology and Visual Science 2002;43:3590-9.

Wild JM. Short wavelength automated perimetry. Acta Ophthalmologica Scandinavica 2001;79:546-59.

Wild JM. Techniques and developments in automated perimetry: a review. Ophthalmic and Physiological Optics 1988;8:295-307.

Wild JM, Cubbidge RP, Pacey IE and Robinson R. Statistical aspects of the normal visual field in short-wavelength automated perimetry. Investigative Ophthalmology and Visual Science 1998;39:54-63.

Wild JM, Dengler-Harles M, Searle AE, O'Neill EC and Crews SJ. The influence of the learning effect on automated perimetry in patients with suspected glaucoma. Acta Ophthalmologica Scandinavica 1989;67:537-45.

Wild JM and Hudson C. The attenuation of blue-on-yellow perimetry by the macular pigment. Ophthalmology 1995;102:911-7.

Wild JM, Hussey MK, Flanagan JG and Trope GE. Pointwise topographical and longitudinal modeling of the visual field in glaucoma. Investigative Ophthalmology and Visual Science 1993;34:1907-16.

Wild JM, Moss ID, Whitaker D and O'Neill EC. The statistical interpretation of blue-yellow visual field loss. Investigative Ophthalmology and Visual Science 1995;36:1398-410.

Wild JM, Pacey IE, O'Neill EC and Cunliffe IA. The SITA perimetric threshold algorithms in glaucoma. Investigative Ophthalmology and Visual Science 1999;40:1998-2009.

Wirtschafter JD, Becker WL, Howe JB and Younge BR. Glaucoma visual field analysis by computed profile of nerve fiber function in optic disc sectors. Ophthalmology 1982;89:255-67.

Wollstein G, Garway-Heath DF, Fontana L and Hitchings RA. Identifying early glaucomatous changes. Comparison between expert clinical assessment of optic disc photographs and confocal scanning ophthalmoscopy. Ophthalmology 2000;107:2272-7.

Wollstein G, Garway-Heath DF and Hitchings RA. Identification of early glaucoma cases with the scanning laser ophthalmoscope. Ophthalmology 1998;105:1557-63.

Wollstein G, Ishikawa H, Wang J, Beaton SA and Schuman JS. Comparison of three optical coherence scanning areas for detection of glaucomatous damage. American Journal of Ophthalmology 2005;139:39-43.

Wollstein G, Schuman JS, Price LL, Aydin A, Beaton SA, Stark PC, Fujimoto JG and Ishikawa H. Optical coherence tomography (OCT) macular and peripappillary retinal nerve fiber layer measurements and visual fields. American Journal of Ophthalmology 2004;138:218-25.

Wollstein G, Schuman JS, Price LL, Aydin A, Stark PC, Hertzmark E, Lai E, Ishikawa H, Mattox C, Fujimoto JG and Paunescu LA. Optical coherence tomography longitudinal evaluation of retinal nerve fiber layer thickness in glaucoma. Archives of Ophthalmology 2005;123:464-70.

Wood JM, Wild JM, Bullimore MA and Gilmartin B. Factors affecting the normal perimetric profile derived by automated static threshold LED perimetry, 1: pupil size. Ophthalmic and Physiological Optics 1988;8:26-31.

Yamagishi N, Anton A, Sample PA, Zangwill L, Lopez A and Weinreb RN. Mapping structural damage of the optic disk to visual field defect in glaucoma. American Journal of Ophthalmology 1997;123:667-76.

Yan X, Tezel G, Wax MB and Edward DP. Matrix metalloproteinases and tumour necrosis factor alpha in glaucomatous optic nerve head. Archives of Ophthalmology 2000;118:666-73.

Yoles E and Schwartz M. Elevation of intraocular glutamate levels in rats with partial lesion of the optic nerve. Archives of Ophthalmology 1998;116:906-10.

Yucel YH, Zhang Q, Gupta N, Kaufman PL and Weinreb RN. Loss of neurons in magnocellular and parvocellular layers of the lateral geniculate nucleus in glaucoma. Archives of Ophthalmology 2000;118:378-84.

Yucel YH, Zhang Q, Weinreb RN, Kaufman PL and Gupta N. Atrophy of relay neurons in magno- and parvocellular layers in the lateral geniculate nucleus in experimental glaucoma. Investigative Ophthalmology and Visual Science 2001;42:3216-22.

Yucel YH, Zhang Q, Weinreb RN, Kaufman PL and Gupta N. Effects of retinal ganglion cell loss on magno-, parvo-, koniocellular pathways in the lateral geniculate nucleus of visual cortex in glaucoma. Progress in Retinal Eye Research 2003;22:465-81.

Zangwill L, Irak I, Berry CC, Garden V, de Souza Lima M and Weinreb RN. Effect of cataract and pupil size on image quality with confocal scanning laser ophthalmoscopy. Archives of Ophthalmology 1997;115:983-90.

Zangwill L, Shakiba S, Caprioli J and Weinreb RN. Agreement between clinicians and a confocal scanning laser ophthalmoscope in estimating cup/disk ratios. American Journal of Ophthalmology 1995;119:415-21.

Zangwill LM, Jain S, Racette L, Ernstrom KB, Bowd C, Medeiros FA, Sample PA and Weinreb RN. The effect of disc size and severity of disease on the diagnostic accuracy of the Heidelberg Retina Tomograph Glaucoma Probability Score. Investigative Ophthalmology and Visual Science 2007;48:2653-60.

Zeimer R, Asrani S, Zou S, Quigley H and Jampel H. Quantitative detection of glaucomatous damage at the posterior pole by retinal thickness mapping. A pilot study. Ophthalmology 1998;105:224-31.

Zeyen T, Miglior S, Pfeiffer N, Cunha-Vaz J and Adamsons I. Reproducibility of evaluation of optic disc change for glaucoma with stereo optic disc photographs. Ophthalmology 2003;110:340-4.

Zhang X, Hood DC, Chen CS and Hong JE. A signal-to-noise analysis of multifocal VEP responses: and objective definition for poor records. Documenta Ophthalmologica 2002;104:287-302.